



HAL
open science

Stationary solutions and well-balanced schemes for the Shallow water model with two velocities

Nelly Boulos Al Makary

► **To cite this version:**

Nelly Boulos Al Makary. Stationary solutions and well-balanced schemes for the Shallow water model with two velocities. General Mathematics [math.GM]. Université Paris-Nord - Paris XIII, 2022. English. NNT : 2022PA131068 . tel-04014568

HAL Id: tel-04014568

<https://theses.hal.science/tel-04014568>

Submitted on 4 Mar 2023

HAL is a multi-disciplinary open access archive for the deposit and dissemination of scientific research documents, whether they are published or not. The documents may come from teaching and research institutions in France or abroad, or from public or private research centers.

L'archive ouverte pluridisciplinaire **HAL**, est destinée au dépôt et à la diffusion de documents scientifiques de niveau recherche, publiés ou non, émanant des établissements d'enseignement et de recherche français ou étrangers, des laboratoires publics ou privés.

UNIVERSITÉ PARIS XIII - SORBONNE PARIS NORD
École Doctorale Sciences, Technologies, Santé Galilée

Prise en compte de la topographie dans un modèle de Saint-Venant à deux vitesses: solutions stationnaires et schémas numériques

THÈSE DE DOCTORAT

présentée par

Nelly BOULOS AL MAKARY

Laboratoire Analyse Géométrie et Applications

pour l'obtention du grade de

DOCTEUR EN MATHÉMATIQUES

soutenue le 13 Décembre 2022 devant le jury d'examen composé de :

OMNES Pascal, Université Sorbonne Paris Nord Président du jury
NOELLE Sebastian, RWTH University Rapporteur
LUCAS Carine, Université d'Orléans Rapporteur
NKONGA Boniface, Université de Nice Sophia-Antipolis Examineur
GODLEWSKI Edwige, Sorbonne Université Examinatrice
AUDUSSE Emmanuel, Université Sorbonne Paris Nord ... Directeur de thèse
AGUILLON Nina, Sorbonne Université Encadrante de thèse
PARISOT Martin, Inria Bordeaux Encadrant de thèse

Abstract

In this work, we are interested in the analysis of the "Shallow water model with two velocities".

First, we study the steady state solutions using the Bernoulli's principle for C^1 regular solutions and the Rankine-Hugoniot relations through discontinuities. Then, we present the types of solutions, their existence and their uniqueness depending on the boundary conditions. Second, we propose several finite volume approximate Riemann solvers for the resolution of the homogeneous Shallow water model with two velocities. The construction of the schemes is based on a recent analysis of the Riemann problem. We present several test cases to illustrate the behavior and the properties of the schemes. Afterwards, we extend these schemes for the model with topography and we propose a suitable numerical approximation of the source term. We prove that the proposed schemes are well-balanced and ensure the positivity of the water heights. Finally, we study the numerical stability of the stationary solutions.

Keywords: Shallow water model with two velocities, steady state solutions, topography, subcritical flow, supercritical flow, discontinuities, Riemann problem, finite volume, well-balanced schemes.

Remerciements

Naturellement, je tiens à adresser mes premiers remerciements à mon directeur de thèse Emmanuel AUDUSSE. Bien de plus que son rôle, il a été une source d'inspiration de par sa rigueur, sa patience, sa motivation et la liste sera encore longue. Je le remercie pour son aide continuelle et pour ses conseils durant ces quatre années de thèse. Je poursuis mes remerciements en exprimant toute ma gratitude à mon encadrante Nina AGUILLON. Je la dois à son encadrement admirable. Elle a fait toujours preuve d'une rigueur scientifique et d'un esprit critique qu'elle s'est efforcée de transmettre. De la même manière, je remercie conjointement mon encadrant Martin PARISOT. Je le remercie chaleureusement pour sa disponibilité, son expertise et son aide en programmation surtout durant mon stage de M2. Je les remercie de m'avoir fait confiance et de m'avoir recrutée pour le stage de Master et la thèse. Pour toutes ces raisons, je tiens à leur exprimer toute ma reconnaissance.

J'exprime toute ma gratitude à Sebastian NOELLE et Carine LUCAS pour leur travail de rapporteurs de thèse. J'ai apprécié toutes vos remarques. À Sebastian Noelle, un grand merci pour les merveilleux séjours à Aachen, merci pour toutes tes conseils et pour ton soutien continu. Merci à Pascal OMNES, Edwige GODLEWSKI et Boniface NKONGA d'avoir accepté de faire partie de mon jury.

De plus, je dis merci à tous les membres de l'équipe ANGE, du LAGA et du LJLL. Je salue et remercie particulièrement mes camarades du bureau au LJLL. Merci pour toutes les discussions ensemble et le soutien qu'on a partagé les un pour les autres. C'est un plaisir d'avoir passé ces dernières années avec vous!

Merci du fond du coeur à tous mes amis au Liban et en France. La liste est si longue pour nommer chacun et chacune parmi vous. Vous vous connaissez tous! Merci d'être un soutien continu, merci d'être toujours là avec votre bonne humeur, merci pour toutes les sorties et le temps passé.

Bien sûr, un très grand merci à ma grande famille! Merci d'être toujours à côté de moi. Merci pour tous les moments agréables et les souvenirs qu'ont vécu au Liban et en France. Vous êtes toujours dans mon coeur et vous le resterez!

À ma soeur "Elissa" et à mon frère "Paul", merci d'être là tout le temps. Merci

d'être mes meilleurs amis. Merci de m'écouter toujours et de ne jamais cesser de prendre soin de moi. Vous m'avez accompagné dans cette épreuve, comme vous l'avez fait dans chaque étape de ma vie. Je vous aime énormément.

À mes parents, qui croient en moi dès le début. Je ne saurais que vous dire merci, vous exprimer ma reconnaissance pour votre soutien à tout égard, même durant les moments difficiles. Merci d'être les gens formidables que je n'ai cessé d'admirer!

Pour finir, je remercie mon mari "Youssef" pour une infinité de choses. Aucun mot peut décrire ma gratitude pour toi. Tu étais et tu seras toujours ma source d'inspiration. Merci d'avoir toujours entendu mes plaintes. Merci de me soutenir sans cesse, d'être fier de moi et de croire toujours en moi. Tu as partagé avec moi les meilleures et les mauvais moments de cette aventure. Maintenant qu'une nouvelle aventure nous attend, j'ai hâte de la vivre avec toi!

À ma famille!

Résumé

Systeme de Saint-Venant à deux vitesses

Les équations de Saint-Venant modélisent les écoulements à surface libre dits "eaux peu profondes". Ces équations occupent une place primordiale dans les études en hydraulique maritime ou fluviale. Elles sont par exemple utilisées pour la protection de l'environnement, le calcul des marées et des ondes de tempête, le transport des sédiments ou encore l'étude des crues. Elles peuvent être obtenues à partir d'une intégration verticale des équations de Navier Stokes [33]. Récemment, des auteurs ont proposé des extensions de ce modèle pour une meilleure description du profil vertical de la vitesse: modèle de Saint-Venant à plusieurs vitesses [7, 8] ou modèle de Saint-Venant à deux vitesses [47, 53]. Dans ce travail nous nous intéressons à l'étude du modèle à deux vitesses qui s'écrit en une dimension d'espace

$$\begin{cases} \partial_t h + \partial_x(h\bar{u}) & = 0, \\ \partial_t(h\bar{u}) + \partial_x(h(\bar{u}^2 + \hat{u}^2) + \frac{g}{2}h^2) & = -gh\partial_x Z, \\ \partial_t \hat{u} + \partial_x(\bar{u}\hat{u}) & = 0. \end{cases} \quad (SW_2)$$

où $h(t, x)$ est la hauteur d'eau, $\bar{u}(t, x) \in \mathbb{R}$ et $\hat{u}(t, x) \in \mathbb{R}$ sont les composantes de la vitesse horizontale et désignent respectivement la moyenne verticale et l'écart type le long de l'axe vertical, $g > 0$ est la gravité et $Z(x)$ représente la topographie. Si nous posons $\hat{u} = 0$, nous retrouvons le modèle de Saint Venant habituel. La solution du problème de Riemann pour ce modèle a été proposée dans [1] pour une topographie constante ($Z = 0$).

L'objectif de ce travail est d'étudier les solutions stationnaires du modèle à deux vitesses et ensuite de développer des solveurs de Riemann dits "well-balanced" ou équilibre capables de préserver toute solution stationnaire régulière en 1D sous une topographie arbitraire continue.

Dans ce but, nous analysons dans un premier temps les solutions stationnaires. Ensuite, nous proposons des solveurs de Riemann pour le système homogène à deux vitesses, i.e sans topographie. Par la suite, nous étendons ces schémas

pour prendre en considération la présence de la topographie. Nous validons les différentes parties de notre étude par des résultats numériques.

Solutions stationnaires du système de Saint Venant à deux vitesses

L'étude des solutions stationnaires du modèle de type de Saint Venant est importante car les écoulements en rivière sont généralement des perturbations autour d'un écoulement stationnaire. Pour le système de Saint-Venant classique, certaines solutions sont données dans [37, 28]. Les solutions stationnaires de (SW_2) sont des fonctions régulières de classe C^1 par morceaux où le débit $h\bar{u}$ est constant ainsi que la quantité $\bar{u}\bar{u}$. Puis, pour mieux comprendre les solutions stationnaires, nous analysons la deuxième équation en suivant le principe de Bernoulli pour les solutions régulières et en préservant les relations de Rankine-Hugoniot pour les solutions discontinues.

L'analyse des solutions stationnaires nous permettra de comprendre leurs allures dans un domaine donné et sous une topographie continue fixée. Plus précisément, nous étudierons la forme des solutions en fonction du type de l'écoulement (souscritique, transcritique, supercritique). Une étude originale concernant la non-unicité de la solution dans le cas de conditions limites supercritiques sera décrite dans ce travail.

Schémas numériques pour le système homogène

Dans ce travail, nous commençons par construire des schémas numériques pour le système homogène qui seront adaptés par la suite pour prendre en considération la présence de la topographie. Le système de Saint-Venant à deux vitesses homogène est un système hyperbolique de lois de conservation. Nous approchons la solution en utilisant la méthode des volumes finis bien adaptées à ce type de problème [34, 17, 54]. Il existe de nombreux schémas volumes finis standards pour ce type de problème, par exemple le schéma le plus connu, le schéma *HLL*, voir [40]. Ce schéma contient un seul état intermédiaire séparé par deux ondes. Les états intermédiaires de ce schéma peuvent être calculés en utilisant seulement les relations de consistance. Ce schéma est couramment utilisé pour approcher le système de Saint-Venant classique et préserve la positivité des hauteurs d'eau et assure la décroissance de l'entropie, voir [17]. Mais, contrairement à ce dernier, le modèle à deux vitesses contient une onde supplémentaire qui est une discontinuité de contact et le schéma *HLL* n'est pas précis autour de cette onde. Par conséquent, nous considérons deux solveurs

approchés avec trois ondes et deux états intermédiaires. Ces solveurs de Riemann approchés sont de type "HLLC", voir [17, 55, 54, 23]. Les trois schémas proposés préservent

- (i) la positivité des hauteurs d'eau,
- (ii) le principe du maximum sur $S = \frac{\hat{u}}{h}$.

Nous prouvons de plus que le deuxième schéma à trois ondes est exacte sur le transport du cisaillement S . À travers une stratégie numérique bien précise, nous constatons que les trois schémas proposés vérifient au niveau discret une dissipation de l'énergie mécanique pour le système de Saint-Venant classique, alors que, ce n'est pas le cas pour le modèle à deux vitesses. En fait, seul le schéma *HLL* est capable de vérifier cette propriété.

Schémas numériques well-balanced pour les solutions stationnaires

En plus de l'analyse des solutions stationnaires, nous nous intéressons à construire des schémas numériques capables de vérifier les propriétés énumérées précédemment et qui sont précis sur la discontinuité de contact tout en préservant les états d'équilibre réguliers pour tous les états stationnaires. Les schémas préservant cette propriété sont appelés "Well-balanced". Plusieurs schémas préservant les états d'équilibre du système de Saint Venant classique ont été introduits ces dernières années, citons par exemple [13, 38, 36, 7].

À notre connaissance, un schéma "well-balanced" pour le modèle à deux vitesses n'a jamais été étudié. La présence de la topographie crée une onde supplémentaire qui doit être ajoutée dans la construction des schémas numériques afin de conserver les états stationnaires. De ce fait, nous étendons les schémas présentés pour le système homogène. Nous proposons d'abord une approximation numérique appropriée du terme source. Ensuite, nous construisons un premier solveur de Riemann approché comme une extension du schéma "HLL" auquel nous ajoutons l'onde stationnaire comme fait dans [44] pour le modèle de Saint-Venant. Ce schéma ne prend pas en considération la discontinuité de contact sur S . Puis, nous construisons deux solveurs de Riemann approchés de 4-ondes différents dont la stratégie de la construction de l'un est similaire à celle utilisée pour approcher la solution du modèle de Ripa dans [29] alors que le second est totalement nouveau et prend en considération les quatre ondes et les invariants de Riemann du modèle. Nous prouvons ainsi que les trois schémas vérifient la propriété de l'équilibre ainsi que le principe du maximum

sur S . Enfin, nous assurons la positivité des hauteurs d'eau intermédiaire dans chacun des schémas.

Résultats numériques

Dans un dernier temps, nous testons les schémas numériques construits sur ces solutions stationnaires étudiées. Nous étudions, à travers les simulations numériques, la stabilité numérique des solutions stationnaires. En particulier, nous observons que les solutions avec un choc à gauche de la bosse ne sont pas stables. Cela a été documenté dans [11] avec des preuves expérimentales.

Summary

The objective of this work is to study the steady state solutions of the "Shallow water model with two velocities" with topographic source term and then to design non linearly stable and well balanced finite volume schemes to compute approximate solutions of this model.

The shallow water model with two velocities is a hyperbolic system, introduced recently in [1] where the authors establish the global well-posedness of the Riemann problem. In $1D$ and for continuous solutions, this system is a bi-layer version of the layerwise hydrostatic model introduced in [9] for a particular choice of the interface velocity and is equivalent to the shear shallow water model introduced in [32].

The first chapter of this thesis is dedicated to the study of the steady state solutions of the $1D$ model with topography source term. We first exhibit the C^1 regular solutions following the Bernouilli's principle and the Rankine-Hugoniot jump conditions through a discontinuity where the dissipation of entropy should be verified. In a second step, we present various types of solutions depending on the boundary conditions. We study in each case the (non) existence and (non) uniqueness of the steady states. When the solution is not unique we analyze the effect of the shape of the topography on the coexistence of the solutions. Some of these solutions were presented for the classical Shallow water equations in [41].

In the second chapter, we propose three numerical schemes for the resolution of the homogeneous shallow water model with two velocities. The solution of the Riemann problem of the homogeneous shallow water model with two velocities contains three waves. The construction of Godunov schemes [35] based on the exact solution of the Riemann problem is possible but is very costly and might not be extended to the model with source term. Hence, we will consider Approximate Riemann solvers "ARS", see [17]. These solvers are Godunov-type finite volume schemes where the exact solution of the Riemann

problem is replaced by an approximate one. The best known ARS is the well known *HLL* scheme, see [40]. This scheme is based on a one state approximate Riemann solver. The *HLL* solver is commonly used to approximate the solutions of the Shallow water model, see [17]. But contrary to the homogeneous shallow water model, the homogeneous shallow water model with two velocities contains an additional wave which corresponds to the contact wave in the Riemann problem and the *HLL* solver is not accurate around this contact wave. Hence, we will describe and analyze two ARS with three waves and two intermediate states. These two solvers are of *HLLC* type, see [17, 55, 54, 23]. We present several test cases to illustrate the behavior and the properties of the schemes.

The third chapter is devoted to the derivation of numerical schemes to approach the solution of the shallow water model with two velocities and topography. In this case, the system is not written under a conservative form and an additional stationary wave is created due to the presence of the source term. This wave must be added in the construction of the ARS in order to preserve the stationary states. To do so, we extend the schemes presented in the second chapter. Therefore, we propose first a suitable numerical approximation of the source term. Then, we construct an approximate Riemann solver as an extension of the *HLL* scheme for which we add the stationary wave as done in [44]. Then, we construct two different 4-waves approximate Riemann solvers. One of them is similar to a scheme proposed in [29] to approximate the solution of the Ripa model whereas the second one is up to our knowledge totally new and takes into consideration the four waves and some Riemann invariants of the model. We prove that the three schemes verify the well-balanced property as well as the positivity of the intermediate water heights.

In the last chapter, we performed numerical simulations to study the stability of the stationary solutions documented in Chapter 2: in particular we observed that solutions with a shock on the left of a bump are unstable. This was mentioned in [11] with experimental evidence.

Contents

1	Introduction	19
1.1	Context	19
1.1.1	The shallow water model	19
1.2	The homogeneous Shallow water model with two velocities and relations with other models	23
1.2.1	2D model	23
1.2.2	The 1D homogeneous Shallow water model with two velocities	24
1.2.3	Properties of the homogeneous Shallow water model with two velocities	24
1.2.4	Relation with the Bilayer Shallow water model	27
1.2.5	Relation with the Shear shallow water model	28
1.2.6	Relation with the full Euler system	28
1.2.7	Relation with the Ripa model	29
1.3	The 1D Shallow water model with two velocities and source term	29
1.3.1	Model	29
1.3.2	Steady state solutions	30
1.3.3	Numerical schemes for the shallow water model with two velocities	35
2	Stationary solutions of the 1D SW_2 model	47
2.1	Brief description of the model	47
2.2	Moving steady state solution: regular part and stationary shock	49
2.2.1	Regular moving steady states	51
2.2.2	Stationary shocks and the entropy condition	60
2.3	(Non) existence and (non) uniqueness of the moving steady states depending on the boundary conditions	64
2.3.1	Preliminaries	65
2.3.2	Subcritical inlet boundary conditions	67
2.3.3	Supercritical inlet boundary conditions	72

3	Numerical schemes for the homogeneous model	87
3.1	Finite volume method	89
3.2	Stability and consistency	91
3.3	<i>HLL</i> approximate Riemann solver	93
3.4	<i>HLL*</i> approximate Riemann solver	97
3.5	<i>HLL_{\bar{u}}</i> approximate Riemann solver	103
3.6	Numerical results	107
3.6.1	Dam break problem	108
3.6.2	Two shock case	109
3.6.3	Two rarefactions case	111
3.6.4	Dam break problem with change of sign on \hat{u}	111
3.6.5	Stationary contact discontinuity	115
3.6.6	Traveling contact discontinuity	119
3.7	Discrete energy inequality of the schemes	121
3.7.1	The case $\hat{u}_L = \hat{u}_R = 0$	122
3.7.2	The case $\hat{u}_L \neq 0$ and $\hat{u}_R \neq 0$	122
4	Numerical schemes for the model with topography	123
4.1	Godunov type schemes	125
4.2	Stability and consistency	125
4.3	Steady state solutions	126
4.4	Determination of the topography source term	128
4.5	The <i>HLL₀</i> approximated Riemann solver	131
4.5.1	Well-balanced version of the <i>HLL₀</i> scheme	134
4.5.2	Positive and well-balanced version of the <i>HLL₀</i> scheme	137
4.5.3	Other correction strategies to ensure the positivity of the intermediate water heights	140
4.6	The <i>HLL₀*</i> approximated Riemann solver	141
4.6.1	Well-balanced version of the <i>HLL₀*</i> scheme	143
4.6.2	Positive and well-balanced version of the <i>HLL₀*</i> scheme	147
4.7	The <i>HLL_{0,\bar{u}}</i> approximated Riemann solver	150
4.7.1	Well-balanced version of the <i>HLL_{0,\bar{u}}</i> scheme	152
4.7.2	Positive and well-balanced version of the <i>HLL_{0,\bar{u}}</i> scheme	156
4.8	Study of positive intermediate water heights corrections	164
5	Numerical stability of the stationary solutions	167
5.1	Subcritical inlet boundary condition	170
5.1.1	Subcritical outlet boundary condition	170
5.2	Supercritical inlet boundary conditions	176
5.2.1	Subcritical outlet boundary conditions	178
5.2.2	Supercritical outlet boundary conditions	183

<i>CONTENTS</i>	17
Conclusion	189
Perspectives	191

Chapter 1

Introduction

1.1 Context

1.1.1 The shallow water model

The Shallow water model was initially introduced by the engineer Adhémar Barré de Saint Venant in 1871 in its $1D$ version in [12]. The shallow water model is a hyperbolic system modeling free surface flows. It is used in many studies such that flooding, dam breaks, tsunami prevention, hydraulic jumps, sediment transport and so on.

The Shallow water equations can be derived from the Navier Stokes equations where we consider that the vertical dimension is much smaller than the horizontal one [33]. Then, it can be seen as a shallow water or as a long wave approximation. It can also be derived from a vertical integration of the Euler equations with the assumptions that the pressure is hydrostatic and that the velocity is vertically averaged [9].

In its $2D$ version, the homogeneous Shallow water model reads

$$\begin{cases} \partial_t h + \nabla \cdot (hU) = 0, \\ \partial_t (hU) + \nabla \cdot (hU \otimes U + \frac{g}{2} h^2 \mathbb{1}) = 0 \end{cases} \quad (SW)$$

with $g > 0$ the gravity acceleration. The unknowns of the system are $h(t, x, y) \in \mathbb{R}_+$ the water depth of the flow and $U(t, x, y) \in \mathbb{R}^2$ the water column velocity. (SW) is a system of conservation law where the first equation represents the mass equation and the second equation is the momentum equation.

Contrary to the free surface Navier Stokes and Euler equations, the Shallow water equations (*SW*) is a model with reduced complexity which facilitates geophysical flows simulations. In fact, the problem of the moving domain no longer arises since the problem can be written in two space dimensions and there exist efficient and robust numerical techniques, see [19].

Limitations of the Shallow water model

The study of flows is limited by the difficult approximation of the vertical velocity, the stratification in the ocean for example, where we are interested in the vertical structure in the flow and in this case we can't only be interested in the average velocity. Moreover, taking into account the hypothesis of hydrostatic pressure can cause some problems. We give for example the case of the swell where the horizontal scale is comparable to the vertical scale and the non-hydrostatic pressure should be taken into consideration.

To solve this issue, many works were presented in the "ANGE team", see [2, 6, 9, 31]. In the present work, we are interested in the Multilayer Shallow water models and mainly the model derived in [9] to better approximate the hydrostatic Euler equations. It is a multilayer shallow water system with mass exchanges where the layer thickness is proportional to the total water height. This model presents some analogy with the σ transformation free surface flows commonly used in oceanography, see [25].

The multilayer Shallow water model

According to [9], the multilayer Shallow water model can be derived by a vertical integration of the hydrostatic and incompressible free surface Euler equation [20, 39] where we suppose that the flow domain is divided in the vertical direction in n layers as seen in Figure 1.1 for

$$t > t_0, \quad x \in \mathbb{R}, \quad z_b(x) \leq z \leq \eta(x, t),$$

where $\eta(x, t)$ represents the elevation of the free surface.

The model reads

$$\begin{cases} \partial_t h + \sum_{i=1}^n \nabla \cdot (h_i U_i) & = 0, \\ \partial_t (h_i U_i) + \nabla \cdot (h_i U_i \otimes U_i + \frac{g}{2} h_i h) & = U_{i+\frac{1}{2}} G_{i+\frac{1}{2}} - U_{i-\frac{1}{2}} G_{i-\frac{1}{2}}, \end{cases} \quad (SW_L)$$

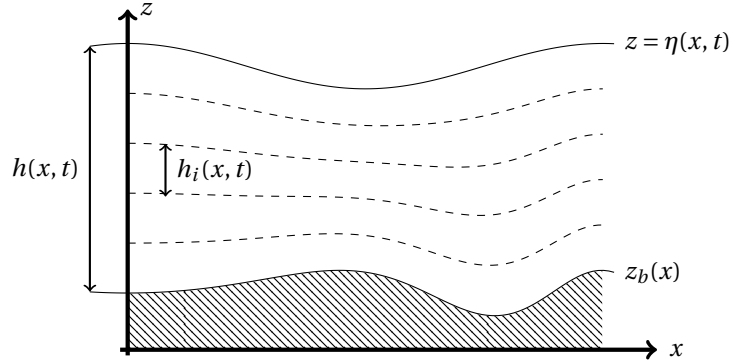


Figure 1.1: Sketch of the multilayer approach

where the unknowns are respectively h the total water height and the mean velocity U_i of each layer.

The rest of the parameters appearing in (SW_L) are:

- h_i the approximation of the layer thickness which is deduced from the total water height through the relation

$$h_i = l_i h,$$

with $l_i, i = 1, \dots, n$

$$l_i > 0, \quad \sum_{i=1}^n l_i = 1.$$

- the mass exchange terms between the interfaces $G_{i+\frac{1}{2}}$ which are computed by

$$G_{i+\frac{1}{2}} = \partial_t \sum_{j=1}^i h_j + \nabla \cdot \sum_{j=1}^i (h_j U_j),$$

- the velocity at the interface $U_{i+\frac{1}{2}} = \mathcal{U}(U_i, U_{i+1})$ that represents a convex combination of U_i and U_{i+1} .

Previously, we presented the multilayer shallow water model. However, in this work, we focus on the two-layers version of this model for which we give the following properties.

Hyperbolicity

In its two layers version, the model reads

$$\left\{ \begin{array}{l} \partial_t h_1 + \nabla \cdot h_1 U_1 = G_{\frac{3}{2}}, \\ \partial_t h_2 + \nabla \cdot h_2 U_2 = -G_{\frac{3}{2}}, \\ \partial_t h_1 U_1 + \nabla \cdot (h_1 U_1 \otimes U_1 + \frac{g}{2} h_1 h \mathbb{1}) = U_{\frac{3}{2}} G_{\frac{3}{2}}, \\ \partial_t h_2 U_2 + \nabla \cdot (h_2 U_2 \otimes U_2 + \frac{g}{2} h_2 h \mathbb{1}) = -U_{\frac{3}{2}} G_{\frac{3}{2}}. \end{array} \right. \quad (1.1)$$

where the unknowns are the water height in each layer h_1 and h_2 , the velocity in each layer U_1 and U_2 , the velocity at the interface $U_{\frac{3}{2}}$ and the term of mass exchange $G_{\frac{3}{2}}$. In the following, this model is called bilayer shallow water model. In [9], this model was proven to be hyperbolic for $U_{\frac{3}{2}} = U_1$ or U_2 whereas in [1], for a homogeneous vertical discretization, i.e $h_1 = h_2$, the model is hyperbolic for $U_{\frac{3}{2}} = \frac{U_1 + U_2}{2}$. The study of the hyperbolicity for the three layers model or more is not done yet.

Riemann problem

After proving the hyperbolicity, a next issue one can face, is the resolution of the Riemann problem for the bilayer model. The Riemann problem is a Cauchy problem with discontinuous data where we consider that the domain of definition is divided in two constant states. This solution is a major improvement in the understanding of the model when it comes to the construction of Approximate Riemann solvers.

The solution of the Riemann problem is a challenging question because the system is not written under a conservative form and a definition of the non conservative products has to be given.

To face this issue a new formulation of the bilayer model was given recently in [1] where the authors introduce a new model called "The shallow water model with two velocities". They prove that it is equivalent for regular solutions to the bilayer shallow water model (1.1) completed with

$$h_1 = h_2 \quad \text{and} \quad U_{\frac{3}{2}} = \frac{U_1 + U_2}{2}. \quad (1.2)$$

1.2. THE HOMOGENEOUS SHALLOW WATER MODEL WITH TWO VELOCITIES AND RELATIONS WITH

Then, the resolution of the Riemann problem of the shallow water model with two velocities is given.

In this thesis, we are interested in the model with two velocities. We first present the model and then we give some detailed properties of the 2D model. However, in the present work, we focus on the 1D model with two velocities.

1.2 The homogeneous Shallow water model with two velocities and relations with other models

1.2.1 2D model

In two space dimensions, the homogeneous shallow water model with two velocities reads

$$\begin{cases} \partial_t h + \nabla \cdot (h\bar{U}) & = 0, \\ \partial_t (h\bar{U}) + \nabla \cdot (h(\bar{U} \otimes \bar{U} + \hat{U} \otimes \hat{U}) + \frac{g}{2} h^2 \mathbb{1}) & = 0, \\ \partial_t \hat{U} + (\bar{U} \cdot \nabla) \hat{U} + (\hat{U} \cdot \nabla) \bar{U} & = 0. \end{cases} \quad (2DSW_2)$$

with $g > 0$ the acceleration of gravity. The unknowns of the system are $h(t, x, y) \in \mathbb{R}_+$ the water depth of the flow, $\bar{U}(t, x, y) = (\bar{u}, \bar{v}) \in \mathbb{R}^2$ the vertical-averaged of the horizontal velocity and $\hat{U}(t, x, y) = (\hat{u}, \hat{v}) \in \mathbb{R}^2$ the signed standard deviation of the horizontal velocity such that

$$(h, \bar{U}, \hat{U}) = \left(h_1 + h_2, \frac{U_1 + U_2}{2}, \frac{U_2 - U_1}{2} \right). \quad (1.3)$$

For $\hat{U} = 0$ we retrieve the classical shallow water model. The (2DSW₂) is an approximation of the free surface Euler equation assuming the pressure is hydrostatic and the horizontal velocity is mainly described by its vertical mean and standard deviation.

1.2.2 The 1D homogeneous Shallow water model with two velocities

In its one dimension version, the homogeneous shallow water model with two velocities reads

$$\begin{cases} \partial_t h + \partial_x(h\bar{u}) & = 0, \\ \partial_t(h\bar{u}) + \partial_x(h(\bar{u}^2 + \hat{u}^2) + \frac{g}{2}h^2) & = 0, \\ \partial_t \hat{u} + \partial_x(\bar{u}\hat{u}) & = 0. \end{cases} \quad (SW_2^H)$$

We can deduce that for regular solutions

$$\partial_t \left(\frac{\hat{u}}{h} \right) + \bar{u} \partial_x \left(\frac{\hat{u}}{h} \right) = 0. \quad (1.4)$$

Hence, the third equation of (SW_2^H) is a transport equation of the quantity $S = \frac{\hat{u}}{h}$ at velocity \bar{u} .

1.2.3 Properties of the homogeneous Shallow water model with two velocities

In this section, we highlight some essential properties of the homogeneous 2D Shallow water model with two velocities $(2DSW_2)$.

Energy conservation

Any smooth enough solution $(2DSW_2)$ satisfies the energy conservation law

$$\partial_t E + \nabla \cdot \left(\left(\left(E + \frac{g}{2}h^2 \right) \mathbb{1} + h\hat{U} \otimes \hat{U} \right) \bar{U} \right) = 0, \quad (1.5)$$

where the energy is defined by

$$E = \frac{h}{2} \left(\|\bar{U}\|^2 + \|\hat{U}\|^2 \right) + \frac{g}{2}h^2. \quad (1.6)$$

In case of discontinuous solutions, the energy acts as a mathematical entropy used to discriminate the admissible solutions for which the left hand side of (1.5) is non positive.

Invariance by rotation

The 2D Shallow water model with two velocities is invariant by rotation. Thus, to study the half space Riemann problem (with transverse velocity) it is sufficient to consider

$$\begin{cases} \partial_t h + \partial_x(h\bar{u}) & = 0 \\ \partial_t(h\bar{u}) + \partial_x(h(\bar{u}^2 + \hat{u}^2) + \frac{g}{2}h^2) & = 0 \\ \partial_t \hat{u} + \partial_x(\bar{u}\hat{u}) & = 0 \\ \partial_t(h\bar{v}) + \partial_x(h(\bar{u}\bar{v} + \hat{u}\hat{v})) & = 0 \\ \partial_t \hat{v} + \hat{u}\partial_x \bar{v} + \bar{u}\partial_x \hat{v} & = 0 \end{cases} \quad (1.7)$$

where (\bar{u}, \hat{u}) are the components of the normal velocity and (\bar{v}, \hat{v}) are the components of the transverse velocity.

The first three equation of system (1.7) correspond to the conservative 1D model (SW_2^H) where the set of unknowns is (h, \bar{u}, \hat{u}) . These equations are independent of the last two equations in (1.7) containing the transverse velocity (\bar{v}, \hat{v}) . We will see that this property will facilitate the study of the model.

Hyperbolicity

In [1], the hyperbolicity of the model was proven and it appears that the eigenvalues of the model depend only on the variables of the 1D model (SW_2^H). More precisely, the quasi-linear form of (1.7) is

$$\partial_t V + A(V) \partial_x V = 0,$$

where $V = (h, \bar{u}, \hat{u}, \bar{v}, \hat{v})$ and $A(V)$ is the matrix defined by

$$A(V) = \begin{pmatrix} \bar{u} & h & 0 & 0 & 0 \\ g + \frac{\hat{u}^2}{h} & \bar{u} & 2\hat{u} & 0 & 0 \\ 0 & \hat{u} & \bar{u} & 0 & 0 \\ \frac{\hat{v}\bar{v}}{2} & 0 & \hat{v} & \bar{u} & \hat{u} \\ 0 & 0 & 0 & \hat{u} & \bar{u} \end{pmatrix}.$$

Therefore, the eigenvalues are given by

$$\lambda_L < \gamma_L < \lambda^* < \gamma_R < \lambda_R,$$

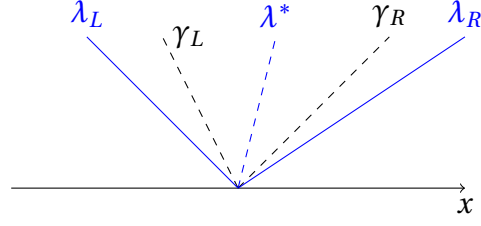


Figure 1.2: Representation of the eigenvalues of the $(2DSW_2)$ model. The blue ones correspond to the 1D model (SW_2^H) .

where

$$\left\{ \begin{array}{l} \lambda_L = \bar{u} - \sqrt{gh + 3\hat{u}^2} \\ \gamma_L = \bar{u} - |\hat{u}|, \\ \lambda^* = \bar{u}, \\ \gamma_R = \bar{u} + |\hat{u}|, \\ \lambda_R = \bar{u} + \sqrt{gh + 3\hat{u}^2}. \end{array} \right.$$

see Figure 1.2. Thus, for $\hat{u} \neq 0$, the 2D shallow water model with two velocities $(2DSW_2)$ is strictly hyperbolic, see [1, Lem 5].

Nature of the characteristic fields

The λ_L -field and the λ_R -field are then genuinely nonlinear, whereas the γ_L -field, the λ^* -field and the γ_R -field are linearly degenerate. All the internal waves are contact discontinuities.

1.2. THE HOMOGENEOUS SHALLOW WATER MODEL WITH TWO VELOCITIES AND RELATIONS WITH

Riemann invariants

A set of independent k -Riemann invariants, denoted \mathcal{I}_k is given by

$$\begin{aligned}\mathcal{I}_{\lambda_L} &= \mathcal{R}_{\lambda_L} \cup \left\{ \bar{v} - \frac{\hat{u}\hat{v}}{\frac{g}{2} + \hat{u}^2} \bar{u}, \frac{\hat{u}\hat{v}}{\frac{g}{2} + \hat{u}^2} \right\}, \\ \mathcal{I}_{\gamma_L} &= \{h, \bar{u}, \hat{u}, \bar{v} + \text{sgn}(\hat{u})\hat{v}\}, \\ \mathcal{I}_{\lambda^*} &= \mathcal{R}_{\lambda^*} \cup \{\bar{v}, h\hat{u}\hat{v}\}, \\ \mathcal{I}_{\gamma_R} &= \{h, \bar{u}, \hat{u}, \bar{v} - \text{sgn}(\hat{u})\hat{v}\}, \\ \mathcal{I}_{\lambda_R} &= \mathcal{R}_{\lambda_R} \cup \left\{ \bar{v} - \frac{\hat{u}\hat{v}}{\frac{g}{2} + \hat{u}^2} \bar{u}, \frac{\hat{u}\hat{v}}{\frac{g}{2} + \hat{u}^2} \right\}.\end{aligned}$$

where

$$\begin{aligned}\mathcal{R}_{\lambda_L} &= \left\{ \bar{u} + \sqrt{gh + 3\hat{u}^2} + \frac{gh}{\sqrt{3}\hat{u}} \log \left(\sqrt{1 + \frac{3\hat{u}^2}{gh}} + \sqrt{\frac{3}{gh}} \hat{u} \right), \frac{\hat{u}}{h} \right\}, \\ \mathcal{R}_{\lambda^*} &= \left\{ \bar{u}, \frac{g}{2h^2} + h\hat{u}^2 \right\}, \\ \mathcal{R}_{\lambda_R} &= \left\{ \bar{u} - \sqrt{gh + 3\hat{u}^2} - \frac{gh}{\sqrt{3}\hat{u}} \log \left(\sqrt{1 + \frac{3\hat{u}^2}{gh}} + \sqrt{\frac{3}{gh}} \hat{u} \right), \frac{\hat{u}}{h} \right\}.\end{aligned}\tag{1.8}$$

are the Riemann invariants of the 1D model (SW_2^H), see [1, Lem 1 and Lem 5].

Next, we exhibit the relation between the model and other models derived from the Euler equations, see Figure 1.3.

1.2.4 Relation with the Bilayer Shallow water model

The bilayer shallow water model (1.1) completed with closure (1.2) is equivalent to the shallow water model with two velocities ($2DSW_2$) where the unknowns are connected by (1.3) and conversely by

$$\left(h_1, h_2, U_1, U_2, U_{\frac{3}{2}}, G_{\frac{3}{3}} \right) = \left(\frac{h}{2}, \frac{h}{2}, \bar{U} - \hat{U}, \bar{U} + \hat{U}, \bar{U}, -\frac{1}{2} \partial_x (h\hat{U}) \right),$$

see [1].

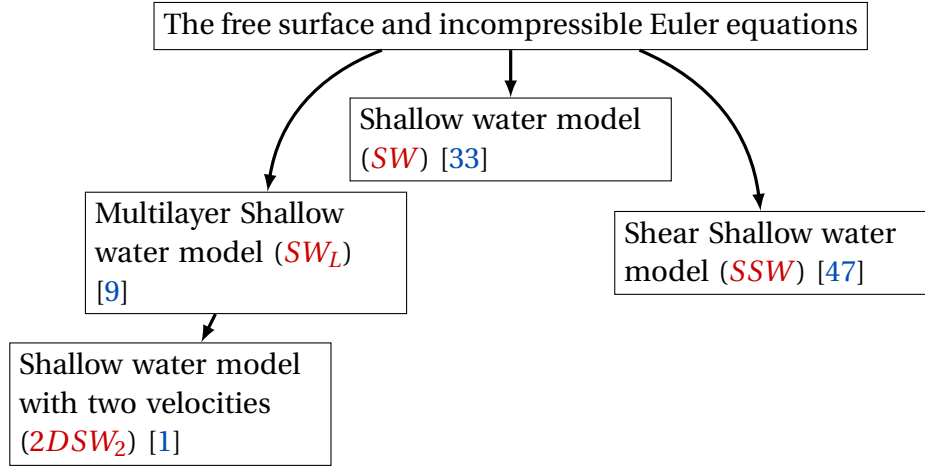


Figure 1.3: Averaged models derived from Euler equations.

1.2.5 Relation with the Shear shallow water model

The "Multi-dimension shear shallow water model" introduced in [46] and in [47] is an extension of the shallow water model where the authors consider a closure momentum equations of the vertical-averaged Euler system. It reads

$$\begin{cases} \partial_t h + \nabla \cdot (h\bar{U}) & = 0, \\ \partial_t (h\bar{U}) + \nabla \cdot \left(h(\bar{U} \otimes \bar{U} + h\mathbf{P} + \frac{g}{2} h^2 \mathbb{I}) \right) & = 0, \\ \partial_t \mathbf{P} + (\bar{U} \cdot \nabla) \mathbf{P} + (\cdot \nabla \bar{U}) \mathbf{P} + \mathbf{P} (\cdot \nabla \bar{U})^T & = 0. \end{cases} \quad (\text{SSW})$$

where \mathbf{P} is the symmetric and positive stress tensor that characterizes the distortion of the horizontal velocity profile in the vertical direction. In one dimension, the (SSW) model is equivalent for smooth solutions to (SW_2^H). It is not the case in $2D$ because the $2D$ models don't have the same number of unknowns.

1.2.6 Relation with the full Euler system

The (SW_2^H) model is equivalent for smooth solutions to the full Euler system for gas dynamics on the variables $(h, h\bar{u}, E)$, for a particular pressure $p = h\hat{u}^2 + \frac{g}{2} h^2$ and where \hat{u} acts as an entropy, see [1].

1.2.7 Relation with the Ripa model

The system (SW_2^H) presents some similarities with the Ripa model which is an also an extension of the Shallow water equations introduced in [48, 49] to take into consideration the horizontal temperature gradients. It writes

$$\begin{cases} \partial_t h + \partial_x(hu) & = 0, \\ \partial_t(hu) + \partial_x(hu^2 + \frac{g}{2}h^2\theta) & = 0, \\ \partial_t(h\theta) + \partial_x(hu\theta) & = 0. \end{cases} \quad (RIPA)$$

where $u(x, t)$ is the velocity and $\theta(x, t)$ is the temperature. Similarly to (SW_2^H), for smooth solutions the third equation of the Ripa model ($RIPA$) is also a transport equation of θ at velocity u whereas the pressure term is different between the two models.

The invariant model (1.7) is not conservative; therefore, it is difficult to approximate its solution and to study its steady state solutions. Therefore, we base our study in this thesis on the 1D model which can form a basis for future research on the transverse model.

1.3 The 1D Shallow water model with two velocities and source term

1.3.1 Model

The shallow water model with two velocities in one space dimension with topography source term reads

$$\begin{cases} \partial_t h + \partial_x(h\bar{u}) & = 0, \\ \partial_t(h\bar{u}) + \partial_x(h(\bar{u}^2 + \hat{u}^2) + \frac{g}{2}h^2) & = -gh\partial_x Z, \\ \partial_t \hat{u} + \partial_x(\bar{u}\hat{u}) & = 0. \end{cases} \quad (SW_2)$$

with Z the topography. In this thesis, we consider for simplicity that there exists a point $x_0 \in I = [x_L, x_R]$ such that Z is a C^1 regular function, increasing on $[x_L, x_0]$ and decreasing on $[x_0, x_R]$.

1.3.2 Steady state solutions

The goal of this manuscript is to study the steady state solutions of this new model which is not trivial. In fact, on intervals where the solution is C^1 , the three quantities

$$h\bar{u}, \quad \bar{u}\hat{u} \quad \text{and} \quad h + Z + \frac{1}{2g}(\bar{u}^2 + 3\hat{u}^2),$$

are constant. The conservation of the last quantity, called the hydraulic head, is nothing but the Bernoulli's principle and denoted K . On the other hand, at a point of discontinuity, the steady solutions should verify the Rankine-Hugoniot jump conditions

$$\begin{cases} [h\bar{u}] = 0, \\ [h(\bar{u}^2 + \hat{u}^2) + \frac{g}{2}h^2] = 0, \\ [\bar{u}\hat{u}] = 0, \end{cases}$$

as well as the dissipation of entropy

$$\left[\left(g(h + Z) + \frac{\bar{u}^2 + 3\hat{u}^2}{2} \right) h\bar{u} \right] \leq 0,$$

see [51]. The notation $[X] = X^+ - X^-$ represents the jump at the discontinuity separating the solution's trace X^- and X^+ .

The previous relations allow us to conclude that $h\bar{u}$ is constant in the whole domain (where the solution is regular and across the discontinuity). Therefore, for steady state solutions, there exists $M \in \mathbb{R}$ such that

$$\forall x \in I, \quad h(x)\bar{u}(x) = M.$$

Lake at rest

We mention a particular steady state solution called "lake at rest" for which the classical and very well known definition is to set the velocities to zero. In other terms, the water is at rest and its surface should not be perturbed. However, the definition of the lake at rest for the shallow water model with two velocities is quite different.

Actually, as the (SW_2) contains two velocities (\hat{u}, \bar{u}) then, if $\bar{u} = 0$ and

- $\hat{u} = 0$, we retrieve the lake at rest of the classical shallow water for which many studies were done, see [17].

1.3. THE 1D SHALLOW WATER MODEL WITH TWO VELOCITIES AND SOURCE TERM 31

- $\hat{u} \neq 0$ then, the water is not at rest and the steady state of (SW_2) is characterized by the following ODE

$$\partial_x \left(h\hat{u}^2 + \frac{g}{2}h^2 \right) = -gh\partial_x Z,$$

where an infinite number of steady states can be defined by fixing h or \hat{u} .

Moving steady states

Other types of steady states solutions are the moving steady states obtained by setting $\bar{u} \neq 0$:

- If $\hat{u} = 0$ then, we retrieve the moving steady states solutions of the classical shallow water system with topography. Some test cases for these moving steady state solutions are presented without an exhaustive study in [37] and [28].
- If $\hat{u} \neq 0$ then, we retrieve the general moving steady states solutions of the model with two velocities (SW_2).

In this thesis and mainly in the second chapter, we choose to study only the moving steady states of (SW_2), i.e for $\bar{u} \neq 0$ and for any value of \hat{u} . In that case, since the quantities $h\bar{u}$ and $\bar{u}\hat{u}$ are constant and for $h \neq 0$, the quantity $\frac{\hat{u}}{h}$ is also constant and we denote it by S . From now on, we fix $M > 0$ and $S \in \mathbb{R}$.

Up to our knowledge, a detailed study describing all the steady states, proving their (non) existence and (non) uniqueness depending on the boundary conditions was never done. Therefore, we present in this thesis all the possible moving steady states for the shallow water model with two velocities with source term according to the boundary conditions. This study encompasses the steady states solutions of the classical shallow water model, i.e for $\hat{u} = 0$.

Boundary conditions

The boundaries are fixed depending on the type of the flow, i.e on the signs of the eigenvalues of the system at the boundary. For $M \in \mathbb{R}_+^*$ and $S \in \mathbb{R}$, the boundaries are fixed as shown in Table 1.1.

Flow regime	Inlet boundary	Outlet boundary
Subcritical	2	1
Supercritical	3	0

Table 1.1: Number of required boundary conditions

Main results

The study of the moving steady state is based on the following properties

- The hydraulic head $h + Z + \frac{1}{2g} \left(\frac{M^2}{h^2} + 3h^2 S^2 \right) = K$ decreases through stationary shocks (Proposition 8) and is constant in between shocks.
- The transition from the subcritical to the supercritical regimes is continuous and occurs only at the top of the topography (Lemma 3).
- If the flow is subcritical at the inlet then, the solution contains at most one shock which can only occur at the right of the top of the topography (Lemma 4).
- If the flow is supercritical at the inlet then, the solution may contain at most one shock on each side of the domain (Lemma 5).

Using the above results, we set some threshold parameters depending on the hydraulic head K and on the water heights at both sides of the domain and at the top of the topography. Equipped with these parameters and the set of boundary conditions, we claim:

- If the inlet boundary is subcritical, the solution is unique and if
 1. the outlet boundaries are subcritical then, depending on the value of the parameters, the solution is either subcritical Figure 1.4a or transcritical with shock Figure 1.4b. (Proposition 10)
 2. the outlet boundaries are supercritical then, only one type of solution might exist: it is called the transcritical solution without shock, see Figure 1.4c. (Proposition 11)
- If the inlet boundary is supercritical and

1.3. THE 1D SHALLOW WATER MODEL WITH TWO VELOCITIES AND SOURCE TERM 33

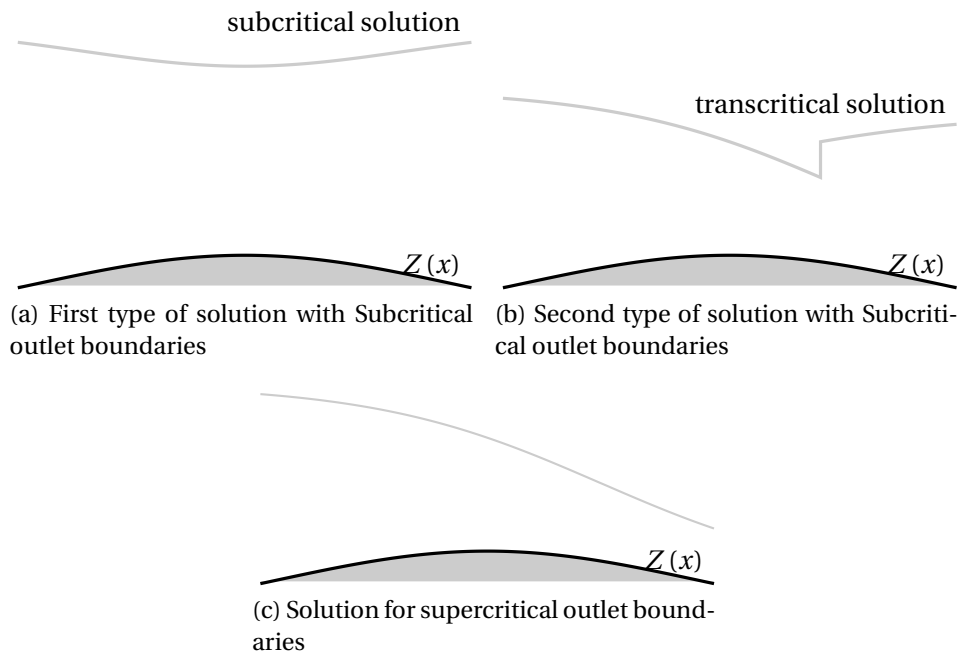


Figure 1.4: Different solutions with subcritical inlet boundaries

1. the outlet boundaries are subcritical then, there are three different types of solutions: one with a shock on the right, see Figure 1.5a, one with a shock on the left, see Figure 1.5c and one with two shocks, see Figure 1.5b. The last two solutions can never coexist but in general the solution is not unique. (Proposition 12 and Proposition 13)
2. the outlet boundaries are supercritical then, two solutions might coexist. The solution can be supercritical everywhere Figure 1.5d or with one shock on the left, see Figure 1.5e. (Proposition 14)

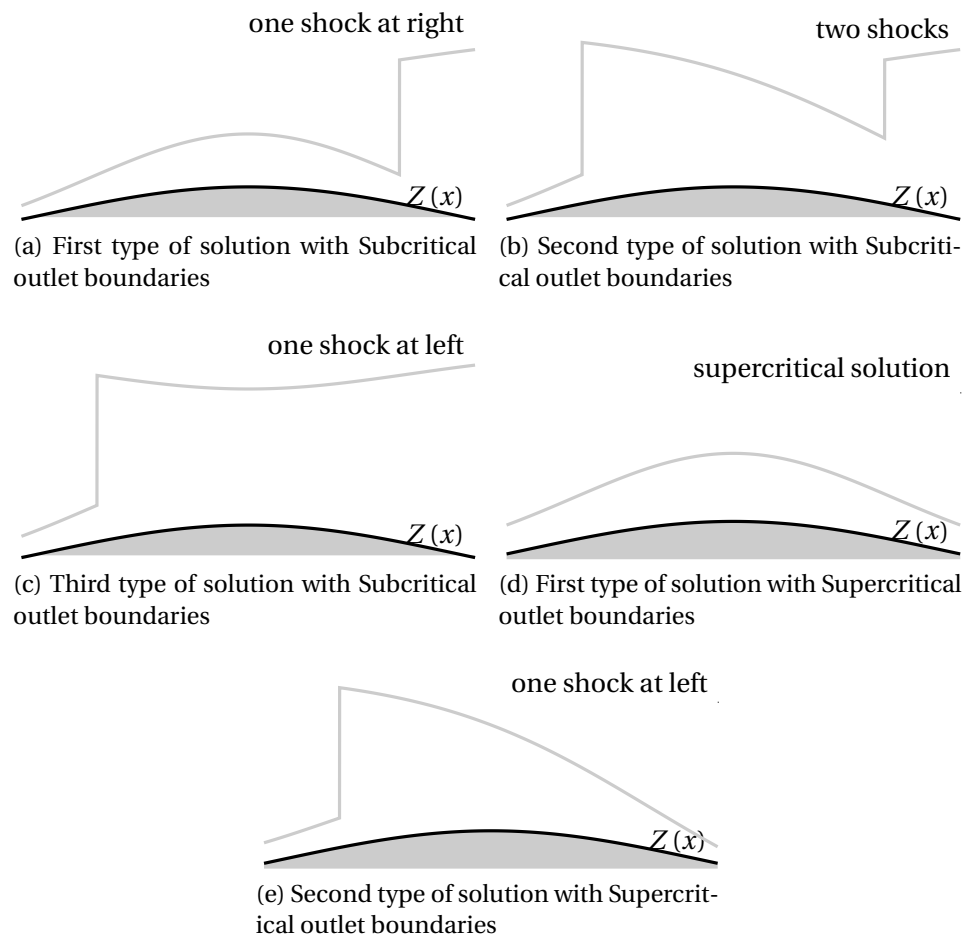


Figure 1.5: Different solutions with supercritical inlet boundaries

1.3.3 Numerical schemes for the shallow water model with two velocities

In the previous sections, we presented the model, proved its hyperbolicity and exhibited its steady state solutions. In this section, we will design numerical schemes to approximate the solution of this model. The goal in this thesis is to derive schemes that

- (i) preserve the positivity of the water height,
- (ii) preserve the maximum principle on $S = \frac{\hat{u}}{h}$
- (iii) are accurate for the transport process associated to the shear velocity
- (iv) preserve the regular steady states solution of the shallow water model with two velocities with topography source term, i.e preserve the well-balanced property.

Therefore, we start by introducing the finite volume method we use in the construction of the schemes.

Finite Volume method

The (SW_2) model can be written under the following form

$$\partial_t W + \partial_x F(W) = B(W), \quad (1.9)$$

where

$$W = \begin{pmatrix} h \\ h\bar{u} \\ \hat{u} \\ Z \end{pmatrix}, \quad F(W) = \begin{pmatrix} h\bar{u} \\ h(\bar{u}^2 + \hat{u}^2) + \frac{g}{2}h^2 \\ \bar{u}\hat{u} \\ 0 \end{pmatrix} \quad \text{and} \quad B(W) = \begin{pmatrix} 0 \\ -gh\partial_x Z \\ 0 \\ 0 \end{pmatrix}.$$

To derive the numerical schemes we privilege the finite volume method that adapts very well to the discontinuous aspects of the solution. For more information on systems of conservation laws we refer to [34, 52]. For a fixed space step Δx , we denote $C_i =]x_{i-\frac{1}{2}}, x_{i+\frac{1}{2}}[$ the cell of length $\Delta x = x_{i+\frac{1}{2}} - x_{i-\frac{1}{2}}$ where $x_{i+\frac{1}{2}}$ is the x - coordinate of the interface between the cell C_i and C_{i+1} . Each

cell is centered at $x_i = x_{i-\frac{1}{2}} + \Delta x/2$ for all $i \in \mathbb{Z}$. The time is discretized using an adaptive time step $t^{n+1} = t^n + \Delta t^n$ with Δt^n satisfying a CFL condition to be described later. W_i^n is an approximation of the mean value of $W(x, t)$ at time t^n on the cell C_i .

An explicit finite volume scheme can be expressed with the following update formula

$$\forall i \in \mathbb{Z}, \forall n \in \mathbb{N} \quad W_i^{n+1} = W_i^n - \frac{\Delta t^n}{\Delta x} \left(\mathcal{F}_{i+\frac{1}{2}}^n - \mathcal{F}_{i-\frac{1}{2}}^n \right) + \Delta t^n \mathcal{B}_i^n,$$

where $\mathcal{F}_{i+\frac{1}{2}}^n$ and \mathcal{B}_i^n are respectively the numerical flux at the interface and the numerical source term. They are respectively an approximation of

$$\frac{1}{\Delta t^n} \int_{t^n}^{t^{n+1}} F \left(W \left(t, x_{i+\frac{1}{2}} \right) \right) dt.$$

and of

$$\frac{1}{\Delta t^n} \frac{1}{\Delta x} \int_{x_{i-\frac{1}{2}}}^{x_{i+\frac{1}{2}}} \int_{t^n}^{t^{n+1}} B(W(t, x)) dt dx.$$

The initialization of the algorithm can be computed with

$$\forall i \in \mathbb{Z} \quad W_i^0 = \frac{1}{\Delta x} \int_{x_{i-\frac{1}{2}}}^{x_{i+\frac{1}{2}}} W(x, 0) dx.$$

Numerical flux

The issue remains in how to compute the numerical flux at the interfaces and the discrete topography source term. Developing a finite volume method consists in defining, from the values of the variables, a stable and a consistent numerical flux. We focus on the simplest case where the numerical flux can be expressed as a function \mathcal{F} depending on the two neighboring states

$$\mathcal{F}_{i+\frac{1}{2}}^n = \mathcal{F} \left(W_i^n, W_{i+1}^n \right).$$

Approximation of the source term

When the system is homogeneous, i.e the topography is flat there is no need to approximate the source term. For systems with source term, it is not trivial to find a suitable approximation of the source term that allows to preserve

the steady states. Here, we choose to construct Approximate Riemann Solvers "ARS" [54] to approach the solutions and to approximate the source term using the strategy done in [16]. This will be done as follows:

- In Chapter 3, we propose three approximate Riemann solvers for the homogeneous model based on some properties of the exact solution of the Riemann problem computed in [1],
- In Chapter 4, we extend the schemes proposed in Chapter 3 to adapt with the model with the source term.

A general introduction to Approximate Riemann Solvers is given in the following.

Approximate Riemann solvers

When the exact solution of the Riemann problem is known, a general strategy to build a finite volume scheme was proposed by Godunov in [35]. The solution of the Riemann problem for the homogeneous shallow water model with two velocities (SW_2^H) was done in [1]. The Riemann problem is a Cauchy problem with a simple initial condition: two constant states W_L and W_R separated by a discontinuity. The problem reads:

$$\begin{cases} \partial_t W + \partial_x F(W) = 0 \\ W(0, x) = W_0(x) = \begin{cases} W_L & \text{if } x < 0 \\ W_R & \text{if } x \geq 0. \end{cases} \end{cases}$$

Godunov observed that since the cell averages W_i^n are constant in each cell C_i , they define at each cell interface $x_{i+\frac{1}{2}}$ and on the interval $]t^n, t^{n+1}]$ a Riemann problem. By solving this Riemann problem on a small time interval and then by averaging the solution, it is possible to obtain a new piecewise constant approximation. The strategy is used as many times as necessary to reach, step by step, a general final time.

However, computing the exact solution of the Riemann problem for the homogeneous Shallow Water model with two velocities at each interface and for each time step is costly since it implies a fix point algorithm and the exact solution of the Riemann problem for the model with topography (SW_2) was never computed yet. Moreover, it was proven that the Riemann problem for the classical

Shallow Water model with topography can sometimes be ill posed since its solution might not be unique, see [24, 5]. Therefore, there is no point in trying to find the solution of the Riemann problem for (SW_2) which is for sure more complicated than the solution of (SW) because the (SW_2) has an additional unknown.

All that being said, we will consider the ARS solvers [50, 40] as an alternative way to define the numerical fluxes for both models. The main idea of these ARS solvers is to replace the exact solution of the Riemann problem with an approximate solution denoted $\tilde{W}\left(\frac{x}{t}, U_L, U_R\right)$. The considered approximated Riemann solvers are constructed on N discontinuities of speed λ_j separating $(N + 1)$ constant states $\tilde{W}_{j+\frac{1}{2}}(t, x)$:

$$\tilde{W}\left(\frac{x}{t}, U_L, U_R\right) = \begin{cases} W_L = W_{\frac{1}{2}} & \text{if } \frac{x}{t} < \lambda_1, \\ \tilde{W}_{j+\frac{1}{2}} & \text{if } \lambda_j < \frac{x}{t} < \lambda_{j+1} \text{ for } j = 1, \dots, N-1, \\ W_R = W_{N+\frac{1}{2}} & \text{if } \frac{x}{t} > \lambda_N. \end{cases} \quad (1.10)$$

The update at time t^{n+1} is then defined by

$$W_i^{n+1} = \frac{1}{\Delta x} \int_0^{\frac{\Delta x}{2}} \tilde{W}\left(\frac{x}{\Delta t^n}, W_{i-1}^n, W_i^n\right) dx + \frac{1}{\Delta x} \int_{-\frac{\Delta x}{2}}^0 \tilde{W}\left(\frac{x}{\Delta t^n}, W_i^n, W_{i+1}^n\right) dx.$$

In order to ensure the stability and the consistency, the approximate Riemann solver has to satisfy three properties, [17, 40]:

1. The external waves λ_1 and λ_N of the approximated solution have to be faster than the external wave speed of the exact solution.
2. The time step has to satisfy the following CFL condition

$$\left(\max_{j,i} |\lambda_{j,i+\frac{1}{2}}^n|\right) \Delta t^n \leq \frac{\Delta x}{2},$$

where $\lambda_{j,i+\frac{1}{2}}^n = \lambda_j(U_i^n, U_{i+1}^n)$ for $j \in [1, N]$. The CFL condition prevents the waves (issued from different interfaces) from interacting during the time step.

3. The approximate Riemann solver $\tilde{W}\left(\frac{x}{t}, W_L, W_R\right)$ has to be consistent with the shallow water model with two velocities equations. The definition of the consistency differs between the homogeneous model and the model with topography by adding the approximation of the source term. Therefore, the definition of the consistency will be given separately in Chapter 3 and Chapter 4.

Numerical schemes for the homogenous model

Many works were devoted to approximate the solution of hyperbolic systems of conservation laws, see [34, 55, 43]. Here, we elected the Approximate Riemann Solvers for their utility later in preserving the steady state solutions. Our aim in Chapter 3 is to derive finite volume schemes that fulfill the properties (i), (ii) and (iii). To do that, let us briefly describe the numerical strategies we develop in this work:

HLL solver § 3.3

The first scheme we will construct is the well known *HLL* solver [40]. This scheme is based on a one intermediate state approximate Riemann solver, see Figure 1.6. This intermediate state $(h_{HLL}, h_{HLL}\bar{u}_{HLL}, \hat{u}_{HLL})$ can be computed using only the consistency properties. This scheme will be used as a basis for the construction of other solvers. The *HLL* solver is commonly used to approximate the solutions of the shallow water model and fulfills properties (i) and (ii). However the model with two velocities contains an additional wave, which corresponds to the contact wave λ^* in the Riemann problem and the *HLL* is not accurate around this wave. The numerical results show that the *HLL* scheme is diffusive, see Figure 1.9.

Hence, we construct two ARS with 3– waves and two intermediate states. These two solvers are of *HLLC* type (with the C referring to the contact wave) since they take into consideration the contact discontinuity λ^* of the model with two velocities, see [17, 55, 54, 23].

HLL^{*} solver § 3.4

The first 3– waves ARS is named *HLL*^{*} where $(h, h\bar{u})$ are computed using the *HLL* scheme but, to take into consideration the transport of $S = \frac{\hat{u}}{h}$, see (1.4), S is updated using an upwind strategy, see [17]. Only \hat{u} is discontinuous through the internal wave separating the left intermediate state $(h_{HLL}, h_{HLL}\bar{u}_{HLL}, \hat{u}_L^*)$ and the right intermediate state $(h_{HLL}, h_{HLL}\bar{u}_{HLL}, \hat{u}_R^*)$, see Figure 1.7. The *HLL*^{*} solver improves the precision around the contact discontinuity but, we observe numerically that the *HLL*^{*} scheme presented a small spurious deviation on \bar{u} , see the black curves in Figure 1.10. Moreover, it is not able to maintain a stationary isolated contact discontinuity.

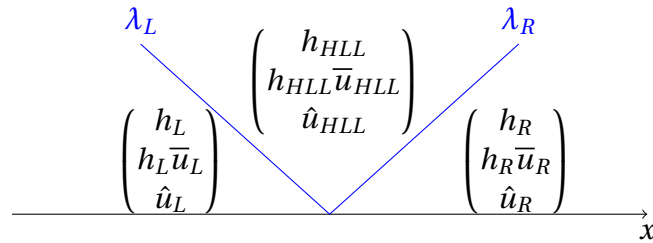


Figure 1.6: The waves representation of the HLL approximate Riemman solver.

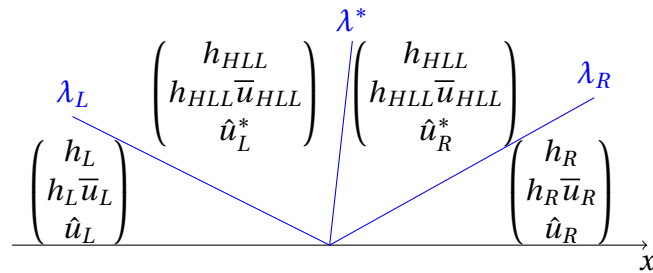


Figure 1.7: The waves representation of the HLL^* approximate Riemman solver.

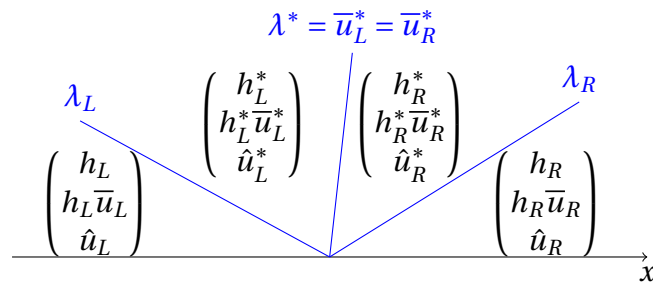


Figure 1.8: The waves representation of the $HLL_{\bar{u}}$ approximate Riemman solver.

1.3. THE 1D SHALLOW WATER MODEL WITH TWO VELOCITIES AND SOURCE TERM 41

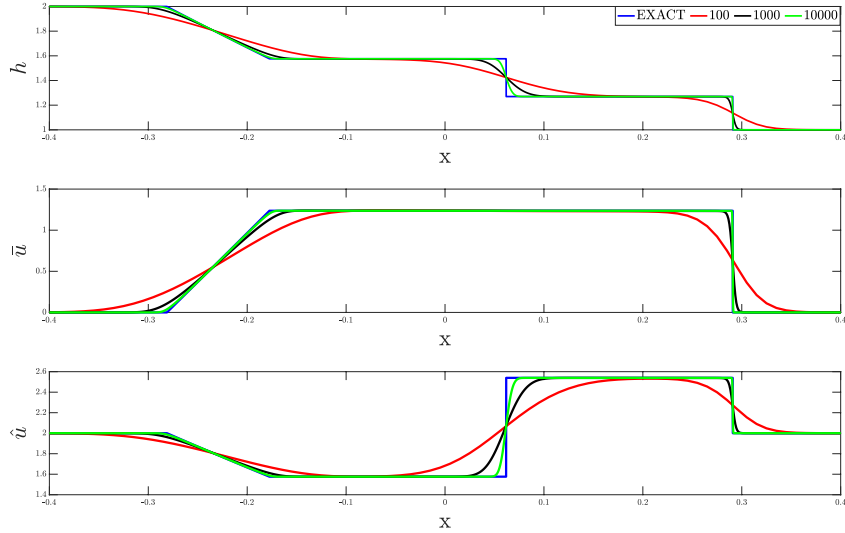


Figure 1.9: The one rarefaction one shock: plots of the variables using the HLL scheme for 100, 1000 and 10000 points.

$HLL_{\bar{u}}$ solver § 3.5

The second 3– waves ARS named $HLL_{\bar{u}}$ is obtained for a more suitable choice of additional relations on the internal wave λ^* to define the two intermediate states, see Figure 1.8. This solver is proved to fulfill properties (i), (ii), (iii) and to maintain a stationary isolated contact discontinuity. It is identical to a solver described in [17, Section 2.4.6.a]. The numerical results shows that the $HLL_{\bar{u}}$ scheme improves the results in comparison with other schemes, see Figure 1.10.

It was difficult to prove if the three schemes ensure the discrete dissipation of energy (1.6) using the definition proposed in [17, §2.2.2]. For this reason, we propose a numerical strategy to study through random Riemann problems, if the schemes verify this property or not, see § 3.7. We were able to conclude that the three schemes verify the discrete dissipation of energy for the classical shallow water model. This was proven for the HLL scheme in [17]. For the model with two velocities (SW_2^H), this property might be true only for the HLL scheme and not for the three waves ARS.

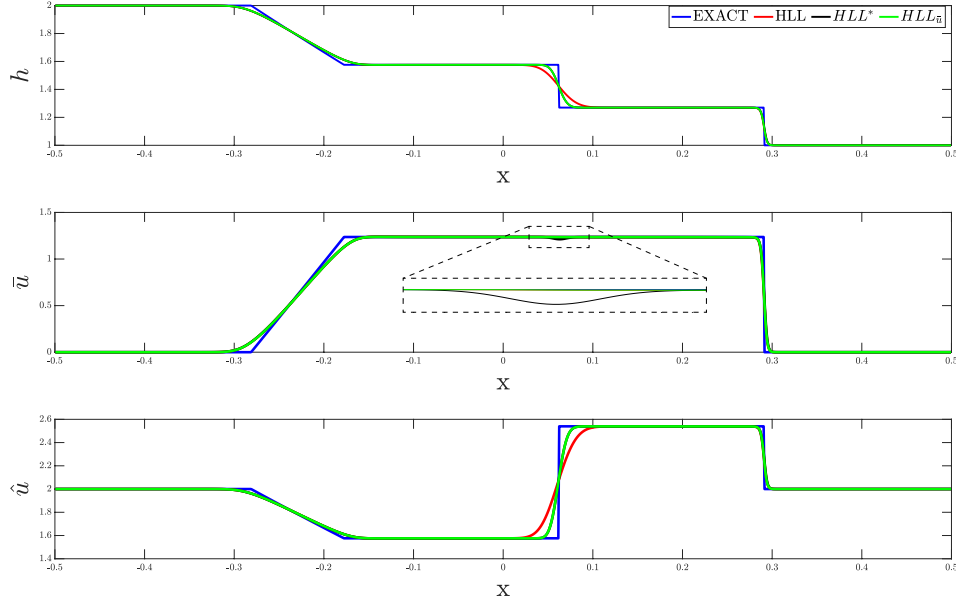


Figure 1.10: One rarefaction one shock case. Plots of the variables using HLL , HLL^* and $HLL_{\bar{u}}$ solvers for 1000 grid cells

Numerical schemes for the model with source term

In Chapter 4, we extend the numerical schemes introduced in Chapter 3 to approach the solutions of the model with topography (SW_2). In addition to the three eigenvalues (3.2), the presence of the new stationary variable Z creates a stationary wave $\lambda_0 = 0$ which should be considered in the construction of the numerical schemes if we want them to be accurate around the stationary states. Thus, our aim in this chapter is to derive finite volume Approximate Riemann Solvers that still verify the properties (i), (ii), (iii) but also the well-balanced property (iv). For all W_L and W_R defining a regular steady state, the well balanced approximate Riemann solver \tilde{W} should verify

$$\tilde{W}\left(\frac{x}{t}, W_L, W_R\right) = \begin{cases} W_L & \text{if } \frac{x}{t} < 0, \\ W_R & \text{if } \frac{x}{t} > 0. \end{cases}$$

Well-balanced property

In the last twenty years, many works were devoted to the derivation of well-balanced schemes in order to preserve the steady state solutions of hyperbolic models. The definition and the relevance of the well-balanced method was initially introduced for the lake at rest ($M = 0$ and $S = 0$) by Bermudez and Vasquez in [13] where they define a compatible approximation of flux terms and source terms. We refer also to [17] where the author presents a detailed literature review listing different numerical schemes. We mention in particular the very well known hydrostatic reconstruction in [7] that consists on deriving a well-balanced scheme from any numerical flux defined for the homogeneous system. This pioneer work was an easy technique to preserve the lake at rest but was not enough to exactly capture all the moving steady states, see [27]. To adapt these schemes for the moving steady states ($M \neq 0$ and $S = 0$), an extension of the hydrostatic reconstruction was proposed in [22] which unfortunately doesn't preserve the positivity of the water heights. Another correction was proposed in [18] for subsonic steady states that preserves the positivity of the water heights.

To deal with all the smooth steady states, a numerical technique based on ARS was proposed in [14, 15] in which the intermediate states are obtained by solving a Bernoulli-type equation. But, in order to introduce the source term within the approximate Riemann solver, this approach needs to solve a non linear equation at each interface, which is costly. A correction was done in [45] by proposing a linearization of this non linear equation. This new strategy exactly captures all the steady solutions but presents some difficulties in the discretization of the topography source term. An alternative approximation of the source term was proposed in [16].

In this thesis, we study three ARS to approximate the solution for $S \neq 0$ which, up to our knowledge, was never done before. These schemes are extensions of the solvers introduced for the homogeneous model and adapted to take into consideration the presence of the topography source term. We proceed by

1. approximating first the source term inspired by the strategy done in [16] for the Shallow water equations (§ 4.4)
2. introducing a scheme named HLL_0 . This solver is an extension of HLL scheme introduced in § 3.3 for which we add the stationary wave λ_0 in order to preserve the steady states. The evolution of the shear S is not

affected by the presence of the topography hence, this scheme is similar to the Riemann solver used to approximate the shallow water equations with topography in [16]. Moreover, the scheme verifies the properties (i) and (iv). However, this scheme doesn't take into account the transport of S , see (§ 4.5)

3. constructing a second numerical scheme named HLL_0^* as done in the HLL^* scheme for the homogeneous model. This scheme can also be seen as a 4-waves ARS where the water height and the mean velocity are constant through the transport wave. A similar strategy was used to approximate the solution of the Ripa model with source term in [29], see (§ 4.6).
4. introducing a scheme named $HLL_{0,\bar{u}}$. This scheme is a 4-waves ARS and can be seen as an extension of the $HLL_{\bar{u}}$ scheme (§ 3.5) in which we consider the stationary wave λ_0 or as an extension of the HLL_0 scheme (§ 4.5) in which we take into consideration the transport on S , see (§ 4.7)

We prove that the three schemes are well-balanced and ensure the positivity of the water heights. We also compare the behavior of the schemes with other strategies proposed in [10, 45] to ensure the positivity of the water heights, see § 4.8.

Numerical stability of the stationary solutions

The behavior of the well-balanced schemes is mostly tested on the steady states solutions with subcritical inlet boundary conditions presented in [37, 28], whereas, few numerical simulations are presented to test the behavior of the numerical schemes on steady solutions with supercritical inlet boundary conditions as well as the numerical stability of such solutions. In fact, a formal analysis was done by physicists in [11] to prove that the left shocks are linearly not stable. In this work, we test numerically the stability of the moving steady state solutions defined in Chapter 2 and the behavior of the numerical schemes on these solutions. Through the numerical results we observe that

1. for subcritical inlet boundary conditions, when the initial conditions are chosen to be the lake at rest, the schemes reach the steady states at machine accuracy except for the $HLL_{0,\bar{u}}$ scheme for the solution with a transition from subcritical to supercritical regimes where we observe a small non-entropic stationary shock on the top of the bump, see Figure 1.11.

1.3. THE 1D SHALLOW WATER MODEL WITH TWO VELOCITIES AND SOURCE TERM 45

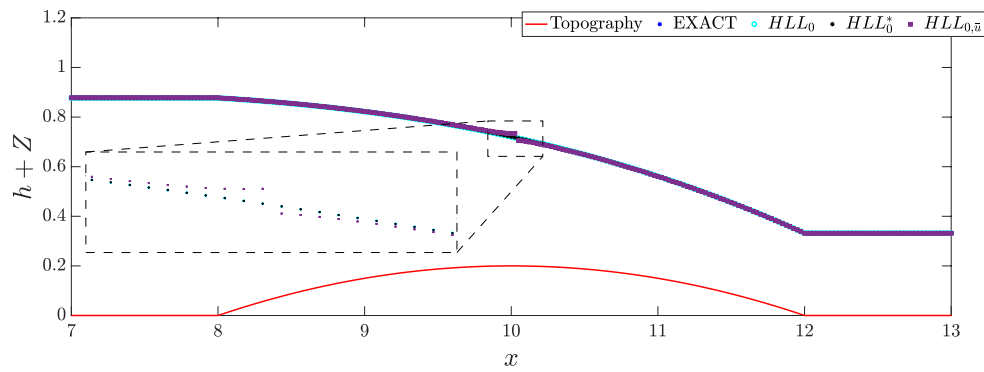


Figure 1.11: Transcritical solution without shock

2. for supercritical inlet boundary conditions, when the initial conditions are chosen to be the exact and regular solution, the schemes are well-balanced.
3. the steady state solutions with one shock at the left are not stable, see Figure 1.12.

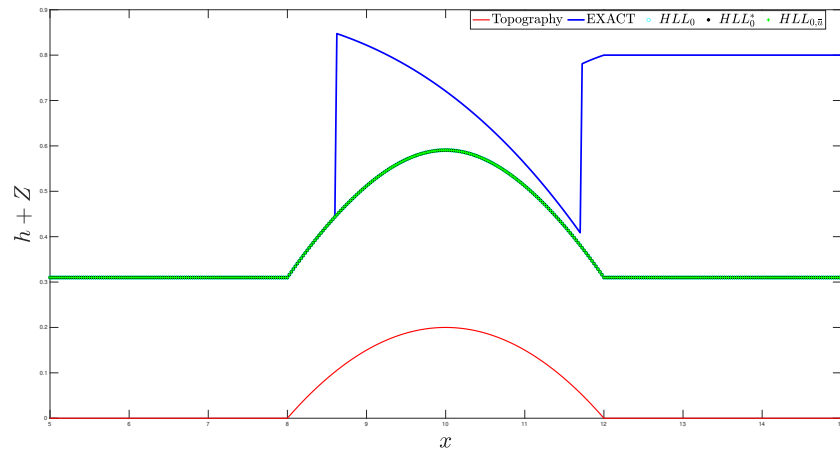


Figure 1.12: The unstable two shocks solution: the numerical solutions converge to a total different regular steady state solution.

Chapter 2

Stationary solutions of the 1D SW_2 model

2.1 Brief description of the model

In previous works, two shallow-water type models were introduced: the shear shallow water model (SSW) presented in [47] and the shallow water model with two velocities ($2DSW_2$) presented in [1]. These two models are equivalent in one dimension and for smooth solutions. This chapter is dedicated to the study of the steady state solutions of the 1D shallow water model with two velocities which reads

$$\begin{cases} \partial_t h + \partial_x(h\bar{u}) & = 0, \\ \partial_t(h\bar{u}) + \partial_x(h(\bar{u}^2 + \hat{u}^2) + \frac{g}{2}h^2) & = -gh\partial_x Z, \\ \partial_t \hat{u} + \partial_x(\bar{u}\hat{u}) & = 0. \end{cases} \quad (SW_2)$$

with $g > 0$ the acceleration of gravity and Z the topography. The unknowns of the system are $h(t, x) \in \mathbb{R}_+$ the water depth of the flow, $\bar{u}(t, x) \in \mathbb{R}$ the vertical-averaged of the horizontal velocity and $\hat{u}(t, x) \in \mathbb{R}$ the signed standard deviation of the horizontal velocity. More precisely, the model (SW_2) is an approximation of the free surface Euler equation assuming the pressure is hydrostatic and by considering a vertical piecewise constant discretization of the horizontal velocity. We refer to [1, 9, 47] for more precision on the modeling. The (SW_2) can be written under the following form

$$\partial_t U + \partial_x F(U) = B(U, Z),$$

where

$$U = \begin{pmatrix} h \\ h\bar{u} \\ \hat{u} \end{pmatrix}, \quad F(U) = \begin{pmatrix} h\bar{u} \\ h(\bar{u}^2 + \hat{u}^2) + \frac{g}{2}h^2 \\ \bar{u}\hat{u} \end{pmatrix} \quad \text{and} \quad B(U, Z) = \begin{pmatrix} 0 \\ -gh\partial_x Z \\ 0 \end{pmatrix}.$$

The (SW₂) system has three eigenvalues:

$$\lambda_1^E = \bar{u} - \sqrt{gh + 3\hat{u}^2}, \quad \lambda_2^E = \bar{u} \quad \text{and} \quad \lambda_3^E = \bar{u} + \sqrt{gh + 3\hat{u}^2}. \quad (2.1)$$

The following defines the Froude number of (SW₂).

Definition 1. *The Froude number corresponds to the ratio between the material celerity and the celerity of the potential waves. In the case of (SW₂), it reads*

$$F_r := \frac{|\bar{u}|}{\sqrt{gh + 3\hat{u}^2}}. \quad (2.2)$$

We distinguish three flow regimes according to the value of the Froude number, if $F_r < 1$, then the flow is called subcritical, if $F_r = 1$ then the flow is critical and if $F_r > 1$ it is called supercritical.

For simplicity, we consider a particular shape of the topography.

Hypothesis 1. *We assume that there exists a point $x_0 \in I = [x_L, x_R]$ such that Z is a C^1 function, increasing on $[x_L, x_0]$ and decreasing on $[x_0, x_R]$.*

Solutions of (SW₂) may develop discontinuities in finite time. The discontinuous solutions are weak solutions and they are characterized by the Rankine Hugoniot relations

$$\sigma(U^+ - U^-) = F(U^+) - F(U^-), \quad (2.3)$$

where σ is the velocity of the discontinuity and $U^-(t, x) = \lim_{\epsilon \rightarrow 0^-} U(t, x + \epsilon)$ and $U^+(t, x) = \lim_{\epsilon \rightarrow 0^+} U(t, x + \epsilon)$ are the solution's trace. The weak solutions are not always admissible thus, we consider that they have to satisfy also the following entropy inequality condition

$$\partial_t E + \partial_x \left(\left(g(h + Z) + \frac{\bar{u}^2 + 3\hat{u}^2}{2} \right) h\bar{u} \right) \leq 0 \quad (2.4)$$

with the total energy, acting as the mathematical entropy reads

$$E = gh \left(Z + \frac{h}{2} \right) + \frac{h}{2} (\bar{u}^2 + \hat{u}^2).$$

2.2. MOVING STEADY STATE SOLUTION: REGULAR PART AND STATIONARY SHOCK 49

More precisely, for any continuous solution equation (2.4) is an equality whereas across shocks the energy is decreasing.

In this work, we are interested in steady state solutions of (SW₂), in particular in their existence and uniqueness depending on the imposed boundary conditions. Indeed, a precise definition of steady solutions is given in the following.

Definition 2. A steady state solution of (SW₂) is a triplet of piecewise C^1 regular functions $(h, h\bar{u}, \hat{u})$. On open intervals where the functions are C^1 regular they verify the following system of ordinary differential equations

$$\begin{cases} \partial_x(h\bar{u}) & = 0, \\ \partial_x(h(\bar{u}^2 + \hat{u}^2) + \frac{g}{2}h^2) & = -gh\partial_x Z, \\ \partial_x(\bar{u}\hat{u}) & = 0. \end{cases} \quad (\text{SSW2})$$

and at a point of discontinuity, the Rankine-Hugoniot jump conditions (2.3) with $\sigma = 0$ hold:

$$\begin{cases} [h\bar{u}] & = 0 \\ [h(\bar{u}^2 + \hat{u}^2) + \frac{g}{2}h^2] & = 0 \\ [\bar{u}\hat{u}] & = 0, \end{cases} \quad (2.5)$$

as well as the dissipation of entropy

$$\left[\left(g(h + Z) + \frac{\bar{u}^2 + 3\hat{u}^2}{2} \right) h\bar{u} \right] \leq 0, \quad (2.6)$$

where $[X] = X^+ - X^-$ represents the jump of the discontinuity separating the solution's left trace X^- and the solution's right trace X^+ .

2.2 Moving steady state solution: regular part and stationary shock

We can remark from (SSW2) and (2.5) that both quantities $h\bar{u}$ and $\bar{u}\hat{u}$ are constant in the whole domain.

Proposition 1. For steady state solutions, there exists $M \in \mathbb{R}$ such that

$$\forall x \in I, \quad h(x)\bar{u}(x) = M.$$

If $M \neq 0$, there exists $S \in \mathbb{R}$ such that

$$\forall x \in I, \quad \frac{\hat{u}(x)}{h(x)} = S.$$

Proof. The first equation of (SSW2) shows that $h\bar{u}$ is constant in the whole domain where the solution is regular. In addition to that, the first equation of (2.5) shows that $h\bar{u}$ is constant across the discontinuity. Hence, there exists $M \in \mathbb{R}$ such that for any $x \in I$ we have $h(x)\bar{u}(x) = M$. If $M \neq 0$, then $h > 0$ and $\bar{u} \neq 0$ hence, the third equation of (SSW2) and (2.5) show that $\bar{u}\hat{u}$ is constant in the whole domain. Therefore, there exists $S \in \mathbb{R}$ such that for any $x \in I$ we have $\frac{\hat{u}(x)}{h(x)} = S$. \square

A different quantity is preserved in the second equation of (SSW2) for C^1 regular solutions and in the second equation of (2.5) at shocks. In this section, we characterize these quantities.

Definition 3. For $M \neq 0$ and $S \in \mathbb{R}$, the strictly positive and piecewise C^1 regular function h is a moving steady state if

- on intervals where h is regular, the function $h + Z + \frac{1}{2g} \left(\frac{M^2}{h^2} + 3h^2 S^2 \right)$ is constant,
- at a point where h is discontinuous, the following relations hold

$$\left[\frac{M^2}{h} + h^3 S^2 + \frac{g}{2} h^2 \right] = 0 \quad (2.7)$$

and

$$\left[\left(g(h + Z) + \frac{M^2}{2h^2} + \frac{3S^2}{2} h^2 \right) M \right] \leq 0. \quad (2.8)$$

Proposition 2. Let $M \neq 0$ and $S \in \mathbb{R}$. Let h be a moving steady state as defined in Definition 3. Then (h, M, hS) is a steady state solution of (SW₂) as defined in Definition 2.

Proof. Introducing the constants $M = h\bar{u}$ and $S = \frac{\hat{u}}{h}$ then for $x \mapsto h(x)$ a piecewise C^1 steady state solution of (SW₂), the second equation of (SSW2) can be written as

$$\partial_x \left(\frac{M^2}{h} + S^2 h^3 + \frac{g}{2} h^2 \right) + gh \partial_x Z = 0$$

which for $h \in C^1$ strictly positive, $M \in \mathbb{R}^*$ and $S \in \mathbb{R}$ is equivalent to

$$-\frac{M^2}{h^2} \partial_x h + 3S^2 h^2 \partial_x h + gh \partial_x h + gh \partial_x Z = 0.$$

2.2. MOVING STEADY STATE SOLUTION: REGULAR PART AND STATIONARY SHOCKS 51

Then, dividing by gh we have

$$-\frac{M^2}{gh^3}\partial_x h + \frac{3S^2}{g}h\partial_x h + \partial_x(h+Z) = 0.$$

and finally

$$\partial_x \left(\frac{M^2}{2gh^2} + \frac{3}{2g}S^2h^2 + (h+Z) \right) = 0.$$

As a consequence, the quantity $\frac{M^2}{2h^2} + \frac{3}{2}S^2h^2 + g(h+Z)$ is constant in the domain where h is C^1 .

Using $M = h\bar{u} \neq 0$ and $S = \frac{\dot{u}}{h}$ in the Rankine Hugoniot equations (2.5) we get that the second equation of (2.5) can be written as

$$\left[h \left(\frac{M^2}{h^2} + h^2 S^2 \right) + \frac{g}{2} h^2 \right] = 0,$$

which is nothing but the relation (2.7). Similarly, replacing $h\bar{u} \neq 0$ and $\frac{\dot{u}}{h}$ respectively by M and S in (2.6) we get the dissipation of entropy at a discontinuity (2.8). \square

From now on, we fix $M > 0$ and $S \in \mathbb{R}$.

2.2.1 Regular moving steady states

In the current section we focus on the description of the C^1 -regular steady state solutions of (SW_2) as seen in Definition 3 and Proposition 2. In order to characterize the regular moving steady states, we start by introducing the following function.

Definition 4. For a given $M \in \mathbb{R}_+^*$, $S \in \mathbb{R}$, we define the function Φ as

$$\begin{aligned} \Phi : \mathbb{R}_+^* \times \mathbb{R} &\rightarrow \mathbb{R}_+^* \\ (h, Z) &\mapsto h + Z + \frac{1}{2g} \left(\frac{M^2}{h^2} + 3h^2 S^2 \right) \end{aligned}$$

The following proposition is introduced to give more details on the smooth part of the solution.

Proposition 3. Consider the function Φ defined in Definition 4, then the function $x \mapsto h(x)$ is a C^1 steady state solution of (SW₂) if and only if there exists $K \in \mathbb{R}$ such that

$$\forall x \in I, \Phi(h, Z) = K \quad (2.9)$$

which is nothing more than the Bernoulli's principle in our context.

Proof. Assume that the function $x \mapsto h(x)$ is a C^1 steady state solution of (SW₂). As proven in Proposition 2, for $M = h\bar{u}$ and $S = \frac{\hat{u}}{h}$ we have

$$\partial_x \left(\frac{M^2}{2gh^2} + \frac{3}{2g} S^2 h^2 + (h + Z) \right) = 0,$$

which means that the quantity $\frac{M^2}{2h^2} + \frac{3}{2} S^2 h^2 + g(h + Z)$ is constant in the whole domain. Therefore, there exists $K \in \mathbb{R}$ and the steady state solutions verify (2.9). □

In the literature, the constant K is sometimes called the hydraulic head or the energy head [37].

Remark 1. We remark that in the case of the classical shallow water equations where $S = 0$, we recover the classical function characterizing the smooth equilibrium of the shallow water equations

$$\Phi^0(h, Z) := h + Z + \frac{M^2}{2gh^2},$$

see [44].

We start by studying the variations of the function $h \mapsto \Phi(h, Z)$.

Proposition 4. Given $M \in \mathbb{R}_+^*$, $S \in \mathbb{R}$ and for any $Z \in \mathbb{R}$, the function $h \mapsto \Phi(h, Z)$ is strictly convex and tends to $+\infty$ when h tends to 0 and h tends to $+\infty$. It reaches its unique minimum at a point h_c which is independent of the bathymetry Z . In the case of moving steady states, the Froude number (2.2) rewrites

$$Fr = \frac{h_c}{h} \sqrt{\frac{gh_c + 3h_c^2 S^2}{gh + 3h^2 S^2}}. \quad (2.10)$$

The flow is supercritical if $h < h_c$, critical if $h = h_c$ and subcritical if $h > h_c$.

2.2. MOVING STEADY STATE SOLUTION: REGULAR PART AND STATIONARY SHOCK53

Proof. We start by differentiating Φ with respect to h

$$\partial_h \Phi(h, Z) = 1 + \frac{1}{2g} \left(\frac{-2M^2}{h^3} + 6hS^2 \right),$$

then, differentiating it again with respect to h we get

$$\partial_h^2 \Phi(h, Z) = \frac{3}{g} \left(\frac{M^2}{h^4} + S^2 \right) > 0.$$

We can conclude that $\Phi(h, Z)$ is strictly convex with respect to h and admits the following limits

$$\lim_{h \rightarrow 0^+} \Phi(h, Z) = \lim_{h \rightarrow +\infty} \Phi(h, Z) = +\infty.$$

Hence, Φ reaches its unique minimum in \mathbb{R}_+^* at the point $h_c > 0$ such that

$$P(h) = 3S^2 h^4 + g h^3 - M^2 = 0, \quad (2.11)$$

which is clearly independent of Z . The Froude number defined in (2.2) reads

$$F_r = \frac{M}{h \sqrt{gh + 3S^2 h^2}}. \quad (2.12)$$

By definition of h_c ,

$$M^2 = 3S^2 h_c^4 + g h_c^3,$$

and therefore for $M \in \mathbb{R}_+^*$ we have $M = \sqrt{3S^2 h_c^4 + g h_c^3}$. Replacing it in (2.12) we get the relation (2.10). \square

To define a C^1 solution on the interval I , we need to find for any $x \in I$ a solution $h(x)$ of the equation

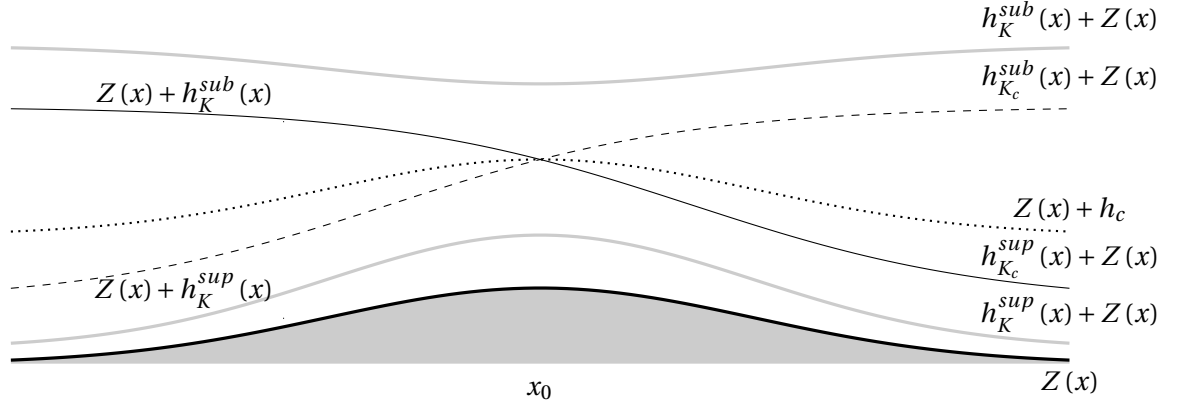
$$\Phi(h(x), Z(x)) = K.$$

This is not possible for any values of K . We start by introducing a critical hydraulic head K_c .

Definition 5. Given $M \in \mathbb{R}_+^*$, $S \in \mathbb{R}$ and the topography Z verifying Hypothesis 1, we define the hydraulic head K_c corresponding to the critical water depth at the maximum of the topography Z_{max} , i.e

$$K_c := \Phi(h_c, Z_{max}).$$

Next, we consider the first case where $K \geq K_c$ and we have the following result.

Figure 2.1: Regular moving steady states for $K \geq K_c$

Proposition 5. *Let Z verifies Hypothesis 1.*

- If $K > K_c$ then, for all $x \in I$ the equation $\Phi(h, Z(x)) = K$ admits two distinct solutions, a subcritical solution $h_K^{sub}(x)$ and a supercritical solution $h_K^{sup}(x)$ verifying

$$h_K^{sup}(x) < h_c < h_K^{sub}(x). \quad (2.13)$$

- If $K = K_c$ then, for all $x \in [x_L, x_0[\cup]x_0, x_R]$ the equation $\Phi(h, Z(x)) = K$ admits two distinct solutions, a subcritical solution $h_{K_c}^{sub}(x)$ and a supercritical solution $h_{K_c}^{sup}(x)$ verifying (2.13).
At $x = x_0$, the equation $\Phi(h, Z_{max}) = K_c$ admits h_c as a unique solution and then $h_{K_c}^{sub}(x_0) = h_{K_c}^{sup}(x_0) = h_c$.

The functions $x \mapsto h_K^{sub}(x)$ and $x \mapsto h_K^{sup}(x)$ are C^1 regular on $[x_L, x_R]$, except if $K = K_c$ where they are only continuous at the point $x = x_0$. The functions $x \mapsto (h_K^{sub}(x), M, Sh_K^{sub}(x))$ and $x \mapsto (h_K^{sup}(x), M, Sh_K^{sup}(x))$ are solutions of (SSW2) on the interval I .

These functions are plotted in Figure 2.1 and their construction is illustrated in Figure 2.2.

Proof. We start the proof by the case $K > K_c$. For $x \in I$, the function $h \mapsto \Phi(h, Z(x))$ is strictly monotone on $]0, h_c]$ and $[h_c, +\infty[$. Moreover, we have

$$\Phi(h_c, Z(x)) = \Phi(h_c, Z_{max}) + Z(x) - Z_{max} \leq K_c < K$$

2.2. MOVING STEADY STATE SOLUTION: REGULAR PART AND STATIONARY SHOCK55

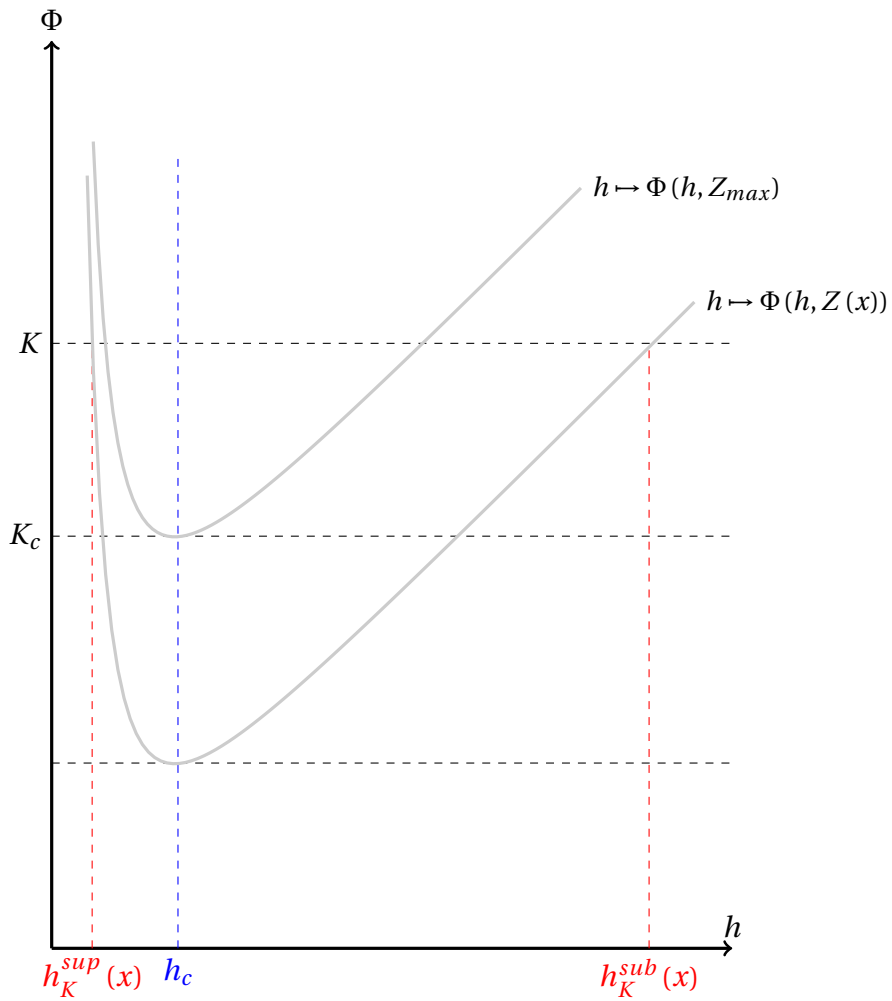


Figure 2.2: Construction of $h_K^{sub}(x)$ and $h_K^{sup}(x)$, solutions of $\Phi(h, Z(x)) = K$ when $K \geq K_c$.

and $\Phi(h, Z(x)) \rightarrow +\infty$ as $h \rightarrow 0^+$ and $h \rightarrow +\infty$. This allows us to conclude using the intermediate value theorem and the monotonicity of $h \mapsto \Phi(h, Z(x))$ on each interval that there exists a unique $h_K^{sup}(x) \in]0, h_c[$ such that $\Phi(h_K^{sup}(x), Z(x)) = K$ and there exists a unique $h_K^{sub}(x) \in]h_c, +\infty[$ such that $\Phi(h_K^{sub}(x), Z(x)) = K$. To study the regularity of these solutions, we introduce the C^1 function F as follows

$$\begin{aligned} F : \mathbb{R}_+^* \times I &\rightarrow \mathbb{R} \\ (h, x) &\mapsto \Phi(h, Z(x)) - K. \end{aligned}$$

For all $x \in I$, we have

$$F(h_K^{sub}(x), x) = \Phi(h_K^{sub}(x), Z(x)) - K = 0.$$

Differentiating F with respect to h , we get

$$\begin{aligned} \frac{\partial F}{\partial h}(h, x) &= \frac{\partial \Phi}{\partial h}(h, Z(x)) \\ &= 1 + \frac{1}{2g} \left(\frac{-2M^2}{h^3} + 6hS^2 \right), \end{aligned}$$

which is null if and only if $h = h_c$. We proved previously that when $K > K_c$, $h_K^{sub}(x) \neq h_c$ therefore, we can conclude using the implicit functions theorem that the function

$$\begin{aligned} h_K^{sub} : I &\rightarrow \mathbb{R}_+^* \\ x &\mapsto h_K^{sub}(x), \end{aligned}$$

is C^1 regular on I . The same result applies for $h_K^{sup}(x)$.

Now, we consider that $K = K_c$. For $x = x_0$, h_c is the unique solution of $\Phi(h, Z_{max}) = K$ and for $x \neq x_0$, $\Phi(h_c, Z(x)) < K$ and we obtain as before that there exists a unique $h_K^{sup}(x) \in]0, h_c[$ and a unique $h_K^{sub}(x) \in]h_c, +\infty[$ verifying $\Phi(h, Z(x)) = K$.

Concerning the regularity of $h_{K_c}^{sub}$, at the top of the topography we have $h_{K_c}^{sub}(x_0) = h_c$ hence, $\frac{\partial F}{\partial h}(h_c, x_0) = 0$ and the implicit functions theorem can't be applied in this specific case where $K = K_c$ and $x = x_0$. At this point, the functions h_K^{sub} and h_K^{sup} are only continuous and not C^1 regular.

□

We have studied the solution of $\Phi(h, Z(x)) = K$ for $K \geq K_c$. Now, we study its solutions for $K < K_c$. We have

$$\Phi(h, Z_{max}) - K > \Phi(h, Z_{max}) - K_c \geq 0. \quad (2.14)$$

and the equation $\Phi(h, Z(x)) = K$ doesn't have a solution in the vicinity of x_0 , but it is possible to define the solution on a smaller interval.

2.2. MOVING STEADY STATE SOLUTION: REGULAR PART AND STATIONARY SHOCK57

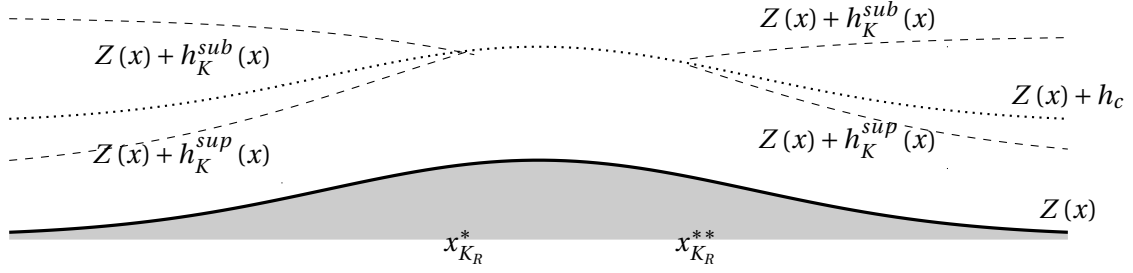


Figure 2.3: Regular moving steady states for $\bar{K}_L < K < K_c$

Proposition 6. *Let Z verify Hypothesis 1 and $K < K_c$. We introduce the following topography height*

$$Z_K^{lim} = K - \left(h_c + \frac{1}{2g} \left(\frac{M^2}{h_c^2} + 3h_c^2 S^2 \right) \right).$$

In addition to that, we define the hydraulic heads

$$\bar{K}_L := \Phi(h_c, Z_L), \quad \text{and} \quad \bar{K}_R := \Phi(h_c, Z_R).$$

We have the following statements:

- *If $\bar{K}_L < K < K_c$ then, the equation $Z(x) = Z_K^{lim}$ admits a unique solution on $[x_L, x_0[$ named x_K^* . For all $x \in [x_L, x_K^*[$ the equation $\Phi(h, Z(x)) = K$ admits two C^1 distinct solutions, a subcritical solution $h_K^{sub}(x)$ and a supercritical solution $h_K^{sup}(x)$. If $x = x_K^*$, the equation $\Phi(h, Z_K^{lim}) = K$ admits h_c as a unique solution and we denote by $h_K^{sub}(x_K^*) = h_K^{sup}(x_K^*) = h_c$.*
- *If $\bar{K}_R < K < K_c$ then, the equation $Z(x) = Z_K^{lim}$ admits a unique solution on $]x_0, x_R]$ named x_K^{**} . For all $x \in]x_K^{**}, x_R]$ the equation $\Phi(h, Z(x)) = K$ admits two C^1 distinct solutions, a subcritical solution $h_K^{sub}(x)$ and a supercritical solution $h_K^{sup}(x)$. If $x = x_K^{**}$, the equation $\Phi(h, Z_K^{lim}) = K$ admits h_c as a unique solution and we denote by $h_K^{sub}(x_K^{**}) = h_K^{sup}(x_K^{**}) = h_c$.*
- *If $K < \bar{K}_L$ and $K < \bar{K}_R$ then, there is no solution to the equation $\Phi(h, Z(x)) = K$.*

The functions h_K^{sub} and h_K^{sup} are continuous on their domain of definition and C^1 regular except on x_K^ and x_K^{**} . These solutions verify (2.13) and they are not*

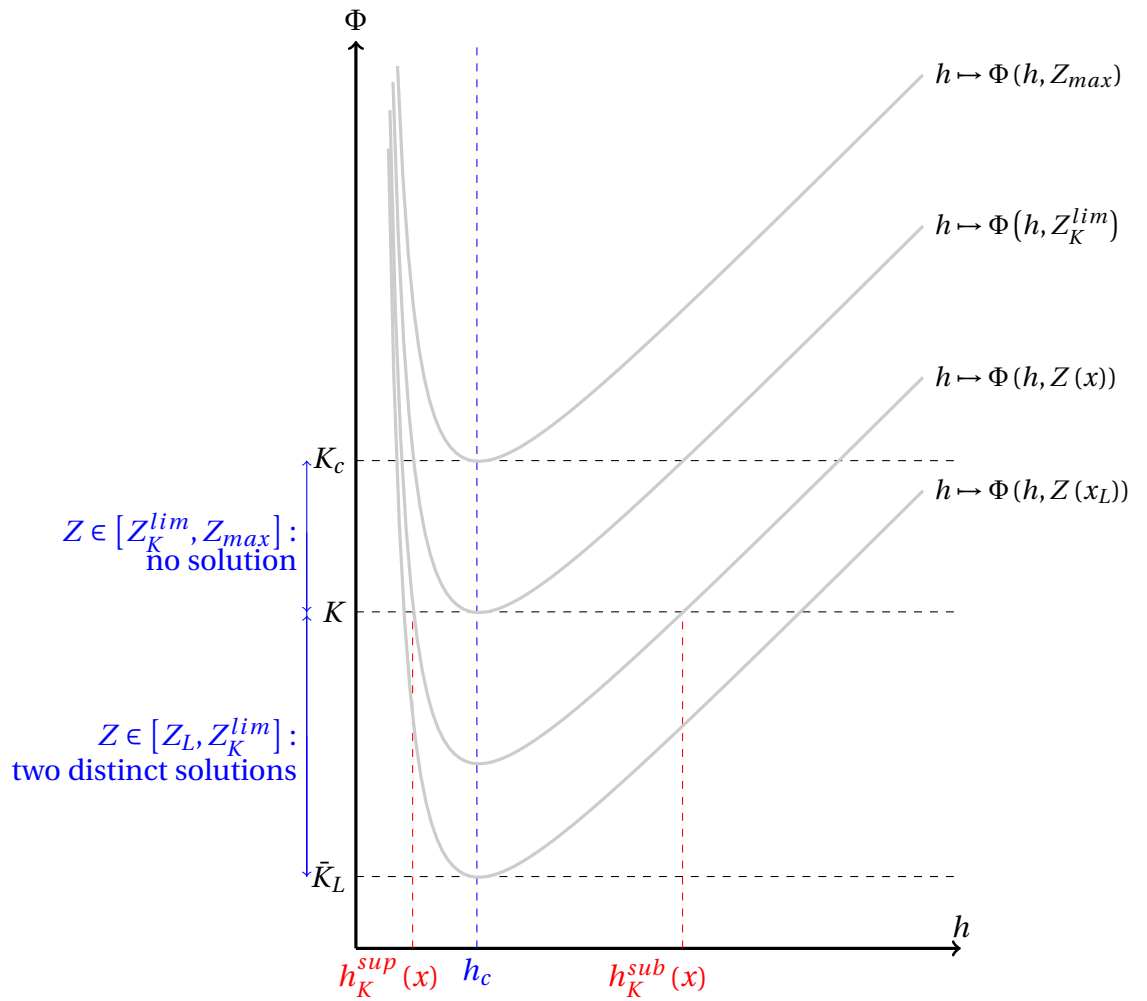


Figure 2.4: Construction of $h_K^{sub}(x)$ and $h_K^{sup}(x)$, solutions of $\Phi(h, Z(x)) = K$ when $\bar{K}_L < K < K_c$.

2.2. MOVING STEADY STATE SOLUTION: REGULAR PART AND STATIONARY SHOCK59

defined for $x \in]x_K^*, x_K^{**}[$. In the corresponding domain of definition, the functions $x \mapsto (h_K^{sub}(x), M, Sh_K^{sub}(x))$ and $x \mapsto (h_K^{sup}(x), M, Sh_K^{sup}(x))$ are "regular" solutions of (SSW2).

The functions are plotted in Figure 2.3 and their construction is explained in Figure 2.4.

Proof. For $\bar{K}_L < K < K_c$, let us prove the existence of x_K^* solution of $Z(x) = Z_K^{lim}$. As $\bar{K}_L < K < K_c$, we have

$$\bar{K}_L - \left(h_c + \frac{1}{2g} \left(\frac{M^2}{h_c^2} + 3h_c^2 S^2 \right) \right) < K - \left(h_c + \frac{1}{2g} \left(\frac{M^2}{h_c^2} + 3h_c^2 S^2 \right) \right) < K_c - \left(h_c + \frac{1}{2g} \left(\frac{M^2}{h_c^2} + 3h_c^2 S^2 \right) \right)$$

which, by definition of \bar{K}_L , Z_K^{lim} and K_c leads to

$$Z(x_L) < Z_K^{lim} < Z_{max}.$$

This allows us to conclude using the intermediate value theorem and the monotonicity of Z on $[x_L, x_0]$ that there exists a unique $x_K^* \in [x_L, x_0[$ such that $Z(x_K^*) = Z_K^{lim}$. Moreover, $\Phi(h, Z(x_K^*)) = K$ admits a unique solution h_c .

Now, we prove that $\Phi(h, Z(x)) = K$ admits two distinct solutions for $x \in [x_L, x_K^*]$. For $Z_L \leq Z(x) < Z(x_K^*)$, we have

$$\Phi(h_c, Z(x)) = \Phi(h_c, Z(x_K^*)) + Z(x) - Z(x_K^*) < K.$$

Thanks to the monotonicity of $h \mapsto \Phi(h, Z)$ on $]0, h_c[$ and on $[h_c, +\infty[$, the properties mentioned in Proposition 4 and the intermediate value theorem, we can conclude that there exists a unique $h_K^{sup}(x) \in]0, h_c[$ and a unique $h_K^{sub}(x) \in]h_c, +\infty[$ such that $\Phi(h_K^{sub}(x), Z(x)) = K$ and $\Phi(h_K^{sup}(x), Z(x)) = K$. The C^1 -regularity of h_K^{sup} and h_K^{sub} away from the point x_K^* where $\partial_h \Phi(h_K^{sub}(x_K^*), Z(x_K^*)) = 0$ follows from the implicit function theorem, see the proof of Proposition 5.

Finally, we treat the case where $K < \bar{K}_L$. In this case, for all $x \in I$

$$\Phi(h, Z(x)) - K > \Phi(h, Z(x)) - \bar{K}_L > \Phi(h, Z_L) - \bar{K}_L \geq 0,$$

therefore, there is no solution to the equation $\Phi(h, Z(x)) = K$ in $[x_L, x_0]$. This results also holds when $K < \bar{K}_R$. The same strategy applies on the right of the domain in the case $\bar{K}_R < K < K_c$. \square

2.2.2 Stationary shocks and the entropy condition

We have detailed earlier in § 2.2.1 the C^1 regular solutions of (SW₂). In the following, we describe the discontinuous part of the solution that verifies the Rankine-Hugoniot jump conditions (2.7) and the dissipation of entropy (2.8). To do so, we start by introducing the following definition.

Definition 6. For a given $M \in \mathbb{R}_+^*$, $S \in \mathbb{R}$, we define the function $F^{h\bar{u}}$ representing the momentum flux as

$$\begin{aligned} F^{h\bar{u}} : \mathbb{R}_+^* &\rightarrow \mathbb{R}_+^* \\ h &\mapsto \frac{M^2}{h} + h^3 S^2 + \frac{g}{2} h^2. \end{aligned}$$

A property of the function $F^{h\bar{u}}$ characterizing the Rankine Hugoniot relations (2.7) is given in the following proposition.

Proposition 7. Let $M \in \mathbb{R}_+^*$ and $S \in \mathbb{R}$ be fixed. For any $h \neq h_c$, there exists a unique $\psi(h) > 0$, $\psi(h) \neq h$ such that

$$F^{h\bar{u}}(h) = F^{h\bar{u}}(\psi(h)). \quad (2.15)$$

Moreover h and $\psi(h)$ are in different regimes:

$$(h - h_c)(\psi(h) - h_c) < 0.$$

We set $\psi(h_c) = h_c$. Then, the function

$$\begin{aligned} \psi : \mathbb{R}_+^* &\rightarrow \mathbb{R}_+^* \\ h &\mapsto \psi(h), \end{aligned} \quad (2.16)$$

is strictly decreasing, continuous on \mathbb{R}_+^* and C^1 on $]0, h_c[\cup]h_c, +\infty[$.

Proof. For h a C^1 regular and a strictly positive function, the derivative of the function $F^{h\bar{u}}$ is

$$\left(F^{h\bar{u}}\right)'(h) = -\frac{M^2}{h^2} + 3h^2 S^2 + gh,$$

such that $\left(F^{h\bar{u}}\right)'(h_c) = 0$, where h_c has been defined in (2.11). In addition, the second derivative is

$$\left(F^{h\bar{u}}\right)''(h) = \frac{2M^2}{h^3} + 6hS^2 + g > 0.$$

2.2. MOVING STEADY STATE SOLUTION: REGULAR PART AND STATIONARY SHOCK61

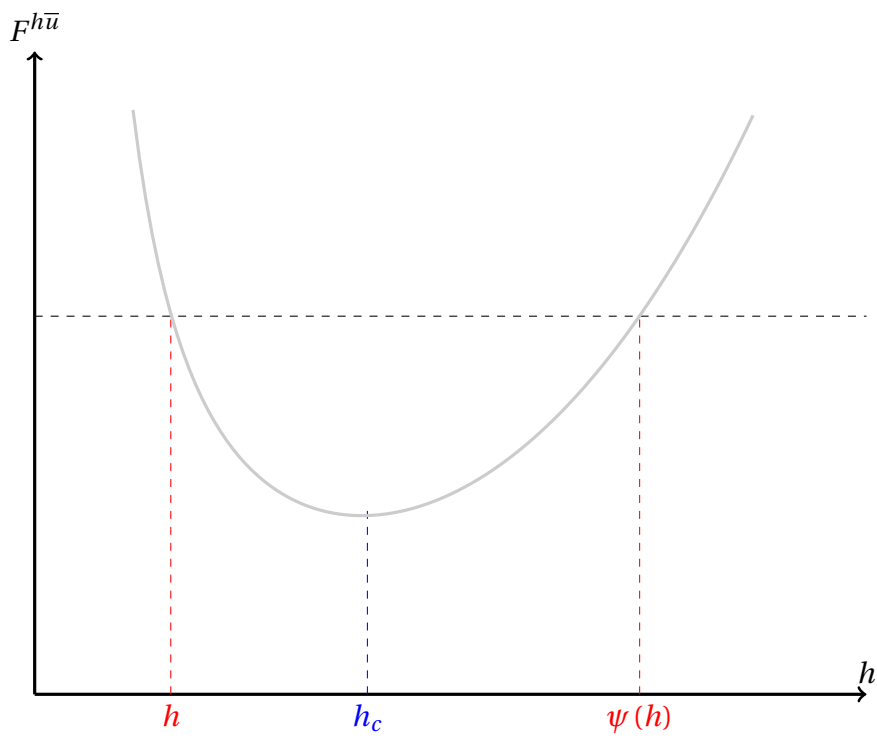


Figure 2.5: Plot of the function $F^{h\bar{u}}$ and construction of $\psi(h)$.

Hence, the function $h \mapsto F^{\bar{h}\bar{u}}(h)$ is strictly convex, strictly monotone on $]0, h_c]$ and $[h_c, +\infty[$ and tends to $+\infty$ when h tends to 0^+ and h tends to $+\infty$, see Figure 2.5. Thus, $F^{\bar{h}\bar{u}}$ admits a unique minimum in \mathbb{R}_+^* . It leads that, using the intermediate value theorem, for any $h < h_c$ (resp. $h > h_c$), there exists a unique $\psi(h) > h_c$ (resp. $\psi(h) < h_c$) verifying (2.15). And if $h = h_c$ then $\psi(h_c) = h_c$ verifies also (2.15).

To study the regularity of the function ψ , we introduce the C^1 function G as follows

$$G : \mathbb{R}_+^* \times \mathbb{R}_+^* \rightarrow \mathbb{R} \\ (h^*, h) \mapsto F^{\bar{h}\bar{u}}(h^*) - F^{\bar{h}\bar{u}}(h).$$

For all $h \in \mathbb{R}_+^*$, we have

$$G(\psi(h), h) = F^{\bar{h}\bar{u}}(\psi(h)) - F^{\bar{h}\bar{u}}(h) = 0.$$

Differentiating G with respect to h^* , we get

$$\frac{\partial G}{\partial h^*}(h^*, h) = \left(F^{\bar{h}\bar{u}}\right)'(h^*),$$

which is null if and only if $h^* = h_c$. Hence, the theorem of implicit function allows us to conclude that the function ψ as defined in (2.16) is C^1 on $]0, h_c[\cup]h_c, +\infty[$. Therefore, for all $h \neq h_c$ we have

$$\left(F^{\bar{h}\bar{u}}\right)'(h) = \left(F^{\bar{h}\bar{u}}\right)'(\psi(h)) \cdot \psi'(h).$$

$F^{\bar{h}\bar{u}}$ is strictly decreasing in $]0, h_c]$ and strictly increasing in $[h_c, +\infty[$ which allows us to conclude that $\left(F^{\bar{h}\bar{u}}\right)'(h)$ and $\left(F^{\bar{h}\bar{u}}\right)'(\psi(h))$ have opposite signs. As a consequence, $\psi'(h) < 0$ and ψ is strictly decreasing. Since ψ is strictly decreasing, continuous on \mathbb{R}_+^* , tends to $+\infty$ when h tends to 0 and tends to 0 when h tends to $+\infty$ then, the function is bijective from \mathbb{R}_+^* to \mathbb{R}_+^* . By definition of ψ , we have

$$F^{\bar{h}\bar{u}}(\psi(h)) = F^{\bar{h}\bar{u}}(\psi(\psi(h))),$$

which by construction of $F^{\bar{h}\bar{u}}$ allows us to conclude that $\psi(\psi(h)) = h$ implying that the function ψ is an involution on \mathbb{R}_+^* .

□

As mentioned in Definition 3, discontinuous solutions have to verify also the dissipation of entropy (2.8). This property is interpreted in the next proposition.

2.2. MOVING STEADY STATE SOLUTION: REGULAR PART AND STATIONARY SHOCK63

Proposition 8. For a given $M \in \mathbb{R}_+^*$ and $S \in \mathbb{R}$, we suppose that $h^- \in \mathbb{R}_+^*$ and $\psi(h^-) = h^+$ are respectively the water heights at the left and at the right of a stationary shock. Then, the shock verifies the entropy dissipation if one of the equivalent conditions below holds:

$$K^+ = \Phi(h^+, Z) \leq K^- = \Phi(h^-, Z) \quad (2.17)$$

or

$$h^- < h_c < h^+. \quad (2.18)$$

Proof. Given $M \in \mathbb{R}_+^*$ and $S \in \mathbb{R}$, the dissipation of entropy (2.8) is

$$\left[\left(g(h+Z) + \frac{M^2}{2h^2} + \frac{3S^2}{2}h^2 \right) M \right] \leq 0, \quad (2.19)$$

which for $M > 0$, writes

$$[\Phi(h, Z)] \leq 0,$$

and yields to (2.17). We note that the inequation (2.19) can also be written as

$$g[h+Z] + \frac{M^2}{2} \left[\frac{1}{h^2} \right] + \frac{3S^2}{2} [h^2] \leq 0.$$

We have already proved in Proposition 7 that h^- and $\psi(h^-) = h^+$ are in different regimes, so $[h] = h^+ - h^- \neq 0$. Also, we assumed in Hypothesis 1 that the topography Z is continuous then $[Z] = 0$. It leads that the previous inequation can be written as

$$[h] \left(g - \frac{M^2}{2(h^+)^2(h^-)^2} (h^- + h^+) + \frac{3S^2}{2} (h^- + h^+) \right) \leq 0. \quad (2.20)$$

In addition, the second equation in the Rankine-Hugoniot (2.7) relations implies

$$M^2 \left[\frac{1}{h} \right] + S^2 [h^3] + \frac{g}{2} [h^2] = 0,$$

which yields for $h^+ - h^- \neq 0$

$$\frac{M^2}{h^+ h^-} = \frac{g}{2} (h^+ + h^-) + S^2 ((h^+)^2 + (h^-)^2 + h^- h^+).$$

Replacing the quantity $\frac{M^2}{h^+ h^-}$ obtained in the above equation by its value in (2.20) we get

$$[h] \left(g - \frac{g}{4h^+ h^-} (h^+ + h^-)^2 - \frac{S^2 ((h^+)^2 + (h^-)^2 + h^- h^+)}{2h^+ h^-} (h^+ + h^-) + \frac{3S^2}{2} (h^- + h^+) \right) \leq 0,$$

which is nothing but

$$[h] \left(-g \frac{[h]^2}{4h^+ h^-} - S^2 \frac{(h^+ + h^-) [h]^2}{2h^+ h^-} \right) \leq 0.$$

which is true if and only if $[h] > 0$. This relation is equivalent to (2.18). \square

2.3 (Non) existence and (non) uniqueness of the moving steady states depending on the boundary conditions

According to [21, 34], the number of boundary conditions depends on the flow regime at the boundary. We are only interested in the boundary conditions inside the domain of definition at the inlet and at the outlet. The inlet boundary conditions are chosen according to the number of positive eigenvalues at the left of the domain, and the outlet boundary conditions are chosen according to the number of negative eigenvalues at the right of the domain. We already fixed $M > 0$ which means that for $h \in \mathbb{R}_+^*$ we have $\bar{u} > 0$. Hence, for the eigenvalues (2.1), we always have $\lambda_2^E > 0$ and $\lambda_3^E > 0$. We fix M and S at the inlet of the domain. It remains to fix the water height h when needed, which depends on the type of the flow.

1. If at the inlet

- the flow regime is subcritical then, $\lambda_1^E < 0$ and two boundary conditions are fixed at the left, i.e we fix only $M > 0$ and S , see Figure 2.6a and 2.6b.
- the flow regime is supercritical then, $\lambda_1^E > 0$ and three boundary conditions are fixed at the left, i.e we fix $h(x_L)$, $M > 0$ and S , see Figure 2.6c and 2.6d.

2. If at the outlet

- the flow regime is subcritical then, $\lambda_1^E < 0$ and one boundary condition is fixed at the right, i.e we fix only $h(x_R)$, see Figure 2.6a and 2.6c.

2.3. (NON) EXISTENCE AND (NON) UNIQUENESS OF THE MOVING STEADY STATES DEPENDING ON

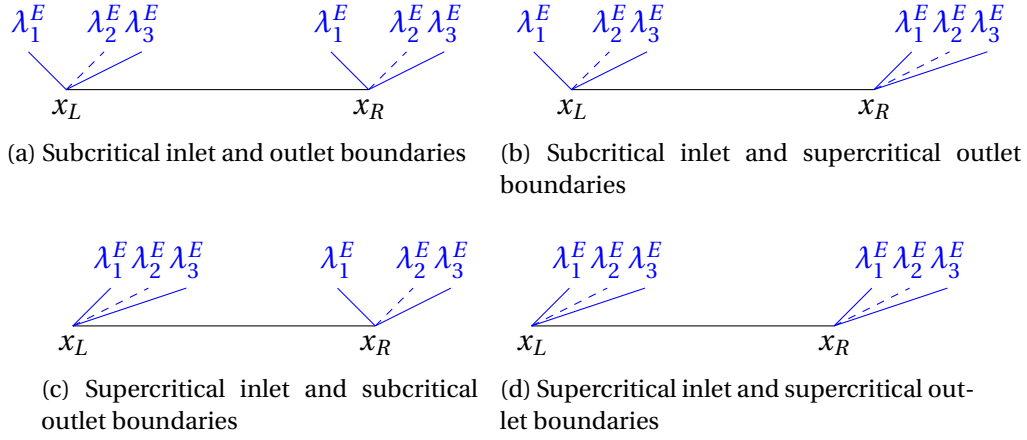


Figure 2.6: Representation of the eigenvalues for the different type of boundaries

- the flow regime is supercritical then, $\lambda_1^E > 0$ and no boundary condition is fixed at the right, see Figure 2.6b and 2.6d.

In the following, we will explain in details the construction of the solutions in each case.

2.3.1 Preliminaries

We now state some general results on the steady state solutions. We recall that the hydraulic head at the left and at the right of the domain are denoted by

$$K_L = \Phi(h_L, Z_L),$$

and

$$K_R = \Phi(h_R, Z_R).$$

where $h_L = h(x_L)$, $h_R = h(x_R)$, $Z_L = Z(x_L)$ and $Z_R = Z(x_R)$

Lemma 1. *If a piecewise C^1 solution exists on I , then $K_L \geq K_c$ and $K_L \geq K_R$.*

Proof. The hydraulic head $K = h + Z + \frac{1}{2g} \left(\frac{M^2}{h^2} + 3h^2 S^2 \right)$ is constant on intervals where the steady state solution is regular and decreases through entropy stationary shocks. This proves that $K_L \geq K_R$. Let us denote by $K_0 = \Phi(h(x_0^-), Z_{max})$

the hydraulic head at the top of the topography where $h(x_0^-) = \lim_{x \rightarrow x_0} h(x)$ with $x < x_0$. Then if $K_L < K_c$, $K_0 < K_c$ and according to Proposition 6, it is not possible to solve $\Phi(h, Z(x)) = K_0$ in the vicinity of $x = x_0$ which means that there is no piecewise C^1 steady state solution of (SW₂) on I . \square

From now on we suppose that the two conditions of Lemma 1 hold. In some cases, we know that the solution must contain a shock.

Lemma 2. *If $K_R < K_c$ then, the solution contains necessarily a shock somewhere on the right of the bump, i.e for $x \in [x_0, x_R]$.*

Proof. Suppose that the steady state solution is C^1 regular on $[x_0, x_R]$. Then, on that interval, the hydraulic head is constant and h is solution of $\Phi(h, Z(x)) = K_R$, which can't be solved in the vicinity of x_0 , see (2.14). \square

The next lemma gives properties concerning the transitions between the different regimes.

Lemma 3. *The transition from the subcritical regime to the supercritical regime is always continuous and can only happen at the top of the topography $x = x_0$ and with a critical hydraulic head K_c .*

Proof. According to Proposition 8, a stationary shock verifies $h^- < h_c < h^+$. This means that if a stationary shock exists then, the water height at the left of the discontinuity must be supercritical. Hence, the transition from the subcritical regime to the supercritical regime is always continuous. Now, let us denote by x_t the position where the transition occurs, i.e $h(x_t) = h_c$. We know that h is continuous on a small interval $x \in]x_t - \epsilon, x_t + \epsilon[$ for some $\epsilon > 0$ in which the hydraulic head is constant, see Proposition 3. Our aim is to solve the equation $\Phi(h(x), Z(x)) = K$ for some $K \leq K_L$. In fact, the transition is continuous which means we should have $h_K^{sub}(x_t) = h_K^{sup}(x_t) = h_c$. This is only true if $K = K_c$ and $x_t = x_0$, see Proposition 5. So we can finally conclude that the transition happens only at $x = x_0$ and with a critical hydraulic head K_c . \square

Remark 2. *The result of Lemma 3 also applies if the transition from the supercritical regime to the subcritical regime is continuous.*

We now state a technical proposition that will be widely used in the proofs.

2.3. (NON) EXISTENCE AND (NON) UNIQUENESS OF THE MOVING STEADY STATES DEPENDING ON

Proposition 9. *Assume that the topography Z verifies Hypothesis 1. Let $x \mapsto h^{sol}(x)$ be a C^1 steady solution of (SW₂), i.e for some $K \in \mathbb{R}$, $h^{sol} = h_K^{sub}$ or $h^{sol} = h_K^{sup}$. Then $(F^{h\bar{u}} \circ h^{sol})' = -gZ' h^{sol}$.*

Proof. At a point x on the interior of the domain of definition of h^{sol} , we have

$$\left(F^{h\bar{u}} \circ h^{sol}\right)'(x) = \left(F^{h\bar{u}}\right)'(h^{sol}(x)) \cdot \left(h^{sol}\right)'(x).$$

Now, we note that for all $h > 0$ at all Z we have

$$\left(F^{h\bar{u}}\right)'(h) = gh\partial_h\Phi(h, Z).$$

On the other hand, h^{sol} is a C^1 regular solution of (SW₂). Hence, $x \mapsto \Phi(h^{sol}(x), Z(x))$ is constant (see Proposition 3), thus its derivative is null, which yields

$$\partial_h\Phi(h^{sol}(x), Z(x)) \cdot \left(h^{sol}\right)'(x) = -Z'(x).$$

Thus,

$$\begin{aligned} \left(F^{h\bar{u}} \circ h^{sol}\right)'(x) &= gh^{sol}(x)\partial_h\Phi(h^{sol}(x), Z(x)) \cdot \left(h^{sol}\right)'(x) \\ &= -gZ'(x)h^{sol}(x), \end{aligned}$$

which concludes the proof. □

2.3.2 Subcritical inlet boundary conditions

In this section, we suppose that the flow is subcritical at the inlet, i.e $h(x_L) > h_c$. Two boundary conditions are required at the left of the domain, where we impose the discharge $M > 0$ and the shear S . We start by introducing the following lemma.

Lemma 4. *If the flow at the left of the domain is subcritical then, the solution contains at most one shock which can only occur at the right part of the topography, i.e for $x \in [x_0, x_R]$.*

Proof. Denote by x_s the position of the first shock in the solution. If $x_s < x_0$, it would mean that the solution is supercritical in x_s^- . But, the flow is subcritical in x_L . which means that there would be a continuous transition between the

regimes in $]x_L, x_s[$, which contradicts Lemma 3. Hence, there is no shock at the left of the bump. Therefore, the solution is necessarily subcritical and C^0 for all $x \in [x_L, x_0]$. Now, if the solution touches h_c at $x = x_0$ and becomes supercritical, there is a possibility that a shock occurs in $x \in]x_0, x_R]$ because the dissipation of entropy (2.18) can be verified. Only one shock can occur. In fact, when the first shock occurs at the right of the bump, the solution becomes again subcritical. It can't become supercritical again neither in a continuous way because this transition is only possible at the top of the topography, see Lemma 3, nor in a discontinuous way because the dissipation of entropy (2.18) can't be verified. \square

In the following, we will describe the type of the steady state solution depending on the outlet boundary conditions.

Subcritical outlet boundary condition

We start with the case $h(x_R) = h_R > h_c$. One characteristic enters the domain at the outlet hence, we fix one boundary condition on the form $h(x_R) = h_R$.

Proposition 10. *Let Z verify Hypothesis 1. Suppose that $h(x_L) > h_c$. For $M > 0$, $S \in \mathbb{R}$ fixed at the inlet and $h_R > h_c$ fixed at the outlet, we have the following:*

- *If $h_R > h_{K_c}^{sub}(x_R)$ then, there exists a unique steady state solution of (SW₂). This solution is C^1 regular on the whole domain and given by $h = h_{K_R}^{sub}$. This solution is called subcritical everywhere.*
- *If $\psi(h_{K_c}^{sup}(x_R)) < h_R < h_{K_c}^{sub}(x_R)$ then, there exists a unique C^1 piecewise solution. More precisely, there exists a unique point $x_{shock} \in [x_0, x_R]$ such that*

$$h(x) = \begin{cases} h_{K_c}^{sub}(x) & \text{if } x \leq x_0, \\ h_{K_c}^{sup}(x) & \text{if } x_0 \leq x < x_{shock}, \\ h_{K_R}^{sub}(x) & \text{if } x > x_{shock}. \end{cases}$$

verifies (2.15) and (2.18). This solution is called transcritical with shock.

- *If $h_R < \psi(h_{K_c}^{sup}(x_R))$ then, there is no steady solution of (SW₂) satisfying the subcritical boundary conditions.*

The different solutions are plotted in Figure 2.7.

2.3. (NON) EXISTENCE AND (NON) UNIQUENESS OF THE MOVING STEADY STATES DEPENDING ON

Proof. We start with the case $h_R > h_{K_c}^{sub}(x_R)$. The water heights h_R and $h_{K_c}^{sub}(x_R)$ are both subcritical. According to Proposition 4, the function $h \mapsto \Phi(h, Z)$ is increasing for $h > h_c$. Thus, $\Phi(h_R, Z_R) > \Phi(h_{K_c}^{sup}(x_R), Z_R)$ or equivalently $K_R > K_c$. Hence, we can conclude from Proposition 5 that $x \mapsto h_{K_R}^{sub}(x)$ is a C^1 subcritical solution of (SSW2) verifying the subcritical boundary conditions. We now prove that there is no solution that satisfies the boundary conditions and that contains a shock. Such a solution would verify $K_L > K_R > K_c$. It follows from Proposition 5 that no transition to the supercritical is possible and the shock can't occur, see Lemma 4. Hence, the solution is subcritical and regular on the whole interval I and is necessarily $h_{K_R}^{sub}$.

Next, we study the case where $\psi(h_{K_c}^{sup}(x_R)) < h_R < h_{K_c}^{sub}(x_R)$. In this case, we have $K_R < K_c$ and we can conclude from Lemma 2 that the solution contains necessarily a shock, which takes place at the right of the top of the topography, see Lemma 4. In addition, the transition from the subcritical regime to the supercritical regime is continuous and thanks to Lemma 3 we can point that the hydraulic head at the left of the shock is $K_L = K_c$. Therefore, the solution starts subcritical on $[x_L, x_0]$ with $h = h_{K_c}^{sub}$, reaches h_c at $x = x_0$ and becomes supercritical in a continuous way with $h = h_{K_c}^{sup}$. Thus, the water height at the left of the shock will be $h_{K_c}^{sup}(x)$ and the water height on its right is $h_{K_R}^{sub}(x)$. It remains to place the shock at a point where the Rankine-Hugoniot relations (2.7) are verified. In other words, we have to prove that the following function has a unique zero

$$\begin{aligned} f : [x_{K_R}^{**}, x_R] &\rightarrow \mathbb{R} \\ x &\mapsto F^{h\bar{u}}(h_{K_R}^{sub}(x)) - F^{h\bar{u}}(h_{K_c}^{sup}(x)). \end{aligned} \quad (2.21)$$

Since $K_R < K_c$, $h_{K_R}^{sub}$ is only defined on $[x_{K_R}^{**}, x_R]$ and $h_{K_R}^{sub}(x_{K_R}^{**}) = h_c$ which explains the domain of definition of the function f , see Proposition 6.

Next, on one hand, h_c is the minimum of $F^{h\bar{u}}$ hence,

$$f(x_{K_R}^{**}) = F^{h\bar{u}}(h_c) - F^{h\bar{u}}(h_{K_c}^{sup}(x_{K_R}^{**})) < 0.$$

On another hand, we have $h_c < \psi(h_{K_c}^{sup}(x_R)) < h_R$ thus, using the fact that the function $h \mapsto F^{h\bar{u}}(h)$ is increasing for $h > h_c$, we get

$$\begin{aligned} f(x_R) &= F^{h\bar{u}}(h_{K_R}^{sub}(x_R)) - F^{h\bar{u}}(h_{K_c}^{sup}(x_R)) \\ &= F^{h\bar{u}}(h_R) - F^{h\bar{u}}(\psi(h_{K_c}^{sup}(x_R))) > 0. \end{aligned} \quad (2.22)$$

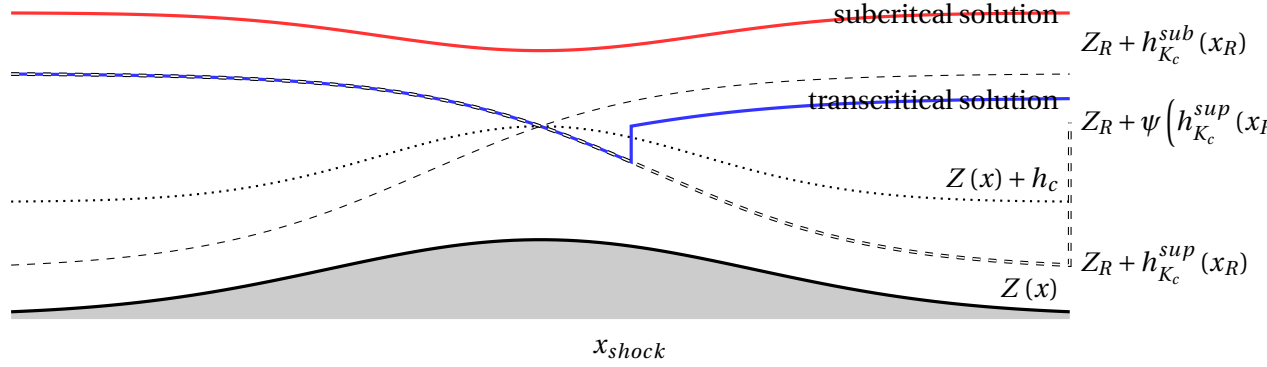


Figure 2.7: General steady states with subcritical boundary conditions at both sides of the domain

Using Proposition 9, we compute the derivative of the function f to get

$$\begin{aligned} f'(x) &= (F^{h\bar{u}})'(h_{K_R}^{sub}(x)) \cdot (h_{K_R}^{sub})'(x) - (F^{h\bar{u}})'(h_{K_c}^{sup}(x)) \cdot (h_{K_c}^{sup})'(x), \\ &= -gZ'(x)(h_{K_R}^{sub}(x) - h_{K_c}^{sup}(x)). \end{aligned}$$

For all $x \in [x_{K_R}^{**}, x_R]$, the function Z is decreasing and $h_{K_R}^{sub} > h_c \geq h_{K_c}^{sup}$. As a consequence, f is strictly increasing on $[x_{K_R}^{**}, x_R]$. Thus, applying the theorem of intermediate value and using the monotonicity of f we can conclude that there exists a unique point x_{shock} where $f(x_{shock}) = 0$.

Finally, we prove that for $h_R < \psi(h_{K_c}^{sup}(x_R))$ there is no steady solution of (SW₂) satisfying the subcritical boundary conditions. In this case, we also have $K_R < K_c$ and the solution has the same structure with a shock on the right. We still have $f(x_{K_R}^{**}) < 0$ and $f'(x) > 0$ but $f(x_R)$ as defined in (2.22) is negative. Hence, the function f defined in (2.21) is always negative for all $x \in [x_{K_R}^{**}, x_R]$. Which means that it is not possible to place a stationary shock joining $h_{K_c}^{sup}$ and $h_{K_R}^{sub}$. \square

Supercritical outlet boundary conditions

In this section, we focus on the subcritical boundary conditions at the inlet and the supercritical boundary conditions at the outlet. We fix $M > 0$ and S at the

2.3. (NON) EXISTENCE AND (NON) UNIQUENESS OF THE MOVING STEADY STATES DEPENDING ON

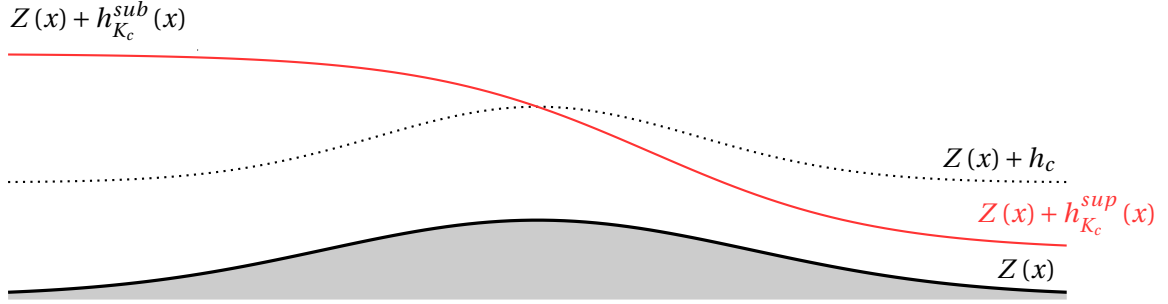


Figure 2.8: Steady state solution with subcritical boundary conditions at the inlet and supercritical boundary conditions at the outlet

inlet. In addition, we assume that $h(x_L) = h_L > h_c$ and $h(x_R) = h_R < h_c$, but none of these values is fixed.

Proposition 11. *Let Z verify Hypothesis 1. For $M > 0$, $S \in \mathbb{R}$ fixed at the inlet, there exists a unique solution*

$$h(x) = \begin{cases} h_{K_c}^{sub}(x) & \text{if } x \leq x_0, \\ h_{K_c}^{sup}(x) & \text{if } x \geq x_0, \end{cases}$$

with subcritical boundary at the inlet and supercritical boundary at the outlet. The plot of this solution is showed in Figure 2.8.

Proof. The inlet boundary conditions are subcritical. Hence, the solution is continuous and subcritical on $[x_L, x_0]$. Thus, on that interval the hydraulic head is constant and the transition to the supercritical occurs at the top of the bump with a hydraulic head K_c hence, $K_L = K_c$, see Lemma 3. According to Lemma 4, there is a possibility that a shock occurs in $]x_0, x_R]$. However, the right boundary condition is supercritical then, the solution can't contain a shock on the right verifying (2.18), pass to subcritical regime and then become again supercritical. This means that the solution is necessarily continuous everywhere. Now, let us prove that h is the unique continuous solution. If the solution is continuous then the hydraulic head is constant in the whole domain. Therefore, K_c is the hydraulic head in the whole domain. Thus, $K_L = K_R = K_c$ and the unique solution is $h_{K_c}^{sub}$ at the left of the top of the topography and $h_{K_c}^{sup}$ at its right. \square

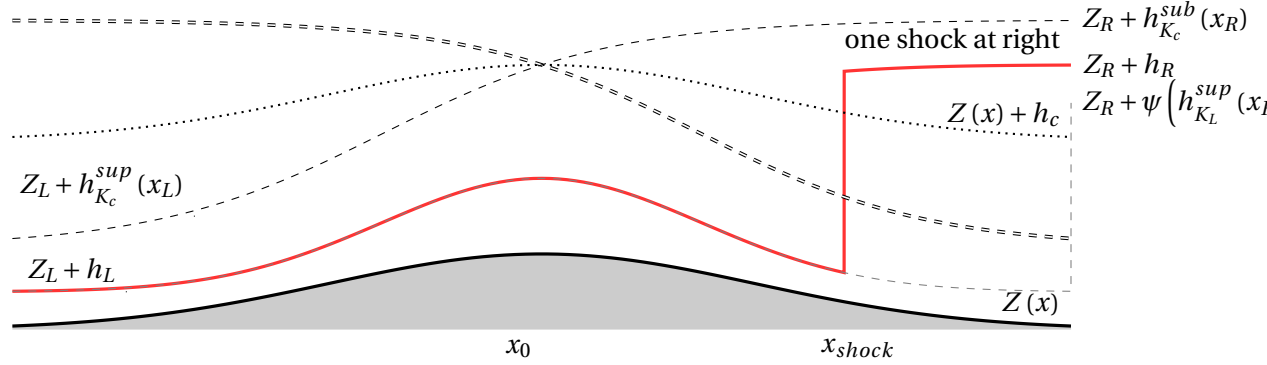


Figure 2.9: Steady state solution with one shock at right for the supercritical boundary conditions at the inlet and subcritical boundary conditions at the outlet when $K_L > K_c > K_R$

2.3.3 Supercritical inlet boundary conditions

In this section, we are interested in supercritical inlet boundary conditions. Three boundary conditions are required at the left of the domain, where we impose the discharge $M > 0$, the shear S and the water height $h_L = h(x_L) < h_c$.

Subcritical outlet boundary conditions

With subcritical boundary conditions at the outlet we also fix $h_R = h(x_R) > h_c$. First, we introduce the following lemma.

Lemma 5. *If the inlet boundary condition is supercritical, the solution may contain at most one shock at each side of the top of the topography.*

Proof. If the inlet boundary condition is supercritical then, there is a possibility that an entropic shock occurs at the left of the bump because the dissipation of entropy can be verified, see Proposition 8. If a shock occurs in $[x_L, x_0]$ then, the solution becomes subcritical and should become supercritical again before a second shock can occur. According to Lemma 3, the transition is continuous and takes place at the top of the bump. A similar argument, developed in Lemma 4, shows that there cannot be two shocks on $[x_0, x_R]$. \square

2.3. (NON) EXISTENCE AND (NON) UNIQUENESS OF THE MOVING STEADY STATES DEPENDING ON

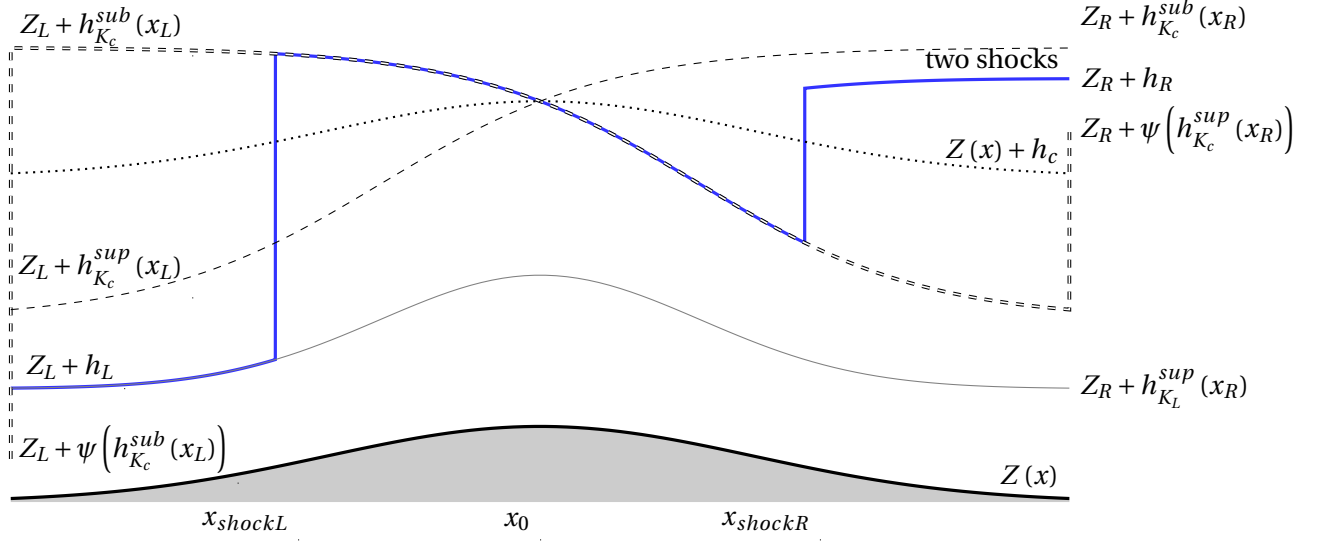


Figure 2.10: Steady state solution with two shocks for the supercritical boundary conditions at the inlet and subcritical boundary conditions at the outlet when $K_L > K_c > K_R$

The main result of this section is that in some cases, there exist two distinct steady state solutions verifying the same set of boundary data. This result is decomposed in two cases:

- In Proposition 12, we suppose that $K_R < K_c$ or equivalently that $h_c < h_R < h_{K_c}^{sub}(x_R)$.
- In Proposition 13, we suppose that $K_R > K_c$ or equivalently that $h_R > h_{K_c}^{sub}(x_R)$.

Proposition 12. *Let Z verify Hypothesis 1. Let $M > 0$, $S \in \mathbb{R}$, $h_L < h_c$ fixed at the inlet and $h_R > h_c$ fixed at the outlet such that $K_L > K_c > K_R$, i.e $h_L < h_{K_c}^{sup}(x_L)$ and $h_R < h_{K_c}^{sub}(x_R)$.*

- *If $\psi(h_{K_L}^{sup}(x_R)) < h_R$ then, there exists a unique $x_{shock} \in]x_{K_R}^{**}, x_R[$ such that*

$$h(x) = \begin{cases} h_{K_L}^{sup}(x) & \text{if } x < x_{shock}, \\ h_{K_R}^{sub}(x) & \text{if } x > x_{shock}. \end{cases}$$

is a C^1 piecewise steady state solution of (SW₂). The plot of the solution is showed in Figure 2.9.

- If $\psi\left(h_{K_c}^{sub}(x_L)\right) < h_L$ and $\psi\left(h_{K_c}^{sup}(x_R)\right) < h_R$ then, there exists a unique $x_{shockL} \in]x_L, x_0[$ and a unique $x_{shockR} \in]x_{K_R}^{**}, x_R[$ such that

$$h(x) = \begin{cases} h_{K_L}^{sup}(x) & \text{if } x < x_{shockL}, \\ h_{K_c}^{sub}(x) & \text{if } x_{shockL} < x \leq x_0, \\ h_{K_c}^{sup}(x) & \text{if } x_0 \leq x < x_{shockR}, \\ h_{K_R}^{sub}(x) & \text{if } x > x_{shockR}, \end{cases}$$

is a C^1 piecewise steady state solution of (SW₂). The plot of the solution is showed in Figure 2.10.

- If neither of these conditions hold, there exist no steady solution for (SW₂) verifying the supercritical boundary conditions on the left and the subcritical boundary conditions on the right.

Proof. First of all, the condition $K_L > K_c > K_R$ implies that

$$\Phi(h_L, Z_L) = K_L > K_c = \Phi(h_c, Z_{max}) = \Phi\left(h_{K_c}^{sup}(x_0), Z(x_0)\right) = \Phi\left(h_{K_c}^{sup}(x_L), Z_L\right),$$

and

$$\Phi(h_R, Z_R) = K_R < K_c = \Phi(h_c, Z_{max}) = \Phi\left(h_{K_c}^{sub}(x_0), Z(x_0)\right) = \Phi\left(h_{K_c}^{sub}(x_R), Z_R\right).$$

Thus, we can conclude from Φ decreasing in $]0, h_c[$ and increasing in $[h_c, +\infty[$ that $h_L < h_{K_c}^{sup}(x_L)$ and $h_R < h_{K_c}^{sub}(x_R)$, see Proposition 4.

Now, in both cases the solution contains necessarily a shock at the right of the topography because $K_R < K_c$, see Lemma 2.

We start with the first type with only one shock at the right. In this case, the solution has the form

$$h(x) = \begin{cases} h_{K_L}^{sup}(x) & \text{if } x < x_{shock}, \\ h_{K_R}^{sub}(x) & \text{if } x > x_{shock}. \end{cases}$$

The Rankine-Hugoniot relations must be verified at the position of the shock, so x_{shock} is a zero of the function

$$\begin{aligned} f_R : [x_{K_R}^{**}, x_R] &\rightarrow \mathbb{R} \\ x &\mapsto F^{h\bar{u}}\left(h_{K_R}^{sub}(x)\right) - F^{h\bar{u}}\left(h_{K_L}^{sup}(x)\right), \end{aligned}$$

The critical water height h_c is the minimum of the function $F^{h\bar{u}}$ so at the point $x_{K_R}^{**}$ we have

$$f_R\left(x_{K_R}^{**}\right) = F^{h\bar{u}}(h_c) - F^{h\bar{u}}\left(h_{K_L}^{sup}\left(x_{K_R}^{**}\right)\right) < 0.$$

2.3. (NON) EXISTENCE AND (NON) UNIQUENESS OF THE MOVING STEADY STATES DEPENDING ON

At the right of the domain we have by hypothesis $h_R > \psi\left(h_{K_L}^{sup}(x_R)\right) > h_c$ and $F^{h\bar{u}}$ increases on $[h_c, +\infty[$ (Proposition 7). It leads

$$\begin{aligned} f_R(x_R) &= F^{h\bar{u}}\left(h_{K_R}^{sub}(x_R)\right) - F^{h\bar{u}}\left(h_{K_L}^{sup}(x_R)\right) \\ &= F^{h\bar{u}}(h_R) - F^{h\bar{u}}\left(\psi\left(h_{K_L}^{sup}(x_R)\right)\right) > 0, \end{aligned}$$

and we can conclude using the intermediate value theorem that there exists a point x_{shock} where $f_R(x_{shock}) = 0$. To prove the uniqueness, we apply Proposition 9 and we get

$$f'_R(x) = -gZ'(x)\left(h_{K_R}^{sub}(x) - h_{K_L}^{sup}(x)\right) > 0.$$

We turn to the case where there is a shock on each side of the top of the topography. The solution starts supercritical with $h(x) = h_{K_L}^{sup}(x)$, the first shock occurs and then the solution becomes subcritical. In order to realize the second shock, the solution must become supercritical again. According to Lemma 3, this transition is continuous and must happen at $x = x_0$ with a critical hydraulic head. Therefore,

- for all x between the position of the first shock and the top of the topography the solution is $h(x) = h_{K_c}^{sub}(x)$
- for all x between the top of the topography and the position of the second shock the solutions is $h(x) = h_{K_c}^{sup}(x)$.

Then, to attend the right subcritical boundaries the water height at the right of the second shock will be $h_{K_R}^{sub}$.

Now, to prove the existence of the first shock we introduce the function

$$\begin{aligned} f_L : [x_L, x_0] &\rightarrow \mathbb{R} \\ x &\mapsto F^{h\bar{u}}\left(h_{K_c}^{sub}(x)\right) - F^{h\bar{u}}\left(h_{K_L}^{sup}(x)\right). \end{aligned} \quad (2.23)$$

Since $F^{h\bar{u}}$ decreases on $]0, h_c[$ at the left of the domain where by hypothesis $\psi\left(h_{K_c}^{sub}(x_L)\right) < h_L$, we have

$$f_L(x_L) = F^{h\bar{u}}\left(h_{K_c}^{sub}(x_L)\right) - F^{h\bar{u}}\left(h_{K_L}^{sup}(x_L)\right) = F^{h\bar{u}}\left(\psi\left(h_{K_c}^{sub}(x_L)\right)\right) - F^{h\bar{u}}(h_L) > 0.$$

At the top of the topography we have,

$$f_L(x_0) = F^{h\bar{u}}\left(h_{K_c}^{sub}(x_0)\right) - F^{h\bar{u}}\left(h_{K_L}^{sup}(x_0)\right) = F^{h\bar{u}}(h_c) - F^{h\bar{u}}\left(h_{K_L}^{sup}(x_0)\right) < 0.$$

We can conclude using the intermediate value theorem that there exists a point x_{shockL} where $f_L(x_{shockL}) = 0$. For all $x \in [x_L, x_0]$,

$$f'_L(x) = -gZ'(x) \left(h_{K_c}^{sub}(x) - h_{K_L}^{sup}(x) \right) < 0,$$

and we get that f_L is strictly decreasing on $[x_L, x_0]$ and the point x_{shockL} such that $f_L(x_{shockL}) = 0$ is unique.

Now, to prove the existence and the uniqueness of the second shock we recall the function f defined in (2.21). We follow the same strategy as done in the proof of the Proposition 10: we prove that $f(x_{K_R}^{**}) < 0$ and for $h_c < \psi(h_{K_c}^{sup}(x_R)) < h_R$ we get that $f(x_R) > 0$. We can conclude that the point x_{shockR} such that $f(x_{shockR}) = 0$ is unique.

If none of the previous conditions hold, the functions f , f_L and f_R defined in the proof have no zeros and it is impossible to construct a solution. \square

Proposition 13. *Let Z verify Hypothesis 1. For $M > 0$, $S \in \mathbb{R}$, $h_L < h_c$ fixed at the inlet and $h_R > h_c$ fixed at the outlet such that $K_L > K_R > K_c$, i.e $h_L < h_{K_c}^{sup}(x_L)$ and $h_R > h_{K_c}^{sub}(x_R)$.*

- If $\psi(h_{K_R}^{sub}(x_L)) < h_L$ and $h_{K_L}^{sup}(x_0) < \psi(h_{K_R}^{sub}(x_0))$ then, there exists a unique $x_{shock} \in]x_L, x_0[$ such that

$$h(x) = \begin{cases} h_{K_L}^{sup}(x) & \text{if } x < x_{shock}, \\ h_{K_R}^{sub}(x) & \text{if } x > x_{shock}. \end{cases}$$

is a C^1 piecewise steady state solution of (SW₂). The plot of the solution is showed in Figure 2.11.

- If $h_{K_L}^{sup}(x_0) < \psi(h_{K_R}^{sub}(x_0))$ and $\psi(h_{K_L}^{sup}(x_R)) < h_R$ then, there exists a unique $x_{shock} \in]x_0, x_R[$ such that

$$h(x) = \begin{cases} h_{K_L}^{sup}(x) & \text{if } x < x_{shock}, \\ h_{K_R}^{sub}(x) & \text{if } x > x_{shock}. \end{cases}$$

is a C^1 piecewise steady state solution of (SW₂). The plot of the solution is showed in Figure 2.12.

- If none of these conditions apply then, there is no steady state solution of (SW₂) verifying the supercritical boundary conditions on the left and the subcritical boundary conditions on the right.

2.3. (NON) EXISTENCE AND (NON) UNIQUENESS OF THE MOVING STEADY STATES DEPENDING ON

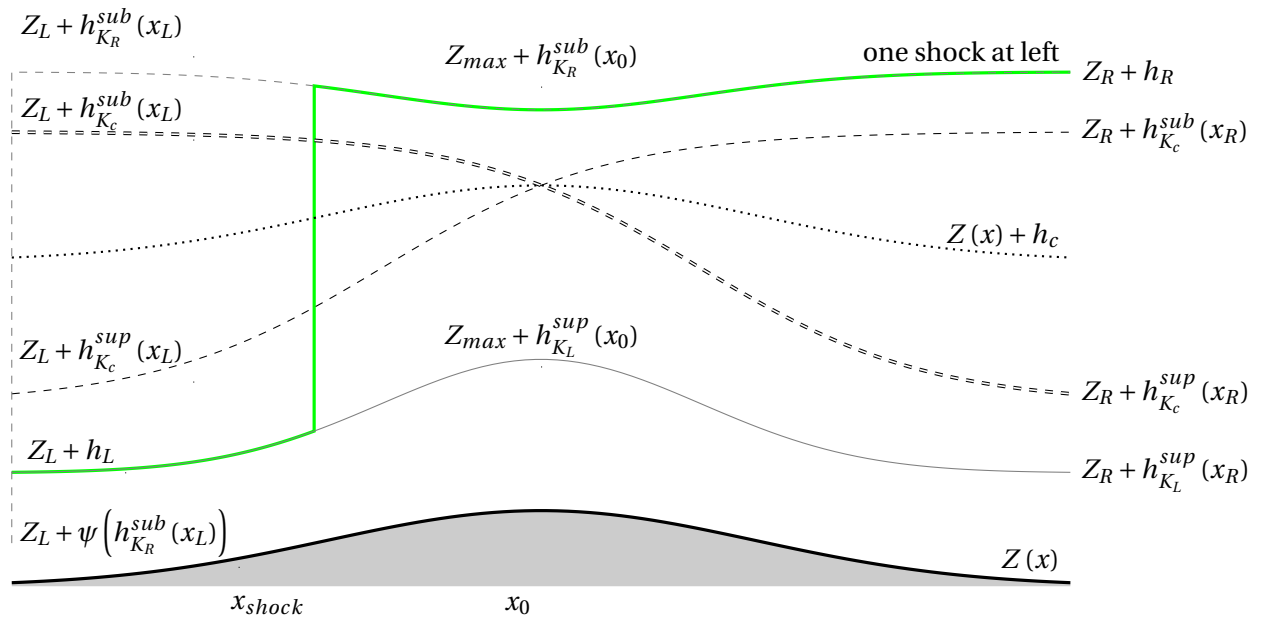


Figure 2.11: Steady state solution with one shock at left for the supercritical boundary conditions at the inlet and subcritical boundary conditions at the outlet when $K_L > K_R > K_C$

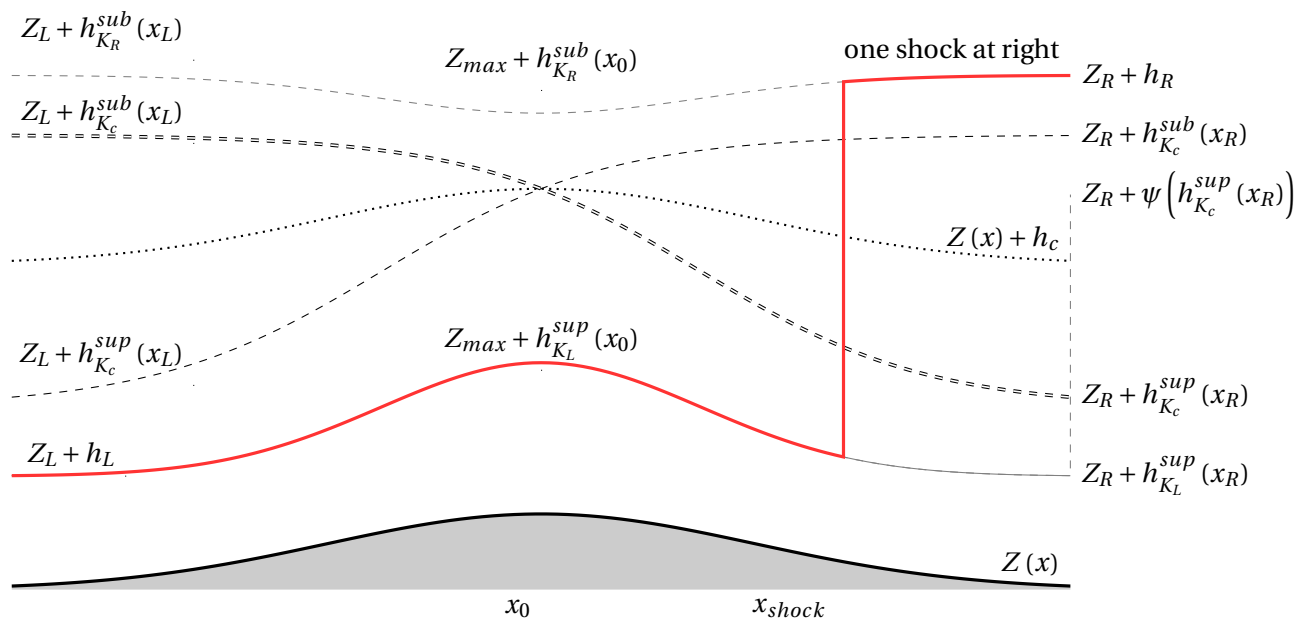


Figure 2.12: Steady state solution with one shock at right for the supercritical boundary conditions at the inlet and subcritical boundary conditions at the outlet when $K_L > K_R > K_C$

Proof. First of all, $K_L > K_R > K_c$ thus $h_{K_R}^{sub}$ and $h_{K_L}^{sup}$ are defined for all $x \in I$ and we have $h_L < h_{K_c}^{sup}(x_L)$ and $h_R > h_{K_R}^{sub}(x_R)$. In addition, $K_L \neq K_R$ so the hydraulic head is not constant in the whole domain. Thus, the solution must contain a shock. The inlet boundary condition is supercritical hence, according to Lemma 5 the solution can contain at most one shock at each side of the domain. But here, the solution can't contain a shock on each side of the bump, because in that case there is a continuous transition from subcritical to supercritical between the shock with hydraulic head K_c . Then after the second shocks we would have $K_R < K_c$, see Proposition 8. In the following, we prove the existence and the uniqueness of the shock in $]x_L, x_0[$ or in $]x_0, x_R[$. We first introduce the function

$$\begin{aligned} f &: I \rightarrow \mathbb{R} \\ x &\mapsto F^{h\bar{u}}\left(h_{K_R}^{sub}(x)\right) - F^{h\bar{u}}\left(h_{K_L}^{sup}(x)\right), \end{aligned}$$

For all $x \in I$, $h_{K_R}^{sub}(x) > h_{K_L}^{sup}(x)$ thus, the derivative of the function f

$$f'(x) = -gZ'(x)\left(h_{K_R}^{sub}(x) - h_{K_L}^{sup}(x)\right),$$

is strictly negative for all $]x_L, x_0[$ and strictly positive for all $]x_0, x_R[$. It follows that, if there is a shock in $]x_L, x_0[$ or in $]x_0, x_R[$ then we necessarily have $f(x_0) < 0$. $F^{h\bar{u}}$ is decreasing on $]0, h_c[$, thus

$$\begin{aligned} f(x_0) &= F^{h\bar{u}}\left(h_{K_R}^{sub}(x_0)\right) - F^{h\bar{u}}\left(h_{K_L}^{sup}(x_0)\right) \\ &= F^{h\bar{u}}\left(\psi\left(h_{K_R}^{sub}(x_0)\right)\right) - F^{h\bar{u}}\left(h_{K_L}^{sup}(x_0)\right), \end{aligned}$$

is strictly negative if and only if $\psi\left(h_{K_R}^{sub}(x_0)\right) > h_{K_L}^{sup}(x_0)$.

At the left,

$$\begin{aligned} f(x_L) &= F^{h\bar{u}}\left(h_{K_R}^{sub}(x_L)\right) - F^{h\bar{u}}\left(h_{K_L}^{sup}(x_L)\right) \\ &= F^{h\bar{u}}\left(\psi\left(h_{K_R}^{sub}(x_L)\right)\right) - F^{h\bar{u}}(h_L), \end{aligned}$$

is strictly positive if and only if $\psi\left(h_{K_R}^{sub}(x_L)\right) < h_L$.

At the right, the water height is subcritical, so $F^{h\bar{u}}$ is increasing and if $\psi\left(h_{K_L}^{sup}(x_R)\right) < h_R$, we have

$$\begin{aligned} f(x_R) &= F^{h\bar{u}}\left(h_{K_R}^{sub}(x_R)\right) - F^{h\bar{u}}\left(h_{K_L}^{sup}(x_R)\right) \\ &= F^{h\bar{u}}(h_R) - F^{h\bar{u}}\left(\psi\left(h_{K_L}^{sup}(x_R)\right)\right) > 0. \end{aligned}$$

2.3. (NON) EXISTENCE AND (NON) UNIQUENESS OF THE MOVING STEADY STATES DEPENDING ON

The theorem of intermediate value allows us to conclude that there exists a point x_{shock} where $f(x_{shock}) = 0$ in $]x_0, x_R[$ or in $]x_L, x_0[$ depending on each case. The uniqueness of the shocks follows from the monotonicity of the function f as usual. □

Now that we have presented the different steady state solutions verifying the supercritical boundary conditions at the inlet and the subcritical boundary conditions at the outlet, we present in the next corollaries the possible coexistence of the solution depending on $Z(x_L)$ and $Z(x_R)$.

Corollary 1. *Let Z verify Hypothesis 1 and $Z(x_L) = Z(x_R)$. For $M > 0$, $S \in \mathbb{R}$, $h_L < h_c$ fixed at the inlet and $h_R > h_c$ fixed at the outlet.*

- *If $K_L > K_c > K_R$ and if the solution with one shock at right exists then, the solution with two shocks exists too as well.*
- *If $K_L > K_R > K_c$, the two sets of conditions of Proposition 13 are equivalent and both solutions coexist.*

The uniqueness and the coexistence of the solutions are illustrated in Figure 2.15.

Proof. Suppose $Z(x_L) = Z(x_R)$ thus, x_L and x_R play symmetric roles : $h_K^{sub}(x_L) = h_K^{sub}(x_R)$ and similarly $h_K^{sup}(x_L) = h_K^{sup}(x_R)$. Let us first focus on Proposition 12 where $K_R < K_c < K_L$. If the solution with one shock at right exists then, $\psi(h_{K_L}^{sup}(x_R)) < h_R$. First, $K_L > K_c$ implies that $h_{K_L}^{sup}(x_L) < h_{K_c}^{sup}(x_L)$. Second, ψ decreases and $\psi(h_{K_L}^{sup}(x_R)) < h_R$ thus,

$$h_R > \psi(h_{K_L}^{sup}(x_R)) = \psi(h_{K_L}^{sup}(x_L)) > \psi(h_{K_c}^{sup}(x_L)) = \psi(h_{K_c}^{sup}(x_R)),$$

and, the second condition for the existence of the two shocks solution is verified. In addition, as $K_R < K_c$ we get that $h_R = h_{K_R}^{sub}(x_R) < h_{K_c}^{sub}(x_R)$. Hence, the condition $\psi(h_{K_L}^{sup}(x_R)) < h_R$ implies $\psi(h_{K_L}^{sup}(x_R)) < h_{K_c}^{sub}(x_R)$ or equivalently $h_{K_L}^{sup}(x_R) > \psi(h_{K_c}^{sub}(x_R))$. With $Z(x_L) = Z(x_R)$ we obtain $h_L = h_{K_L}^{sup}(x_L) > \psi(h_{K_c}^{sub}(x_L))$ which is nothing but the first condition for the existence of the two shocks solution.

Next, we focus on Proposition 13 where $K_L > K_R > K_c$. In this case, $h_{K_L}^{sup}(x_0) < \psi\left(h_{K_R}^{sub}(x_0)\right)$ is a common condition for the existence of both solutions. For $Z(x_L) = Z(x_R)$ we have

$$\psi(h_L) = \psi\left(h_{K_L}^{sup}(x_L)\right) = \psi\left(h_{K_L}^{sup}(x_R)\right) < h_R = h_{K_R}^{sub}(x_R) = h_{K_R}^{sub}(x_L)$$

which is equivalent to $h_L > \psi\left(h_{K_R}^{sub}(x_L)\right)$. Hence, the first condition of the existence of the solution with a shock at left is equivalent to the second condition of the existence of the solution with a shock at right. Therefore, both solutions coexist. \square

We detailed in Corollary 1 the effect of $Z(x_L) = Z(x_R)$ on the solution. In the next corollaries, we exhibit the different consequences of $Z(x_L) \neq Z(x_R)$ on the solution.

Corollary 2. *Let Z verify Hypothesis 1. For $M > 0$, $S \in \mathbb{R}$, $h_L < h_c$ fixed at the inlet and $h_R > h_c$ fixed at the outlet. For $Z(x_L) < Z(x_R)$,*

- *If $K_L > K_c > K_R$ and if the solution with one shock at right exists then, the solution with two shocks exists too.*
- *If $K_L > K_R > K_c$ and if the solution with one shock at right exists then the solution with one shock at left exists too.*

The uniqueness and the coexistence of the solutions are illustrated in Figure 2.16.

Proof. We begin with $K_L > K_c > K_R$. Since $K_L > K_c$, the condition $\psi\left(h_{K_L}^{sup}(x_R)\right) < h_R$ implies $\psi\left(h_{K_c}^{sup}(x_R)\right) < h_R$. Hence, the second condition for the existence of the solution with two shocks is verified. Moreover, for $Z(x_L) < Z(x_R)$ there exists a unique point $\tilde{x} \in]x_L, x_0[$ where $Z(\tilde{x}) = Z(x_R)$ then,

$$\psi\left(h_{K_L}^{sup}(\tilde{x})\right) = \psi\left(h_{K_L}^{sup}(x_R)\right) < h_{K_c}^{sub}(x_R) = h_{K_c}^{sub}(\tilde{x}).$$

Therefore, $f(\tilde{x})$ with f defined in (2.23) is positive. Hence, there exists a unique $x_{shockL} \in]\tilde{x}, x_0[$ verifying $f(x_{shockL}) = 0$, see Figure 2.13. Now, for $K_L > K_R > K_c$ suppose that the solution with one shock at right exists, i.e $\psi\left(h_{K_L}^{sup}(x_R)\right) < h_R$ and $x_{shock} \in]x_0, x_R[$. Thus, there exists a unique point $x_{shockL} \in]x_L, x_0[$ such that $Z(x_{shockL}) = Z(x_{shockR})$ leading to $f(x_{shockL}) = 0$,

2.3. (NON) EXISTENCE AND (NON) UNIQUENESS OF THE MOVING STEADY STATES DEPENDING ON

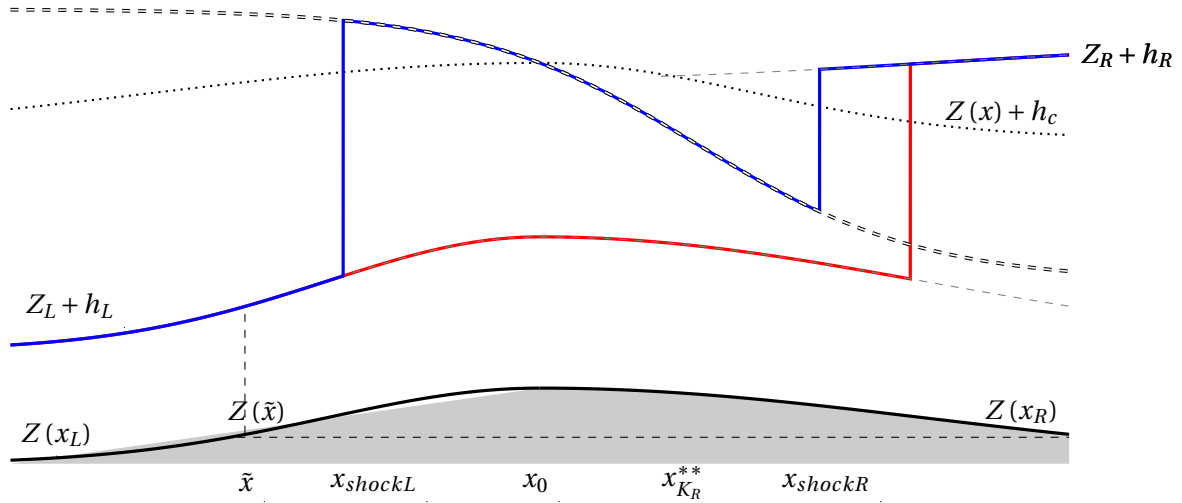


Figure 2.13: Steady state solutions for the supercritical boundary conditions at the inlet and subcritical boundary conditions at the outlet when $K_L > K_c > K_R$ and $Z(x_L) < Z(x_R) = Z(\tilde{x})$.

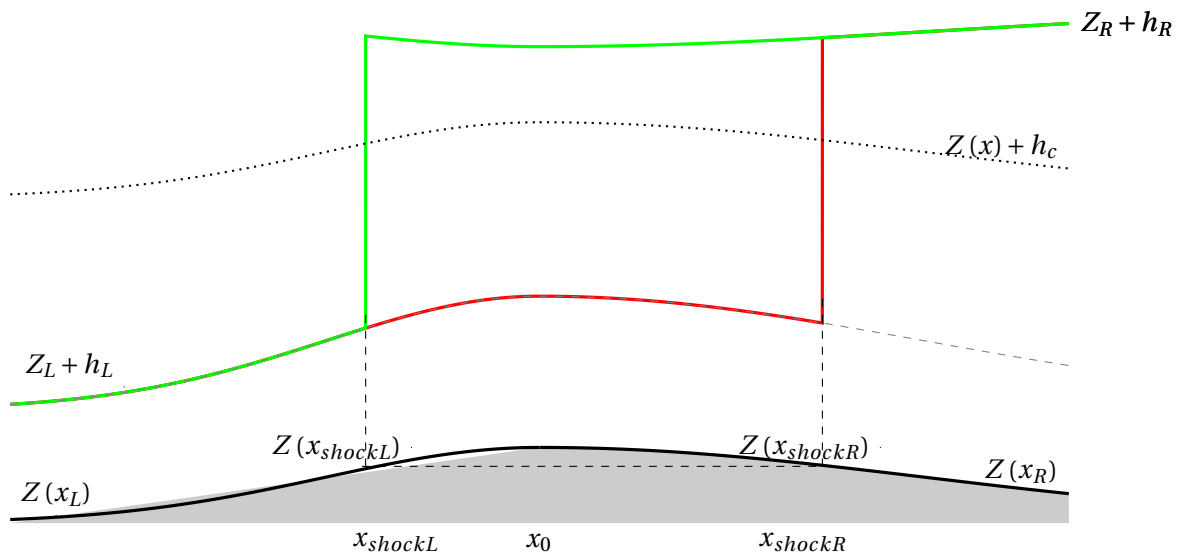


Figure 2.14: Steady state solutions for the supercritical boundary conditions at the inlet and subcritical boundary conditions at the outlet when $K_L > K_R > K_c$ and $Z(x_L) < Z(x_R)$

see Figure 2.14. Hence, there exists a shock on the left of the bump too, see Proposition 13. □

Corollary 3. *Let Z verify Hypothesis 1. For $M > 0$, $S \in \mathbb{R}$, $h_L < h_c$ fixed at the inlet and $h_R > h_c$ fixed at the outlet. For $Z(x_L) > Z(x_R)$*

- *If $K_L > K_c > K_R$ and if the solution with one shock at right exists and $\psi(h_{K_c}^{sub}(x_L)) < h_L$ then, the solution with two shocks exists too.*
- *If $K_L > K_R > K_c$ and if the solution with one shock at left exists then the solution with one shock at right exists too.*

The uniqueness and the coexistence of the solutions are illustrated in Figure 2.17.

Proof. Here, we focus on the third type of topography where $Z(x_L) > Z(x_R)$. For the case of $K_L > K_c > K_R$, if the solution with one shock at right exists then, $\psi(h_{K_L}^{sup}(x_R)) < h_R$. This condition implies that $\psi(h_{K_c}^{sup}(x_R)) < h_R$ which is the second condition for the existence of the solutions with two shocks. In addition, if $\psi(h_{K_c}^{sub}(x_L)) < h_L$ then, the two conditions for the existence of the solution with two shocks are verified.

Second, for the case of $K_L > K_R > K_c$, we follow the same strategy as done in the proof of Corollary 2 but this time assuming that the shock at left exists to prove that the solution with the shock at right exists too. □

Supercritical outlet boundary conditions

In this section, we focus on the supercritical boundaries on each side of the domain. Three boundary conditions are required at the left of the domain, where we impose the discharge $M > 0$, the shear S and the water height $h(x_L) = h_L < h_c$. We assume that the right boundary condition is also supercritical, i.e $h(x_R) < h_c$ but its value is not prescribed. The three characteristics exit the domain and no boundary condition is imposed at the right.

Proposition 14. *Let Z verify Hypothesis 1. Suppose that $h(x_R) < h_c$. For $M > 0$, $S \in \mathbb{R}$ and the water height $h(x_L) = h_L < h_c$ fixed at the inlet, we have:*

2.3. (NON) EXISTENCE AND (NON) UNIQUENESS OF THE MOVING STEADY STATES DEPENDING ON

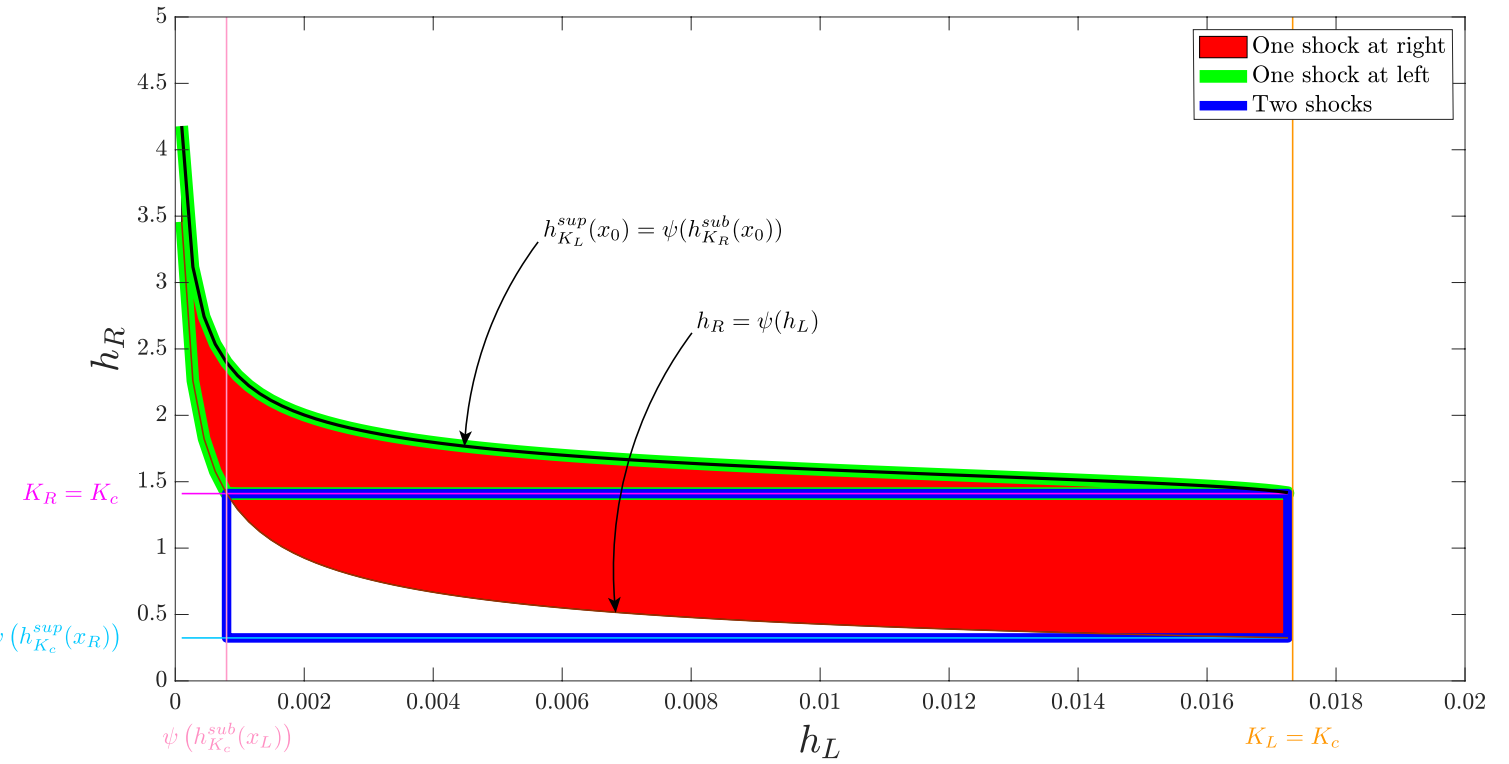


Figure 2.15: Sketch of the different zones of solutions with supercritical boundary condition at the left and subcritical boundary condition at the right for $M = 0.1, S = 1, g = 9.81$ and $Z(x_L) = Z(x_R)$.

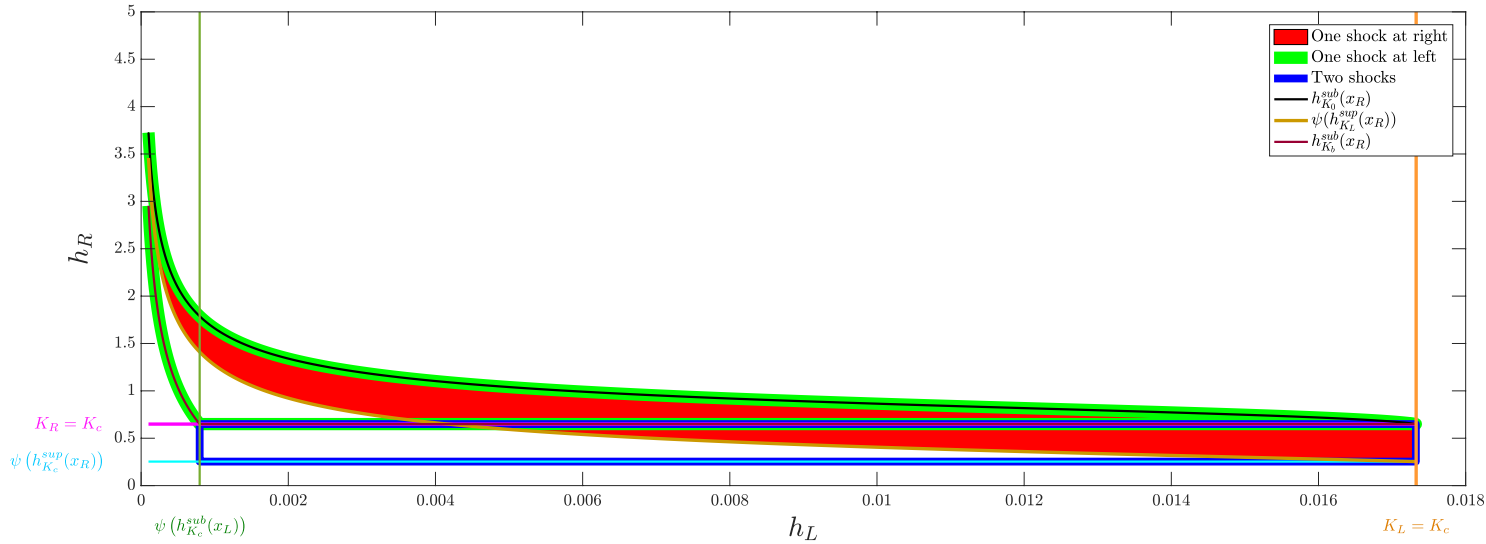


Figure 2.16: Sketch of the different zones of solutions with supercritical boundary condition at the left and subcritical boundary condition at the right for $M = 0.1$, $S = 1$, $g = 9.81$ and $Z(x_L) < Z(x_R)$.

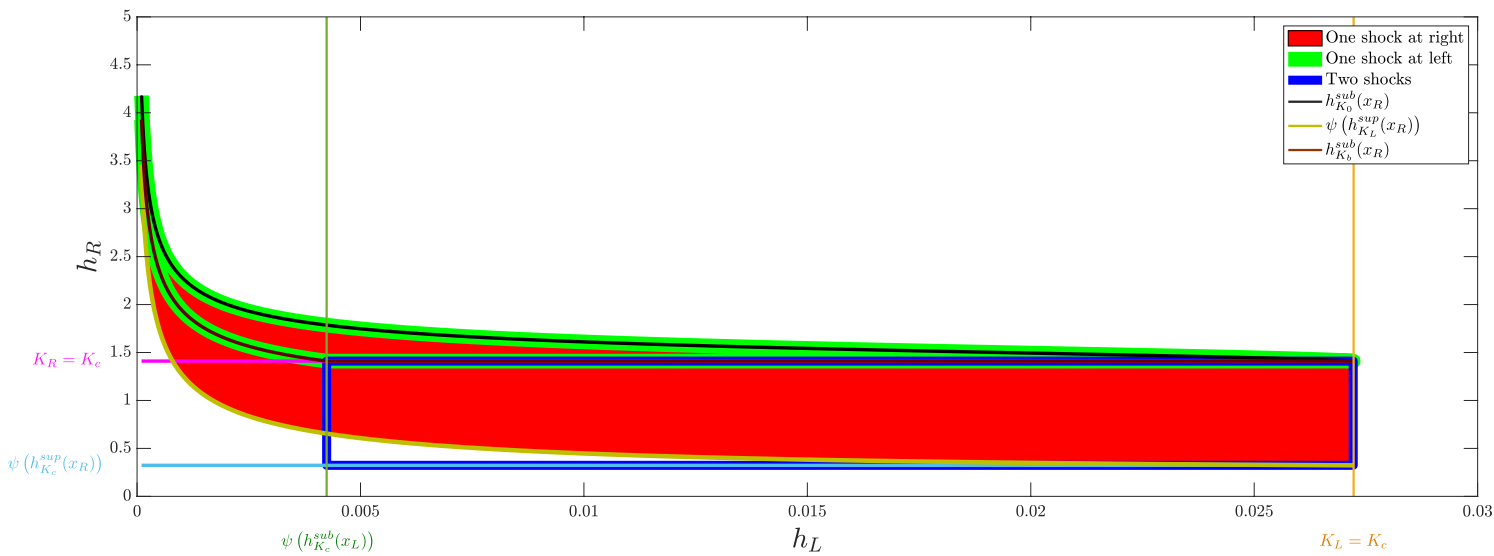


Figure 2.17: Sketch of the different zones of solutions with supercritical boundary condition at the left and subcritical boundary condition at the right for $M = 0.1$, $S = 1$, $g = 9.81$ and $Z(x_L) > Z(x_R)$.

2.3. (NON) EXISTENCE AND (NON) UNIQUENESS OF THE MOVING STEADY STATES DEPENDING ON

- If $h_L > h_{K_c}^{sup}(x_L)$, there is no steady solution of (SW₂) satisfying the supercritical boundary conditions.
- If $h_L < h_{K_c}^{sup}(x_L)$ then, $h_{K_L}^{sup}$ is a C^1 regular steady solution of (SW₂). This solution is called supercritical everywhere.
- If $h_L < h_{K_c}^{sup}(x_L)$ and $\psi\left(h_{K_c}^{sub}(x_L)\right) < h_L$ then, there exists a unique $x_{shock} \in]x_L, x_0[$ such that

$$h(x) = \begin{cases} h_{K_L}^{sup}(x) & \text{if } x_L \leq x < x_{shock}, \\ h_{K_c}^{sub}(x) & \text{if } x_{shock} < x < x_0, \\ h_{K_c}^{sup}(x) & \text{if } x > x_0. \end{cases} \quad (2.24)$$

is a piecewise C^1 steady state solution of (SW₂) verifying (2.15) and (2.18).

The different solutions are plotted in Figure 2.18.

Proof. First of all, if $h_L < h_{K_c}^{sup}(x_L)$ then $K_L < K_c$ and there is no steady state solution of (SW₂) with supercritical boundary conditions at both sides of the domain, see Lemma 1. According to Lemma 5 the solution may contain at most one shock on each side of the domain. However, since the boundaries at the outlet are also supercritical, there is no possibility that a shock occurs at the right of the domain. In fact, if there is a shock at the right of the bump, then the solution must become supercritical again to attend the boundary conditions. But, this is not possible on $]x_0, x_R[$, see Lemma 3 and Proposition 8.

We start with the first type of solution where there is no shock at the left of the bump. $K_L > K_c$ hence, according to Proposition 5 the function $x \mapsto h_{K_L}^{sup}(x)$ is a C^1 supercritical solution of (SSW₂) verifying the supercritical boundary conditions. Now, if the solution contains a shock at the left of the bump then, the solution has the form (2.24) For the existence and the uniqueness of the shock on $[x_L, x_0]$ we should necessarily have $\psi\left(h_{K_c}^{sub}(x_L)\right) < h_L$. We recall the function f defined in (2.23) and we follow the same strategy done in the proof of Proposition 12. We prove that $f(x_L) < 0$ and $f(x_0) > 0$ thus, there exists a point x_{shock} such that $f(x_{shock}) = 0$. The function f is strictly decreasing on that interval. As a consequence, the point x_{shock} is unique. □

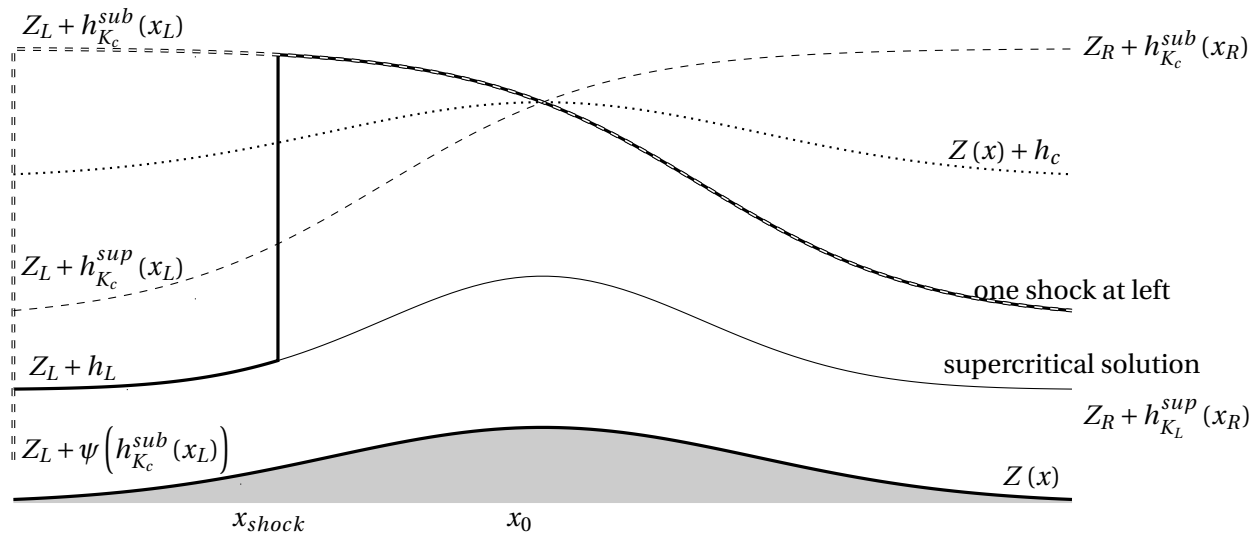


Figure 2.18: General steady states with supercritical boundary conditions at both sides of the domain

Chapter 3

Numerical schemes for the homogeneous model

In this chapter, we propose a numerical method for the resolution of the homogeneous Shallow-water model with two velocities (SW_2^H)

$$\begin{cases} \partial_t h + \partial_x(h\bar{u}) & = 0, \\ \partial_t(h\bar{u}) + \partial_x(h(\bar{u}^2 + \hat{u}^2) + \frac{g}{2}h^2) & = 0, \\ \partial_t \hat{u} + \partial_x(\bar{u}\hat{u}) & = 0. \end{cases} \quad (SW_2^H)$$

The model can be written under the following conservative form

$$\partial_t U + \partial_x F(U) = 0, \quad (3.1)$$

where

$$U = \begin{pmatrix} h \\ h\bar{u} \\ \hat{u} \end{pmatrix} \quad \text{and} \quad F(U) = \begin{pmatrix} h\bar{u} \\ h(\bar{u}^2 + \hat{u}^2) + \frac{g}{2}h^2 \\ \bar{u}\hat{u} \end{pmatrix}.$$

The system is completed by the initial value problem

$$U(0, x) = U_0(x),$$

and by Neumann boundary conditions. For $h > 0$, the homogeneous (SW_2^H) system is strictly hyperbolic with the following eigenvalues

$$\lambda_1^E = \bar{u} - \sqrt{gh + 3\hat{u}^2}, \quad \lambda_2^E = \bar{u} \quad \text{and} \quad \lambda_3^E = \bar{u} + \sqrt{gh + 3\hat{u}^2}. \quad (3.2)$$

The characteristic field associated to λ_2^E is linearly degenerate, while the characteristic fields associated to λ_1^E and λ_3^E are genuinely nonlinear. A set of independent k -Riemann invariants, denoted \mathcal{R}_k is given by

$$\begin{aligned}\mathcal{R}_{\lambda_1^E} &= \left\{ \bar{u} + \sqrt{gh + 3\hat{u}^2} + \frac{gh}{\sqrt{3}\hat{u}} \log \left(\sqrt{1 + \frac{3\hat{u}^2}{gh}} + \sqrt{\frac{3}{gh}} \hat{u} \right), \frac{\hat{u}}{h} \right\}, \\ \mathcal{R}_{\lambda_2^E} &= \left\{ \bar{u}, \frac{g}{2} h^2 + h\hat{u}^2 \right\}, \\ \mathcal{R}_{\lambda_3^E} &= \left\{ \bar{u} - \sqrt{gh + 3\hat{u}^2} - \frac{gh}{\sqrt{3}\hat{u}} \log \left(\sqrt{1 + \frac{3\hat{u}^2}{gh}} + \sqrt{\frac{3}{gh}} \hat{u} \right), \frac{\hat{u}}{h} \right\}.\end{aligned}\quad (3.3)$$

The semi space $\{h \geq 0\}$ is an invariant region of (SW_2^H) . The mechanical energy of (SW_2^H) reads

$$E = g \frac{h^2}{2} + \frac{h}{2} (\bar{u}^2 + \hat{u}^2), \quad (3.4)$$

and the associated energy flux is

$$G = \left(gh + \frac{\bar{u}^2 + 3\hat{u}^2}{2} \right) h\bar{u}. \quad (3.5)$$

Smooth solutions of (SW_2^H) satisfy the energy conservation law

$$\partial_t E + \partial_x G = 0$$

whereas discontinuous solutions are selected to satisfy the following energy inequality condition

$$\partial_t E + \partial_x G \leq 0. \quad (3.6)$$

We choose to approximate the solution using the finite volume method for its inherent ability to ensure discrete local conservation property and to approximate discontinuous solutions, see [34, 43, 17, 54]. Our aim in this chapter is to derive finite volume schemes that

- (i) preserve the positivity of the water height
- (ii) preserve the maximum principle on $S = \frac{\hat{u}}{h}$
- (iii) are accurate for the transport process associated to the shear velocity.

We choose to consider Approximate Riemann solvers "ARS", see [17]. These solvers are Godunov-type finite volume schemes where the exact solution of the Riemann problem is replaced by an approximate one. The best known ARS is the well known *HLL* scheme, see [40] for the first description of the scheme and [17] for its interpretation as an ARS. This scheme is based on a two

waves and one intermediate state approximate Riemann solver. The intermediate state of this solver can be computed by using only consistency properties and will be used in the construction of the other solvers. The *HLL* solver is commonly used to approximate the solutions of the Shallow water model and fulfills the stability property (i) and verifies the discrete energy inequality, see [17]. But contrary to the homogeneous shallow water model, the homogeneous shallow water model with two velocities contains an additional wave λ_2^E , which corresponds to the contact wave in the Riemann problem and the *HLL* solver is not accurate around this contact wave. Hence, we will describe two ARS with three waves and two intermediate states. These two solvers are of *HLLC* type, see [17, 55, 54, 23]. These two solvers are proved to fulfill properties (i), (ii) and (iii). We are not able to prove if these solvers verify a discrete energy inequality. However, we propose a numerical strategy on random Riemann problems to test this property. We are able to conclude that the three waves ARS might verify it for the classical shallow water model but not the model with two velocities (*SW*₂).

3.1 Finite volume method

Let us introduce the finite volume framework we will use to propose a numerical approximation of (*SW*₂^H). For a fixed space step Δx , we denote $C_i = \left] x_{i-\frac{1}{2}}, x_{i+\frac{1}{2}} \right[$ the cell of length $\Delta x = x_{i+\frac{1}{2}} - x_{i-\frac{1}{2}}$ where $x_{i+\frac{1}{2}}$ is the x -coordinate of the interface between the cell C_i and C_{i+1} . Each cell is centered at $x_i = x_{i-\frac{1}{2}} + \Delta x/2$ for all $i \in \mathbb{Z}$. The time is discretized using an adaptive time step $t^{n+1} = t^n + \Delta t^n$ with Δt^n satisfying a CFL condition to be described later. U_i^n will denote a computed approximation of the average of $U(x, t)$ at time t^n on the cell C_i . By analogy with the conservation law (3.1) integrated with respect to x and t over the space-time control volume $C_i \times]t^n, t^{n+1}[$, we propose the following finite volume update formula

$$\forall i \in \mathbb{Z}, \forall n \in \mathbb{N} \quad U_i^{n+1} = U_i^n - \frac{\Delta t^n}{\Delta x} \left(\mathcal{F}_{i+\frac{1}{2}}^n - \mathcal{F}_{i-\frac{1}{2}}^n \right), \quad (3.7)$$

where $\mathcal{F}_{i+\frac{1}{2}}^n$ the numerical flux at the interface will be defined later to be an approximation of

$$\frac{1}{\Delta t^n} \int_{t^n}^{t^{n+1}} F \left(U \left(t, x_{i+\frac{1}{2}} \right) \right) dt. \quad (3.8)$$

The initialization of the algorithm can be computed with a piecewise constant approximation of the initial solution

$$\forall i \in \mathbb{Z} \quad U_i^0 = \frac{1}{\Delta x} \int_{x_{i-\frac{1}{2}}}^{x_{i+\frac{1}{2}}} U_0(x) dx. \quad (3.9)$$

The issue remains in how to compute the numerical flux at the interfaces. For the first order schemes we consider here a function \mathcal{F} depending on the two neighboring states

$$\mathcal{F}_{i+\frac{1}{2}}^n = \mathcal{F}(U_i^n, U_{i+1}^n).$$

The first finite-volume scheme was proposed in [35]. Godunov observed that since the cell averages U_i^n are constant in each cell C_i , they define at each cell interface $x_{i+\frac{1}{2}}$ and on the interval $]t^n, t^{n+1}]$ a Riemann problem

$$\begin{cases} \partial_t U + \partial_x F(U) = 0 \\ U(t^n, x) = \begin{cases} U_L & \text{if } x < x_{i+\frac{1}{2}} \\ U_R & \text{if } x \geq x_{i+\frac{1}{2}} \end{cases} \end{cases} \quad (3.10)$$

These Riemann problems do not interact on the interval $]t^n, t^{n+1}]$ if the time step Δt^n is chosen sufficiently small to ensure that the waves emanating from the interface $x_{i+\frac{1}{2}}$ remain in the interval $[x_i, x_{i+1}]$ which is always possible since in hyperbolic problems, information travels with a finite speed. Let $U_r(\frac{x}{t}, U_L, U_R)$ be the solution of the exact Riemann problem associated to (3.10). For (SW₂^H), this solution was computed in [1]. At time t^{n+1} , it is possible to construct an approximation of the solution on the whole space by merging the solution of each Riemann problem on subdomain around each interface

$$U_{l,r}(t^{n+1}, x) = U_r\left(\frac{x - x_{i+\frac{1}{2}}}{\Delta t^n}, U_i^n, U_{i+1}^n\right) \text{ for } x \in [x_i, x_{i+1}]. \quad (3.11)$$

Then we obtain a piecewise constant approximation U_i^{n+1} at time t^{n+1} by computing

$$U_i^{n+1} = \frac{1}{\Delta x} \int_{x_{i-\frac{1}{2}}}^{x_{i+\frac{1}{2}}} U_{l,r}(t^{n+1}, x) dx.$$

which, using (3.11) reads

$$U_i^{n+1} = \frac{1}{\Delta x} \int_0^{\frac{\Delta x}{2}} U_r\left(\frac{x}{\Delta t^n}, U_{i-1}^n, U_i^n\right) dx + \frac{1}{\Delta x} \int_{-\frac{\Delta x}{2}}^0 U_r\left(\frac{x}{\Delta t^n}, U_i^n, U_{i+1}^n\right) dx. \quad (3.12)$$

Note that (3.12) is indeed a finite volume scheme since it can be written under the flux form (3.7) with the following numerical flux, see [34]

$$\mathcal{F}(U_i^n, U_{i+1}^n) = F(U_r(0, U_i^n, U_{i+1}^n)).$$

The Godunov's scheme relies on the knowledge of the exact solution of the Riemann problem. For the shallow water model with two velocities (SW_2^H), computing the exact solution of the Riemann problem at each interface and for each time step is costly since it implies a fix point algorithm, see [1]. Moreover, it can not be extended to the case with topography that we consider in the next chapter. So we will consider approximate Riemann solvers as an alternative way to define the numerical fluxes, see [42, 17, 54]. The main idea of these ARS is to replace the exact solution of the Riemann problem by an approximate solution denoted $\tilde{U}(\frac{x}{t}, U_L, U_R)$. The considered approximated Riemann solvers are constructed on N discontinuities of speed λ_j separating $(N + 1)$ constant states $\tilde{U}_{j+\frac{1}{2}}(t, x)$:

$$\tilde{U}\left(\frac{x}{t}, U_L, U_R\right) = \begin{cases} U_{\frac{1}{2}} = U_L & \text{if } \frac{x}{t} < \lambda_1, \\ \tilde{U}_{j+\frac{1}{2}} & \text{if } \lambda_j < \frac{x}{t} < \lambda_{j+1} \text{ for } j = 1, \dots, N-1, \\ U_{N+\frac{1}{2}} = U_R & \text{if } \frac{x}{t} > \lambda_N. \end{cases} \quad (3.13)$$

The update at time t^{n+1} is then defined, as before, by

$$U_i^{n+1} = \frac{1}{\Delta x} \int_0^{\frac{\Delta x}{2}} \tilde{U}\left(\frac{x}{\Delta t^n}, U_{i-1}^n, U_i^n\right) dx + \frac{1}{\Delta x} \int_{-\frac{\Delta x}{2}}^0 \tilde{U}\left(\frac{x}{\Delta t^n}, U_i^n, U_{i+1}^n\right) dx.$$

Here also a flux form (3.7) can be associated to this strategy as it will be exhibited later.

3.2 Stability and consistency

In order to ensure stability and consistency properties, the approximate Riemann solver has to satisfy three properties, see [17, 40]:

1. The external waves λ_1 and λ_N of the approximated solution have to be faster than the external wave speed λ_1^E and λ_3^E of the exact solution (3.2). To satisfy this property, following [17, Section 2.4.3], we choose $\lambda_1 = \lambda_L$ and $\lambda_N = \lambda_R$ with

$$\begin{aligned} \lambda_L &= \min(\bar{u}_L - c_L, \bar{u}_R - c_R), \\ \lambda_R &= \max(\bar{u}_L + c_L, \bar{u}_R + c_R), \end{aligned} \quad (3.14)$$

where $c_X = \sqrt{gh_X + 3\hat{u}_X^2}$ denotes the sound speed with X referring to the indexes L or R , see [1]. These external waves will be used to construct all the solvers. Other choices of external waves celerity are possible, see [54, Chap 10.5].

2. The time step has to satisfy the following CFL condition

$$\max_i \left(|\lambda_{L,i+\frac{1}{2}}^n|, |\lambda_{R,i+\frac{1}{2}}^n| \right) \Delta t^n \leq \frac{\Delta x}{2}, \quad (3.15)$$

which prevents the waves from interacting during the time step.

3. According to [17, Def 2.1], the approximate Riemman solver $\tilde{U}(\frac{x}{t}, U_L, U_R)$ has to satisfy the consistency relation

$$\tilde{U}\left(\frac{x}{t}, U, U\right) = U, \quad \forall x \in [x_i, x_{i+1}] \quad \text{and} \quad \forall t \in]t^n, t^{n+1}]. \quad (3.16)$$

Moreover, in the sense of Harten and Lax in [40, Thm 3.1] the consistency property

$$\frac{1}{\Delta x} \int_{-\frac{\Delta x}{2}}^{\frac{\Delta x}{2}} \tilde{U}\left(\frac{x}{\Delta t^n}, U_L, U_R\right) dx = \frac{1}{\Delta x} \int_{-\frac{\Delta x}{2}}^{\frac{\Delta x}{2}} U_r\left(\frac{x}{\Delta t^n}, U_L, U_R\right) dx, \quad (3.17)$$

ensures the conservativity identity

$$\mathcal{F}_L(U_L, U_R) = \mathcal{F}_R(U_L, U_R) \quad (3.18)$$

where

$$\mathcal{F}_L(U_L, U_R) = F(U_L) + \sum_{\lambda_j \leq 0} \lambda_j \left(\tilde{U}_{j+\frac{1}{2}} - \tilde{U}_{j-\frac{1}{2}} \right),$$

and

$$\mathcal{F}_R(U_L, U_R) = F(U_R) - \sum_{\lambda_j \geq 0} \lambda_j \left(\tilde{U}_{j+\frac{1}{2}} - \tilde{U}_{j-\frac{1}{2}} \right).$$

This allows us to define the flux form (3.7) of the solver with

$$\mathcal{F}_{i+\frac{1}{2}}^n = \mathcal{F}(U_i^n, U_{i+1}^n) = \mathcal{F}_L(U_i^n, U_{i+1}^n) = \mathcal{F}_R(U_i^n, U_{i+1}^n), \quad (3.19)$$

In fact, since the left hand side of (3.17) reads

$$\begin{aligned} \frac{1}{\Delta x} \int_{-\frac{\Delta x}{2}}^{\frac{\Delta x}{2}} \tilde{U}\left(\frac{x}{\Delta t^n}, U_L, U_R\right) dx &= \frac{U_L + U_R}{2} + \frac{\Delta t^n}{\Delta x} (\lambda_1 U_L - \lambda_N U_R) \\ &\quad + \frac{\Delta t^n}{\Delta x} \sum_{j=1}^{N-1} \tilde{U}_{j+\frac{1}{2}} (\lambda_{j+1} - \lambda_j) \\ &= \frac{U_L + U_R}{2} - \frac{\Delta t^n}{\Delta x} \sum_{j=1}^N \lambda_j \left(\tilde{U}_{j+\frac{1}{2}} - \tilde{U}_{j-\frac{1}{2}} \right), \end{aligned}$$

and the right hand side reads

$$\frac{1}{\Delta x} \int_{-\frac{\Delta x}{2}}^{\frac{\Delta x}{2}} U_r \left(\frac{x}{\Delta t^n}, U_L, U_R \right) dx = \frac{U_L + U_R}{2} - \frac{\Delta t^n}{\Delta x} (F(U_R) - F(U_L)),$$

the consistency relation (3.17) reads

$$F(U_R) - F(U_L) = \sum_{j=1}^N \lambda_j \left(\tilde{U}_{i+\frac{1}{2}} - \tilde{U}_{i-\frac{1}{2}} \right). \quad (3.20)$$

which implies (3.18). Finally, (3.16) and (3.19) imply the classical consistency relation for the numerical flux, see [17, Prop 2.2]

$$\mathcal{F}(U, U) = F(U).$$

In the following we will construct three Approximate Riemann Solvers:

- the well known *HLL* solver [40], see also [17].
- a scheme named *HLL** where $(h, h\bar{u})$ are computed using the *HLL* scheme but $S = \frac{\hat{u}}{h}$ is updated using an upwind strategy, see [17]. We then prove that the *HLL** scheme can be seen as a 3-waves ARS for a particular choice of the internal wave celerity and additional relations on the internal wave.
- a 3-waves ARS named *HLL \bar{u}* that is obtained for a more suitable choice of additional relations on the internal wave. This solver is proved to be identical to a solver described in [17] which is an HLLC-type scheme, see [54].

Throughout this chapter, we assume h_L and h_R are non-negative and we will prove that the solution of the ARS remains non-negative.

3.3 *HLL* approximate Riemann solver

The *HLL* solver was first introduced by Harten, Lax and van Leer in [40]. This approximate Riemann solver consists of three constant states separated by two discontinuities. In that case (3.13) reads

$$\tilde{U}_{HLL} \left(\frac{x}{t}, U_L, U_R \right) = \begin{cases} U_L & \text{if } \frac{x}{t} < \lambda_L, \\ U_{HLL} & \text{if } \lambda_L < \frac{x}{t} < \lambda_R, \\ U_R & \text{if } \frac{x}{t} > \lambda_R. \end{cases}$$

where $U_{HLL} = (h_{HLL}, h_{HLL}\bar{u}_{HLL}, \hat{u}_{HLL})$. The consistency relations (3.20) are sufficient to entirely compute the intermediate state U_{HLL} which reads under vector form

$$U_{HLL} = \frac{\lambda_R U_R - \lambda_L U_L}{\lambda_R - \lambda_L} - \frac{F(U_R) - F(U_L)}{\lambda_R - \lambda_L},$$

and component by component

$$\begin{cases} h_{HLL} &= \frac{[h(\lambda - \bar{u})]}{[\lambda]}, \\ h_{HLL}\bar{u}_{HLL} &= \frac{[\lambda h\bar{u} - h(\bar{u}^2 + \hat{u}^2) - \frac{g}{2}h^2]}{[\lambda]}, \\ \hat{u}_{HLL} &= \frac{[\hat{u}(\lambda - \bar{u})]}{[\lambda]}. \end{cases} \quad (\text{HLL})$$

where $[X] = X_R - X_L$.

According to (3.19), the *HLL* numerical flux is defined by

$$\mathcal{F}_{HLL}(U_L, U_R) = \begin{cases} F(U_L) & \text{if } \lambda_L > 0, \\ \frac{\lambda_R F(U_L) - \lambda_L F(U_R)}{\lambda_R - \lambda_L} - \frac{\lambda_L \lambda_R}{\lambda_R - \lambda_L} (U_R - U_L) & \text{if } \lambda_L < 0 < \lambda_R, \\ F(U_R) & \text{if } \lambda_R < 0. \end{cases} \quad (\mathcal{F}_{HLL})$$

In the next proposition, we prove that the *HLL* approximate solver preserves the positivity of the water heights.

Proposition 15. *Assume h_L and h_R to be positive and the characteristic velocities defined in (3.14). Then, the intermediate state h_{HLL} in (HLL) is positive.*

Proof. We can deduce from the definition of the characteristic velocities (3.14) that if $h_L > 0$ or $h_R > 0$ then $\lambda_R - \lambda_L > 0$. Therefore, the expression of h_{HLL} in (HLL) allows us to deduce that h_{HLL} is positive if and only if the numerator is positive. This numerator can be written as

$$[h(\lambda - u)] = h_R(\lambda_R - \bar{u}_R) + h_L(\bar{u}_L - \lambda_L) \geq h_R c_R + h_L c_L > 0.$$

If h_L and h_R are positive hence, h_{HLL} is positive. \square

We prove as well that the *HLL* scheme verifies the maximum principle on S .

Proposition 16. *For a any choice of the external waves λ_L and λ_R , the *HLL* scheme satisfies the maximum principle on S .*

Proof. Using the update (3.12) for the HLL scheme, in the case of a general approximate Riemann solver, the finite volume scheme can be written as

$$\begin{aligned}
U_i^{n+1} &= \left(1 - \frac{\Delta t^n}{\Delta x} \left(\lambda_{N+1, i-\frac{1}{2}}^+ - \lambda_{1, i+\frac{1}{2}}^-\right)\right) U_i^n \\
&+ \frac{\Delta t^n}{\Delta x} \lambda_{1, i-\frac{1}{2}}^+ U_{i-1}^n - \frac{\Delta t^n}{\Delta x} \lambda_{N+1, i+\frac{1}{2}}^- U_{i+1}^n \\
&+ \frac{\Delta t^n}{\Delta x} \sum_{k=1}^N \left(\lambda_{k+1, i-\frac{1}{2}}^+ - \lambda_{k, i-\frac{1}{2}}^+\right) U_{k^*, i-\frac{1}{2}} \\
&+ \frac{\Delta t^n}{\Delta x} \sum_{k=1}^N \left(\lambda_{k+1, i+\frac{1}{2}}^- - \lambda_{k, i+\frac{1}{2}}^-\right) U_{k^*, i+\frac{1}{2}},
\end{aligned} \tag{3.21}$$

such that $\lambda_k^- = \min(0, \lambda_k)$, $\lambda_k^+ = \max(0, \lambda_k)$ and U_{k^*} is the intermediate state separated by the waves λ_{k+1} and λ_k for $k \in \{1, \dots, N\}$.

Relation (3.21) applies for h_i^{n+1} and \hat{u}_i^{n+1} . For the HLL scheme, we have only one intermediate state, i.e $N = 1$. Hence, h_i^{n+1} can be written as

$$h_i^{n+1} = \sum \alpha_k \tilde{h}_k$$

where \tilde{h}_k can take the values $h_{HLL, i-\frac{1}{2}}$ or $h_{HLL, i+\frac{1}{2}}$ or h_j^n for $j \in \{i-1, i, i+1\}$ and α_k represents respectively the coefficient of \tilde{h}_k in (3.21). The coefficients α_k are positive due to the CFL condition (3.6) and the order of the waves. Moreover, for all k , the water heights \tilde{h}_k are positive too. Similarly, \hat{u}_i^{n+1} can be written as

$$\hat{u}_i^{n+1} = \sum \alpha_k \tilde{u}_k$$

where $\tilde{u}_k = \tilde{h}_k \tilde{S}_k$ such that \tilde{S}_k can take the values $S_{HLL, i-\frac{1}{2}}$ or $S_{HLL, i+\frac{1}{2}}$ or S_j^n for $j \in \{i-1, i, i+1\}$. According to the intermediate states (HLL), we have

$$S_{HLL} = \frac{\hat{u}_{HLL}}{h_{HLL}} = \frac{S_R h_R (\lambda_R - \bar{u}_R) + S_L h_L (\bar{u}_L - \lambda_L)}{h_R (\lambda_R - \bar{u}_R) + h_L (\bar{u}_L - \lambda_L)}.$$

We proved previously that $(\lambda_R - \bar{u}_R) > 0$ and $(\bar{u}_L - \lambda_L) > 0$. Hence, for $h_L > 0$ and $h_R > 0$, S_{HLL} is a convex combination of S_L and S_R . Therefore, $S_{HLL, i-\frac{1}{2}}$ and $S_{HLL, i+\frac{1}{2}}$ are both a convex combination of S_{i-1} , S_i and S_{i+1} .

In addition, for $h_i^{n+1} > 0$, we have

$$S_i^{n+1} = \frac{\hat{u}_i^{n+1}}{h_i^{n+1}} = \frac{\sum \alpha_k \tilde{h}_k \tilde{S}_k}{\sum \alpha_k \tilde{h}_k} \tag{3.22}$$

Since all the coefficients α_k and all the water heights \tilde{h}_k are positive and since \tilde{S}_k is convex combination of S_{i-1} , S_i and S_{i+1} , we can finally conclude that S_i^{n+1}

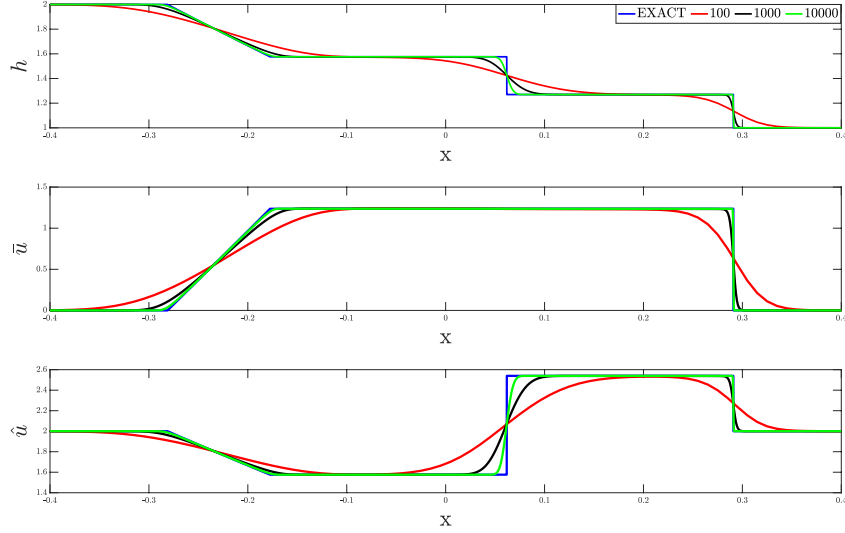


Figure 3.1: Dam Break case: Plots of the variables using the *HLL* scheme for 100, 1000 and 10000 points.

is as a convex combination of S_{i-1} , S_i and S_{i+1} and

$$\frac{\sum \alpha_k \tilde{h}_k \min(S_{i-1}, S_i, S_{i+1})}{\sum \alpha_k \tilde{h}_k} \leq S_i^{n+1} \leq \frac{\sum \alpha_k \tilde{h}_k \max(S_{i-1}, S_i, S_{i+1})}{\sum \alpha_k \tilde{h}_k}.$$

The maximum principle on S is then verified. □

We plot a first test case using the *HLL* scheme where we solve the Riemann problem for a case that contains one rarefaction wave and one shock. The initial conditions are

$$\begin{aligned} U_L &= (2, 0, 2), \\ U_R &= (1, 0, 2). \end{aligned} \tag{3.23}$$

We see that the *HLL* scheme is very diffusive even if it is consistent and stable. A very small space step Δx is needed to obtain an accurate approximation, see Figure 3.1. This is particularly true for the internal wave for which the solution computed with 1000 cells is still very diffusive. The *HLL* scheme does not take into consideration that the Riemann invariant $S = \frac{\hat{u}}{h}$ of the exact Riemann solver jumps only through the middle wave λ_2^E as seen in (3.3). To compute a better approximation of the solution of the homogeneous shallow water model with two velocities (SW_2^H), we propose in the next section an improvement of the *HLL* scheme that takes into account the transport equation on $S = \frac{\hat{u}}{h}$.

3.4 HLL^* approximate Riemann solver

Here, to construct the solver we use the fact that the quantity $S = \frac{\hat{u}}{h}$ jumps only along the intermediate contact discontinuity. Indeed, from (SW_2^H) , we can deduce for regular solutions the transport equation

$$\partial_t S + \bar{u} \partial_x S = 0. \quad (3.24)$$

Hence, a way to improve the HLL scheme is to use it only to update the classical shallow water variables $(h, h\bar{u})$ and to compute the interface mass and momentum fluxes, respectively \mathcal{F}_{HLL}^h and $\mathcal{F}_{HLL}^{h\bar{u}}$. Then, the shear velocity \hat{u} is updated using an upwind strategy as it is done for passive transport, see [17, §2.7]. This upwinding is based on the sign of the mass flux. More precisely, if we consider the flux form of the scheme, the mass and the momentum fluxes are computed using (\mathcal{F}_{HLL}) but the shear velocity flux is computed by

$$\mathcal{F}_{\{HLL, up, i+\frac{1}{2}\}}^{\hat{u}} = \frac{\hat{u}_i^n}{h_i^n} \mathcal{F}_{\{HLL, i+\frac{1}{2}\}}^{h+} + \frac{\hat{u}_{i+1}^n}{h_{i+1}^n} \mathcal{F}_{\{HLL, i+\frac{1}{2}\}}^{h-}, \quad (3.25)$$

where $X^- = \min(0, X)$ and $X^+ = \max(0, X)$.

Lemma 6. *Assume h_L or h_R to be positive. For λ_L and λ_R defined in (3.14), the intermediate state h_{HLL} is positive.*

Proof. As the water height is computed using the HLL strategy, it remains obviously positive as proved in proposition 15. \square

The HLL^* solver improves the precision around the contact discontinuity but while plotting the results of the test case (3.23) we also observe small spurious deviation on \bar{u} , see Figure 3.2. Moreover, the HLL^* solver is not able to maintain a stationary isolated contact discontinuity as exhibited later. In the following, we propose an interpretation of the HLL^* as a 3-waves approximate Riemann solver. It will help us later in the construction of a better approximate Riemann solver.

Interpretation of HLL^* as a 3-waves approximate Riemann solver

In the following we will exhibit that the HLL^* solver can also be seen as a 3-waves solver where we consider that the water depth h and the velocity \bar{u} are

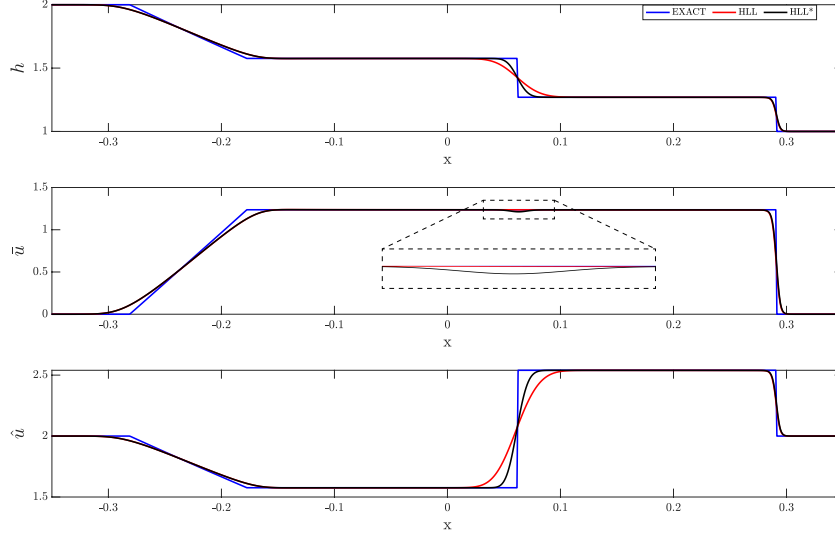


Figure 3.2: Dam Break case: Plots of the variables using the *HLL* and *HLL** scheme for 1000 points.

constant through the internal wave. Let us consider a three waves approximate Riemann solver where $U_L^* = (h_L^*, h_L^* \bar{u}_L^*, \hat{u}_L^*)$ and $U_R^* = (h_R^*, h_R^* \bar{u}_R^*, \hat{u}_R^*)$ are the intermediate states separated by the discontinuity with an unknown velocity $\lambda^* \in [\lambda_L, \lambda_R]$. The approximate Riemann solver reads

$$\tilde{U}_{HLL^*} \left(\frac{x}{t}, U_L, U_R \right) = \begin{cases} U_L & \text{if } \frac{x}{t} < \lambda_L, \\ U_L^* & \text{if } \lambda_L < \frac{x}{t} < \lambda^*, \\ U_R^* & \text{if } \lambda^* < \frac{x}{t} < \lambda_R, \\ U_R & \text{if } \frac{x}{t} > \lambda_R. \end{cases}$$

We are looking for a system composed of seven equations to fully determine the seven unknowns. The consistency relation (3.20) reads

$$\begin{aligned} [h\bar{u}] &= \lambda_L (h_L^* - h_L) + \lambda^* (h_R^* - h_L^*) + \lambda_R (h_R - h_R^*), \\ \left[h(\bar{u}^2 + \hat{u}^2) + \frac{g}{2} h^2 \right] &= \lambda_L (h_L^* \bar{u}_L^* - h_L \bar{u}_L) + \lambda^* (h_R^* \bar{u}_R^* - h_L^* \bar{u}_L^*) + \lambda_R (h_R \bar{u}_R - h_R^* \bar{u}_R^*), \\ [\bar{u}\hat{u}] &= \lambda_L (\hat{u}_L^* - \hat{u}_L) + \lambda^* (\hat{u}_R^* - \hat{u}_L^*) + \lambda_R (\hat{u}_R - \hat{u}_R^*). \end{aligned}$$

which, using the intermediate states of the *HLL* solver (**HLL**) can be written as

$$\begin{cases} \lambda_R h_R^* - \lambda_L h_L^* + \lambda^* (h_L^* - h_R^*) &= (\lambda_R - \lambda_L) h_{HLL}, \\ \lambda_R h_R^* \bar{u}_R^* - \lambda_L h_L^* \bar{u}_L^* + \lambda^* (h_L^* \bar{u}_L^* - h_R^* \bar{u}_R^*) &= (\lambda_R - \lambda_L) h_{HLL} \bar{u}_{HLL}, \\ \lambda_R \hat{u}_R^* - \lambda_L \hat{u}_L^* + \lambda^* (\hat{u}_L^* - \hat{u}_R^*) &= (\lambda_R - \lambda_L) \hat{u}_{HLL}. \end{cases} \quad (3.26)$$

In addition, since the water height and the mean velocity have to be the same as the ones of the HLL solver (HLL), we impose the continuity of h and \bar{u} through the λ^* -wave

$$h_L^* = h_R^* \quad \text{and} \quad \bar{u}_L^* = \bar{u}_R^*. \quad (3.27)$$

Finally, since we want to include the transport equation (3.24) in our ARS, we impose that the quantity $\frac{\hat{u}}{h}$ jumps only through the internal waves and then it is continuous through the external waves λ_L and λ_R

$$\frac{\hat{u}_L^*}{h_L^*} = \frac{\hat{u}_L}{h_L} \quad \text{and} \quad \frac{\hat{u}_R^*}{h_R^*} = \frac{\hat{u}_R}{h_R}. \quad (3.28)$$

Proposition 17. Assume that h_L and h_R are positive and $\frac{\hat{u}_R}{h_R} \neq \frac{\hat{u}_L}{h_L}$. The system (3.26)-(3.27)-(3.28) admits a unique solution $(h_L^*, h_R^*, \bar{u}_L^*, \bar{u}_R^*, \hat{u}_L^*, \hat{u}_R^*, \lambda^*) \in \mathbb{R}^7$ given by

$$\left\{ \begin{array}{l} h_L^* = h_{HLL}, \\ h_R^* = h_{HLL}, \\ \bar{u}_L^* = \bar{u}_{HLL}, \\ \bar{u}_R^* = \bar{u}_{HLL}, \\ \hat{u}_L^* = \hat{u}_L \frac{h_{HLL}}{h_L}, \\ \hat{u}_R^* = \hat{u}_R \frac{h_{HLL}}{h_R}, \\ \lambda^* = \lambda_R - \frac{h_R(\lambda_R - \bar{u}_R)}{h_{HLL}}. \end{array} \right. \quad (HLL^*)$$

Proof. Using the relations (3.27), first two equations of the system (3.26) imply

$$\left\{ \begin{array}{l} h_L^* = h_R^* = h_{HLL}, \\ \bar{u}_L^* = \bar{u}_R^* = \bar{u}_{HLL}. \end{array} \right.$$

Then, equation (3.28) leads to

$$\hat{u}_L^* = \hat{u}_L \frac{h_{HLL}}{h_L} \quad \text{and} \quad \hat{u}_R^* = \hat{u}_R \frac{h_{HLL}}{h_R},$$

and the third equation reads

$$\lambda_R \hat{u}_R \frac{h_{HLL}}{h_R} - \lambda_L \hat{u}_L \frac{h_{HLL}}{h_L} + \lambda^* \left(\hat{u}_L \frac{h_{HLL}}{h_L} - \hat{u}_R \frac{h_{HLL}}{h_R} \right) = \lambda_R \hat{u}_R - \lambda_L \hat{u}_L - \bar{u}_R \hat{u}_R + \bar{u}_L \hat{u}_L,$$

that leads to

$$\lambda^* h_{HLL} \left(\frac{\hat{u}_L}{h_L} - \frac{\hat{u}_R}{h_R} \right) = \frac{\hat{u}_L}{h_L} (\lambda_L h_{HLL} - \lambda_L h_L + \bar{u}_L h_L) + \frac{\hat{u}_R}{h_R} (-\lambda_R h_{HLL} + \lambda_R h_R - \bar{u}_R h_R),$$

First equation of (HLL) implies

$$\lambda_L h_{HLL} - \lambda_L h_L + \bar{u}_L h_L = \lambda_R h_{HLL} - \lambda_R h_R + \bar{u}_R h_R.$$

Hence, if $\frac{\hat{u}_R}{h_R} \neq \frac{\hat{u}_L}{h_L}$

$$\lambda^* = \lambda_L + \frac{h_L}{h_{HLL}} (\bar{u}_L - \lambda_L) = \lambda_R - \frac{h_R}{h_{HLL}} (\lambda_R - \bar{u}_R).$$

□

Remark 3. If $\frac{\hat{u}_R}{h_R} = \frac{\hat{u}_L}{h_L}$, we get $\hat{u}_L^* = \hat{u}_R^* = \hat{u}_{HLL}$ and we choose

$$\lambda^* = \lambda_R - \frac{h_R}{h_{HLL}} (\lambda_R - \bar{u}_R).$$

Then, relations (HLL*) are then valid for all cases.

We supposed that $\lambda_L < \lambda^* < \lambda_R$ in order to write the relations (3.26). Now, we have to prove that this is true.

Proposition 18. Assume that h_L and h_R are positive, then $\lambda_L < \lambda^* < \lambda_R$.

Proof. In proposition (15) we proved that h_{HLL} is positive. Definition (3.14) leads to $\lambda_R - \bar{u}_R > 0$ and $\bar{u}_L - \lambda_L > 0$. Hence,

$$\begin{aligned} \lambda_R - \lambda^* &= \lambda_R - \lambda_R + \frac{h_R (\lambda_R - \bar{u}_R)}{h_{HLL}} \\ &= \frac{h_R (\lambda_R - \bar{u}_R)}{h_{HLL}} > 0. \end{aligned}$$

In the same way

$$\begin{aligned} \lambda^* - \lambda_L &= \lambda_L + \frac{h_L}{h_{HLL}} (\bar{u}_L - \lambda_L) - \lambda_L \\ &= \frac{h_L (\bar{u}_L - \lambda_L)}{h_{HLL}} > 0. \end{aligned}$$

□

Remark 4. We note that for dry areas, i.e $h = 0$ we impose $\bar{u} = 0$ and $\hat{u} = 0$. Hence, if $h_L = 0$ and $h_R \neq 0$, we have $\lambda^* = \lambda_L$ and we retrieve the HLL scheme. Similarly, if $h_R = 0$ and $h_L \neq 0$, we have $\lambda^* = \lambda_R$ and then we also retrieve the HLL scheme.

It remains to prove that the two strategies, namely the "HLL on (h, \bar{u}) and upwind on S " strategy and the 3-waves ARS HLL* lead to the same formula to compute U_i^{n+1} from U_i^n . Since the water height and the mean velocity intermediate state are equal for both strategies then, it is clear that they define the same update for the water height and mean velocity. It remains to prove that the update for the shear velocity is also the same for both strategies. To do that, we will prove that the shear flux $\mathcal{F}_{\{HLL,up\}}^{\hat{u}}$ computed by the upwind strategy (3.25) is equal to the shear flux $\mathcal{F}_{\{HLL^*\}}^{\hat{u}}$ computed by (3.19) for (HLL*) scheme.

Proposition 19. *The shear flux at the interface $\mathcal{F}_{\{HLL,up\}}^{\hat{u}}$ computed by (3.25) is equal to the one computed using (3.19) for (HLL*).*

Proof. Using (3.19) we have

$$\begin{aligned}\mathcal{F}_{\{HLL,i+\frac{1}{2}\}}^h &= h_L \bar{u}_L + \sum_{\lambda_j \leq 0} \lambda_j (h_{j+\frac{1}{2}} - h_{j-\frac{1}{2}}) \\ &= h_R \bar{u}_R - \sum_{\lambda_j \geq 0} \lambda_j (h_{j+\frac{1}{2}} - h_{j-\frac{1}{2}}),\end{aligned}$$

and

$$\begin{aligned}\mathcal{F}_{\{HLL,i+\frac{1}{2}\}}^{\hat{u}} &= \bar{u}_L \hat{u}_L + \sum_{\lambda_j \leq 0} \lambda_j (\hat{u}_{j+\frac{1}{2}} - \hat{u}_{j-\frac{1}{2}}) \\ &= \bar{u}_R \hat{u}_R - \sum_{\lambda_j \geq 0} \lambda_j (\hat{u}_{j+\frac{1}{2}} - \hat{u}_{j-\frac{1}{2}}).\end{aligned}$$

Then , we consider the following cases

- If $\lambda_L \geq 0$ we have $\bar{u}_L \geq 0$, then

$$\mathcal{F}_{\{HLL,i+\frac{1}{2}\}}^h = h_L \bar{u}_L \geq 0,$$

and

$$\begin{aligned}\mathcal{F}_{\{HLL^*,i+\frac{1}{2}\}}^{\hat{u}} &= \bar{u}_L \hat{u}_L = \frac{\hat{u}_L}{h_L} \mathcal{F}_{\{HLL,i+\frac{1}{2}\}}^h \\ &= \mathcal{F}_{\{HLL,up,i+\frac{1}{2}\}}^{\hat{u}}.\end{aligned}$$

- If $\lambda_R \leq 0$ we have $\bar{u}_R \leq 0$, then

$$\mathcal{F}_{\{HLL,i+\frac{1}{2}\}}^h = h_R \bar{u}_R \leq 0,$$

and

$$\mathcal{F}_{\{HLL^*,i+\frac{1}{2}\}}^{\hat{u}} = \bar{u}_R \hat{u}_R = \frac{\hat{u}_R}{h_R} \mathcal{F}_{\{HLL,i+\frac{1}{2}\}}^h = \mathcal{F}_{\{HLL,up,i+\frac{1}{2}\}}^{\hat{u}}.$$

- If $\lambda_L \leq 0 \leq \lambda_R$, supposing $\lambda^* \geq 0$ then

$$\begin{aligned}\mathcal{F}_{\{HLL, i+\frac{1}{2}\}}^h &= h_L \bar{u}_L + \lambda_L (h_{HLL} - h_L) \\ &= h_{HLL} \lambda^* \geq 0.\end{aligned}$$

In addition,

$$\begin{aligned}\mathcal{F}_{\{HLL^*, i+\frac{1}{2}\}}^{\hat{u}} &= \bar{u}_L \hat{u}_L + \lambda_L (\hat{u}_L^* - \hat{u}_L) \\ &= \frac{\hat{u}_L}{h_L} (h_L \bar{u}_L + \lambda_L (h_{HLL} - h_L)) \\ &= \frac{\hat{u}_L}{h_L} \mathcal{F}_{\{HLL, i+\frac{1}{2}\}}^h = \mathcal{F}_{\{HLL, up, i+\frac{1}{2}\}}^{\hat{u}}.\end{aligned}$$

In the same way, supposing $\lambda^* \leq 0$, we also get $\mathcal{F}_{\{HLL^*, i+\frac{1}{2}\}}^{\hat{u}} = \mathcal{F}_{\{HLL, up, i+\frac{1}{2}\}}^{\hat{u}}$.

To sum up, we have proved that both strategies lead to the same computation of the shear flux. \square

In this section, we constructed the HLL^* scheme as an improvement of the HLL scheme. Then, we showed that the HLL^* scheme is a 3-waves approximated Riemann solver. We imposed a constant water height through the internal wave, i.e $h_L^* = h_R^*$ but, unfortunately, this is not the case for the water depth of the exact solution of Riemann problem. In the next section we propose an alternative improvement of the HLL^* scheme.

Proposition 20. *For any choice of the external waves λ_L and λ_R , the HLL^* scheme satisfies the maximum principle on S .*

Proof. We apply the same proof as in Proposition 16 but, in this case we have two intermediate states hence, $N = 2$ and S_{j^*} is equal to S_L or S_R . \square

3.5 $HLL_{\bar{u}}$ approximate Riemann solver

In this section, we propose another three waves approximate Riemann solver. As for the HLL^* solver, the approximate Riemann solver reads

$$\tilde{U}_{HLL_{\bar{u}}}\left(\frac{x}{t}, U_L, U_R\right) = \begin{cases} U_L & \text{if } \frac{x}{t} < \lambda_L, \\ U_L^* & \text{if } \lambda_L < \frac{x}{t} < \lambda^*, \\ U_R^* & \text{if } \lambda^* < \frac{x}{t} < \lambda_R, \\ U_R & \text{if } \frac{x}{t} > \lambda_R. \end{cases}$$

where $U_L^* = (h_L^*, h_L^* \bar{u}_L^*, \hat{u}_L^*)$ and $U_R^* = (h_R^*, h_R^* \bar{u}_R^*, \hat{u}_R^*)$. We still consider the consistency relations

$$\begin{cases} \lambda_R h_R^* - \lambda_L h_L^* + \lambda^* (h_L^* - h_R^*) & = (\lambda_R - \lambda_L) h_{HLL}, \\ \lambda_R h_R^* \bar{u}_R^* - \lambda_L h_L^* \bar{u}_L^* + \lambda^* (h_L^* \bar{u}_L^* - h_R^* \bar{u}_R^*) & = (\lambda_R - \lambda_L) h_{HLL} \bar{u}_{HLL}, \\ \lambda_R \hat{u}_R^* - \lambda_L \hat{u}_L^* + \lambda^* (\hat{u}_L^* - \hat{u}_R^*) & = (\lambda_R - \lambda_L) \hat{u}_{HLL}. \end{cases} \quad (3.29)$$

We also keep three relations that were used to construct the HLL^* scheme, namely the continuity of the mean velocity across the internal wave (3.27) and the continuity of the shear velocity across the external waves (3.28). These relations are in accordance with the Riemann invariants of the exact Riemann problem, see (3.3). The fourth relation used to construct HLL^* , namely the continuity of the water height across the internal waves in (3.27), is not considered here. This last relation will be replaced by imposing that the intermediate velocities are equal to the celerity of the internal wave

$$\bar{u}_L^* = \bar{u}_R^* = \lambda^*. \quad (3.30)$$

This new relation is in agreement with the property of the system since the celerity of the internal wave is equal to \bar{u} , see (3.2).

Let us now determine the value of the intermediate states.

Proposition 21. *Assume that h_L and h_R are positive and $\frac{\hat{u}_R}{h_R} \neq \frac{\hat{u}_L}{h_L}$. The system (3.29), (3.28) and (3.30) admits a unique solution $(h_L^*, h_R^*, \bar{u}_L^*, \bar{u}_R^*, \hat{u}_L^*, \hat{u}_R^*, \lambda^*) \in \mathbb{R}^7$*

given by

$$\left\{ \begin{array}{l} h_L^* = h_L \left(\frac{\lambda_L - \bar{u}_L}{\lambda_L - \bar{u}_{HLL}} \right), \\ h_R^* = h_R \left(\frac{\lambda_R - \bar{u}_R}{\lambda_R - \bar{u}_{HLL}} \right), \\ \bar{u}_L^* = \bar{u}_{HLL}, \\ \bar{u}_R^* = \bar{u}_{HLL}, \\ \hat{u}_L^* = \hat{u}_L \left(\frac{\lambda_L - \bar{u}_L}{\lambda_L - \bar{u}_{HLL}} \right), \\ \hat{u}_R^* = \hat{u}_R \left(\frac{\lambda_R - \bar{u}_R}{\lambda_R - \bar{u}_{HLL}} \right), \\ \lambda^* = \bar{u}_{HLL}. \end{array} \right. \quad (HLL_{\bar{u}})$$

Proof. Using the definition of h_{HLL} in (HLL), the first equation of (3.29) reads

$$h_R^*(\lambda_R - \lambda^*) + h_L^*(\lambda^* - \lambda_L) = h_R(\lambda_R - \bar{u}_R) + h_L(\bar{u}_L - \lambda_L), \quad (3.31)$$

is strictly positive since $\lambda_R > \bar{u}_R$ and $\lambda_L < \bar{u}_L$. The second equation of the same system is equivalent to

$$\lambda^* (h_R^*(\lambda_R - \lambda^*) + h_L^*(\lambda^* - \lambda_L)) = (h_R(\lambda_R - \bar{u}_R) - h_L(\lambda_L - \bar{u}_L)) \bar{u}_{HLL},$$

It follows that $\lambda^* = \bar{u}_{HLL}$. Third equation of (3.29) and (3.28) lead to

$$\frac{\hat{u}_R}{h_R} (h_R^*(\lambda_R - \lambda^*) - h_R(\lambda_R - \bar{u}_R)) + \frac{\hat{u}_L}{h_L} (h_L^*(\lambda^* - \lambda_L) - h_L(\bar{u}_L - \lambda_L)) = 0. \quad (3.32)$$

The linear system (3.31) and (3.32) on (h_L^*, h_R^*) is well posed if $\frac{\hat{u}_R}{h_R} \neq \frac{\hat{u}_L}{h_L}$ and yields the values of h_L^* and h_R^* in $(HLL_{\bar{u}})$. Finally, (3.28) gives \hat{u}_L^* and \hat{u}_R^* and (3.30) gives \bar{u}_L^* and \bar{u}_R^* . \square

Remark 5. For $\frac{\hat{u}_R}{h_R} = \frac{\hat{u}_L}{h_L}$, $(HLL_{\bar{u}})$ is also a solution of the system (3.29)-(3.28) and (3.30).

It remains to prove that $\lambda_L < \lambda^* = \bar{u}_{HLL} < \lambda_R$ is verified.

Proposition 22. Assume that $h_L > 0$ and $h_R > 0$. Let λ_L , λ_R and \bar{u}_{HLL} be defined respectively by (3.14) and (HLL). We get that $\lambda_L < \lambda^* < \lambda_R$.

Proof. We first prove that $\lambda_R - \bar{u}_{HLL}$ is positive. Definitions (HLL) and (3.14) lead to

$$\begin{aligned} \lambda_R - \bar{u}_{HLL} &= \lambda_R - \frac{\lambda_R h_R \bar{u}_R - \lambda_L h_L \bar{u}_L - [h(\bar{u}^2 + \hat{u}^2) + \frac{g}{2} h^2]}{(\lambda_R - \lambda_L) h_{HLL}} \\ &= \frac{\lambda_R (\lambda_R - \lambda_L) h_{HLL} - \lambda_R h_R \bar{u}_R + \lambda_L h_L \bar{u}_L + [h(\bar{u}^2 + \hat{u}^2) + \frac{g}{2} h^2]}{(\lambda_R - \lambda_L) h_{HLL}}. \end{aligned} \quad (3.33)$$

According to (3.14), $\lambda_R - \lambda_L$ is positive. Then, we proved in Proposition 15 that h_{HLL} is positive. Hence, $(\lambda_R - \lambda_L) h_{HLL}$ is always positive. Therefore the positivity of $\lambda_R - \bar{u}_{HLL}$ depends on the positivity of the numerator in (3.33). Let us define

$$P_R(\lambda_L, \lambda_R) := \lambda_R(\lambda_R - \lambda_L) h_{HLL} - \lambda_R h_R \bar{u}_R + \lambda_L h_L \bar{u}_L + \left[h(\bar{u}^2 + \hat{u}^2) + \frac{g}{2} h^2 \right].$$

Using the definition of h_{HLL} in (HLL), it reads

$$\begin{aligned} P_R(\lambda_L, \lambda_R) &= \lambda_R h_R (\lambda_R - \bar{u}_R) + \lambda_R h_L (\bar{u}_L - \lambda_L) - h_R \bar{u}_R (\lambda_R - \bar{u}_R) - h_L \bar{u}_L (\bar{u}_L - \lambda_L) \\ &\quad + h_R \hat{u}_R^2 - h_L \hat{u}_L^2 + \frac{g}{2} h_R^2 - \frac{g}{2} h_L^2 \\ &= h_R (\lambda_R - \bar{u}_R)^2 + h_L (\lambda_R - \bar{u}_L) (\bar{u}_L - \lambda_L) + h_R \hat{u}_R^2 - h_L \hat{u}_L^2 + \frac{g}{2} h_R^2 - \frac{g}{2} h_L^2. \end{aligned}$$

The definition of λ_L and λ_R in (3.14) ensures that $\lambda_R - \bar{u}_R \geq c_R \geq 0$, $\bar{u}_L - \lambda_L \geq c_L \geq 0$ and $\lambda_R - \bar{u}_L \geq c_L \geq 0$. Therefore, using the definition of c_L ,

$$\begin{aligned} P_R(\lambda_L, \lambda_R) &> h_R c_R^2 + h_L c_L^2 + h_R \hat{u}_R^2 - h_L \hat{u}_L^2 + \frac{g}{2} h_R^2 - \frac{g}{2} h_L^2 \\ &> h_R \left(c_R^2 + \hat{u}_R^2 + \frac{g}{2} h_R \right) + h_L \left(2\hat{u}_L^2 + \frac{g}{2} h_L \right). \end{aligned}$$

It follows that $\lambda_R - \bar{u}_{HLL}$ is positive.

In a similar way we prove that $\bar{u}_{HLL} - \lambda_L$ is positive

$$\bar{u}_{HLL} - \lambda_L > \frac{h_L \left(c_L^2 + \hat{u}_L^2 + \frac{g}{2} h_L \right) + h_R \left(2\hat{u}_R^2 + \frac{g}{2} h_R \right)}{(\lambda_R - \lambda_L) h_{HLL}} > 0.$$

Hence, we can finally conclude that $\lambda_L < \lambda^* = \bar{u}_{HLL} < \lambda_R$. \square

It remains now to prove the positivity of the intermediate water heights.

Proposition 23. *Assume that h_L and h_R are positive, then the intermediate water heights h_L^* and h_R^* defined in (HLL $_{\bar{u}}$) are positive.*

Proof. In proposition (22) we established that $\lambda_L < \bar{u}_{HLL} < \lambda_R$. Since $\lambda_R - \bar{u}_R > 0$ and $\bar{u}_L - \lambda_L > 0$, it follows from (HLL $_{\bar{u}}$) that h_L^* and h_R^* are positive if h_L and h_R are positive. \square

Proposition 24. *For any choice of the external waves λ_L and λ_R , the $HLL_{\bar{u}}$ scheme satisfies the following properties:*

- the maximum principle on S ,
- the preservation of the stationary contact discontinuity where $\bar{u} = 0$ and $h\hat{u}^2 + \frac{g}{2}h^2$ is constant.

Proof. To prove that the $HLL_{\bar{u}}$ scheme ($HLL_{\bar{u}}$) satisfies the maximum principle of S , we follow the proof of Proposition 16 considering that, in this case we have two intermediate states hence, $N = 2$ and S_{j^*} is equal to S_L or S_R . Concerning the preservation of the stationary contact discontinuity, for $\bar{u}_L = \bar{u}_R = 0$ we get that $\bar{u}_{HLL} = 0$ and then we can conclude from ($HLL_{\bar{u}}$) that

$$\begin{aligned}\bar{u}_L^* &= \bar{u}_R^* = \lambda^* = 0, \\ h_L^* &= h_L, \\ h_R^* &= h_R, \\ \hat{u}_L^* &= \hat{u}_L, \\ \hat{u}_R^* &= \hat{u}_R.\end{aligned}$$

As a consequence, the stationary contact discontinuity is preserved. □

Remark 6. We can also prove that the ARS used in $HLL_{\bar{u}}$ scheme ($HLL_{\bar{u}}$) is exact on the stationary contact discontinuity even with $\bar{u} = cte \neq 0$ and $h\hat{u}^2 + \frac{g}{2}h^2 = cte$ but the whole scheme is not due the averaging step (3.9).

Remark 7. Note that in [17] a inequality (2.162) is associated to the scheme (2.161). The proof uses the fact that the opposite of the specific energy is a convex function of $(\frac{1}{e}, e)$. It is not the case for the shear S in our model and we are not able to prove a discrete energy inequality.

Remark 8. We mention that the ($HLL_{\bar{u}}$) scheme was also used in the approximation of the Shear shallow water model in [23]. This work was published during this PHD. The authors do not prove any stability properties.

Figure 3.3 shows that the $HLL_{\bar{u}}$ scheme improves the results $HLL_{\bar{u}}$ in comparison with other schemes. In particular, the spurious deviation on \bar{u} disappears.

Remark 9. If $\hat{u}_L = \hat{u}_R = 0$, then $\hat{u}_L^* = \hat{u}_R^* = 0$ and \hat{u} remains equal to zero at the next time step. However, since the water height is discontinuous through λ^* , the intermediate water heights h_L^* and h_R^* are different from h_{HLL} and then we do not retrieve the HLL scheme for the classical shallow water (SW) contrary to the HLL^* solver. But, we retrieve the Siliciu scheme proposed in [17, §2.4.5].

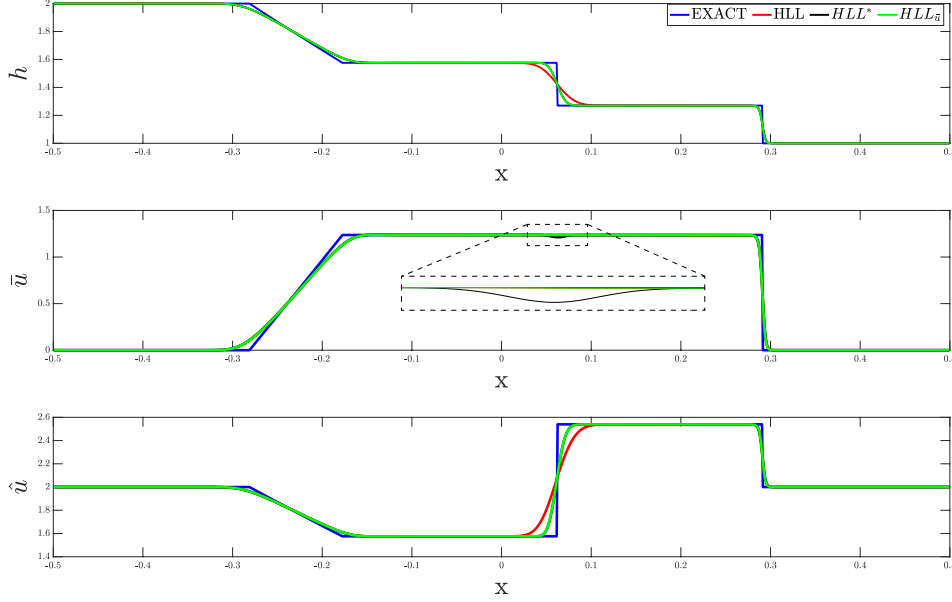


Figure 3.3: Dam Break case: Plots of the variables using HLL , HLL^* and $HLL_{\bar{u}}$ solvers for 1000 grid cells

3.6 Numerical results

In this section, we will illustrate the behavior of the schemes for several Riemann problems introduced in [1]. All these problems contain a contact discontinuity. For each numerical test we will show the differences between the three schemes described before. To ensure that the CFL condition is satisfied, we set

$$\Delta t^n = \alpha_{CFL} \frac{\Delta x}{2\Gamma} \quad , \quad \Gamma = \max_i \left(|\lambda_{L,i+\frac{1}{2}}^n|, |\lambda_{R,i+\frac{1}{2}}^n| \right)$$

with $0 < \alpha_{CFL} \leq 1$. In the following, we set $\alpha_{CFL} = 0.9$.

We compare the solutions computed by the several schemes with the analytical solution of the Riemann problems, see [1]. In addition to that, for a domain discretized with nx cells we compute the L^2 errors using the following expression

$$L^2 = \sqrt{\frac{1}{nx} \sum_{i=1}^{nx} (U_i - U_i^{ex})^2} \quad (3.34)$$

where U_i and U_i^{ex} are respectively the approximate and the exact solutions at the cell C_i and at the physical time t_{end} .

nx	err_{HLL}	$order_{HLL}$	err_{HLL}^*	$order_{HLL}^*$	$err_{HLL_{\bar{u}}}$	$order_{HLL_{\bar{u}}}$
10^2	4.9e-02	-	4.5e-02	-	4.4e-02	-
10^3	2.1e-02	0.37	1.6e-02	0.43	1.6e-02	0.43
10^4	1.08e-02	0.29	7.7e-03	0.33	7.6e-03	0.32
10^5	6e-03	0.25	4.1e-03	0.27	4.2e-03	0.27
10^6	3e-03	0.25	2.2e-03	0.25	2e-03	0.25

Table 3.1: Height error and order of accuracy of the three schemes for the Dam break case

nx	err_{HLL}	$order_{HLL}$	err_{HLL}^*	$order_{HLL}^*$	$err_{HLL_{\bar{u}}}$	$order_{HLL_{\bar{u}}}$
10^2	1.17e-01	-	1.2e-01	-	1.15e-01	-
10^3	3.7e-02	0.54	3.7e-02	0.53	3.6e-02	0.53
10^4	1.1e-02	0.53	1e-02	0.52	1e-02	0.52
10^5	5e-03	0.34	4.2e-03	0.43	4.1e-03	0.4
10^6	2e-03	0.33	1.4e-03	0.35	1.5e-03	0.34

Table 3.2: Mean velocity error and order of accuracy of the three schemes for the Dam break case

3.6.1 Dam break problem

During the construction of the schemes, we presented their behavior on a first test case with one rarefaction and one shock. In addition to the qualitative results of Figure 3.3, we now present the L^2 errors and orders for h , \bar{u} and \hat{u} respectively in Table 3.1, 3.2 and 3.3. The error tables show that the L^2 errors for the HLL solver are around 50% larger than the errors of 3-waves schemes for h and \hat{u} because they are affected by the contact discontinuity whereas the errors of \bar{u} are very close for the three schemes. The three schemes present a very close order of accuracy. This order of accuracy is better for \bar{u} than h and \hat{u} . We retrieve that the convergence is faster on rarefaction or shock than contact discontinuity. For h and \hat{u} , we observe that the order is around 0.25 whereas we should refine more to exhibit the asymptotic order for \bar{u} .

Now, we present another test case with two shocks.

nx	err_{HLL}	$order_{HLL}$	err_{HLL}^*	$order_{HLL}^*$	$err_{HLL_{\bar{u}}}$	$order_{HLL_{\bar{u}}}$
10^2	1.2e-01	-	9.9e-02	-	9e-02	-
10^3	6.1e-02	0.29	4.3e-02	0.35	4.3e-02	0.34
10^4	3.3e-02	0.26	2.3e-02	0.27	2.3e-02	0.27
10^5	1.8e-02	0.25	1.2e-02	0.25	1.2e-02	0.25
10^6	1e-02	0.24	7e-03	0.25	7e-03	0.25

Table 3.3: Standard deviation error and order of accuracy of the three schemes for the Dam break case

nx	err_{HLL}	$order_{HLL}$	err_{HLL}^*	$order_{HLL}^*$	$err_{HLL_{\bar{u}}}$	$order_{HLL_{\bar{u}}}$
10^2	1.5e-01	-	1.4e-01	-	1.1e-01	-
10^3	7.3e-02	0.33	5.5e-02	0.41	5.1e-02	0.36
10^4	3.8e-02	0.27	2.7e-02	0.31	2.5e-02	0.3
10^5	2.1e-02	0.26	1.4e-02	0.28	1.3e-02	0.26
10^6	1.2e-02	0.25	4.1e-03	0.25	4.2e-03	0.25

Table 3.4: Height error and order of accuracy of the three schemes for the two shocks problem § 3.6.2

3.6.2 Two shock case

The initial conditions are

$$\begin{aligned} U_L &= (2, 6, 2), \\ U_R &= (1, -6, 2). \end{aligned}$$

In this test case, the two external waves of the exact solution are shock waves. The numerical simulations in Figure 3.4 present the same characteristic as for the previous test case: *HLL* solver is more diffusive on the contact wave and *HLL** solver presents a small spurious deviation on \bar{u} on this wave. The errors in Table 3.4, 3.5 and 3.6 are a bit larger than for the Dam break problem but the orders of convergence are similar for h and \hat{u} .

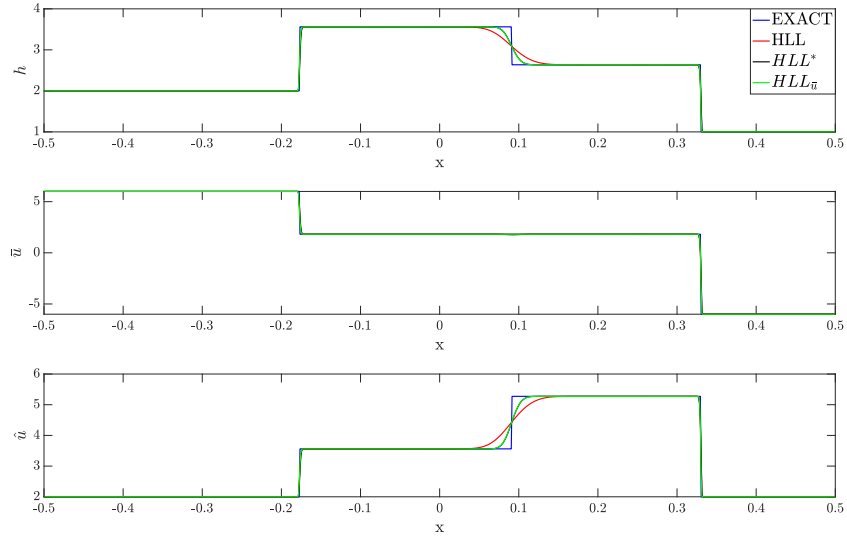


Figure 3.4: The two shock problem § 3.6.2. Plots of the variables using HLL , HLL^* and $HLLC_{\bar{u}}$ solvers for 1000 grid cells

nx	err_{HLL}	$order_{HLL}$	err_{HLL^*}	$order_{HLL^*}$	$err_{HLL_{\bar{u}}}$	$order_{HLL_{\bar{u}}}$
10^2	4.4e-01	-	4.9e-01	-	3.9e-01	-
10^3	1.2e-01	0.53	1.4e-01	0.54	1.1e-01	0.54
10^4	4.8e-02	0.42	5.3e-02	0.42	4.4e-02	0.4
10^5	1.8e-02	0.42	1.8e-02	0.45	1.6e-02	0.44
10^6	1.4e-03	0.44	1.1e-03	0.45	1e-03	0.45

Table 3.5: Mean velocity error and order of accuracy of the three schemes for the two shocks problem § 3.6.2

nx	err_{HLL}	$order_{HLL}$	err_{HLL^*}	$order_{HLL^*}$	$err_{HLL_{\bar{u}}}$	$order_{HLL_{\bar{u}}}$
10^2	2.7e-01	-	2.1e-01	-	1.9e-01	-
10^3	1.3e-01	0.31	9.6e-02	0.38	9.4e-02	0.33
10^4	7.1e-02	0.27	4.9e-02	0.29	4.7e-02	0.28
10^5	3.9e-02	0.25	2.6e-02	0.27	2.5e-02	0.26
10^6	3e-02	0.25	1.6e-02	0.25	1.4e-02	0.25

Table 3.6: Standard deviation error and order of accuracy of the three schemes for the two shocks problem § 3.6.2

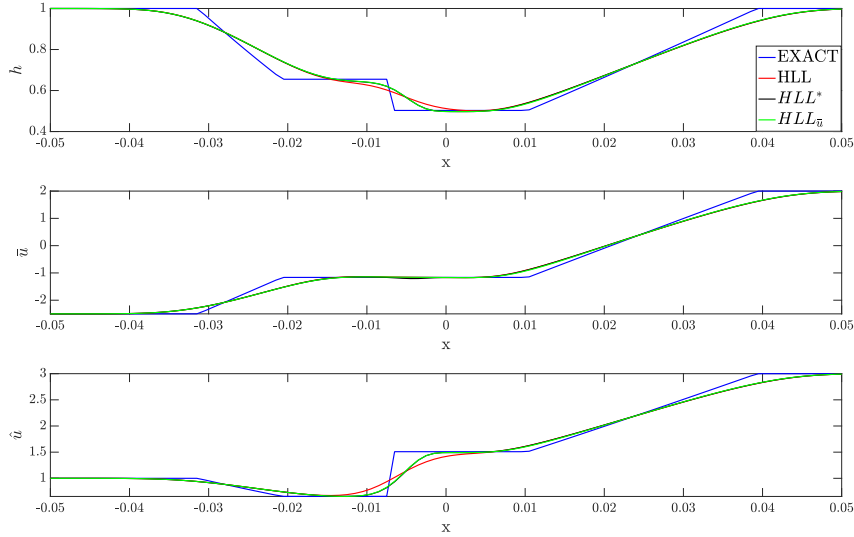


Figure 3.5: The two rarefactions case § 3.6.3. Plots of the variables using HLL , HLL^* and $HLL_{\bar{u}}$ solvers for 1000 grid cells

3.6.3 Two rarefactions case

The initial conditions are

$$\begin{aligned} U_L &= (1, -2.5, 1), \\ U_R &= (1, 2.5, 3). \end{aligned}$$

In this test case, the two external waves of the exact solution are rarefaction waves. Results on Figure 3.5 are similar to the previous one. Errors on Table 3.7, Table 3.8 and 3.9 are, for the finest mesh, ten times smaller than for the two shocks problem § 3.6.2. Moreover, the orders of convergence are much better (around 0.7) for the mean velocity (for which the solutions is here C^0 and piecewise C^1). But, for h and \hat{u} , the orders are almost the same as the two shocks problem due to the presence of the contact discontinuity.

3.6.4 Dam break problem with change of sign on \hat{u}

We plotted in the first three test cases the numerical solutions for Riemann problems with a constant sign of \hat{u} on the left and the right of the domain. In this section, we look for a Riemann problem with initial conditions of different signs on the left and the right of the domain for \hat{u} . More precisely, we consider

nx	err_{HLL}	$order_{HLL}$	err_{HLL}^*	$order_{HLL}^*$	$err_{HLL_{\bar{u}}}$	$order_{HLL_{\bar{u}}}$
10^2	3.6e-02	-	3.8e-012	-	3.8e-02	-
10^3	1.1e-02	0.56	9.7e-03	0.59	9.6e-03	0.59
10^4	3.3e-03	0.47	2.9e-03	0.51	2.9e-03	0.51
10^5	1.5e-03	0.34	1.2e-03	0.39	1.2e-03	0.39
10^6	8e-04	0.26	6e-04	0.28	6e-04	0.28

Table 3.7: Height error and order of accuracy of the three schemes for the two rarefactions problem § 3.6.3

nx	err_{HLL}	$order_{HLL}$	err_{HLL}^*	$order_{HLL}^*$	$err_{HLL_{\bar{u}}}$	$order_{HLL_{\bar{u}}}$
10^2	1.6e-01	-	1.6e-01	-	1.6e-01	-
10^3	4.4e-02	0.57	4.4e-02	0.55	4.3e-02	0.56
10^4	1e-02	0.63	1e-02	0.63	1e-02	0.62
10^5	2.1e-03	0.7	2e-03	0.7	2e-03	0.69
10^6	3e-04	0.73	3e-04	0.73	4e-04	0.73

Table 3.8: Mean velocity error and order of accuracy of the three schemes for the two rarefactions problem § 3.6.3

nx	err_{HLL}	$order_{HLL}$	err_{HLL}^*	$order_{HLL}^*$	$err_{HLL_{\bar{u}}}$	$order_{HLL_{\bar{u}}}$
10^2	1.1e-01	-	1.1e-01	-	1.1e-01	-
10^3	3.3e-02	0.49	3.1e-02	0.55	3e-02	0.55
10^4	1.5e-02	0.35	1.2e-02	0.41	1.2e-02	0.41
10^5	8e-03	0.26	6e-03	0.27	6e-03	0.27
10^6	4e-03	0.25	3e-03	0.25	3.5e-03	0.25

Table 3.9: Standard deviation error and order of accuracy of the three schemes for the two rarefactions problem § 3.6.3

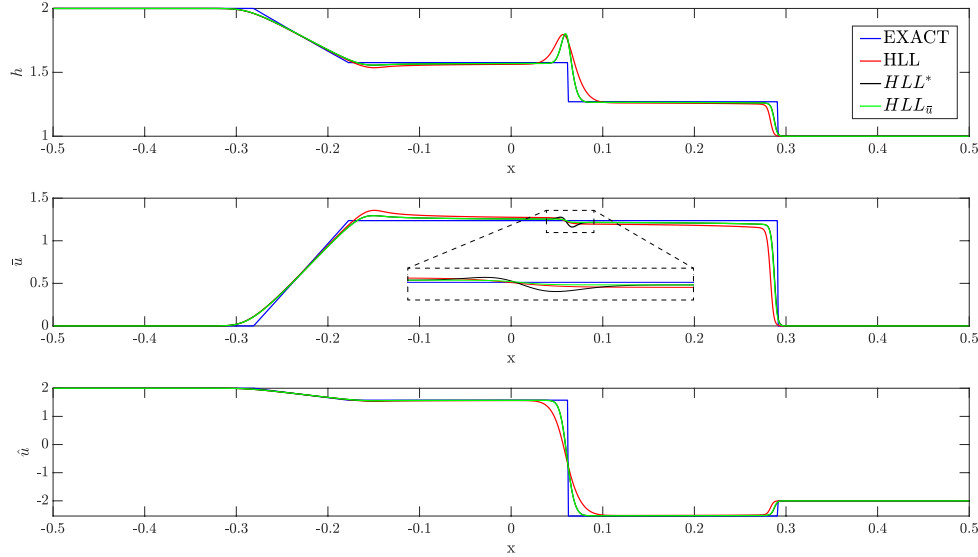


Figure 3.6: Rarefaction/Shock case 2. Plots of the variables using HLL , HLL^* and $HLL_{\bar{u}}$ solvers for 1000 grid cells

a Dam break problem for which \hat{u}_L and \hat{u}_R don't have the same sign and the initial conditions are

$$\begin{aligned} U_L &= (2, 0, 2), \\ U_R &= (1, 0, -2). \end{aligned}$$

In Figure 3.6, we show the numerical results for the three solvers. We can clearly remark when comparing Figure 3.6 and Figure 3.3 that the behavior of the schemes differs when the initial conditions of \hat{u} have not the same sign. We observe a large spurious deviation on h at the contact discontinuity and a small one on \bar{u} for the HLL^* scheme. Moreover, we observe a delay on the position of the numerical shock. This delay on the shock can be explained by the presence of the spurious deviation on h near the contact discontinuity which is a mass gain that has to be removed somewhere else since the scheme is mass conservative. This spurious deviation on h in the numerical results is related to the fact that the numerical approximation of \hat{u} goes from $\hat{u}_L > 0$ to $\hat{u}_R < 0$ through a smooth solution (due to numerical viscosity) that passes then necessarily by zero, see Proposition 25.

Proposition 25. Consider a regular solution that depends only on the variable $z = x - \bar{u}t$ for the Riemann problem associated to (SW_2^H) with a change of sign on \hat{u} . If \hat{u} is monotone then h is not.

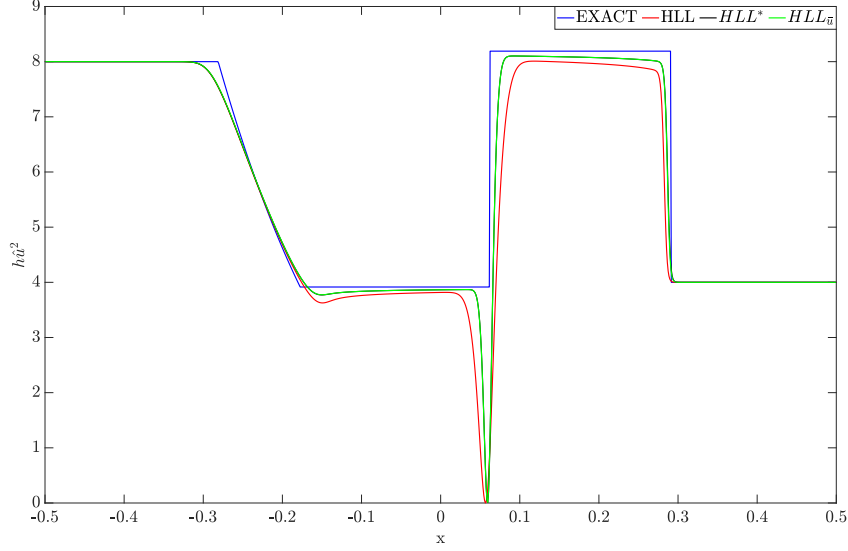


Figure 3.7: Dam break problem with change of sign on \hat{u} § 3.6.4. Plots of the $h\hat{u}^2$ using HLL , HLL^* and $HLL_{\bar{u}}$ solvers for 1000 grid cells

Proof. When the solution $(h, h\bar{u}, \hat{u})$ of (SW_2^H) is a C^1 regular function of $z = x - \bar{u}t$, the system (SW_2^H) becomes a system of three ODE's

$$\begin{cases} -\bar{u}h' + \bar{u}h' + h\bar{u}' & = 0, \\ -\bar{u}(h\bar{u})' + \bar{u}h\bar{u}' + \bar{u}(h\bar{u})' + (h\hat{u}^2 + \frac{g}{2}h^2)' & = 0, \\ -\bar{u}\hat{u}' + \bar{u}\hat{u}' + \hat{u}\bar{u}' & = 0, \end{cases}$$

which, for $h > 0$ is equivalent to

$$\begin{cases} \bar{u}' & = 0, \\ (h\hat{u}^2 + \frac{g}{2}h^2)' & = 0, \end{cases} \quad (3.35)$$

leading to

$$2h\hat{u}\hat{u}' + h'\hat{u}^2 + gh h' = 0.$$

Hence, we get

$$h' = -\frac{2h\hat{u}\hat{u}'}{\hat{u}^2 + gh}.$$

It allows us to conclude that if S changes its sign and is monotone, the sign of h' is equal (or opposite) to the sign of S . Hence, if the sign of S changes, h is not monotone. \square

Remark 10. According to (3.35), the pressure $h\hat{u}^2 + \frac{g}{2}h^2$ is constant. Hence, if h is not monotone across the contact discontinuity then, $h\hat{u}^2$ isn't monotone as well and its numerical approximation also contains a large spurious deviation, see Figure 3.7.

Remark 11. The errors reported in Table 3.10, 3.11 and 3.12 for the case when \hat{u} changes its sign are much larger than the ones reported in Table 3.1, 3.2 and 3.3 where the sign of \hat{u} remains the same. Moreover, the order of convergence for \bar{u} is worse and is now the same as the order of convergence for h and \hat{u} . This can be related to the bad approximation of the pressure on the contact discontinuity and to the delay on the shock wave.

In the following, we test two different Riemann problems to verify the third property of Proposition 24.

3.6.5 Stationary contact discontinuity

We proved in Proposition 24 that the $HLL_{\bar{u}}$ solver exactly preserves a stationary contact discontinuity. Here, we investigate the behavior of HLL and HLL^* solvers for this test case. Hence, we consider a Riemann problem for which \bar{u} is zero and $h\hat{u}^2 + \frac{g}{2}h^2 = cte$. More precisely, the initial conditions are

$$\begin{aligned} U_L &= (1, 0, 1), \\ U_R &= (0.5, 0, 3.509). \end{aligned}$$

In Figure 3.8, we see that the HLL solver is very diffusive for h and \hat{u} on the contact discontinuity. The results of the HLL^* solver are much better for h and \hat{u} but present spurious deviations: a large stationary one on \bar{u} at the contact discontinuity and two small ones that travel to the left and to the right that one can see on the three quantities h , \bar{u} and \hat{u} . This can also be concluded from Table 3.13, 3.14 and 3.15.

nx	err_{HLL}	$order_{HLL}$	err_{HLL}^*	$order_{HLL}^*$	$err_{HLL_{\bar{u}}}$	$order_{HLL_{\bar{u}}}$
10^2	8.8e-02	-	6.6e-02	-	6.8e-02	-
10^3	5.3e-02	0.24	3.8e-02	0.3	3.8e-02	0.31
10^4	3.1e-02	0.24	2.2e-02	0.24	2.2e-02	0.24
10^5	1.7e-02	0.24	1.2e-02	0.24	1.2e-02	0.24
10^6	9e-03	0.25	7e-03	0.25	7e-03	0.25

Table 3.10: Height error and order of accuracy of the three schemes for the Dam break problem with change of sign on \hat{u} § 3.6.4

nx	err_{HLL}	$order_{HLL}$	err_{HLL}^*	$order_{HLL}^*$	$err_{HLL_{\bar{u}}}$	$order_{HLL_{\bar{u}}}$
10^2	2e-01	-	1.4e-01	-	1.4e-01	-
10^3	1e-01	0.23	5e-02	0.32	6e-02	0.29
10^4	6e-02	0.21	4.2e-02	0.2	4e-02	0.21
10^5	3e-02	0.24	2.4e-02	0.22	2.5e-02	0.22
10^6	2e-02	0.24	1.4e-02	0.24	1.4e-02	0.24

Table 3.11: Mean velocity error and order of accuracy of the three schemes for the Dam break problem with change of sign on \hat{u} § 3.6.4

nx	err_{HLL}	$order_{HLL}$	err_{HLL}^*	$order_{HLL}^*$	$err_{HLL_{\bar{u}}}$	$order_{HLL_{\bar{u}}}$
10^2	4.1e-01	-	2.8e-01	-	2.9e-01	-
10^3	2.3e-01	0.24	1.6e-01	0.31	1.6e-01	0.3
10^4	1.3e-01	0.25	9e-02	0.25	9e-02	0.24
10^5	7e-02	0.24	5e-02	0.24	5e-02	0.24
10^6	4e-02	0.24	2e-02	0.24	2.e-02	0.24

Table 3.12: Standard deviation error and order of accuracy of the three schemes for the Dam break problem with change of sign on \hat{u} § 3.6.4

nx	err_{HLL}	$order_{HLL}$	err_{HLL}^*	$order_{HLL}^*$
10^2	5e-02	-	3e-02	-
10^3	2.8e-02	0.26	1.2e-02	0.5
10^4	1.6e-02	0.25	3e-03	0.5
10^5	9e-03	0.24	1.2e-03	0.49
10^6	5e-03	0.24	4e-04	0.48

Table 3.13: Height error and order of accuracy of the three schemes for the stationary contact discontinuity § 3.6.5

nx	err_{HLL}	$order_{HLL}$	err_{HLL}^*	$order_{HLL}^*$
10^2	3e-03	-	1e-01	-
10^3	1e-03	0.57	3.2e-02	0.51
10^4	3e-04	0.49	1e-02	0.5
10^5	1e-04	0.46	3e-03	0.5
10^6	3e-05	0.46	9.7e-04	0.5

Table 3.14: Mean velocity error and order of accuracy of the three schemes for the stationary contact discontinuity § 3.6.5

nx	err_{HLL}	$order_{HLL}$	err_{HLL}^*	$order_{HLL}^*$
10^2	2.2e-01	-	2.2e-01	-
10^3	1.2e-01	0.25	7.1e-02	0.5
10^4	6.9e-02	0.25	2.2e-02	0.5
10^5	3e-02	0.24	7e-03	0.49
10^6	2e-02	0.24	2e-03	0.48

Table 3.15: Standard deviation error and order of accuracy of the three schemes for stationary contact discontinuity § 3.6.5

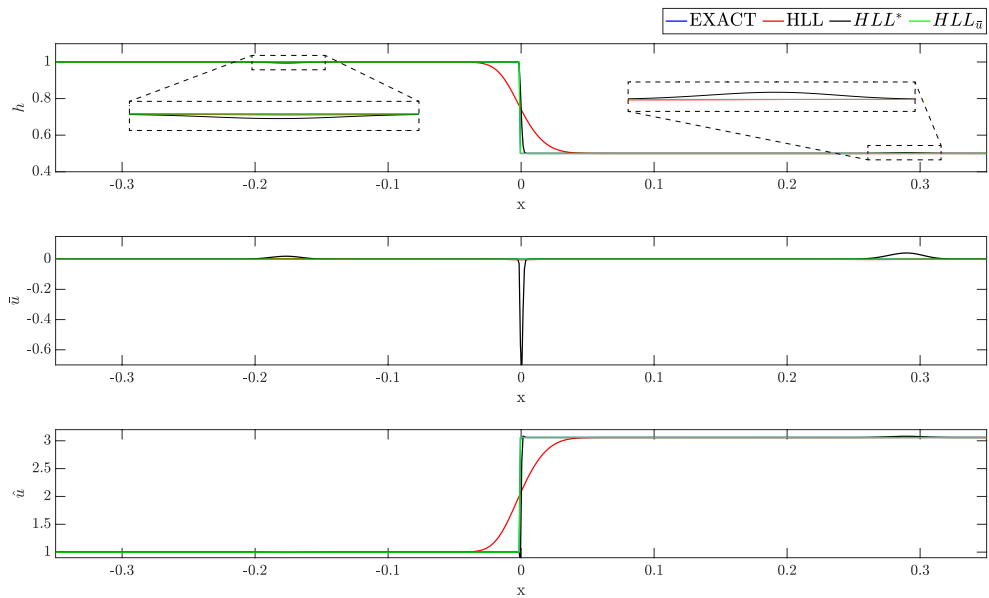


Figure 3.8: Stationary contact discontinuity § 3.6.5. Plots of the variables using HLL , HLL^* and $HLL_{\bar{u}}$ solvers for 1000 grid cells

3.6.6 Traveling contact discontinuity

Here, we investigate the case of a traveling isolated contact discontinuity. In this case we proved in Remark 6 that the approximated Riemann problem associated to the $HLL_{\bar{u}}$ solver is exact and we would like to see if it has an impact on the numerical results. Hence, we consider a Riemann problem where \bar{u} and $h\hat{u}^2 + \frac{g}{2}h^2 = cte$ are constant but not zero. More precisely, the initial conditions are

$$\begin{aligned} U_L &= (1, 1, 1), \\ U_R &= (0.5, 1, 3.509). \end{aligned}$$

We see in Figure 3.9 that in that case none of the schemes exactly preserves the

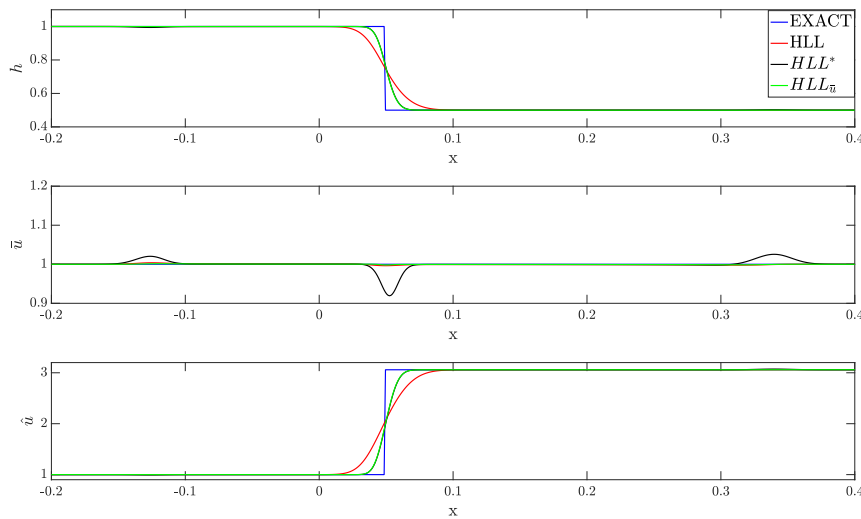


Figure 3.9: Traveling contact discontinuity § 3.6.6. Plots of the variables using HLL , HLL^* and $HLL_{\bar{u}}$ solvers for 1000 grid cells

contact discontinuity. Nevertheless, the $HLL_{\bar{u}}$ solver gives better results since the HLL solver is much more diffusive on the contact discontinuity and the HLL^* solver presents the same spurious deviations as in the stationary case. Errors on Table 3.16, 3.17 and 3.18 are similar for the HLL^* and $HLL_{\bar{u}}$ schemes on h and \hat{u} and better than the HLL scheme. But, for the mean velocity the $HLL_{\bar{u}}$ gives better errors whereas the HLL^* scheme has better order of convergence. But, we can't know if that order is relevant due to the presence of the numerical artifacts in the HLL^* scheme.

nx	err_{HLL}	$order_{HLL}$	err_{HLL}^*	$order_{HLL}^*$	$err_{HLL_{\bar{u}}}$	$order_{HLL_{\bar{u}}}$
10^2	5.2e-02	-	4.1e-02	-	3.9e-02	-
10^3	2.8e-02	0.26	1.9e-02	0.31	1.9e-02	0.29
10^4	1.6e-02	0.25	1e-02	0.25	1e-02	0.25
10^5	9.1e-03	0.24	6.1e-03	0.25	6.1e-03	0.25
10^6	5e-03	0.25	3e-03	0.25	3e-03	0.25

Table 3.16: Height error and order of accuracy of the three schemes for the traveling contact discontinuity § 3.6.6

nx	err_{HLL}	$order_{HLL}$	err_{HLL}^*	$order_{HLL}^*$	$err_{HLL_{\bar{u}}}$	$order_{HLL_{\bar{u}}}$
10^2	3.9e-03	-	5.5e-02	-	1.5e-03	-
10^3	1e-03	0.57	9.8e-03	0.75	5e-04	0.47
10^4	3.4e-04	0.49	1.7e-03	0.75	1.8e-04	0.44
10^5	1.1e-04	0.46	3e-04	0.75	6.4e-05	0.45
10^6	4.e-05	0.46	5e-05	0.75	2.e-05	0.45

Table 3.17: Mean velocity error and order of accuracy of the three schemes for the traveling contact discontinuity § 3.6.6

nx	err_{HLL}	$order_{HLL}$	err_{HLL}^*	$order_{HLL}^*$	$err_{HLL_{\bar{u}}}$	$order_{HLL_{\bar{u}}}$
10^2	2.2e-01	-	1.6e-01	-	1.6e-01	-
10^3	1.2e-01	0.25	8.4e-02	0.3	8.4e-02	0.28
10^4	6.9.3e-02	0.24	4.6e-02	0.25	4.6e-02	0.25
10^5	3.8e-02	0.24	2.6e-02	0.25	2.6e-02	0.25
10^6	2.1e-02	0.25	1.4e-02	0.25	1e-02	0.25

Table 3.18: Standard deviation error and order of accuracy of the three schemes for the traveling contact discontinuity § 3.6.6

3.7 Discrete energy inequality of the schemes

In [1], the solution of (SW_2^H) is defined as weak solution of this system of PDE that moreover dissipates the mechanical energy (3.4). Here, we are interested in verifying if the schemes satisfy a discrete energy inequality.

According to [17, §2.2.2], a scheme verifies a discrete energy inequality associated to an energy, if there exists a numerical energy flux $\mathcal{G}(U_L, U_R)$ which is consistent with the exact energy flux, i.e $\mathcal{G}(U, U) = G(U)$ defined in (3.5) such that under some CFL condition, the discrete values computed by (3.7) automatically verify

$$\forall i \in \mathbb{Z}, \forall n \in \mathbb{N}, \quad E(U_i^{n+1}) - E(U_i^n) + \frac{\Delta t^n}{\Delta x} \left(\mathcal{G}_{i+\frac{1}{2}}^n - \mathcal{G}_{i-\frac{1}{2}}^n \right) \leq 0, \quad (3.36)$$

where

$$\mathcal{G}_{i+\frac{1}{2}}^n = \mathcal{G}(U_{i+1}^n, U_i^n).$$

If the energy is a convex function of the conserved variables, there is a general theory for discrete entropy inequality (3.36) where the flux is an approximate Riemann solver, see for example [17, §2.3]. We can't use this general theory in this work because in our case the energy (3.4) is not a convex function of $(h, h\bar{u}, \hat{u})$, see [1]. Therefore, we choose to investigate numerically whether (3.36) holds or not. This strategy consists in exploring for a single time step, 10^4 random Riemann problems to test on two cells if (3.36) holds or not. Neumann boundary conditions are used on both boundaries, where we use the consistency property of \mathcal{G} to determine the numerical energy flux. The variables are chosen randomly between $]0, 1[$.

More precisely, if (3.36) is verified then, it is necessarily true in the two cells. In other words, for one time step, we have

$$\begin{aligned} E(U_1^1) - E(U_1^0) + \frac{\Delta t^n}{\Delta x} \left(\mathcal{G}_{\frac{3}{2}}^0 - \mathcal{G}_{\frac{1}{2}}^0 \right) &\leq 0, \\ E(U_2^1) - E(U_2^0) + \frac{\Delta t^n}{\Delta x} \left(\mathcal{G}_{\frac{5}{2}}^0 - \mathcal{G}_{\frac{3}{2}}^0 \right) &\leq 0, \end{aligned}$$

where $\mathcal{G}_{\frac{5}{2}}^n = G(U_2^n)$ and $\mathcal{G}_{\frac{1}{2}}^n = G(U_1^n)$ due to the consistency with the exact energy flux.

Adding the above inequalities lead to the following global necessary condition

$$\Delta E^{0,1} := E(U_2^1) + E(U_1^1) - (E(U_2^0) + E(U_1^0)) + \frac{\Delta t^n}{\Delta x} \left(\mathcal{G}_{\frac{5}{2}}^0 - \mathcal{G}_{\frac{1}{2}}^0 \right) \leq 0. \quad (3.37)$$

When (3.37) is not verified then, (3.36) is not verified too.

nx	HLL^*	$HLL_{\bar{u}}$
$Max(\Delta E^n)$	0.05	0.001
j	487	15
$U_{L_{Max(\Delta E^n)}}$	$U_L = [0.58, 0.08, 0.74]$	$U_L = [0.85, 0.4, 0.25]$
$U_{R_{Max(\Delta E^n)}}$	$U_R = [0.62, 0.18, 0.68]$	$U_R = [0.77, 0.33, 0.89]$

Table 3.19: Interesting values corresponding to the cases where the schemes are non-dissipative.

3.7.1 The case $\hat{u}_L = \hat{u}_R = 0$

We start with the case of the classical Shallow water model. We mention that in this case the energy is convex and it was proven in [17] that the HLL scheme verifies the dissipative energy inequality (3.36). This was also true using (3.37) not only for the HLL scheme but for other schemes as well.

3.7.2 The case $\hat{u}_L \neq 0$ and $\hat{u}_R \neq 0$

For the model with two velocities, we conclude through the numerical results that the HLL scheme verifies (3.37). In this case, we might think that it is dissipative even if it is very diffusive on the transport wave. Concerning the other schemes, we present in Table 3.19 the number of times j where (3.37) is increasing, the maximum value $Max(\Delta E^n)$ of the non dissipative energy obtained as well as the Riemann problem $U_{Max(\Delta E^n)}$ associated to this maximum value. We can conclude from Table 3.19 that the HLL^* and the $HLL_{\bar{u}}$ schemes don't verify the discrete energy inequality. However, we can remark that for the HLL^* there are more Riemann problems for which the (3.37) relation is not true than for the $HLL_{\bar{u}}$ scheme.

Chapter 4

Numerical schemes for the model with topography

In this chapter we extend the numerical schemes introduced in Chapter 3 to approach the solutions of the model with topography (SW_2)

$$\begin{cases} \partial_t h + \partial_x(h\bar{u}) & = 0, \\ \partial_t(h\bar{u}) + \partial_x(h(\bar{u}^2 + \hat{u}^2) + \frac{g}{2}h^2) & = -gh\partial_x Z, \\ \partial_t \hat{u} + \partial_x(\bar{u}\hat{u}) & = 0, \end{cases} \quad (SW_2)$$

where Z is a C^1 function representing the topography. The difference between the homogeneous system (SW_2^H) and the system with topography (SW_2) is that it presents non-constant stationary solutions $(h, h\bar{u}, \hat{u})$. Thus, our aim in this chapter is to derive finite volume Approximate Riemann solvers "ARS" that preserve the stability properties in the previous chapter (i), (ii), (iii) and the accuracy on the contact discontinuity while verifying a well-balanced property for all regular steady states of the system (SW_2).

First, we begin with some general results on the model with topography that we will use to derive and analyze our ARS. Adding Z as a stationary new variable, the shallow water model with two velocities (SW_2) can be written under the following form

$$\partial_t W + \partial_x F(W) = B(W), \quad (4.1)$$

where

$$W = \begin{pmatrix} h \\ h\bar{u} \\ \hat{u} \\ Z \end{pmatrix}, \quad F(W) = \begin{pmatrix} h\bar{u} \\ h(\bar{u}^2 + \hat{u}^2) + \frac{g}{2}h^2 \\ \bar{u}\hat{u} \\ 0 \end{pmatrix} \quad \text{and} \quad B(W) = \begin{pmatrix} 0 \\ -gh\partial_x Z \\ 0 \\ 0 \end{pmatrix}.$$

with U the vector of the conservative variables of the homogeneous (SW_2) . The system is completed by the initial value

$$W(0, x) = W_0(x),$$

and the boundary conditions that we will detail when we test the behavior of the numerical schemes in the next chapter. The system (SW_2) rewrites under the quasi-linear form

$$\partial_t V + A(V) \partial_x V = 0,$$

where $V = (h, \bar{u}, \hat{u}, Z)$ and $A(V)$ is the matrix defined by

$$A(V) = \begin{pmatrix} \bar{u} & h & 0 & 0 \\ g + \frac{\hat{u}^2}{h} & \bar{u} & 2\hat{u} & g \\ 0 & \hat{u} & \bar{u} & 0 \\ 0 & 0 & 0 & 0 \end{pmatrix}.$$

The matrix $A(V)$ possesses four eigenvalues, three of them are the eigenvalues of the homogeneous system, see (3.2) and the fourth one λ_0 is related to the new stationary variable Z . The eigenvalues are

$$\lambda_1^{E'} = \bar{u} - \sqrt{gh + 3\hat{u}^2}, \quad \lambda_2^{E'} = \bar{u}, \quad \lambda_3^{E'} = \bar{u} + \sqrt{gh + 3\hat{u}^2}, \quad \text{and} \quad \lambda_0 = 0. \quad (4.2)$$

The characteristic fields associated to $\lambda_2^{E'}$ and λ_0 are linearly degenerate, while the characteristic fields associated to $\lambda_1^{E'}$ and $\lambda_3^{E'}$ are genuinely nonlinear. A set of independent k -Riemann invariants, denoted \mathcal{R}_k is given by

$$\begin{aligned} \mathcal{R}_{\lambda_1^{E'}} &= \left\{ \mathcal{R}_{\lambda_1^E}, Z \right\}, \\ \mathcal{R}_{\lambda_2^{E'}} &= \left\{ \mathcal{R}_{\lambda_2^E}, Z \right\}, \\ \mathcal{R}_{\lambda_3^{E'}} &= \left\{ \mathcal{R}_{\lambda_3^E}, Z \right\}, \\ \mathcal{R}_{\lambda_0} &= \left\{ h\bar{u}, \frac{\bar{u}^2}{2} + \frac{3\hat{u}^2}{2} + g(h + Z), \bar{u}\hat{u} \right\}. \end{aligned} \quad (4.3)$$

The mechanical energy of (SW_2) reads

$$E = g \frac{h^2}{2} + \frac{h}{2} (\bar{u}^2 + \hat{u}^2) + ghZ,$$

and the associated energy flux is

$$G = \left(gh + \frac{\bar{u}^2 + 3\hat{u}^2}{2} + gZ \right) h\bar{u}.$$

4.1 Godunov type schemes

The main objective of this work is to derive numerical schemes able to preserve the smooth steady state solutions of (SW₂) presented in Chapter 2. To construct these schemes, as in Chapter 3, we use the finite volume strategy. The method is similar to the finite volume framework proposed in § 3.1 for the conservative schemes (3.7) but with a slight difference due to the presence of the topography source term. We propose then the following update formula

$$\forall i \in \mathbb{Z}, \forall n \in \mathbb{N} \quad W_i^{n+1} = W_i^n - \frac{\Delta t^n}{\Delta x} \left(\mathcal{F}_{i+\frac{1}{2}}^n - \mathcal{F}_{i-\frac{1}{2}}^n \right) + \Delta t^n \mathcal{B}_i^n,$$

where as previously W_i^n should be a piecewise constant approximation of $W(x, t)$ at time t^n on the cell C_i , $\mathcal{F}_{i+\frac{1}{2}}^n$ is the numerical flux at the interface that will be defined later to be an approximation of (3.8) and the new quantity \mathcal{B}_i^n is the numerical source term on the cell C_i to be defined later to be an approximation of

$$\frac{1}{\Delta t^n} \frac{1}{\Delta x} \int_{x_{i-\frac{1}{2}}}^{x_{i+\frac{1}{2}}} \int_{t^n}^{t^{n+1}} B(W(t, x)) dt dx.$$

The initialization of the algorithm can be computed with

$$\forall i \in \mathbb{Z} \quad W_i^0 = \frac{1}{\Delta x} \int_{x_{i-\frac{1}{2}}}^{x_{i+\frac{1}{2}}} W_0(x) dx.$$

As previously, we will consider approximate Riemann solvers. We already mentioned that for the homogeneous shallow water model with two velocities, the Riemann problem was solved in [1] but its computation needs the solution of a nonlinear problem. For the classical shallow water model with topography, the Riemann problem was studied in [3, 24, 5]. Its computation also needs the solution of a non linear problem and it was proven that the solution is not always unique. For the (SW₂) system no solution of the Riemann problem is available. Hence, approximate Riemann solvers are a good alternative to Godunov schemes for which the exact solution of the Riemann problem is needed.

4.2 Stability and consistency

We have introduced in §3.2 the properties the approximate Riemann solver has to satisfy to ensure stability and consistency. Here, we recall these properties to adapt with the presence of the stationary wave:

1. To preserve the order of the waves, see (4.2), we modify (3.14) and we choose the following two external waves

$$\begin{aligned}\lambda_L &= \min(\bar{u}_L - c_L, \bar{u}_R - c_R, 0), \\ \lambda_R &= \max(\bar{u}_L + c_L, \bar{u}_R + c_R, 0),\end{aligned}\quad (4.4)$$

2. Since λ_L and λ_R are still the external waves, we use the same definition of the CFL condition

$$\max_i \left(|\lambda_{L,i+\frac{1}{2}}^n|, |\lambda_{R,i+\frac{1}{2}}^n| \right) \Delta t^n \leq \frac{\Delta x}{2},$$

3. The main difference between (SW_2^H) and (SW_2) is that (3.1) is written under a conservative form while (4.1) is not. Hence, the presence of the source term affects the consistency property introduced in [40, Thm 3.1]. According to [4, Prop 4] the consistency relation now reads

$$F(W_R) - F(W_L) - \Delta x \cdot \tilde{B}(\Delta x, \Delta t^n, W_L, W_R) = \sum_{j=1}^N \lambda_j \left(\tilde{W}_{j+\frac{1}{2}} - \tilde{W}_{j-\frac{1}{2}} \right). \quad (4.5)$$

where \tilde{B} is a numerical approximation of the source term verifying

$$\lim_{\substack{\Delta x, \Delta t^n \rightarrow 0 \\ W_L, W_R \rightarrow W}} \tilde{B}(\Delta x, \Delta t^n, W_L, W_R) = B(W).$$

For the sake of simplicity, we denote $\tilde{B} = \tilde{B}(\Delta x, \Delta t^n, W_L, W_R)$.

4.3 Steady state solutions

According to Chapter 2 Definition 2, the steady states of (SW_2) system are governed by

$$\begin{cases} \partial_x(h\bar{u}) & = 0, \\ \partial_x\left(h(\bar{u}^2 + \hat{u}^2) + \frac{g}{2}h^2\right) & = -gh\partial_x Z, \\ \partial_x(\bar{u}\hat{u}) & = 0 \end{cases} \quad (\text{SSW2})$$

which for smooth steady states leads to

$$\begin{cases} h\bar{u} & = M, \\ \frac{\bar{u}^2}{2} + \frac{3\hat{u}^2}{2} + g(h+Z) & = K, \\ \bar{u}\hat{u} & = MS. \end{cases} \quad (4.6)$$

where $M \in \mathbb{R}$, $S \in \mathbb{R}$ and $K \in \mathbb{R}$. For $M \in \mathbb{R}^*$ and $h \in \mathbb{R}_+^*$, we note $S = \frac{\hat{u}}{h}$. The study of the general steady state solutions for (SW_2) was done in detail in Chapter 2. Here, we will construct numerical schemes to preserve the smooth steady states. Such schemes are called well-balanced and were first introduced for the lake at rest ($M = 0$ and $S = 0$) in [13]. We refer also to [17] where the author presents a detailed literature review listing different numerical schemes for the lake at rest. Then, to adapt these schemes for $M \neq 0$ and $S = 0$, an extension of the hydrostatic reconstruction was proposed by the authors in [22] which unfortunately doesn't preserve the positivity of the water heights. Another correction was proposed for subsonic steady states that preserves the positivity of the water heights [18]. To deal with all the smooth steady states, a numerical technique was proposed for ARS based on [14, 15] in which the intermediate states are obtained by solving a Bernoulli-type equation. But, in order to introduce the source term within the approximate Riemann solver, this approach consists on solving a non linear equation at each interface and is very costly. More recently, a linearization of this non linear equation was done in [45]. However, the proposed scheme involves some difficulties regarding the discretization of the source term. To deal with this issue, a correction of the topography source term discretization was presented in [16]. Up to our knowledge a construction of a well-balanced scheme for $S \neq 0$ was never studied.

In the context of approximate Riemann solver, the well-balanced property is defined as follows:

For all $W_L = (h_L, h_L \bar{u}_L, \hat{u}_L, Z_L)$ and $W_R = (h_R, h_R \bar{u}_R, \hat{u}_R, Z_R)$ at steady state, i.e verifying (4.6), the well-balanced approximate Riemann solver \tilde{W} should verify

$$\tilde{W}\left(\frac{x}{t}, W_L, W_R\right) = \begin{cases} W_L & \text{if } \frac{x}{t} < 0, \\ W_R & \text{if } \frac{x}{t} > 0. \end{cases} \quad (4.7)$$

In the following, we study three ARS that are extensions of the solvers introduced in Chapter 3 and adapted to take into consideration the presence of the topography source term, i.e the presence of the additional contact discontinuity λ_0 . We will proceed as follows:

- We first construct an ARS named HLL_0 . This solver is an extension of HLL scheme introduced in § 3.3 for which we add the discontinuity λ_0 . It is a direct extension to the case $S \neq 0$ of the scheme proposed in [45]. This first solver doesn't take into account the contact discontinuity on S .
- Then, we construct a second numerical scheme named HLL_0^* as done in the HLL^* scheme for the homogeneous model (SW_2^H) in § 3.4. We prove that the HLL_0^* scheme can also be seen as a 4-waves approximate

Riemann solver where we consider that the water height and the mean velocity are constant through the transport wave. A similar strategy was used to approximate the solution of the Ripa model with source term in [29].

- Finally, to take into consideration the four waves and the Riemann invariants of the model, we construct a 4-waves approximate Riemann solver, named $HLL_{0,\bar{u}}$ which can be seen as variation of the HLL_0^* scheme and a combination of HLL_0 and $HLL_{\bar{u}}$.

The three ARS verify the maximum principle on S but they don't verify a discrete dissipative energy.

In this section, we will assume that $h_L \geq 0$, $h_R \geq 0$ and $M \in \mathbb{R}_+^*$. In addition, we consider for all ARS that the topography is only discontinuous through λ_0 . Hence, all the intermediate states at the left and right of λ_0 are equal respectively to Z_L and Z_R .

Before constructing the schemes, we will start by giving a consistent approximation of the source term.

4.4 Determination of the topography source term

One of the crucial issues one faces in the derivation of numerical schemes to accurately approximate the weak solutions of systems with topography such as (SW_2) is to verify the well-balanced property (4.7). To do that, we need to find a suitable approximation of the source term. In a series of paper [44, 45, 16], two strategies were proposed to define this approximation. Both of them allow to construct well-balanced schemes for the shallow-water model. Each one of them has a drawback:

- The strategy proposed in [44, 45] is not exact for a flat bottom since the approximated one is of order $O(\Delta x^2)$ in this case.
- The strategy proposed in [16] is difficult to extend to dry areas.

Here, we choose to extend to our case the strategy proposed in [16]. But all our ARS could be used with an extension of the strategy proposed in [44, 45].

Let us introduce the quantity

$$\epsilon_{L,R} = |K_R - K_L| + |M_R - M_L| + |S_R - S_L|. \quad (4.8)$$

where M , S and K were defined in (4.6).

The smooth steady state solutions of (SW₂) for a Riemann problem are then characterized by

$$\epsilon_{L,R} = 0.$$

Definition 7. Suppose that $h_L > 0$ and $h_R > 0$. We define

$$\overline{M^2} = |M_L M_R|, \quad \overline{S^2} = |S_L S_R|, \quad \bar{h} = \frac{h_L + h_R}{2}, \quad \tilde{F}_{\bar{h},M,S} = \frac{\overline{M^2} \bar{h}}{g h_L^2 h_R^2} - 3 \frac{\overline{S^2} \bar{h}}{g}. \quad (4.9)$$

When $\tilde{F}_{\bar{h},M,S} \neq 1$ or $\epsilon_{L,R} \neq 0$, let us define an approximation of the interface topography source term by

$$\Delta x \cdot \tilde{B}^M = -g \bar{h} (Z_R - Z_L) + \left(\frac{\overline{M^2}}{4 h_L^2 h_R^2} + \frac{\overline{S^2}}{4} \right) \frac{(h_R - h_L) (Z_R - Z_L)^2}{(1 - \tilde{F}_{\bar{h},M,S})^2} + \epsilon_{L,R}. \quad (4.10)$$

Proposition 26. When $\tilde{F}_{\bar{h},M,S} \neq 1$ or $\epsilon_{L,R} \neq 0$, the approximation (4.10) is well defined, consistent with $-gh \partial_x Z$ and vanishes for a flat topography.

Proof. The proof of this proposition was done in [16, Section 3] for the classical Shallow water model with topography and can be easily adapted here for the model with two velocities (SW₂). \square

Proposition 27. Suppose that $W_L = (U_L, Z_L)$ and $W_R = (U_R, Z_R)$ define a smooth steady state solution (4.7). The approximation of the topography source term (4.10) ensures the relation

$$\Delta x \cdot \tilde{B}^M = M^2 \left[\frac{1}{h} \right]_L^R + S^2 [h^3]_L^R + \frac{g}{2} [h^2]_L^R. \quad (4.11)$$

which is a discrete version of the second equation of (SSW2).

Proof. For W_L and W_R verifying the smooth steady relations (4.7) we have $\overline{M^2} = M^2$, $\overline{S^2} = S^2$ and $\epsilon_{L,R} = 0$. In addition, for smooth steady states the energy flux is constant, i.e $K_L = K_R$ which leads to

$$\frac{M^2}{2} \left[\frac{1}{h^2} \right]_L^R + \frac{3S^2}{2} [h^2]_L^R + g [h + Z]_L^R = 0,$$

which reads

$$\frac{M^2}{2} \frac{(h_L - h_R)(h_R + h_L)}{h_R^2 h_L^2} + \frac{3S^2}{2} (h_R + h_L)(h_R - h_L) + g(h_R - h_L) + g(Z_R - Z_L) = 0,$$

which, for $\bar{h} = \frac{h_L + h_R}{2}$ gives

$$(h_R - h_L) \left(1 - \frac{M^2 \bar{h}}{g h_L^2 h_R^2} + 3 \frac{S^2 \bar{h}}{g} \right) + (Z_R - Z_L) = 0 \quad (4.12)$$

and then, if $\tilde{F}_{\bar{h}, M, S} \neq 1$

$$(h_R - h_L) = - \frac{(Z_R - Z_L)}{(1 - \tilde{F}_{\bar{h}, M, S})} \quad (4.13)$$

where $\tilde{F}_{\bar{h}, M, S}$ was introduced in (4.9).

For W_L and W_R verifying the smooth steady relations (4.7) and using the water height jump (4.13), the approximation (4.10) reads

$$\Delta x \cdot \tilde{B}^M = -g \bar{h} (Z_R - Z_L) - \left(\frac{M^2}{4 h_L^2 h_R^2} + \frac{S^2}{4} \right) \frac{(h_R - h_L)^2 (Z_R - Z_L)}{(1 - \tilde{F}_{\bar{h}, M, S})}.$$

After some computations, the above equation leads to

$$\Delta x \cdot \tilde{B}^M = -g \bar{h} \left((1 - \tilde{F}_{\bar{h}, M, S}) + \left(\tilde{F}_{\bar{h}, M, S} - \frac{M^2}{g \bar{h} h_R h_L} + \frac{S^2}{g \bar{h}} (h_R^2 + h_L^2 + h_R h_L) \right) \right) \frac{(Z_R - Z_L)}{(1 - \tilde{F}_{\bar{h}, M, S})}.$$

which is equivalent to

$$\Delta x \cdot \tilde{B}^M = -g \bar{h} \left(1 - \frac{M^2}{g \bar{h} h_R h_L} + \frac{S^2}{g \bar{h}} (h_R^2 + h_L^2 + h_R h_L) \right) \frac{(Z_R - Z_L)}{(1 - \tilde{F}_{\bar{h}, M, S})},$$

which is nothing but

$$\Delta x \cdot \tilde{B}^M = - \left(g \bar{h} - \frac{M^2}{h_R h_L} + S^2 (h_R^2 + h_L^2 + h_R h_L) \right) \frac{(Z_R - Z_L)}{(1 - \tilde{F}_{\bar{h}, M, S})}.$$

Plugging again the jump water height relation (4.13) in the above equation, we obtain

$$\Delta x \cdot \tilde{B}^M = -M^2 \left(\frac{h_R - h_L}{h_R h_L} \right) + S^2 (h_R - h_L) (h_R^2 + h_L^2 + h_R h_L) + \frac{g}{2} (h_R + h_L) (h_R - h_L).$$

or equivalently

$$\Delta x \cdot \tilde{B}^M = \left(g \bar{h} - \frac{M^2}{h_R h_L} + S^2 (h_R^2 + h_L^2 + h_R h_L) \right) (h_R - h_L).$$

which is nothing but (4.11). □

Remark 12. The approximation of the source term (4.10) is ill-defined if $\tilde{F}_{\tilde{h},M,S} = 1$ and $\epsilon_{L,R} = 0$. Let us note that in that case $Z_R - Z_L = 0$, see (4.12). Then, as in [16], we choose to set $\Delta x \cdot \tilde{B}^M = 0$. Other choices can be made. For example in [30], the authors imposed $\Delta x \cdot \tilde{B}^M = \frac{g}{4\tilde{h}} [h]^3$ which is a consistent approximation with $\epsilon = 0$ and in the limit of $\tilde{F}_{\tilde{h},M,S}$ to 1.

Now that we have defined the approximation of the source term, the next step is to construct the numerical schemes.

4.5 The HLL_0 approximated Riemann solver

In this section, we will construct the first well-balanced approximate Riemann solver named HLL_0 . This solver is similar to the scheme initially proposed for the shallow water equations with topography in [16]. This approximate Riemann solver is an extension of the HLL scheme proposed in § 3.3 to take into consideration the stationary wave. Hence, it consists of two intermediate states separated by the discontinuity $\lambda_0 = 0$.

The construction of this scheme is a first step toward the construction of the other schemes for which we add a fourth wave to be an adaptation of HLL^* and $HLL_{\bar{u}}$ scheme proposed in Chapter 3.

The approximate Riemann solver reads

$$\tilde{W}_{HLL_0} \left(\frac{x}{t}, U_L, Z_L, U_R, Z_R \right) = \begin{cases} W_L & \text{if } \frac{x}{t} < \lambda_L, \\ W_L^* & \text{if } \lambda_L < \frac{x}{t} < \lambda_0, \\ W_R^* & \text{if } \lambda_0 < \frac{x}{t} < \lambda_R, \\ W_R & \text{if } \frac{x}{t} > \lambda_R, \end{cases}$$

where $W_L^* = (h_L^*, h_L^* \bar{u}_L^*, \hat{u}_L^*, Z_L)$ and $W_R^* = (h_R^*, h_R^* \bar{u}_R^*, \hat{u}_R^*, Z_R)$, see Figure 4.1.

The integral consistency relation (4.5) for HLL_0 reads

$$\lambda_R W_R^* - \lambda_L W_L^* = \lambda_R W_R - \lambda_L W_L - (F(W_R) - F(W_L)) + \Delta x \cdot \tilde{B}.$$

which component by component can be written as

$$\begin{aligned} [h\bar{u}] &= \lambda_L (h_L^* - h_L) + \lambda_R (h_R - h_R^*), \\ \left[h(\bar{u}^2 + \hat{u}^2) + \frac{g}{2} h^2 \right] &= \lambda_L (h_L^* \bar{u}_L^* - h_L \bar{u}_L) + \lambda_R (h_R \bar{u}_R - h_R^* \bar{u}_R^*) + \Delta x \cdot \tilde{B}, \\ [\bar{u}\hat{u}] &= \lambda_L (\hat{u}_L^* - \hat{u}_L) + \lambda_R (\hat{u}_R - \hat{u}_R^*), \end{aligned}$$

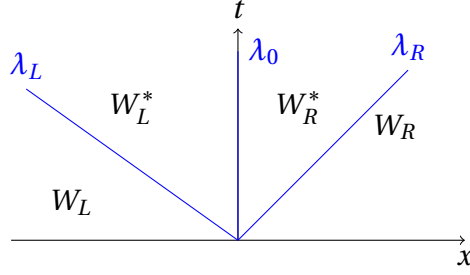


Figure 4.1: The waves representation of the HLL_0 approximate Riemann solver.

We introduce the following notation that will be used all along this chapter

$$A_{h_{HLL}\bar{u}_{HLL},\tilde{B}} = (\lambda_R - \lambda_L) h_{HLL} \bar{u}_{HLL} + \Delta x \cdot \tilde{B}. \quad (4.14)$$

Combining the previous system with the (HLL) intermediate states in § 3.3, we get

$$\begin{cases} \lambda_R h_R^* - \lambda_L h_L^* &= (\lambda_R - \lambda_L) h_{HLL}, \\ \lambda_R h_R^* \bar{u}_R^* - \lambda_L h_L^* \bar{u}_L^* &= A_{h_{HLL}\bar{u}_{HLL},\tilde{B}}, \\ \lambda_R \hat{u}_R^* - \lambda_L \hat{u}_L^* &= (\lambda_R - \lambda_L) \hat{u}_{HLL}, \end{cases} \quad (4.15)$$

It is clear that the system has six unknowns since the celerity of the intermediate wave is imposed to be equal to zero. The relations (4.15) give us three equations but we need three more equations to close the system. To do so, we consider that the states L^* and R^* verify through the contact discontinuity λ_0 , a discrete version of (SSW2).

$$\begin{cases} [h\bar{u}]_{L^*}^{R^*} &= 0, \\ [h(\bar{u}^2 + \hat{u}^2) + \frac{g}{2}h^2]_{L^*}^{R^*} &= \Delta x \cdot \tilde{B}, \\ [\hat{u}\bar{u}]_{L^*}^{R^*} &= 0 \end{cases} \quad (4.16)$$

The first and third equations of (4.16) are nothing but the first and third Riemann invariants (4.3) across λ_0 which, for $h_L^* \neq 0$, $h_R^* \neq 0$, $\bar{u}_L^* \neq 0$ and $\bar{u}_R^* \neq 0$ are equivalent to

$$\begin{cases} h_R^* \bar{u}_R^* = h_L^* \bar{u}_L^* := M^*, \\ \frac{\hat{u}_R^*}{h_R^*} = \frac{\hat{u}_L^*}{h_L^*} := S^*. \end{cases} \quad (4.17)$$

Then, the second equation of (4.16) can be written as

$$M^{*2} \left[\frac{1}{h} \right]_{L^*}^{R^*} + S^{*2} [h^3]_{L^*}^{R^*} + \frac{g}{2} [h^2]_{L^*}^{R^*} = \Delta x \cdot \tilde{B}, \quad (4.18)$$

which is equivalent to

$$M^{*2} \left(\frac{1}{h_R^*} - \frac{1}{h_L^*} \right) + S^{*2} (h_R^{*3} - h_L^{*3}) + \frac{g}{2} (h_R^{*2} - h_L^{*2}) = \Delta x \cdot \tilde{B}.$$

and rewrites

$$\left(\frac{-M^{*2}}{h_L^* h_R^*} + \frac{g}{2} (h_R^* + h_L^*) + S_0^{*2} (h_R^{*2} + h_L^* h_R^* + h_L^{*2}) \right) (h_R^* - h_L^*) = \Delta x \cdot \tilde{B}. \quad (4.19)$$

We can remark that the above relation is nonlinear. So instead of the above formula and in order to give explicit formulas for h_L^* and h_R^* , we consider a linearization as done in [16].

Proposition 28. For $h_L \neq 0$ and $h_R \neq 0$, we define

$$\alpha_{L,R} = \frac{-\overline{M^2}}{h_L h_R} + \frac{g}{2} (h_R + h_L) + \overline{S^2} (h_R^2 + h_L h_R + h_L^2),$$

and when $\alpha_{L,R} \neq 0$ or $\epsilon_{L,R} \neq 0$, we define

$$C_{\alpha_{L,R}, \tilde{B}} := \frac{\alpha_{L,R} \Delta x \cdot \tilde{B}}{\alpha_{L,R}^2 + \epsilon_{L,R}}. \quad (4.20)$$

Then, the relation

$$(h_R^* - h_L^*) = C_{\alpha_{L,R}, \tilde{B}}, \quad (4.21)$$

is an approximated of (4.19).

Proof. The proof of this proposition is done in [16] for the classical Shallow water model. Here, we give the proof for $S \neq 0$. For $h_L \neq 0$ and $h_R \neq 0$, the linearization of (4.19) reads

$$\left(\frac{-\overline{M^2}}{h_L h_R} + \frac{g}{2} (h_R + h_L) + \overline{S^2} (h_R^2 + h_L h_R + h_L^2) \right) (h_R^* - h_L^*) = \Delta x \cdot \tilde{B}.$$

or equivalently

$$\alpha_{L,R} (h_R^* - h_L^*) = \Delta x \cdot \tilde{B}, \quad \text{where} \quad \alpha_{L,R} = \frac{-\overline{M^2}}{h_L h_R} + \frac{g}{2} (h_R + h_L) + \overline{S^2} (h_R^2 + h_L h_R + h_L^2). \quad (4.22)$$

However, the parameter $\alpha_{L,R}$ can be equal to zero as long as

$$\frac{\overline{M^2}}{h_L h_R} = \frac{g}{2} (h_R + h_L) + \overline{S^2} (h_R^2 + h_L h_R + h_L^2).$$

So, for $\alpha_{L,R} \neq 0$ or $\epsilon_{L,R} \neq 0$ the relation (4.22) is replaced in [16] by

$$(\alpha_{L,R}^2 + \epsilon_{L,R})(h_R^* - h_L^*) = \alpha_{L,R} \Delta x \cdot \tilde{B}. \quad (4.23)$$

Finally, relation (4.23) can be written as (4.21). \square

Remark 13. *The linearization (4.21) is ill-posed for $\alpha_{L,R} = \epsilon_{L,R} = 0$. After straight forward computations, we get*

$$\lim_{\alpha_{L,R} \rightarrow 0} \lim_{\epsilon_{L,R} \rightarrow 0} \frac{\alpha_{L,R} \Delta x \cdot \tilde{B}}{(\alpha_{L,R}^2 + \epsilon_{L,R})} = h_R - h_L,$$

but

$$\lim_{\epsilon_{L,R} \rightarrow 0} \lim_{\alpha_{L,R} \rightarrow 0} \frac{\alpha_{L,R} \Delta x \cdot \tilde{B}}{(\alpha_{L,R}^2 + \epsilon_{L,R})} = 0.$$

Here, as in [16], when $\alpha_{L,R} = \epsilon_{L,R} = 0$ we choose to impose

$$(h_R^* - h_L^*) = (h_R - h_L).$$

4.5.1 Well-balanced version of the HLL_0 scheme

Proposition 29. *Assume that h_L and h_R are positive, the system (4.15), (4.17) and (4.21) admits a unique solution $(h_L^*, h_R^*, \bar{u}_L^*, \bar{u}_R^*, \hat{u}_L^*, \hat{u}_R^*) \in \mathbb{R}^6$ given by*

$$\left\{ \begin{array}{l} h_L^* = h_{HLL} - \frac{\lambda_R C_{\alpha_{L,R}, \tilde{B}}}{(\lambda_R - \lambda_L)}, \\ h_R^* = h_{HLL} - \frac{\lambda_L C_{\alpha_{L,R}, \tilde{B}}}{(\lambda_R - \lambda_L)}, \\ \bar{u}_L^* = \frac{h_{HLL} \bar{u}_{HLL} + \frac{\Delta x \cdot \tilde{B}}{\lambda_R - \lambda_L}}{h_L^*}, \\ \bar{u}_R^* = \frac{h_{HLL} \bar{u}_{HLL} + \frac{\Delta x \cdot \tilde{B}}{\lambda_R - \lambda_L}}{h_R^*}, \\ \hat{u}_L^* = \hat{u}_{HLL} \frac{h_L^*}{h_{HLL}}, \\ \hat{u}_R^* = \hat{u}_{HLL} \frac{h_R^*}{h_{HLL}}, \end{array} \right. \quad (HLL_0)$$

where the HLL intermediate states $(h_{HLL}, h_{HLL} \bar{u}_{HLL}, \hat{u}_{HLL})$ are defined in (HLL).

Proof. Considering the water height consistency relation in (4.15) and the relation (4.21) we get the following linear system

$$\begin{cases} \lambda_R h_R^* - \lambda_L h_L^* = (\lambda_R - \lambda_L) h_{HLL}, \\ (h_R^* - h_L^*) = C_{\alpha_{L,R}, \tilde{B}}. \end{cases}$$

which can be easily solved

$$\begin{cases} h_L^* = h_{HLL} - \frac{\lambda_R C_{\alpha_{L,R}, \tilde{B}}}{(\lambda_R - \lambda_L)}, \\ h_R^* = h_{HLL} - \frac{\lambda_L C_{\alpha_{L,R}, \tilde{B}}}{(\lambda_R - \lambda_L)}. \end{cases} \quad (4.24)$$

Then we can deduce from the second equation of the relations (4.15)

$$(\lambda_R - \lambda_L) M^* = A_{h_{HLL} \bar{u}_{HLL}, \tilde{B}}$$

which is equivalent for $A_{h_{HLL} \bar{u}_{HLL}, \tilde{B}}$ defined in (4.14) to

$$M^* = h_{HLL} \bar{u}_{HLL} + \frac{\Delta x \cdot \tilde{B}}{\lambda_R - \lambda_L}.$$

The mean intermediate velocity \bar{u}_L^* and \bar{u}_R^* are then computed from (4.17). The third equation of (4.15) can be written as

$$\lambda_R h_R^* \frac{\hat{u}_R^*}{h_R^*} - \lambda_L h_L^* \frac{\hat{u}_L^*}{h_L^*} = (\lambda_R - \lambda_L) \hat{u}_{HLL}$$

which for $\frac{\hat{u}_R^*}{h_R^*} = \frac{\hat{u}_L^*}{h_L^*} = S^*$ yields to

$$(\lambda_R h_R^* - \lambda_L h_L^*) S^* = (\lambda_R - \lambda_L) \hat{u}_{HLL}.$$

Using the first equation of (4.15) and for $h_{HLL} > 0$ we can conclude that

$$S^* = \frac{\hat{u}_{HLL}}{h_{HLL}} = S_{HLL}.$$

□

Remark 14. If $S_L = 0$ and $S_R = 0$ then we retrieve the classical HLL scheme with topography source term.

Proposition 30. Assume that h_L and h_R are positive and W_L and W_R define a smooth steady state. Then, the intermediate states (HLL₀) satisfy the well-balanced property (4.7), i.e

$$h_L^* = h_L, \quad h_R^* = h_R, \quad M^* = M \quad \text{and} \quad S^* = S.$$

Proof. For W_L and W_R defining a smooth steady state, the relation (??) holds and we have $\overline{M^2} = M^2$, $\overline{S^2} = S^2$ and $\epsilon_{L,R} = 0$. Thus, following the definition of $C_{\alpha_{L,R},\tilde{B}}$ in (4.20) we have

$$C_{\alpha_{L,R},\tilde{B}} = \frac{M^2 \left[\frac{1}{h}\right]_L^R + S^2 [h^3]_L^R + \frac{g}{2} [h^2]_L^R}{\frac{-M^2}{h_L h_R} + \frac{g}{2} (h_R + h_L) + S^2 (h_R^2 + h_L h_R + h_L^2)} = h_R - h_L.$$

Also, the intermediate water height h_{HLL} defined in (HLL) reads

$$h_{HLL} = \frac{\lambda_R h_R - \lambda_L h_L - [h\bar{u}]_L^R}{\lambda_R - \lambda_L} = \frac{\lambda_R h_R - \lambda_L h_L}{\lambda_R - \lambda_L}$$

and \hat{u}_{HLL} reads, as $\bar{u}\hat{u} = MS$,

$$\hat{u}_{HLL} = \frac{\lambda_R \hat{u}_R - \lambda_L \hat{u}_L - [\bar{u}\hat{u}]_L^R}{\lambda_R - \lambda_L} = \frac{\lambda_R \hat{u}_R - \lambda_L \hat{u}_L}{\lambda_R - \lambda_L}.$$

Then, we start by proving that $M^* = M$.

$$\begin{aligned} M^* &= \frac{\lambda_R M - \lambda_L M}{\lambda_R - \lambda_L} - \frac{1}{\lambda_R - \lambda_L} \left(M^2 \left[\frac{1}{h}\right]_L^R + S^2 [h^3]_L^R + \frac{g}{2} [h^2]_L^R \right) + \frac{\Delta x \cdot \tilde{B}}{\lambda_R - \lambda_L} \quad (4.25) \\ &= M - \frac{1}{\lambda_R - \lambda_L} \left(M^2 \left[\frac{1}{h}\right]_L^R + S^2 [h^3]_L^R + \frac{g}{2} [h^2]_L^R - M^2 \left[\frac{1}{h}\right]_L^R - S^2 [h^3]_L^R - \frac{g}{2} [h^2]_L^R \right) \\ &= M. \end{aligned}$$

Next, we prove that $S^* = S$

$$\begin{aligned} S^* &= \frac{\hat{u}_{HLL}}{h_{HLL}} \\ &= \frac{\lambda_R \hat{u}_R - \lambda_L \hat{u}_L - [\hat{u}\bar{u}]_L^R}{\lambda_R h_R - \lambda_L h_L - [h\bar{u}]_L^R} \\ &= \frac{\lambda_R h_R S - \lambda_L h_L S}{\lambda_R h_R - \lambda_L h_L} \\ &= S. \end{aligned}$$

It remains to prove that $h_L^* = h_L$ and $h_R^* = h_R$. In fact,

$$\begin{aligned} h_L^* &= h_{HLL} - \frac{\lambda_R \Delta x \cdot \tilde{B}}{\alpha(\lambda_R - \lambda_L)} \\ &= \frac{\lambda_R h_R - \lambda_L h_L - [h\bar{u}]_L^R}{\lambda_R - \lambda_L} - \frac{\lambda_R \Delta x \cdot \tilde{B}}{\alpha(\lambda_R - \lambda_L)} \\ &= \frac{\lambda_R h_R - \lambda_L h_L - \lambda_R (h_R - h_L)}{\lambda_R - \lambda_L} \\ &= h_L. \end{aligned}$$

and

$$\begin{aligned} h_R^* &= h_{HLL} - \frac{\lambda_L \Delta x \cdot \tilde{B}}{\alpha(\lambda_R - \lambda_L)} \\ &= \frac{\lambda_R h_R - \lambda_L h_L - [h\bar{u}]_L^R}{\lambda_R - \lambda_L} - \frac{\lambda_L \Delta x \cdot \tilde{B}}{\alpha(\lambda_R - \lambda_L)} \\ &= \frac{\lambda_R h_R - \lambda_L h_L - \lambda_R (h_R - h_L)}{\lambda_R - \lambda_L} \\ &= h_R. \end{aligned}$$

□

Remark 15. We note that when the topography is flat, both water height intermediate states are positive. In this case $h_L^* = h_R^* = h_{HLL} > 0$.

4.5.2 Positive and well-balanced version of the HLL_0 scheme

We claimed Proposition 30 supposing that both intermediate water heights are positive. However, the intermediate water heights defined in (4.24) are not always positive. Nevertheless, let us note that

- If the left and right states are at steady states then, the intermediate water heights are necessarily positive, see Proposition 30.
- Due to the water height consistency relation (4.15), only one of the intermediate water heights can be negative.

To define a positive and well-balanced HLL_0 scheme, our strategy is to test the positivity of the quantities \tilde{h}_L^* and \tilde{h}_R^* defined by

$$\tilde{h}_L^* = h_{HLL} - \frac{\lambda_R C_{\alpha_{L,R}, \tilde{B}}}{(\lambda_R - \lambda_L)} \quad \text{and} \quad \tilde{h}_R^* = h_{HLL} - \frac{\lambda_L C_{\alpha_{L,R}, \tilde{B}}}{(\lambda_R - \lambda_L)}. \quad (4.26)$$

The case $\tilde{h}_L^* > 0$ and $\tilde{h}_R^* > 0$

In this case, we consider the intermediate states defined in (HLL_0). The ARS ensures then the positivity of the water heights and the well-balanced property, see Proposition 36.

The case $\tilde{h}_L^* < 0$ and $\tilde{h}_R^* > 0$

In this case, the well-balanced property is lost for sure. Therefore, we propose another ARS that still verifies the consistency relations (4.15) but where we replace the equilibrium relations (4.16) by the fact that one of the intermediate state is equal to zero.

More precisely, we define a 3-waves ARS by the consistency relations (4.15) and the fact that the L^* intermediate state vanishes

$$\begin{cases} h_L^* = 0, \\ \bar{u}_L^* = 0, \\ \hat{u}_L^* = 0 \end{cases} \quad (4.27)$$

In that case, the consistency relations (4.15) and (4.27) imply

$$\begin{cases} \lambda_R h_R^* = (\lambda_R - \lambda_L) h_{HLL}, \\ \lambda_R h_R^* \bar{u}_R^* = A_{h_{HLL}, \bar{u}_{HLL}, \tilde{B}}, \\ \lambda_R \hat{u}_R^* = (\lambda_R - \lambda_L) \hat{u}_{HLL}, \end{cases} \quad (4.28)$$

Proposition 31. *Assume that h_L and h_R are positive. The system (4.27) and (4.28) admits a unique solution*

$$(h_L^*, h_R^*, \bar{u}_L^*, \bar{u}_R^*, \hat{u}_L^*, \hat{u}_R^*) \in \mathbb{R}^6$$

given by

$$\begin{cases} h_L^* = 0, \\ h_R^* = \frac{(\lambda_R - \lambda_L) h_{HLL}}{\lambda_R}, \\ \bar{u}_L^* = 0, \\ \bar{u}_R^* = \frac{A_{h_{HLL} \bar{u}_{HLL}, \tilde{B}}}{\lambda_R h_R^*}, \\ \hat{u}_L^* = 0, \\ \hat{u}_R^* = \frac{(\lambda_R - \lambda_L) \hat{u}_{HLL}}{\lambda_R}, \end{cases} \quad (4.29)$$

where the water height intermediate state h_R^* is positive.

The case $\tilde{h}_L^* > 0$ and $\tilde{h}_R^* < 0$

Similarly, we define a 3-waves ARS by vanishing the R^* intermediate state

$$\begin{cases} h_R^* = 0, \\ \bar{u}_R^* = 0, \\ \hat{u}_R^* = 0 \end{cases} \quad (4.30)$$

and considering relations (4.15).

Proposition 32. *Assume that h_L and h_R are positive. The system (4.30) and (4.15) admits a unique solution*

$$(h_L^*, h_R^*, \bar{u}_L^*, \bar{u}_R^*, \hat{u}_L^*, \hat{u}_R^*) \in \mathbb{R}^6$$

given by

$$\begin{cases} h_L^* = -\frac{(\lambda_R - \lambda_L) h_{HLL}}{\lambda_L}, \\ h_R^* = 0, \\ \bar{u}_L^* = -\frac{A_{h_{HLL} \bar{u}_{HLL}, \tilde{B}}}{\lambda_L h_L^*}, \\ \bar{u}_R^* = 0, \\ \hat{u}_L^* = -\frac{(\lambda_R - \lambda_L) \hat{u}_{HLL}}{\lambda_L}, \\ \hat{u}_R^* = 0, \end{cases} \quad (4.31)$$

where the water height intermediate state h_L^* is positive.

Remark 16. *The HLL_0 verify the maximum principle on S . This is due to the fact that the intermediate states of S are always equal to S_{HLL} and in this case the proof of Proposition 16 is totally applicable.*

Moreover, using the strategy proposed in § 3.7 we are able to conclude that the HLL_0 doesn't verify a discrete energy inequality.

4.5.3 Other correction strategies to ensure the positivity of the intermediate water heights

The choices made to ensure the positivity of the intermediate water heights are similar to those made in other works such as [10, 16]. Up to our knowledge, it is the first time that the correction is interpreted as the solution of a new ARS with vanishing intermediate states. This interpretation is interesting because it is easy to extend for schemes with three intermediate water heights.

First strategy

One of them consists in replacing only the second and the third equilibrium relation (4.16) by setting the intermediate water height and the standard deviation to zero, see [10]. In other words, they set

$$\begin{cases} h_{k^*} = 0, \\ M_{k^*} = M^*, \\ \hat{u}_{k^*} = 0 \end{cases}$$

where k corresponds to L or R depending on the state of the negative quantity in (4.26).

Second strategy

The second strategy done in [16] consists on introducing a parameter γ such that

$$0 \leq \gamma \leq \min(h_L, h_R, h_{HLL}).$$

Then, the method consists in setting $h_{k^*} = \gamma$ and to consider the consistency relations (4.15) and the equilibrium relation (4.17).

Remark 17. *The source term defined in (4.10) is ill posed if $h_L = 0$ or $h_R = 0$. To deal with dry areas for the classical shallow water model, the authors in [16] choose to enforce $\frac{u}{h} = 0$ in the limit of h to zero. This strategy can be adapted also for the model with two velocities. However, the numerical simulations of the discharge show a bad behavior of the scheme. Another treatment can be considered*

in this case that consists in taking the definition of the source term proposed in [45],

$$\Delta x \cdot \tilde{B}^M = -2g[Z] \frac{h_L h_R}{h_L + h_R} + \frac{g}{2} \frac{[h]^3}{h_L + h_R},$$

but, this topography doesn't vanish for flat topography.

In this section, we constructed the HLL_0 scheme. We proved that this scheme is well balanced and preserves the water height positivity. This scheme is the simplest version to approximate the steady state solutions of (SW₂). It is a direct extension of the scheme proposed in [16]. In the next section, we propose a second numerical scheme to be either an extension of HLL^* scheme presented in § 3.4 to take into consideration the presence of the topography or an extension of HLL_0 scheme for which we add a transport equation on S .

4.6 The HLL_0^* approximated Riemann solver

A first possibility is to construct a HLL_0^* solver following the same upwind strategy done for the construction of the HLL^* scheme in §3.4 but starting from the HLL_0 solver instead of the HLL solver. This strategy is possible since the transport process in HLL^* is not affected by the topography source term and the well-balanced property in HLL_0 is not affected by the transport process since S is constant for stationary solutions.

A second possibility is to show as done in § 3.4 that this scheme can also be seen as an ARS, here with four waves, that is a mixture between the 3–waves HLL^* scheme that takes into consideration the presence of the stationary wave λ_0 and the HLL_0 scheme that takes into consideration the transport wave λ^* . However, the main difference with HLL^* and HLL_0 schemes is that we have to check the order of the waves. More precisely, in HLL_0 scheme we have ordered λ_L , λ_0 and λ_R by choosing (4.4) and in HLL^* we have ordered λ_L , λ^* and λ_R by construction. But, here the internal waves λ^* and λ_0 are not ordered yet, see Figure 4.2. The approximate Riemann solver reads

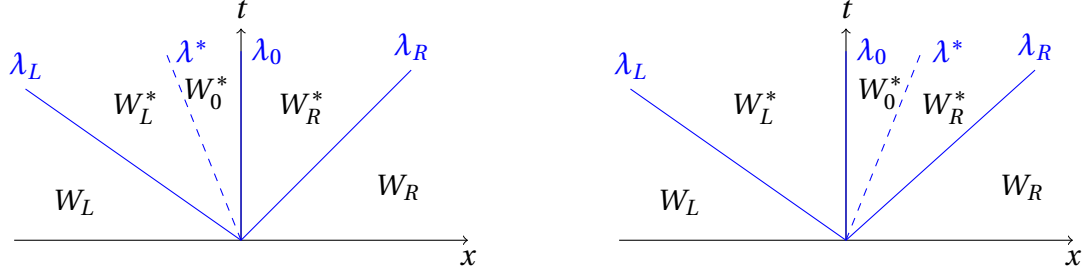


Figure 4.2: The waves representation of the HLL_0^* approximate Riemann solver with $\lambda^* < 0$ on the left and $\lambda^* > 0$ on the right.

$$\tilde{W}_{HLL_0^*} \left(\frac{x}{t}, U_L, Z_L, U_R, Z_R \right) = \begin{cases} W_L & \text{if } \frac{x}{t} < \lambda_L, \\ W_L^* & \text{if } \lambda_L < \frac{x}{t} < \lambda^* \mathbb{1}_{\{\lambda^* < 0\}} \\ W_0^* & \text{if } \lambda^* \mathbb{1}_{\{\lambda^* < 0\}} < \frac{x}{t} < \lambda^* \mathbb{1}_{\{\lambda^* > 0\}} \\ W_R^* & \text{if } \lambda^* \mathbb{1}_{\{\lambda^* > 0\}} < \frac{x}{t} < \lambda_R, \\ W_R & \text{if } \frac{x}{t} > \lambda_R, \end{cases}$$

where $W_0^* = (h_0^*, \bar{u}_0^*, \hat{u}_0^*, Z_0^*)$.

To ensure the consistency of the scheme, we start by considering the consistency relation (4.5) to get

$$[h\bar{u}] = \lambda_L (h_L^* - h_L) + \lambda^* \mathbb{1}_{\{\lambda^* < 0\}} (h_0^* - h_L^*) + \lambda^* \mathbb{1}_{\{\lambda^* > 0\}} (h_R^* - h_0^*) + \lambda_R (h_R - h_R^*), \quad (4.32)$$

$$\begin{aligned} \left[h(\bar{u}^2 + \hat{u}^2) + \frac{g}{2} h^2 \right] &= \lambda_L (h_L^* \bar{u}_L^* - h_L \bar{u}_L) + \lambda^* \mathbb{1}_{\{\lambda^* < 0\}} (h_0^* \bar{u}_0^* - h_L^* \bar{u}_L^*) \\ &\quad + \lambda^* \mathbb{1}_{\{\lambda^* > 0\}} (h_R^* \bar{u}_R^* - h_0^* \bar{u}_0^*) \\ &\quad + \lambda_R (h_R \bar{u}_R - h_R^* \bar{u}_R^*) + \Delta x \cdot \bar{B}, \end{aligned}$$

$$[\bar{u}\hat{u}] = \lambda_L (\hat{u}_L^* - \hat{u}_L) + \lambda^* \mathbb{1}_{\{\lambda^* < 0\}} (\hat{u}_0^* - \hat{u}_L^*) + \lambda^* \mathbb{1}_{\{\lambda^* > 0\}} (\hat{u}_R^* - \hat{u}_0^*) + \lambda_R (\hat{u}_R - \hat{u}_R^*).$$

Similarly to the HLL_0 approximate Riemann solver, we consider the Riemann invariants (4.3) across the stationary wave. They read here

$$(h_0^* \bar{u}_0^*, \bar{u}_0^* \hat{u}_0^*) = \begin{cases} (h_R^* \bar{u}_R^*, \bar{u}_R^* \hat{u}_R^*) & \text{if } \lambda^* < 0, \\ (h_L^* \bar{u}_L^*, \bar{u}_L^* \hat{u}_L^*) & \text{if } \lambda^* > 0 \end{cases} \quad (4.33)$$

Moreover, the linearization across the stationary wave (4.21) implies

$$C_{\alpha_{L,R}, \bar{B}} = \begin{cases} (h_R^* - h_0^*) & \text{if } \lambda^* < 0, \\ (h_0^* - h_L^*) & \text{if } \lambda^* > 0 \end{cases} \quad (4.34)$$

Similarly to the HLL^* ARS, we impose the continuity of h and \bar{u} across the transport wave.

$$(h_0^*, \bar{u}_0^*) = \begin{cases} (h_L^*, \bar{u}_L^*) & \text{if } \lambda^* < 0, \\ (h_R^*, \bar{u}_R^*) & \text{if } \lambda^* > 0 \end{cases} \quad (4.35)$$

and we impose the continuity of $\frac{\hat{u}}{h}$ on the external waves λ_L and λ_R

$$\frac{\hat{u}_L}{h_L} = \frac{\hat{u}_L^*}{h_L^*} \quad \text{and} \quad \frac{\hat{u}_R}{h_R} = \frac{\hat{u}_R^*}{h_R^*}. \quad (4.36)$$

4.6.1 Well-balanced version of the HLL_0^* scheme

Proposition 33. *Assume that h_L and h_R are positive. For $\frac{\hat{u}_R}{h_R} \neq \frac{\hat{u}_L}{h_L}$, the left and right intermediate states are given by*

$$\left\{ \begin{array}{l} h_L^* = h_{HLL} - \frac{\lambda_R C_{\alpha_{L,R}, \tilde{B}}}{(\lambda_R - \lambda_L)}, \\ h_R^* = h_{HLL} - \frac{\lambda_L C_{\alpha_{L,R}, \tilde{B}}}{(\lambda_R - \lambda_L)}, \\ \bar{u}_L^* = \frac{h_{HLL} \bar{u}_{HLL} + \frac{\Delta x \cdot \tilde{B}}{\lambda_R - \lambda_L}}{h_L^*}, \\ \bar{u}_R^* = \frac{h_{HLL} \bar{u}_{HLL} + \frac{\Delta x \cdot \tilde{B}}{\lambda_R - \lambda_L}}{h_R^*}, \\ \hat{u}_L^* = \frac{\hat{u}_L}{h_L} h_L^*, \\ \hat{u}_R^* = \frac{\hat{u}_R}{h_R} h_R^*, \end{array} \right. \quad (HLL_0^*)$$

Proof. Using the relations (4.35), the linearization (4.34) gives

$$(h_R^* - h_L^*) = C_{\alpha_{L,R}, \tilde{B}}.$$

In addition, the relations (4.33) and (4.35) imply

$$h_L^* \bar{u}_L^* = h_0^* \bar{u}_0^* = h_R^* \bar{u}_R^* \quad (4.37)$$

which will denote by M^* . Therefore, the first two relations of consistency relations (4.32) can be written as

$$\left\{ \begin{array}{l} \lambda_R h_R^* - \lambda_L h_L^* = (\lambda_R - \lambda_L) h_{HLL}, \\ M^* (\lambda_R - \lambda_L) = A_{h_{HLL} \bar{u}_{HLL}, \tilde{B}}, \end{array} \right. \quad (4.38)$$

The same relations were used in the HLL_0 scheme. Thus, the explicit values of the left and right intermediate water heights and the intermediate mean velocities are the same as in (HLL_0) . Moreover, $\frac{\hat{u}}{\hat{h}}$ is continuous on the external waves as mentioned in (4.36) thus,

$$\hat{u}_L^* = \frac{\hat{u}_L}{h_L} h_L^* \quad \text{and} \quad \hat{u}_R^* = \frac{\hat{u}_R}{h_R} h_R^*.$$

□

For the computation of the W_0^* intermediate state, the strategy is first to compute the value of λ^* and then, depending on its sign to set the values of the intermediate state.

Proposition 34. *Assume that $h_L^* > 0$ and $h_R^* > 0$. The consistency relations (4.38) and the relations (4.34), (4.35) and (4.36) impose*

$$\lambda^* = \begin{cases} \frac{I}{h_R^*} & \text{if } I > 0, \\ \frac{I}{h_L^*} & \text{if } I < 0 \end{cases} \quad (4.39)$$

where

$$I := \lambda_L h_L^* - \lambda_L h_L + \bar{u}_L h_L = \lambda_R h_R^* - \lambda_R h_R + \bar{u}_R h_R, \quad (4.40)$$

and satisfies

$$\lambda_L < \lambda^* < \lambda_R$$

Proof. The idea here is to prove that the value of λ^* is coherent with its sign, such as it respects the order of the waves as shown in Figure 4.2.

First, we consider the case $I > 0$. Suppose that $\lambda^* > 0$. Then, using the water height continuity in (4.35) and the second Riemann invariant in (4.33), we can conclude

$$\hat{u}_0^* = h_R^* \frac{\hat{u}_L}{h_L}.$$

In addition, the third equation of (4.38) reads

$$\lambda_R \hat{u}_R \frac{h_R^*}{h_R} - \lambda_L \hat{u}_L \frac{h_L^*}{h_L} + \lambda^* \left(\hat{u}_L \frac{h_R^*}{h_L} - \hat{u}_R \frac{h_R^*}{h_R} \right) = \lambda_R \hat{u}_R - \lambda_L \hat{u}_L - \bar{u}_R \hat{u}_R + \bar{u}_L \hat{u}_L.$$

that leads to

$$\lambda^* h_R^* \left(\frac{\hat{u}_L}{h_L} - \frac{\hat{u}_R}{h_R} \right) = \frac{\hat{u}_L}{h_L} (\lambda_L h_L^* - \lambda_L h_L + \bar{u}_L h_L) + \frac{\hat{u}_R}{h_R} (-\lambda_R h_R^* + \lambda_R h_R - \bar{u}_R h_R),$$

The first equation of (HLL) implies

$$\lambda_L h_L^* - \lambda_L h_L + \bar{u}_L h_L = \lambda_R h_R^* - \lambda_R h_R + \bar{u}_R h_R.$$

which is nothing but the definition of I in (4.40). Hence, if $\frac{\hat{u}_R}{h_R} \neq \frac{\hat{u}_L}{h_L}$

$$\lambda^* = \frac{\lambda_R h_R^* - h_R(\lambda_R - \bar{u}_R)}{h_R^*} > 0.$$

Thus, the hypothesis $\lambda^* > 0$ is true.

Now, we consider the case $I < 0$. Suppose that $\lambda^* < 0$. Then, (4.35) and (4.33) imply

$$\hat{u}_0^* = h_L^* \frac{\hat{u}_R}{h_R}.$$

We follow the same strategy as before and we get

$$\lambda^* = \frac{\lambda_L h_L^* - h_L(\lambda_L - \bar{u}_L)}{h_L^*} < 0,$$

and the hypothesis $\lambda^* < 0$ is true.

In addition, the definition (4.39) ensures that

- If $\lambda^* > 0$ then

$$\begin{aligned} \lambda_R - \lambda^* &= \lambda_R - \lambda_R + \frac{h_R(\lambda_R - \bar{u}_R)}{h_R^*} \\ &= \frac{h_R(\lambda_R - \bar{u}_R)}{h_R^*} > 0. \end{aligned}$$

- If $\lambda^* < 0$ then

$$\begin{aligned} \lambda^* - \lambda_L &= \lambda_L + \frac{h_L(\bar{u}_L - \lambda_L)}{h_L^*} - \lambda_L \\ &= \frac{h_L(\bar{u}_L - \lambda_L)}{h_L^*} > 0. \end{aligned}$$

□

Remark 18. If $h_L^* = 0$ or $h_R^* = 0$, the definition of λ^* in (4.39) remains true.

Now, that we have proved that the value of λ^* preserves the order of the waves, we give in the next proposition the value of the W_0^* intermediate state.

Proposition 35. Assume that h_L and h_R are positive and $\frac{\hat{u}_R}{h_R} \neq \frac{\hat{u}_L}{h_L}$. The intermediate state W_0^* is given by

- If $\lambda^* > 0$

$$\left\{ \begin{array}{l} h_0^* = h_{HLL} - \frac{\lambda_L C_{\alpha_{L,R}, \tilde{B}}}{(\lambda_R - \lambda_L)} \\ \bar{u}_0^* = \frac{h_{HLL} \bar{u}_{HLL} + \frac{\Delta x \cdot \tilde{B}}{\lambda_R - \lambda_L}}{h_0^*}, \\ \hat{u}_0^* = \frac{\hat{u}_L}{h_L} h_0^*, \end{array} \right. \quad (4.41)$$

- If $\lambda^* < 0$

$$\left\{ \begin{array}{l} h_0^* = h_{HLL} - \frac{\lambda_R C_{\alpha_{L,R}, \tilde{B}}}{(\lambda_R - \lambda_L)}, \\ \bar{u}_0^* = \frac{h_{HLL} \bar{u}_{HLL} + \frac{\Delta x \cdot \tilde{B}}{\lambda_R - \lambda_L}}{h_0^*}, \\ \hat{u}_0^* = \frac{\hat{u}_R}{h_R} h_0^*. \end{array} \right. \quad (4.42)$$

Proof. Given the sign of λ^* the W_0^* intermediate states can be directly deduced from relations (4.35) and (4.33). \square

Remark 19. If $\frac{\hat{u}_R}{h_R} = \frac{\hat{u}_L}{h_L}$, we get from (4.36) that $\frac{\hat{u}_R^*}{h_R^*} = \frac{\hat{u}_L^*}{h_L^*}$ and we retrieve the intermediate standard velocities of the HLL_0 approximate Riemann solver in (HLL_0) . We choose to define λ^* as done in (4.39). Therefore, relations (HLL_0^*) and (4.41) for $\lambda^* > 0$ or (HLL_0^*) and (4.42) for $\lambda^* < 0$ are valid for all cases. If $\lambda^* = 0$, we get $\lambda^* = \lambda_0$ and we retrieve the intermediate states of the HLL_0 approximate Riemann solver in (HLL_0) .

Remark 20. We note that for dry areas, i.e $h = 0$, we impose $\bar{u} = 0$ and $\hat{u} = 0$. Hence, if $h_L = 0$ and $h_R \neq 0$ then $I = \lambda_L h_L^* < 0$ as defined in (4.40) and we have $\lambda^* = \lambda_L$. Similarly, if $h_R = 0$ and $h_L \neq 0$ then, $I = \lambda_R h_R^* > 0$ and we have $\lambda^* = \lambda_R$. In both cases, we retrieve the HLL_0 scheme for which the dry areas are studied in Remark 17.

It remains to prove that the scheme preserves the well-balanced property. We will only do that for the case $\lambda^* > 0$ but for $\lambda^* < 0$ the same method applies.

Proposition 36. *Assume that h_L and h_R are positive. For W_L and W_R defining a smooth steady state and for $\lambda^* > 0$, the intermediate states (HLL_0^*) and (4.41) satisfy the well-balanced property (4.7).*

Proof. Since the left W_L^* and the right W_R^* water height and mean velocity intermediate states are equal to those defined in HLL_0 then, they obviously verify the well-balanced property, see Proposition 30. In addition, we can conclude from relation (4.35) that also the W_0^* intermediate water height and velocity verify the well-balanced property.

Concerning the shear, for W_L and W_R defining a steady state (4.7), we have $S_L = S_R$ then, we retrieve the shear of the HLL_0 , see Remark 19. This leads to $S^* = S$. Therefore, the system (HLL_0^*) and (4.41) satisfy the well-balanced property. \square

4.6.2 Positive and well-balanced version of the HLL_0^* scheme

All the above results hold if the intermediate water heights are positive, but these water heights can be also negative. However, as in the previous scheme, we can prove that one and only one intermediate water height can be negative. In fact, according to the water height consistency relation (4.38), only one quantity among h_L^* or h_R^* can be negative. Let us suppose that $h_L^* < 0$ then, we necessarily have $h_R^* > 0$ and we can conclude from (4.40) that $I > 0$ leading to $\lambda^* > 0$, see Proposition 34. Hence, we get from the continuity relation (4.35) that $h_0^* = h_R^* > 0$. In the same way, for $\lambda^* < 0$, if $h_R^* < 0$ then, we get that $h_0^* = h_L^* > 0$ and we can conclude that at most one water height is negative.

To ensure the positivity of all intermediate water heights we will follow the strategy proposed in § 4.5 for HLL_0 , which consists in testing the sign of

$$\tilde{h}_L^* = h_{HLL} - \frac{\lambda_R C_{\alpha_{L,R}, \tilde{B}}}{(\lambda_R - \lambda_L)} \quad \text{and} \quad \tilde{h}_R^* = h_{HLL} - \frac{\lambda_L C_{\alpha_{L,R}, \tilde{B}}}{(\lambda_R - \lambda_L)}.$$

The case of $\tilde{h}_L^* > 0$ and $\tilde{h}_R^* > 0$

In this case, we consider:

- for $\lambda^* > 0$, the intermediate states (HLL_0^*) and (4.41),

- for $\lambda^* < 0$, the intermediate states (HLL_0^*) and (4.42).

Hence, the positivity of the intermediate water heights is ensured and the scheme verifies the well-balanced property, see Proposition 36.

The case of $\tilde{h}_L^* < 0$ and $\tilde{h}_R^* > 0$

In this case, $\lambda^* > 0$ and the well-balanced property is lost. As a consequence, we replace the equilibrium relations (4.33) and (4.34) by the fact that the L^* intermediate state vanishes

$$\begin{cases} h_L^* = 0, \\ \bar{u}_L^* = 0, \\ \hat{u}_L^* = 0, \end{cases} \quad (4.43)$$

the continuities (4.35) across $\lambda^* > 0$

$$\begin{cases} h_0^* = h_R^*, \\ \bar{u}_0^* = \bar{u}_R^*. \end{cases} \quad (4.44)$$

and the continuity of $\frac{\hat{u}}{h}$ across the external wave λ_R

$$\frac{\hat{u}_R}{h_R} = \frac{\hat{u}_R^*}{h_R^*}, \quad (4.45)$$

To close the system of ten unknowns, we set as previously

$$\lambda^* = \frac{\lambda_R h_R^* - h_R (\lambda_R - \bar{u}_R)}{h_R^*}. \quad (4.46)$$

Note that the consistency relations (4.32) combined with all the relations above give

$$\begin{cases} \lambda_R h_R^* &= (\lambda_R - \lambda_L) h_{HLL}, \\ \lambda_R h_R^* \bar{u}_R^* &= A_{h_{HLL} \bar{u}_{HLL}, \tilde{B}}, \\ \lambda_R \hat{u}_R^* + \lambda^* (\hat{u}_0^* - \hat{u}_R^*) &= (\lambda_R - \lambda_L) \hat{u}_{HLL}, \end{cases} \quad (4.47)$$

Proposition 37. Assume that h_L and h_R are positive. For $\frac{\hat{u}_L}{h_L} \neq \frac{\hat{u}_R}{h_R}$, the system (4.43)-(4.44)-(4.47)-(4.45) and (4.46) admits a unique solution

$$(h_L^*, h_0^*, h_R^*, \bar{u}_L^*, \bar{u}_0^*, \bar{u}_R^*, \hat{u}_L^*, \hat{u}_0^*, \hat{u}_R^*, \lambda^*) \in \mathbb{R}^{10}$$

given by

$$\left\{ \begin{array}{l} \lambda^* = \frac{h_L \bar{u}_L - \lambda_L h_L}{(\lambda_R - \lambda_L) h_{HLL}} \lambda_R, \\ h_L^* = 0, \\ h_0^* = \frac{(\lambda_R - \lambda_L) h_{HLL}}{\lambda_R}, \\ h_R^* = \frac{(\lambda_R - \lambda_L) h_{HLL}}{\lambda_R}, \\ \bar{u}_L^* = 0, \\ \bar{u}_0^* = \frac{A_{h_{HLL} \bar{u}_{HLL}, \bar{B}}}{\lambda_R h_R^*}, \\ \bar{u}_R^* = \frac{A_{h_{HLL} \bar{u}_{HLL}, \bar{B}}}{\lambda_R h_R^*}, \\ \hat{u}_L^* = 0, \\ \hat{u}_0^* = \frac{(\lambda_R - \lambda_L) \hat{u}_{HLL}}{\lambda_R}, \\ \hat{u}_R^* = \frac{\hat{u}_R}{h_R} \left(\frac{\lambda^* (\lambda_R - \lambda_L) h_{HLL}}{\lambda_R} \right), \end{array} \right. \quad (4.48)$$

where the contact discontinuity λ^* is positive as well as the intermediate water heights h_0^* and h_R^* .

Remark 21. For $\frac{\hat{u}_R}{h_R} = \frac{\hat{u}_L}{h_L}$, (4.48) is also a solution of the system.

Remark 22. We show that $\lambda_L < \lambda^* < \lambda_R$ as in Proposition 34.

The case of $\tilde{h}_L^* > 0$ and $\tilde{h}_R^* < 0$

Similarly, the scheme should verify the consistency relations (4.38) but, since the well-balanced property is lost then, the equilibrium relations (4.33) and (4.34) are replaced by the fact that R^* intermediate states vanishes

$$\left\{ \begin{array}{l} h_R^* = 0, \\ \bar{u}_R^* = 0, \\ \hat{u}_R^* = 0, \end{array} \right. \quad (4.49)$$

Moreover, we consider the continuities (4.35) across $\lambda^* < 0$ and the continuity of $\frac{\hat{u}}{h}$ across the external wave λ_L in (4.36). Here also, to close the system of ten unknowns, we set as previously

$$\lambda^* = \frac{\lambda_L h_L^* - h_L (\lambda_L - \bar{u}_L)}{h_L^*}. \quad (4.50)$$

Proposition 38. Assume that h_L and h_R are positive. For $\frac{\hat{u}_L}{h_L} \neq \frac{\hat{u}_R}{h_R}$, the system (4.38)-(4.49)-(4.35)-(4.36) and (4.50) admits a unique solution

$$(h_L^*, h_0^*, h_R^*, \bar{u}_L^*, \bar{u}_0^*, \bar{u}_R^*, \hat{u}_L^*, \hat{u}_0^*, \hat{u}_R^*, \lambda^*) \in \mathbb{R}^{10}$$

given by

$$\left\{ \begin{array}{l} \lambda^* = \frac{\lambda_R h_R - h_R \bar{u}_R}{(\lambda_R - \lambda_L) h_{HLL}} \lambda_L, \\ h_L^* = -\frac{\lambda_L}{(\lambda_R - \lambda_L) h_{HLL}}, \\ h_0^* = -\frac{(\lambda_R - \lambda_L) h_{HLL}}{\lambda_L}, \\ h_R^* = 0, \\ \bar{u}_L^* = -\frac{A_{h_{HLL}} \bar{u}_{HLL, \bar{B}}}{\lambda_L h_L^*}, \\ \bar{u}_0^* = -\frac{A_{h_{HLL}} \bar{u}_{HLL, \bar{B}}}{\lambda_L h_L^*}, \\ \bar{u}_R^* = 0, \\ \hat{u}_L^* = \frac{\hat{u}_L}{h_L} \frac{\lambda_L h_L - h_L \bar{u}_L}{\lambda_L}, \\ \hat{u}_0^* = \frac{(\lambda_R - \lambda_L) \hat{u}_{HLL}}{\lambda^*}, \\ \hat{u}_R^* = 0, \end{array} \right. \quad (4.51)$$

where the contact discontinuity λ^* is negative and the intermediate water heights h_L^* and h_0^* are positive.

Remark 23. For $\frac{\hat{u}_R}{h_R} = \frac{\hat{u}_L}{h_L}$, (4.51) is also a solution of the system.

Remark 24. We show that $\lambda_L < \lambda^* < \lambda_R$ as done in Proposition 34.

The HLL_0^* scheme is well-balanced and takes into consideration the transport of S which is not the case in the HLL_0 scheme but has the same failures as the HLL^* scheme. The scheme verifies the maximum principle on S since the intermediate states of S are either S_L or S_R but doesn't verify a discrete energy inequality.

4.7 The $HLL_{0, \bar{u}}$ approximated Riemann solver

Here we propose a second 4-waves ARS that is a mixture between HLL_0 and $HLL_{\bar{u}}$.

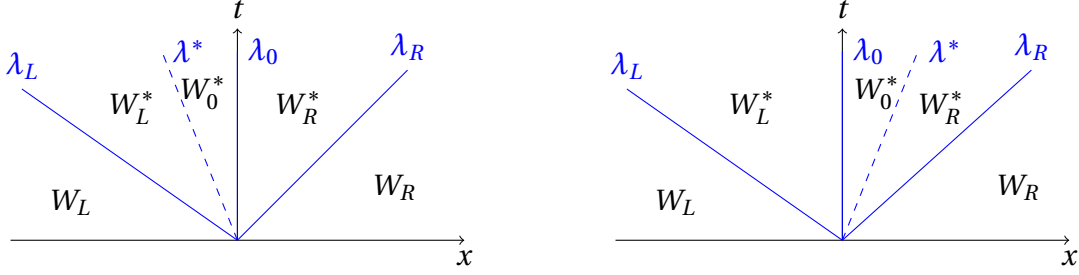


Figure 4.3: The waves representation of the $HLL_{0,\bar{u}}$ approximate Riemann solver with $\lambda^* < 0$ on the left and $\lambda^* > 0$ on the right.

The approximate Riemann solver reads

$$\tilde{W}_{HLL_{0,\bar{u}}}\left(\frac{x}{t}, U_L, Z_L, U_R, Z_R\right) = \begin{cases} W_L & \text{if } \frac{x}{t} < \lambda_L, \\ W_L^* & \text{if } \lambda_L < \frac{x}{t} < \lambda^* \mathbb{1}_{\{\lambda^* < 0\}}, \\ W_0^* & \text{if } \lambda^* \mathbb{1}_{\{\lambda^* < 0\}} < \frac{x}{t} < \lambda^* \mathbb{1}_{\{\lambda^* > 0\}}, \\ W_R^* & \text{if } \lambda^* \mathbb{1}_{\{\lambda^* > 0\}} < \frac{x}{t} < \lambda_R, \\ W_R & \text{if } \frac{x}{t} > \lambda_R. \end{cases}$$

Following the same strategy done in the HLL_0^* solver, we start by the consistency relation (4.32) and the equilibrium relations (4.33) and (4.34). Moreover, we take into account the second Riemann invariant on the external waves (4.36). Finally, contrary to (4.35), we consider only that the mean velocity is constant through λ^* contact discontinuity and we impose that it is equal to λ^* :

$$\lambda^* = \begin{cases} \bar{u}_L^* = \bar{u}_0^* & \text{if } \lambda^* < 0, \\ \bar{u}_R^* = \bar{u}_0^* & \text{if } \lambda^* > 0. \end{cases} \quad (4.52)$$

Remark 25. *The computation of the intermediate states of this scheme is more complicated than in the previous schemes $HLL_{\bar{u}}$ and HLL_0^* since there is no equal intermediate water heights leading to different intermediate discharges.*

We can remark that given the two states W_L and W_R , we are able to know the sign and the explicit form of $A_{h_{HLL}\bar{u}_{HLL},\tilde{B}}$. Hence, we claim the next proposition that gives a property concerning the sign of λ^* .

Proposition 39. *Assume that h_L, h_R, h_L^*, h_0^* and h_R^* are positive. Let λ_L, λ_R and \bar{u}_{HLL} be defined respectively in (4.4) and (HLL). Suppose that $\lambda_L < \lambda^* < \lambda_R$ therefore, the sign of $\bar{u}_L^*, \bar{u}_0^*, \bar{u}_R^*$ and λ^* is the same as the sign of $A_{h_{HLL}\bar{u}_{HLL},\tilde{B}}$.*

Proof. Suppose that $\lambda^* > 0$. Then, we can conclude from (4.52) that \bar{u}_0^* , \bar{u}_R^* and λ^* have the same sign. In addition, for $h_L^* > 0$ and $h_0^* > 0$, relation (4.33) implies that the sign of \bar{u}_L^* is the same as \bar{u}_0^* . Moreover, the second equation of (4.32) can be written as

$$h_R^* \bar{u}_R^* (\lambda_R - \lambda^*) + h_L^* \bar{u}_L^* (\lambda^* - \lambda_L) = A_{h_{HLL} \bar{u}_{HLL}, \tilde{B}},$$

which for $\lambda_L < \lambda^* < \lambda_R$, $h_L^* > 0$ and $h_R^* > 0$ ensures that the sign of \bar{u}_L^* and \bar{u}_R^* is the same as the sign of $A_{h_{HLL} \bar{u}_{HLL}, \tilde{B}}$. Finally, we can conclude that the sign of \bar{u}_L^* , \bar{u}_0^* , \bar{u}_R^* and λ^* is the same as the sign of $A_{h_{HLL} \bar{u}_{HLL}, \tilde{B}}$. Same conclusion holds for $\lambda^* < 0$ \square

Let us now determine the value of the intermediate states based on the sign of $A_{h_{HLL} \bar{u}_{HLL}, \tilde{B}}$.

4.7.1 Well-balanced version of the $HLL_{0, \bar{u}}$ scheme

Proposition 40. *Assume that $h_L > 0$, $h_R > 0$ and $\lambda_L < \lambda^* < \lambda_R$. Assume that Proposition 39 is verified. The system (4.32)-(4.33)-(4.34)-(4.36) and (4.52) admits a unique solution*

$$(h_L^*, h_0^*, h_R^*, \bar{u}_L^*, \bar{u}_0^*, \bar{u}_R^*, \hat{u}_L^*, \hat{u}_0^*, \hat{u}_R^*, \lambda^*) \in \mathbb{R}^{10}$$

given by

- for $A_{h_{HLL} \bar{u}_{HLL}, \tilde{B}} > 0$

$$\left\{ \begin{array}{l}
\lambda^* = \frac{A_{h_{HLL}\bar{u}_{HLL},\tilde{B}}}{(\lambda_R - \lambda_L)h_{HLL} - \lambda_L C_{\alpha_{L,R},\tilde{B}}}, \\
h_L^* = \frac{h_L\bar{u}_L - \lambda_L h_L - \lambda^* C_{\alpha_{L,R},\tilde{B}}}{\lambda^* - \lambda_L}, \\
h_0^* = \frac{h_L\bar{u}_L - \lambda_L h_L - \lambda_L C_{\alpha_{L,R},\tilde{B}}}{\lambda^* - \lambda_L}, \\
h_R^* = \frac{\lambda_R h_R - h_R \bar{u}_R}{\lambda_R - \lambda^*}, \\
\bar{u}_L^* = \frac{h_0^*}{h_L^*} \lambda^*, \\
\bar{u}_0^* = \frac{A_{h_{HLL}\bar{u}_{HLL},\tilde{B}}}{(\lambda_R - \lambda_L)h_{HLL} - \lambda_L C_{\alpha_{L,R},\tilde{B}}}, \\
\bar{u}_R^* = \frac{A_{h_{HLL}\bar{u}_{HLL},\tilde{B}}}{(\lambda_R - \lambda_L)h_{HLL} - \lambda_L C_{\alpha_{L,R},\tilde{B}}}, \\
\hat{u}_L^* = \frac{\hat{u}_L}{h_L} \left(\frac{\lambda_L h_L - h_L \bar{u}_L + \lambda^* C_{\alpha_{L,R},\tilde{B}}}{\lambda_L - \lambda^*} \right), \\
\hat{u}_0^* = \frac{\hat{u}_L}{h_L} \left(\frac{\lambda_L h_L - h_L \bar{u}_L + \lambda_L C_{\alpha_{L,R},\tilde{B}}}{\lambda_L - \lambda^*} \right), \\
\hat{u}_R^* = \frac{\hat{u}_R}{h_R} \left(\frac{\lambda_R h_R - h_R \bar{u}_R}{\lambda_R - \lambda^*} \right),
\end{array} \right. \quad (4.53)$$

- for $A_{h_{HLL}\bar{u}_{HLL},\bar{B}} < 0$

$$\left\{ \begin{array}{l} \lambda^* = \frac{A_{h_{HLL}\bar{u}_{HLL},\bar{B}}}{(\lambda_R - \lambda_L) h_{HLL} - \lambda_R C_{\alpha_{L,R},\bar{B}}}, \\ h_L^* = \frac{h_L \bar{u}_L - \lambda_L h_L}{\lambda^* - \lambda_L}, \\ h_0^* = \frac{\lambda_R h_R - h_R \bar{u}_R - \lambda_R C_{\alpha_{L,R},\bar{B}}}{\lambda_R - \lambda^*}, \\ h_R^* = \frac{\lambda_R h_R - h_R \bar{u}_R - \lambda^* C_{\alpha_{L,R},\bar{B}}}{\lambda_R - \lambda^*}, \\ \bar{u}_L^* = \frac{A_{h_{HLL}\bar{u}_{HLL},\bar{B}}}{(\lambda_R - \lambda_L) h_{HLL} - \lambda_R C_{\alpha_{L,R},\bar{B}}}, \\ \bar{u}_0^* = \frac{A_{h_{HLL}\bar{u}_{HLL},\bar{B}}}{(\lambda_R - \lambda_L) h_{HLL} - \lambda_R C_{\alpha_{L,R},\bar{B}}}, \\ \bar{u}_R^* = \frac{h_0^*}{h_R^*} \lambda^*, \\ \hat{u}_L^* = \frac{\hat{u}_L}{h_L} \left(\frac{\lambda_L h_L - h_L \bar{u}_L}{\lambda_L - \lambda^*} \right), \\ \hat{u}_0^* = \frac{\hat{u}_R}{h_R} \left(\frac{\lambda_R h_R - h_R \bar{u}_R - \lambda_R C_{\alpha_{L,R},\bar{B}}}{\lambda_R - \lambda^*} \right), \\ \hat{u}_R^* = \frac{\hat{u}_R}{h_R} \left(\frac{\lambda_R h_R - h_R \bar{u}_R - \lambda^* C_{\alpha_{L,R},\bar{B}}}{\lambda_R - \lambda^*} \right), \end{array} \right. \quad (4.54)$$

Proof. We will start by proving the computations for $A_{h_{HLL}\bar{u}_{HLL},\bar{B}} > 0$ which, according to Proposition 39 leads to $\lambda^* > 0$. In this case the consistency relations (4.32) are equivalent to

$$\left\{ \begin{array}{l} \lambda_R h_R^* - \lambda_L h_L^* + \lambda^* (h_0^* - h_R^*) = (\lambda_R - \lambda_L) h_{HLL}, \\ \lambda_R h_R^* \bar{u}_R^* - \lambda_L h_L^* \bar{u}_L^* + \lambda^* (h_0^* \bar{u}_0^* - h_R^* \bar{u}_R^*) = A_{h_{HLL}\bar{u}_{HLL},\bar{B}}, \\ \lambda_R \hat{u}_R^* - \lambda_L \hat{u}_L^* + \lambda^* (\hat{u}_0^* - \hat{u}_R^*) = (\lambda_R - \lambda_L) \hat{u}_{HLL}, \end{array} \right. \quad (4.55)$$

Multiplying the first equation of (4.55) by λ^* and using the *HLL* intermediate states (*HLL*) we get

$$\lambda^* (\lambda_R h_R - h_R \bar{u}_R + h_L \bar{u}_L - \lambda_L h_L - \lambda_L C_{\alpha_{L,R},\bar{B}}) = h_R^* \bar{u}_R^* (\lambda_R - \lambda^*) + h_L^* \bar{u}_L^* (\lambda^* - \lambda_L).$$

The sum of the above equation with the second one of (4.55) leads to

$$\lambda^* (\lambda_R h_R - h_R \bar{u}_R + h_L \bar{u}_L - \lambda_L h_L - \lambda_L C_{\alpha_{L,R},\bar{B}}) = A_{h_{HLL}\bar{u}_{HLL},\bar{B}},$$

which using (HLL) and (4.52), is nothing but the explicit value of $\lambda^* = \bar{u}_0^* = \bar{u}_R^*$. Now, using the water height continuity in (4.33) and the second Riemann invariant in (4.36), we can conclude

$$\hat{u}_0^* = h_R^* \frac{\hat{u}_L}{h_L}. \quad (4.56)$$

In addition, the third equation of (4.55) reads

$$\lambda_R \hat{u}_R \frac{h_R^*}{h_R} - \lambda_L \hat{u}_L \frac{h_L^*}{h_L} + \lambda^* \left(\hat{u}_L \frac{h_R^*}{h_L} - \hat{u}_R \frac{h_R^*}{h_R} \right) = \lambda_R \hat{u}_R - \lambda_L \hat{u}_L - \bar{u}_R \hat{u}_R + \bar{u}_L \hat{u}_L.$$

that leads to

$$\lambda^* h_R^* \left(\frac{\hat{u}_L}{h_L} - \frac{\hat{u}_R}{h_R} \right) = \frac{\hat{u}_L}{h_L} (\lambda_L h_L^* - \lambda_L h_L + \bar{u}_L h_L) + \frac{\hat{u}_R}{h_R} (-\lambda_R h_R^* + \lambda_R h_R - \bar{u}_R h_R).$$

The first equation of (HLL) implies

$$\lambda_L h_L^* - \lambda_L h_L + \bar{u}_L h_L = \lambda_R h_R^* - \lambda_R h_R + \bar{u}_R h_R.$$

Hence, if $\frac{\hat{u}_R}{h_R} \neq \frac{\hat{u}_L}{h_L}$

$$\lambda^* = \frac{\lambda_R h_R^* - h_R (\lambda_R - \bar{u}_R)}{h_R^*}.$$

leading to the expression of h_R^* . Next, using (4.34) in the first equation of (4.55) we get h_L^* leading to h_0^* . Finally, the intermediate shear velocities \hat{u}_L^* and \hat{u}_R^* are obtained using (4.36) and (4.56).

The same strategy applies for $A_{h_{HLL}\bar{u}_{HLL},\bar{B}} < 0$. \square

Remark 26. For $\frac{\hat{u}_R}{h_R} = \frac{\hat{u}_L}{h_L}$, (4.53) is also a solution of the system for $A_{h_{HLL}\bar{u}_{HLL},\bar{B}} > 0$ and (4.54) is also a solution of the system for $A_{h_{HLL}\bar{u}_{HLL},\bar{B}} < 0$.

Proposition 41. Suppose $\lambda^* > 0$ verifying $\lambda_L < \lambda^* < \lambda_R$. For W_L and W_R defining a smooth steady state, if h_L^* and h_0^* are positive then the scheme satisfies the well-balanced property (4.7), i.e

$$h_L^* = h_L, \quad h_R^* = h_0^* = h_R, \quad h_L^* \bar{u}_L^* = h_0^* \bar{u}_0^* = h_R^* \bar{u}_R^* = M \text{ and } \frac{\hat{u}_L}{h_L} = \frac{\hat{u}_0^*}{h_0^*} = \frac{\hat{u}_R^*}{h_R^*} = S.$$

Proof. For W_L and W_R defining a smooth steady state (4.7), we have

$$[h\bar{u}]_L^R = 0, \quad \left[\frac{\bar{u}^2}{2} + \frac{3\hat{u}^2}{2} + g(h+Z) \right]_L^R = 0 \quad \text{and} \quad [\bar{u}\hat{u}]_L^R = 0.$$

Following the proof of Proposition 30, we get

$$\begin{aligned} C_{\alpha_{L,R},\bar{B}} &= h_R - h_L, \\ A_{h_{HLL}\bar{u}_{HLL},\bar{B}} &= M(\lambda_R - \lambda_L), \\ (\lambda_R - \lambda_L)h_{HLL} &= \lambda_R h_R - \lambda_L h_L. \end{aligned} \quad (4.57)$$

In this case,

$$\lambda^* = \frac{M(\lambda_R - \lambda_L)}{\lambda_R h_R - \lambda_L h_L - \lambda_R(h_R - h_L)} = \frac{M}{h_R} = \bar{u}_R.$$

According to (4.36), we have $\bar{u}_0^* = \bar{u}_R^* = \bar{u}_R$. At smooth steady states, the right intermediate water height reads

$$h_R^* = \frac{\lambda_R h_R - M}{\lambda_R - \frac{M}{h_R}} = h_R,$$

and the middle intermediate water height reads

$$h_0^* = \frac{h_L \bar{u}_L - \lambda_L h_L - \lambda_L(h_R - h_L)}{\frac{M}{h_R} - \lambda_L} = h_R,$$

hence, $h_0^* = h_R^* = h_R$. Therefore, $h_R^* \bar{u}_R^* = h_R \lambda^* = M$ and $h_0^* \bar{u}_0^* = h_R \frac{M}{h_R} = M$ which leads using (4.33) to $h_L^* \bar{u}_L^* = M$. In addition, the left intermediate water height verifies

$$h_L^* = \frac{h_L \bar{u}_L - \lambda_L h_L - \lambda^*(h_R - h_L)}{\frac{M}{h_R} - \lambda_L} = \frac{h_L \bar{u}_L - \lambda_L h_L - \frac{M}{h_R}(h_R - h_L)}{\frac{M}{h_R} - \lambda_L} = h_L,$$

It remains, to prove the well balanced property on S . From relation (4.36), we can directly conclude that $\frac{\hat{u}_L}{h_L} = \frac{\hat{u}_R}{h_R} = S$. Then, using (4.33) we get $\hat{u}_0^* = h_0^* S$ leading to $\frac{\hat{u}_0^*}{h_0^*} = S$. \square

Remark 27. For $\lambda^* < 0$ verifying $\lambda_L < \lambda^* < \lambda_R$ the scheme is also well-balanced.

4.7.2 Positive and well-balanced version of the $HLL_{0,\bar{u}}$ scheme

We have determined the value of the intermediate states considering that

- (i) the middle wave λ^* have the same sign as $A_{h_{HLL}\bar{u}_{HLL},\bar{B}}$ and verifies $\lambda_L < \lambda^* < \lambda_R$,

(ii) the intermediate water heights h_L^* , h_0^* and h_R^* are positive.

However, this assumptions may not be true. Let us suppose that (i) is true then, as in the previous sections we can remark that only one of the intermediate states can be negative. More precisely, consider the case $\lambda^* > 0$, then the right water height intermediate state h_R^* defined in (4.53) is always positive but, h_L^* and h_0^* might not be positive. In fact,

- for $C_{\alpha_{L,R},\bar{B}} > 0$, h_0^* is positive but nothing can be concluded concerning the sign of h_L^* .
- for $C_{\alpha_{L,R},\bar{B}} < 0$, h_L^* is positive but nothing can be concluded concerning the sign of h_0^* .

Hence, either h_L^* or h_0^* can be negative and not both of them. In the same way, we prove that when $\lambda^* < 0$, $h_L^* > 0$ and either h_0^* or h_R^* can be negative but not both of them.

Our strategy is then to ensure first that (i) is true by modifying the external waves λ_L and λ_R when needed. Then, ensure (ii) as done in the previous section.

(I) **The case** $A_{h_{HLL}\bar{u}_{HLL},\bar{B}} > 0$

Suppose that $\lambda^* > 0$. The denominator of λ^* must be necessarily positive, see (4.53). We denote it by

$$D_p = (\lambda_R - \lambda_L) h_{HLL} - \lambda_L C_{\alpha_{L,R},\bar{B}}.$$

In addition, $\lambda^* - \lambda_L > 0$ but nothing can be concluded for $\lambda_R - \lambda^*$. Therefore,

- if $\lambda_R - \lambda^* > 0$ then, $\lambda_L < \lambda^* < \lambda_R$.
- if $\lambda_R - \lambda^* < 0$ then, a correction for λ_R is needed to ensure that $\lambda_R - \lambda^* > 0$.

When a correction is needed, we exhibit, for $\lambda^* > 0$, the quantity $\lambda_R - \lambda^*$

$$\begin{aligned} \lambda_R - \lambda^* &= \lambda_R - \frac{A_{h_{HLL}\bar{u}_{HLL},\bar{B}}}{D_p} \\ &= \frac{\lambda_R D_p - A_{h_{HLL}\bar{u}_{HLL},\bar{B}}}{D_p}. \end{aligned}$$

As $D_p > 0$ then, the positivity of $\lambda_R - \lambda^*$ depends on the positivity of its numerator. Let us define

$$P_{\lambda^*, \lambda_R} := \lambda_R D_p - A_{h_{HLL} \bar{u}_{HLL}, \bar{B}}$$

Using the definition of h_{HLL} in (HLL), we have

$$\begin{aligned} P_{\lambda^*, \lambda_R} &= \lambda_R h_R (\lambda_R - \bar{u}_R) + \lambda_R h_L (\bar{u}_L - \lambda_L) - \lambda_L \lambda_R C_{\alpha_{L,R}, \bar{B}} - A_{h_{HLL} \bar{u}_{HLL}, \bar{B}} \\ &= \lambda_R^2 h_R + \lambda_R \left(-h_R \bar{u}_R + h_L \bar{u}_L - \lambda_L h_L - \lambda_L C_{\alpha_{L,R}, \bar{B}} \right) - A_{h_{HLL} \bar{u}_{HLL}, \bar{B}} \\ &= \lambda_R^2 h_R - T \lambda_R - A_{h_{HLL} \bar{u}_{HLL}, \bar{B}}, \end{aligned}$$

where $T = h_R \bar{u}_R + \lambda_L h_L - h_L \bar{u}_L + \lambda_L C_{\alpha_{L,R}, \bar{B}}$.

P_{λ^*, λ_R} is a second degree polynomial with a single variable λ_R where the corresponding discriminant is

$$\Delta_1 = T^2 + 4h_R A_{h_{HLL} \bar{u}_{HLL}, \bar{B}} > 0.$$

To ensure $P_{\lambda^*, \lambda_R} > 0$, we choose $\lambda_R > \lambda_R^c = \frac{T + \sqrt{\Delta_1}}{2h_R}$. The relation $P_{\lambda^*, \lambda_R} > 0$ also leads to $D_p > 0$ and in this case the hypothesis $\lambda^* > 0$ is true.

Now that we ensured the order of the waves, we turn to the positivity of the intermediate water heights by testing for $\lambda^* > 0$ the quantities

$$\tilde{h}_L^* = \frac{h_L \bar{u}_L - \lambda_L h_L - \lambda^* C_{\alpha_{L,R}, \bar{B}}}{\lambda^* - \lambda_L} \quad \text{and} \quad \tilde{h}_0^* = \frac{h_L \bar{u}_L - \lambda_L h_L - \lambda_L C_{\alpha_{L,R}, \bar{B}}}{\lambda^* - \lambda_L}. \quad (4.58)$$

The case $\tilde{h}_L^* > 0$ and $\tilde{h}_0^* > 0$

In this case, the intermediate states are given by (4.53). The intermediate water heights are positive and the scheme verifies the well-balanced property, see Proposition 41.

The case $\tilde{h}_L^* < 0$ and $\tilde{h}_0^* > 0$

If one of the quantities defined in (4.58) is negative then, the well-balanced property is lost. Hence, we consider the consistency relations (4.55) and we replace the equilibrium relations by the fact that the L^* intermediate state vanishes

$$\begin{cases} h_L^* = 0, \\ \bar{u}_L^* = 0, \\ \hat{u}_L^* = 0 \end{cases} \quad (4.59)$$

We also consider respectively the relation (4.52) for $\lambda^* > 0$. Finally, contrary to (4.36) on both external waves, we will only consider the Riemann invariant for the right wave

$$\frac{\hat{u}_R}{h_R} = \frac{\hat{u}_R^*}{h_R^*}, \quad (4.60)$$

and we will replace the Riemann invariant on the left wave by

$$\frac{\hat{u}_L}{h_L} = \frac{\hat{u}_0^*}{h_0^*}. \quad (4.61)$$

Proposition 42. *Assume that h_L and h_R are positive. For $\frac{\hat{u}_L}{h_L} \neq \frac{\hat{u}_R}{h_R}$, the system (4.55)-(4.59)-(4.52)-(4.60) and (4.61) admits a unique solution*

$$(h_L^*, h_0^*, h_R^*, \bar{u}_L^*, \bar{u}_0^*, \bar{u}_R^*, \hat{u}_L^*, \hat{u}_0^*, \hat{u}_R^*, \lambda^*) \in \mathbb{R}^{10}$$

given by

$$\left\{ \begin{array}{l} \lambda^* = \frac{A_{h_{HLL}\bar{u}_{HLL},\bar{B}}}{(\lambda_R - \lambda_L) h_{HLL}}, \\ h_R^* = \frac{\lambda_R h_R - h_R \bar{u}_R}{\lambda_R - \lambda^*}, \\ h_0^* = \frac{h_L \bar{u}_L - \lambda_L h_L}{\lambda^*}, \\ h_L^* = 0, \\ \bar{u}_L^* = 0, \\ \bar{u}_0^* = \frac{A_{h_{HLL}\bar{u}_{HLL},\bar{B}}}{(\lambda_R - \lambda_L) h_{HLL}}, \\ \bar{u}_R^* = \frac{A_{h_{HLL}\bar{u}_{HLL},\bar{B}}}{(\lambda_R - \lambda_L) h_{HLL}}, \\ \hat{u}_L^* = 0, \\ \hat{u}_0^* = \frac{\hat{u}_L}{h_L} \left(\frac{h_L \bar{u}_L - \lambda_L h_L}{\lambda^*} \right), \\ \hat{u}_R^* = \frac{\hat{u}_R}{h_R} \left(\frac{\lambda_R h_R - h_R \bar{u}_R}{\lambda_R - \lambda^*} \right), \end{array} \right. \quad (4.62)$$

where the contact discontinuity λ^* is positive as well as the water height intermediate states h_0^* and h_R^* .

Remark 28. For $\frac{\hat{u}_R}{h_R} = \frac{\hat{u}_L}{h_L}$, (4.62) is also a solution of the system.

However, we still have to verify that $\lambda_L < \lambda^* < \lambda_R$. To do that, we follow the same strategy done previously and we choose to correct λ_R when needed by taking $\lambda_R > \lambda_R^{c,1}$ where $\lambda_R^{c,1} = \lambda_R^c$ for $C_{\alpha_{L,R},\bar{B}} = 0$.

The case $\tilde{h}_L^* > 0$ and $\tilde{h}_0^* < 0$

Here, the 4-waves numerical scheme verifies the consistency relations (4.55). In addition, the 0^* intermediate state vanishes

$$\begin{cases} h_0^* = 0, \\ \bar{u}_0^* = 0, \\ \hat{u}_0^* = 0 \end{cases} \quad (4.63)$$

We consider also the relations (4.36). To complete the system we replace the continuity of the mean velocities on λ^* (4.52) by considering only that the right mean velocity is equal to λ^*

$$\lambda^* = \bar{u}_R^*, \quad (4.64)$$

and setting

$$\lambda^* = \frac{A_{h_{HLL}\bar{u}_{HLL},\bar{B}}}{(\lambda_R - \lambda_L) h_{HLL}}, \quad (4.65)$$

Proposition 43. *Assume that h_L and h_R are positive. For $\frac{\hat{u}_L}{h_L} \neq \frac{\hat{u}_R}{h_R}$, the system (4.55)-(4.63)-(4.36)-(4.64) and (4.65) admits a unique solution*

$$(h_L^*, h_0^*, h_R^*, \bar{u}_L^*, \bar{u}_0^*, \bar{u}_R^*, \hat{u}_L^*, \hat{u}_0^*, \hat{u}_R^*, \lambda^*) \in \mathbb{R}^{10}$$

given by

$$\left\{ \begin{array}{l} \lambda^* = \frac{A_{h_{HLL}\bar{u}_{HLL},\bar{B}}}{(\lambda_R - \lambda_L) h_{HLL}}, \\ h_L^* = \frac{\lambda_L h_L - h_L \bar{u}_L}{\lambda_L}, \\ h_0^* = 0, \\ h_R^* = \frac{\lambda_R h_R - h_R \bar{u}_R}{\lambda_R - \lambda^*}, \\ \bar{u}_0^* = 0, \\ \bar{u}_L^* = \frac{A_{h_{HLL}\bar{u}_{HLL},\bar{B}}}{(\lambda_R - \lambda_L) h_{HLL}}, \\ \bar{u}_R^* = \frac{A_{h_{HLL}\bar{u}_{HLL},\bar{B}}}{(\lambda_R - \lambda_L) h_{HLL}}, \\ \hat{u}_L^* = \frac{\hat{u}_L}{h_L} \left(\frac{\lambda_L h_L - h_L \bar{u}_L}{\lambda_L} \right), \\ \hat{u}_0^* = 0, \\ \hat{u}_R^* = \frac{\hat{u}_R}{h_R} \left(\frac{\lambda_R h_R - h_R \bar{u}_R}{\lambda_R - \lambda^*} \right), \end{array} \right. \quad (4.66)$$

where the contact discontinuity λ^* is positive as well as the water height intermediate states h_L^* and h_R^* .

Remark 29. For $\frac{\hat{u}_R}{h_R} = \frac{\hat{u}_L}{h_L}$, (4.66) is also a solution of the system.

Similarly, to ensure that $\lambda_L < \lambda^* < \lambda_R$ we correct λ_R when needed by choosing $\lambda_R > \lambda_R^{c,1}$ where $\lambda_R^{c,1} = \lambda_R^c$ for $C_{\alpha_{L,R},\tilde{B}} = 0$.

(II) **The case** $A_{h_{HLL}\bar{u}_{HLL},\tilde{B}} < 0$

We follow the same strategy. Suppose that $\lambda^* < 0$. According to (4.54) the denominator of λ^* must be necessarily positive. This denominator is denoted by

$$D_n = (\lambda_R - \lambda_L) h_{HLL} - \lambda_R C_{\alpha_{L,R},\tilde{B}}. \quad (4.67)$$

If $\lambda^* < 0$, $\lambda_R - \lambda^* > 0$ but $\lambda_L - \lambda^*$ can be positive. However,

- if $\lambda_L - \lambda^* < 0$ then, $\lambda_L < \lambda^* < \lambda_R$.
- if $\lambda_L - \lambda^* > 0$ then, a correction of λ_L is needed to ensure that $\lambda_L - \lambda^* < 0$ and then $\lambda_L < \lambda^* < \lambda_R$.

In fact,

$$\begin{aligned} \lambda_L - \lambda^* &= \lambda_L - \frac{A_{h_{HLL}\bar{u}_{HLL},\tilde{B}}}{D_n} \\ &= \frac{\lambda_L D_n - A_{h_{HLL}\bar{u}_{HLL},\tilde{B}}}{D_n}. \end{aligned}$$

$D_n > 0$ then, the positivity of $\lambda^* - \lambda_L$ depends on the negativity of its numerator

$$P_{\lambda_L,\lambda^*} := \lambda_L D_n - A_{h_{HLL}\bar{u}_{HLL},\tilde{B}}.$$

Using the definition of h_{HLL} in (HLL), we have

$$\begin{aligned} P_{\lambda_L,\lambda^*} &= \lambda_L h_L (\bar{u}_L - \lambda_L) + \lambda_L h_R (\lambda_R - \bar{u}_R) - \lambda_L \lambda_R C_{\alpha_{L,R},\tilde{B}} - A_{h_{HLL}\bar{u}_{HLL},\tilde{B}} \\ &= -\lambda_L^2 h_L + \lambda_L \left(\lambda_R h_R - h_R \bar{u}_R - \lambda_R C_{\alpha_{L,R},\tilde{B}} + h_L \bar{u}_L \right) + A_{h_{HLL}\bar{u}_{HLL},\tilde{B}} \\ &= -\lambda_L^2 h_L + Q \lambda_L - A_{h_{HLL}\bar{u}_{HLL},\tilde{B}}, \end{aligned}$$

where $Q = \lambda_R h_R - h_R \bar{u}_R + h_L \bar{u}_L - \lambda_R C_{\alpha_{L,R},\tilde{B}}$. In the same way, P_{λ_L,λ^*} is a second degree polynomial with a single variable λ_L where the corresponding discriminant is

$$\Delta_2 = Q^2 + 4h_L A_{h_{HLL}\bar{u}_{HLL},\tilde{B}} > 0.$$

Therefore, we choose $\lambda_L < \lambda_L^c = \frac{Q - \sqrt{\Delta_2}}{2h_L}$. As a consequence, $P_{\lambda_L,\lambda^*} < 0$ hence $D_n > 0$ which verifies the hypothesis of $\lambda^* < 0$.

Now, that we verified that λ^* has the same sign as $A_{h_{HLL}\bar{u}_{HLL},\bar{B}}$ and $\lambda_L < \lambda^* < \lambda_R$, the next step will be to ensure the positivity of the water heights by testing the sign of

$$\tilde{h}_0^* = \frac{\lambda_R h_R - h_R \bar{u}_R - \lambda_R C_{\alpha_{L,R},\bar{B}}}{\lambda_R - \lambda^*} \quad \text{and} \quad \tilde{h}_R^* = \frac{\lambda_R h_R - h_R \bar{u}_R - \lambda^* C_{\alpha_{L,R},\bar{B}}}{\lambda_R - \lambda^*}. \quad (4.68)$$

The case $\tilde{h}_0^* > 0$ and $\tilde{h}_R^* > 0$

The intermediate states are then defined in (4.54). In this case, the scheme ensures the positivity of the intermediate water heights and verifies the well-balanced property Remark 27.

The case $\tilde{h}_0^* > 0$ and $\tilde{h}_R^* < 0$

Since one of the quantities (4.68) is negative then, the scheme is not well-balanced. Hence, we consider the consistency relations (4.38) and we replace the equilibrium relations by the fact that the R^* intermediate state vanishes

$$\begin{cases} h_R^* = 0, \\ \bar{u}_R^* = 0, \\ \hat{u}_R^* = 0 \end{cases} \quad (4.69)$$

In addition, we consider for $\lambda^* < 0$ the relation (4.52). Finally, contrary to (4.36), we will only consider the Riemann invariant for the left wave

$$\frac{\hat{u}_L^*}{h_L^*} = \frac{\hat{u}_L}{h_L}, \quad (4.70)$$

and we will replace the riemann invariants on the right wave by

$$\frac{\hat{u}_0^*}{h_0^*} = \frac{\hat{u}_R}{h_R}. \quad (4.71)$$

Proposition 44. *Assume that h_L and h_R are positive. For $\frac{\hat{u}_L}{h_L} \neq \frac{\hat{u}_R}{h_R}$, the system (4.38)-(4.69)-(4.52)-(4.70) and (4.71) admits a unique solution*

$$(h_L^*, h_0^*, h_R^*, M_L^*, M_0^*, M_R^*, \hat{u}_L^*, \hat{u}_0^*, \hat{u}_R^*, \lambda^*) \in \mathbb{R}^{10}$$

given by

$$\left\{ \begin{array}{l} \lambda^* = \frac{A_{h_{HLL}\bar{u}_{HLL},\tilde{B}}}{(\lambda_R - \lambda_L) h_{HLL}}, \\ h_L^* = \frac{\lambda_L h_L - h_L \bar{u}_L}{\lambda_L - \lambda^*}, \\ h_0^* = \frac{\lambda_R h_R - h_R \bar{u}_R}{-\lambda^*}, \\ h_R^* = 0, \\ \bar{u}_L^* = \frac{A_{h_{HLL}\bar{u}_{HLL},\tilde{B}}}{(\lambda_R - \lambda_L) h_{HLL}}, \\ \bar{u}_0^* = \frac{A_{h_{HLL}\bar{u}_{HLL},\tilde{B}}}{(\lambda_R - \lambda_L) h_{HLL}}, \\ \bar{u}_R^* = 0, \\ \hat{u}_L^* = \frac{\hat{u}_L}{h_L} \left(\frac{\lambda_L h_L - h_L \bar{u}_L}{\lambda_L - \lambda^*} \right), \\ \hat{u}_0^* = \frac{\hat{u}_L}{h_L} \left(\frac{\lambda_L h_L - h_L \bar{u}_L}{\lambda_L - \lambda^*} \right), \\ \hat{u}_R^* = 0, \end{array} \right. \quad (4.72)$$

where the contact discontinuity λ^* is negative and the water height intermediate states h_L^* and h_0^* are positive.

Remark 30. For $\frac{\hat{u}_R}{h_R} = \frac{\hat{u}_L}{h_L}$, (4.72) is also a solution of the system.

To ensure that $\lambda_L < \lambda^* < \lambda_R$ is true, we follow the strategy done previously and we correct λ_L when needed by taking $\lambda_L < \lambda_L^{c,1}$ where $\lambda_L^{c,1} = \lambda_L^c$ for $C_{\alpha_{L,R},\tilde{B}} = 0$.

The case $\tilde{h}_0^* < 0$ and $\tilde{h}_R^* > 0$

Similarly, this scheme verifies the consistency relations (4.32) but, it is not well balanced. Thus, we consider that the 0^* intermediate state vanishes

$$\left\{ \begin{array}{l} h_0^* = 0, \\ \bar{u}_0^* = 0, \\ \hat{u}_0^* = 0 \end{array} \right. \quad (4.73)$$

and the relations (4.36). To complete the system we replace the continuity of the mean velocities on λ^* (4.52) by considering only that the right mean velocity is equal to λ^*

$$\lambda^* = \bar{u}_L^*, \quad (4.74)$$

and setting

$$\lambda^* = \frac{A_{h_{HLL}\bar{u}_{HLL},\tilde{B}}}{(\lambda_R - \lambda_L) h_{HLL}}, \quad (4.75)$$

Proposition 45. Assume that h_L and h_R are positive. For $\frac{\hat{u}_L}{h_L} \neq \frac{\hat{u}_R}{h_R}$, the system (4.32)-(4.73)-(4.36)-(4.74) and (4.75) admits a unique solution

$$(h_L^*, h_0^*, h_R^*, \bar{u}_L^*, \bar{u}_0^*, \bar{u}_R^*, \hat{u}_L^*, \hat{u}_0^*, \hat{u}_R^*, \lambda^*) \in \mathbb{R}^{10}$$

given by

$$\left\{ \begin{array}{l} \lambda^* = \frac{A_{h_{HLL}\bar{u}_{HLL},\bar{B}}}{(\lambda_R - \lambda_L) h_{HLL}}, \\ h_R^* = \frac{\lambda_R h_R - h_R \bar{u}_R}{\lambda_R - \lambda^*}, \\ h_L^* = \frac{\lambda_L h_L - h_L \bar{u}_L}{\lambda_L}, \\ h_0^* = 0, \\ \bar{u}_L^* = \frac{A_{h_{HLL}\bar{u}_{HLL},\bar{B}}}{(\lambda_R - \lambda_L) h_{HLL}}, \\ \bar{u}_0^* = 0, \\ \bar{u}_R^* = \frac{A_{h_{HLL}\bar{u}_{HLL},\bar{B}}}{(\lambda_R - \lambda_L) h_{HLL}}, \\ \hat{u}_L^* = \frac{\hat{u}_L}{h_L} \left(\frac{\lambda_L h_L - h_L \bar{u}_L}{\lambda_L - \lambda^*} \right), \\ \hat{u}_0^* = 0, \\ \hat{u}_R^* = \frac{\hat{u}_R}{h_R} \left(\frac{\lambda_R h_R - h_R \bar{u}_R}{\lambda_R - \lambda^*} \right), \end{array} \right. \quad (4.76)$$

where the contact discontinuity λ^* is negative and the water height intermediate states h_L^* and h_R^* are positive.

Remark 31. For $\frac{\hat{u}_R}{h_R} = \frac{\hat{u}_L}{h_L}$, (4.76) is also a solution of the system.

We correct λ_L when needed by choosing $\lambda_L < \lambda_L^{c,1}$ where $\lambda_L^{c,1} = \lambda_L^c$ for $C_{\alpha_{L,R},\bar{B}} = 0$ to ensure that $\lambda_L < \lambda^* < \lambda_L$.

Remark 32. Since the intermediate states of S are either S_L or S_R then, the scheme verifies maximum principle on S , see the proof of Proposition 16. But, it doesn't verify a discrete energy inequality. This was seen using the numerical strategy proposed in § 3.7.

4.8 Study of positive intermediate water heights corrections

The aim in this section is to compare the behavior of the positive and well-balanced ARS schemes constructed in § 4.5.2 (positive and well-balanced ver-

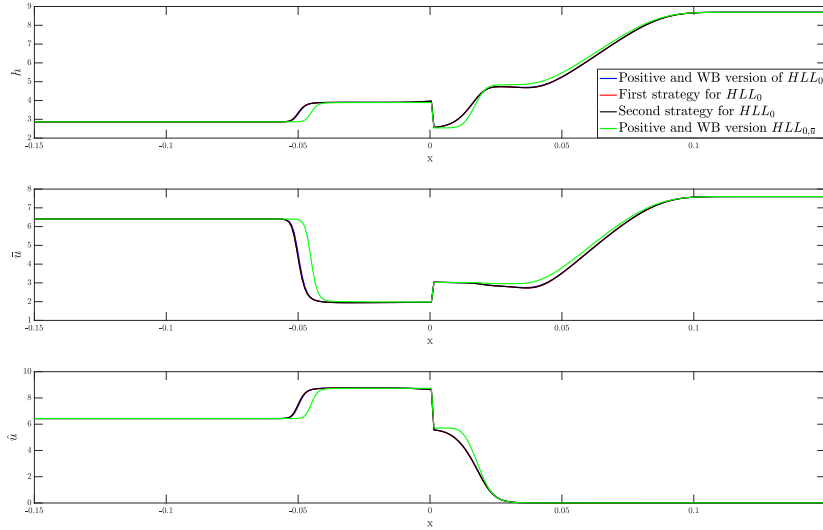


Figure 4.4: Riemann problem with negative intermediate water heights

sion of $HLL_{\bar{u}}$) and in § 4.7.2 (positive and well-balanced version of $HLL_{0,\bar{u}}$) with the strategy proposed in [10] (first strategy of § 4.5.3) and the strategy proposed in [45] to correct the negative intermediate water heights (second strategy of § 4.5.3) with the HLL_0 scheme. The initial conditions of the Riemann problem are

$$U_L = (2.8648, 6.4022, 6.4304, 3.5875),$$

$$U_R = (8.6924, 7.6, 0.0096, 11.3603).$$

We mention that in this case, the exact solution can't be computed because the exact solution of the Riemann problem for (SW_2) with topography was never done. Figure 4.4 shows that the results of the positive version of the HLL_0 scheme, the first strategy and the second strategy with HLL_0 are almost the same regarding the results of the the positive version of the $HLL_{0,\bar{u}}$ scheme. This allows us to conclude that the difference is between the schemes and not between the several strategies used to ensure the positivity of the water heights.

Remark 33. We mention that the first and second strategies proposed in § 4.5.3, see [10, 45], can't be applied to correct the negative intermediate water heights of the $HLL_{0,\bar{u}}$ scheme. In fact, this scheme has three different intermediate states and it will be very difficult to rely on the consistency relations to ensure the positivity of the intermediate water heights.

Chapter 5

Numerical stability of the stationary solutions

This chapter is dedicated to the numerical simulations. In particular, we are interested in two points:

- studying the influence of the water height positivity corrections on the numerical solution
- studying the behavior of the well-balanced schemes around stationary solutions described in Chapter 2 with a focus on the numerical stability on these stationary states.

Stationary solutions

For all the moving steady states we will consider the space domain $I =]0, L[$ where $L = 25$ is the length of the domain and a continuous topography given by

$$Z(x) = \max(0, 0.2 - 0.05(x - x_0)^2), \quad (5.1)$$

verifying Hypothesis 1 for $x \in [8, 12]$ and equal to 0 otherwise.

As mentioned in Chapter 2, §2.3, both quantities $M = h\bar{u} \in \mathbb{R}_+^*$ and $S = \frac{\hat{u}}{h} \in \mathbb{R}_+$ are fixed at the inlet whatever the boundaries are. Here, we choose to fix

$$M = 1.2m/s \quad \text{and} \quad S = 0.5m/s.$$

h_c	0.52
$h_{K_c}^{sub}(x_L) = h_{K_c}^{sub}(x_R)$	0.8769
$h_{K_c}^{sup}(x_L) = h_{K_c}^{sup}(x_R)$	0.3321
$\psi\left(h_{K_c}^{sub}(x_L)\right) = \psi\left(h_{K_c}^{sub}(x_R)\right)$	0.2768
$\psi\left(h_{K_c}^{sup}(x_L)\right) = \psi\left(h_{K_c}^{sup}(x_R)\right)$	0.7689

Table 5.1: Water heights depending on the critical hydraulic head $K_c = 1.0018$

With M and S known we are able to compute the critical water height $h_c > 0$ which by definition verifies

$$M^2 = 3S^2 h_c^4 + g h_c^3,$$

corresponding to $F_r = 1$, see (2.12). For $M = 1.2$ and $S = 0.5$ the critical water height is $h_c = 0.52m$.

Another useful quantity is the critical hydraulic head K_c which is computed using

$$K_c = \Phi(h_c, Z_{max}).$$

where $Z_{max} = 0.2m$ is the maximum of the topography (5.1) and

$$\Phi(h, Z) = h + Z + \frac{1}{2g} \left(\frac{M^2}{h^2} + 3h^2 S^2 \right). \quad (5.2)$$

Hence, we get $K_c = 1.0018$.

Knowing K_c , we can compute $h_{K_c}^{sub}$ and $h_{K_c}^{sup}$ respectively the C^1 regular sub-critical and supercritical solutions of $\Phi(h, Z(x)) = K_c$ for all $x \in I$. According to Proposition 7, this will lead us to the knowledge of a unique $\psi\left(h_{K_c}^{sub}\right)$ and a unique $\psi\left(h_{K_c}^{sup}\right)$ verifying respectively

$$F^{h\bar{u}}\left(h_{K_c}^{sub}\right) = F^{h\bar{u}}\left(\psi\left(h_{K_c}^{sub}\right)\right),$$

and

$$F^{h\bar{u}}\left(h_{K_c}^{sup}\right) = F^{h\bar{u}}\left(\psi\left(h_{K_c}^{sup}\right)\right),$$

where, for all $h \in \mathbb{R}_+^*$

$$F^{h\bar{u}}(h) = \frac{M^2}{h} + h^3 S^2 + \frac{g}{2} h^2.$$

These water heights are computed in Table 5.1.

Numerical schemes

Equipped with all the values in Table 5.1, we now present the numerical simulations of the solutions described in Chapter 2. We mention that all the numerical simulations are done for $t_{end} = 2000s$ and for a domain discretized with $nx = 1000$ cells. In addition, the behavior of the schemes is estimated by computing the L^2 errors using the following expression

$$L^2 = \sqrt{\frac{1}{nx} \sum_{i=1}^{nx} (W_i - W_i^{SS})^2}, \quad (5.3)$$

where W_i is the approximate solution on the cell C_i and

$$W_i^{SS} = \frac{1}{\Delta x} \int_{C_i} W^{SS}(x) dx,$$

is the average of the steady state solution studied in Chapter 2 at the cell C_i . Moreover, to ensure that the CFL condition 3.6 is satisfied, we set $\alpha_{CFL} = 0.5$.

Initial Conditions

The initial conditions are set depending on the type of the flow at the inlet. More precisely

- When the inlet boundary conditions are subcritical, the initial conditions satisfy the lake at rest, i.e

$$h + z = h_R, \quad M = 0 \quad \text{and} \quad S = 0. \quad (5.4)$$

- When the inlet boundary conditions are supercritical, the initial conditions are chosen to be equal to the analytical solution.

Boundary conditions

The boundary conditions are determined according to the type of the flow and the sign of M . More precisely, if at the left

1. $M > 0$ and

- the flow is subcritical then, M and S are fixed and the water height follows a Neumann boundary condition.
 - the flow is supercritical then, M and S are fixed and the water height is equal to $h(x_L)$ that will be given in each section.
2. $M < 0$ then, we set the boundaries according to the type of the flow at the right, i.e if at the right
- the flow is subcritical then, M and S follow a homogeneous Neumann boundary condition and the water height is equal to $h(x_R)$ that will be given in each section.
 - the flow is supercritical then, M , S and the water height follow a Neumann boundary condition.

5.1 Subcritical inlet boundary condition

In this section, we compare the behavior of the different well-balanced numerical schemes constructed in Chapter 4 for the solutions with subcritical inlet boundary conditions, i.e supposing that $h(x_L) > h_c$. These steady state solutions were experimented in [37, 28]. These test cases are widely used in the literature. Here, instead of using the same test case as done in [37, ?, 28], we will construct our own test cases depending on the study done in Chapter 2 and on the parameters fixed in Table 5.1.

On the left boundary, the water height verifies a homogeneous Neumann boundary. Then, we will divide our tests depending on the outlet boundary condition.

5.1.1 Subcritical outlet boundary condition

For the subcritical outlet boundary condition, we fix one boundary condition at the right on the form $h_R = h(x_R) > h_c$.

Based on Proposition 10 we present in Table 5.2 the two possible steady state solutions according to the value of the water height fixed on the right of the domain.

Conditions on the right	Type of the solution	$h(x) =$
$h_R > h_{K_c}^{sub}(x_R)$	Subcritical everywhere	$h_{K_R}^{sub}(x)$
$\psi(h_{K_c}^{sup}(x_R)) < h_R < h_{K_c}^{sub}(x_R)$	Transcritical with shock	$\begin{cases} h_{K_c}^{sub}(x) & \text{if } x \leq x_0, \\ h_{K_c}^{sup}(x) & \text{if } x_0 \leq x < x_{shock}, \\ h_{K_R}^{sub}(x) & \text{if } x > x_{shock}. \end{cases}$

Table 5.2: The two possible solutions with subcritical boundary conditions on both sides of the domain.

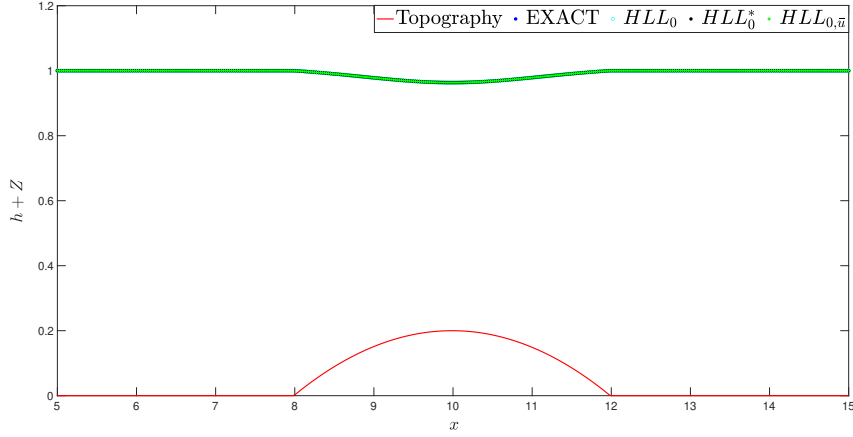


Figure 5.1: Subcritical Solution

Subcritical solution

Here $h_R = 1\text{ m}$ is chosen to verify $h_R > h_{K_c}^{sub}(x_R)$ as shown in Table 5.2. In this case, the steady state solution is continuous and subcritical everywhere. According to Proposition 10, the water height is $h_{K_R}^{sub}$, the C^1 subcritical solution of

$$\Phi(h, Z(x)) = K_R, \forall x \in I$$

where $K_R = \Phi(h_R, Z_R)$, see (5).

We display in Figure 5.1 the results of the three schemes and we present in Table 5.3 the L^2 errors. These errors show that the three well-balanced schemes recover the subcritical steady state solution with the same order of accuracy.

	$h + Z$	M	S
HLL_0	$5.6e - 14$	$2.02e - 14$	$2.7e - 14$
HLL_0^*	$6e - 14$	$1.7e - 14$	$3.2e - 14$
$HLL_{0,\bar{u}}$	$5.4e - 14$	$1.9e - 14$	$3.2e - 14$

Table 5.3: Free surface, discharge and shear errors for the subcritical solution

	$h + Z$	M	S
HLL_0	$8.6e - 03$	$1.9e - 03$	$1.45e - 10$
HLL_0^*	$8.6e - 03$	$1.9e - 03$	$1.45e - 10$
$HLL_{0,\bar{u}}$	$9.1e - 03$	$1.8e - 03$	$8.71e - 16$

Table 5.4: Free surface, discharge and shear errors for the transcritical with shock solution

Transcritical flow with shock

We fix $h_R = 0.8m$ such that $\psi\left(h_{K_c}^{sup}(x_R)\right) < h_R < h_{K_c}^{sub}(x_R)$ as mentioned in Table 5.2. In this case, the steady state solution is a transcritical flow with a shock. According to Proposition 10, the steady state solution on the left of the top of the bump is the C^1 subcritical solution $h_{K_c}^{sub}$ of

$$\Phi(h, Z(x)) = K_c \quad \forall x \in [x_L, x_0],$$

then, between the top of the bump and the shock, it is the C^1 supercritical solution $h_{K_c}^{sup}$ of the same equation for $x \in [x_L, x_0]$ and then after the shock it is the C^1 subcritical solution $h_{K_R}^{sub}$ of

$$\Phi(h, Z(x)) = K_R \quad \forall x \in]x_{shock}, x_R]. \quad (5.5)$$

At the point of discontinuity x_{shock} , the water height upstream $h_{K_c}^{sup}(x)$ and the water height downstream $h_{K_R}^{sub}(x)$ must verify the Rankine-Hugoniot condition, i.e $F^{h\bar{u}}\left(h_{K_c}^{sup}(x_{shock})\right) = F^{h\bar{u}}\left(h_{K_R}^{sub}(x_{shock})\right)$.

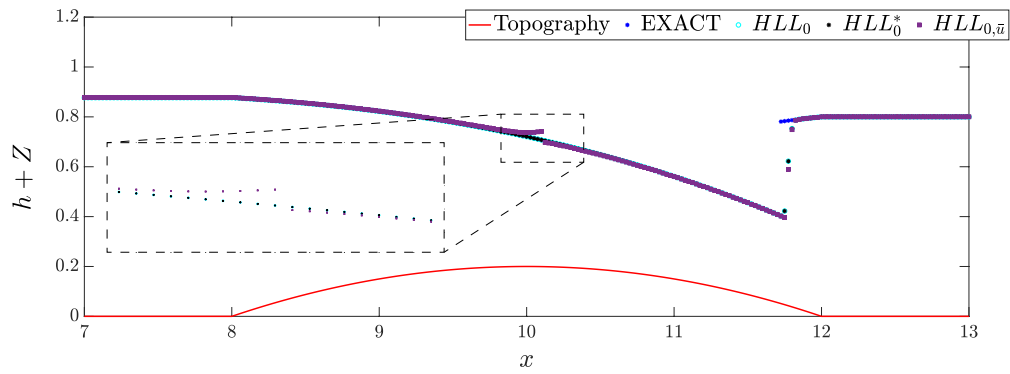


Figure 5.2: Free surface and topography for the transcritical solution with shock solution

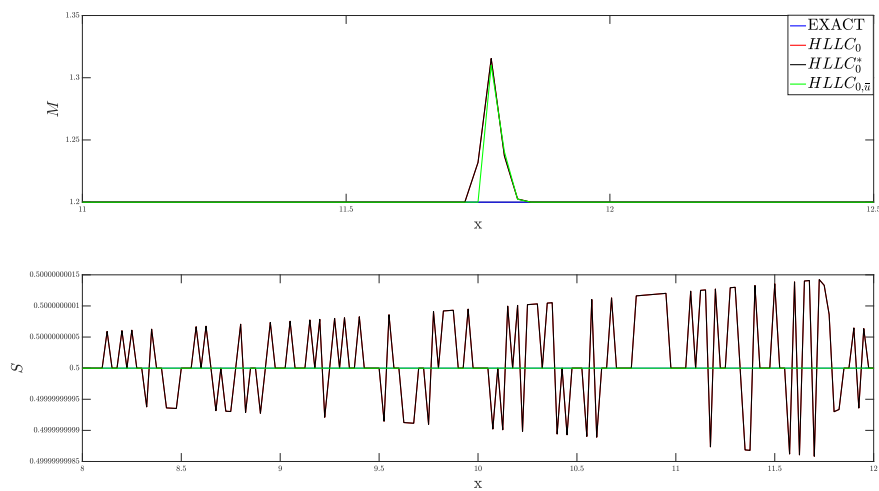


Figure 5.3: Discharge and shear for the transcritical solution with shock solution

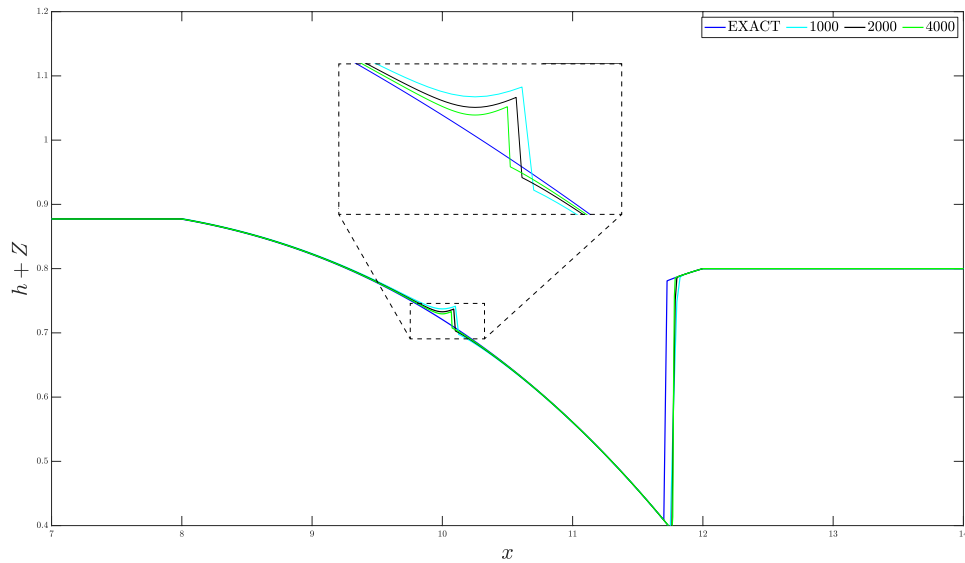


Figure 5.4: Transcritical solution without shock using the $HLL_{0, \bar{u}}$ scheme for different cell sizes.

In Figure 5.2 we present the numerical results using the three well-balanced schemes. Table 5.4 shows that the transcritical solution with shock is not exactly recovered by the well-balanced schemes. The schemes are exact almost everywhere except in the vicinity of the shock which is due to the fact that the schemes are constructed to preserve the regular steady state solutions. The discharge M is also affected by the shock whereas the shear remains constant up to the machine accuracy, see in Figure 5.3 and Table 5.4. In addition to that, we observe in Figure 5.2 a small non-entropic shock at the top of the bump for the $HLL_{0, \bar{u}}$ scheme. This non-entropic shock doesn't affect the L^2 norm errors because the error on the shock is much larger. The amplitude of this non-entropic shock decreases with the mesh size, see Figure 5.4.

Supercritical outlet boundary conditions

To set the initial conditions (5.4), we choose $h_R = 0.3 < h_c$. For this set of boundary conditions, only one C^1 steady state solution is possible see Proposition 2.3.2.

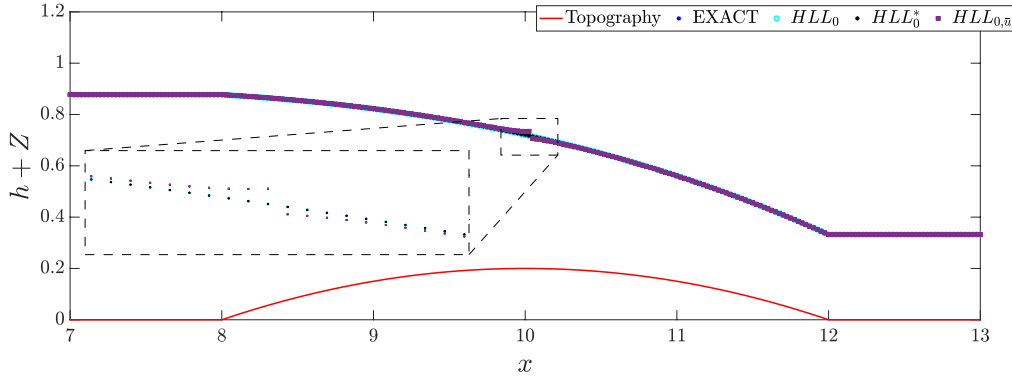


Figure 5.5: Transcritical solution without shock

	$h + Z$	M	S
HLL_0	$5.8e - 15$	$8.2e - 15$	$1.3e - 15$
HLL_0^*	$5.6e - 15$	$1.1e - 14$	$8.1e - 16$
$HLL_{0,\bar{u}}$	$5.9e - 04$	$1.72e - 14$	$1.05e - 15$

Table 5.5: Free surface, discharge and shear errors for the transcritical without shock solution

Transcritical flow without shock

The steady state solution in this case is the transcritical solution without shock over a bump which on the left of the bump, is the C^1 subcritical solution $h_{K_c}^{sub}$ of

$$\Phi(h, Z(x)) = K_c, \quad \forall x \in [x_L, x_0],$$

and on the right of the bump, the C^1 supercritical solution $h_{K_c}^{sup}$ of the same equation for $x \in [x_0, x_R]$.

In Figure 5.5, we present the different numerical results using the schemes. Here also, we can observe a small discontinuity at the top of the bump in the $HLL_{0,\bar{u}}$ scheme. Table 5.5 shows that the HLL_0 and HLL_0^* schemes captures exactly the transcritical solution without shock whereas the non-entropic shock affects the free surface errors for the $HLL_{0,\bar{u}}$ scheme but not the discharge and the shear errors. In this case as well, the error is reduced when we refine the mesh, see Table 5.6

nx	$h + Z$
1000	$5.9e - 04$
2000	$3e - 04$
4000	$2.3e - 04$

Table 5.6: Free surface errors of the $HLL_{0,\bar{u}}$ scheme for the transcritical without shock solution

5.2 Supercritical inlet boundary conditions

In this section, we test the numerical schemes constructed in Chapter 4 for the steady state solutions with supercritical inlet boundary conditions, i.e we fix $h_L = h(x_L) < h_c$.

Up to our knowledge the test cases with supercritical inlet and subcritical outlet boundary conditions are not often studied in the literature. The steady state solution with supercritical inlet and outlet boundary conditions with one shock at the left of the bump was studied in [11] where a formal analysis was done to prove that the left shock is linearly non stable. No numerical results were proposed.

Here, we will present the solutions we obtain for both types of outlet boundaries according to Proposition 12, 13 and 14 so that we can study the numerical stability of such stationary solutions through numerical simulations.

We recall that according to Lemma 1, when the piecewise C^1 solution exists then we have $h_{K_L}^{sup}(x) < h_{K_c}^{sup}(x)$ for all $x \in I$. Therefore, the supercritical water height at the left of the domain should verify $h_L < h_{K_c}^{sup}(x_L)$.

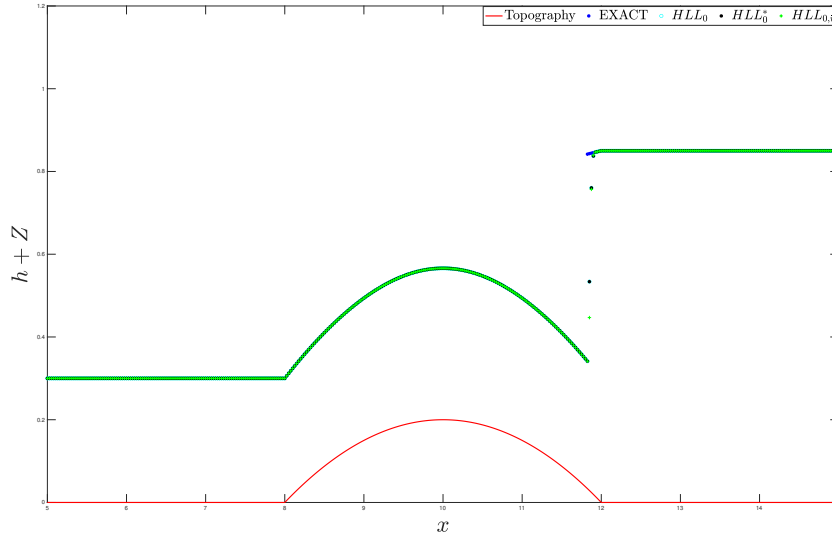


Figure 5.6: One shock at right for $h_R < h_{K_c}^{sub}(x_R)$

Conditions on the left	Conditions on the right	Type of the solution	$h(x) =$
	$\psi(h_{K_L}^{sup}(x_R)) < h_R$	One shock at right	$\begin{cases} h_{K_L}^{sup}(x) & \text{if } x < x_{shock}, \\ h_{K_R}^{sub}(x) & \text{if } x > x_{shock}. \end{cases}$
$\psi(h_{K_c}^{sub}(x_L)) < h_L$	$\psi(h_{K_c}^{sup}(x_R)) < h_R$	Two shocks	$\begin{cases} h_{K_L}^{sup}(x) & \text{if } x < x_{shockL}, \\ h_{K_c}^{sub}(x) & \text{if } x_{shockL} < x \leq x_0, \\ h_{K_c}^{sup}(x) & \text{if } x_0 \leq x < x_{shockR}, \\ h_{K_R}^{sub}(x) & \text{if } x > x_{shockR}, \end{cases}$

Table 5.7: The two possible solutions for the supercritical inlet and subcritical outlet boundary condition with $h_R < h_{K_c}^{sub}(x_R)$.

	$h + Z$	M	S
HLL_0	$9.3e - 03$	$3.4e - 03$	$8.85e - 15$
HLL_0^*	$9.3e - 03$	$3.4e - 03$	$4.82e - 15$
$HLL_{0,\bar{u}}$	$1e - 02$	$2.5e - 03$	$2.72e - 14$

Table 5.8: Free surface, discharge and shear errors for the solution with one shock at right for $h_R < h_{K_c}^{sub}(x_R)$

5.2.1 Subcritical outlet boundary conditions

We first consider the subcritical outlet boundary conditions where we fix at the outlet $h_R = h(x_R) > h_c$. According to § 2.3.3 the type of the solution depends on the value of h_R regarding $h_{K_c}^{sub}(x_R)$.

The case $h_R < h_{K_c}^{sub}(x_R)$

We start by the first case $h_R < h_{K_c}^{sub}(x_R)$ where the steady states solution was constructed in Proposition 12. We show it also here in Table 5.7. We have

- For the one shock at right steady solution, we choose to fix $h_L = 0.3 < h_{K_c}^{sup}(x_L)$ at the left of the domain and $h_R = 0.85 > \psi\left(h_{K_L}^{sup}(x_R)\right)$ at the right of the domain.

At the left of the domain and before the shock, the water height is the C^1 supercritical steady state solution $h_{K_L}^{sup}$ of

$$\Phi(h, Z(x)) = K_L, \forall x \in [x_L, x_{shock}], \quad (5.6)$$

with $K_L = \Phi(h_L, Z_L)$.

After the shock and at the right of the domain, the flow is subcritical then, the water height $h_{K_R}^{sub}$ is the steady state C^1 subcritical solution of (5.5).

In addition, at the shock we have

$$F^{h\bar{u}}\left(h_{K_L}^{sup}(x_{shock})\right) = F^{h\bar{u}}\left(h_{K_R}^{sub}(x_{shock})\right).$$

The numerical simulations obtained with the three schemes are displayed in Figure 5.6. We can conclude from Table 5.8 that the steady state solution with one shock at right is not exactly preserved by the well-balanced schemes. This is due to the presence of the shock. But, this solution is numerically stable since the numerical solution remains very close to the exact one. We can also remark that there is no discontinuity on the top of the bump in the $HLL_{0,\bar{u}}$ scheme plot because there is no transition between the regimes at the top of the bump in this solution.

- When the solution contains two shocks an additional condition is required at the left of the domain where we should have $\psi\left(h_{K_c}^{sub}(x_L)\right) < h_L$. For this reason we fix $h_L = 0.31m$.

At the left of the domain and before the first shock, the steady state solution is the supercritical solution $h_{K_L}^{sup}$ of

$$\Phi(h, Z(x)) = K_L, \quad \forall x \in [x_0, x_{shockL}[,$$

and between the first shock and the top of the bump, it is the subcritical solution $h_{K_c}^{sub}$ of

$$\Phi(h, Z(x)) = K_c, \quad \forall x \in]x_{shockL}, x_0],$$

At x_{shockL} , the steady state solution should verify

$$F^{h\bar{u}}\left(h_{K_L}^{sup}(x_{shockL})\right) = F^{h\bar{u}}\left(h_{K_c}^{sub}(x_{shockL})\right),$$

Moreover, between the top of the bump, and the second shock, it is the supercritical solution $h_{K_c}^{sup}$ of

$$\Phi(h, Z(x)) = K_c, \quad \forall x \in [x_0, x_{shockR}[,$$

and finally, between the second shock and the right of the domain, it is the subcritical solution $h_{K_R}^{sub}$ of

$$\Phi(h, Z(x)) = K_R, \quad \forall x \in]x_{shockR}, x_R], \quad (5.7)$$

At x_{shockR} , the following relation is satisfied

$$F^{h\bar{u}}\left(h_{K_c}^{sup}(x_{shockR})\right) = F^{h\bar{u}}\left(h_{K_R}^{sub}(x_{shockR})\right).$$

It is clear from the results presented in Figure 5.7 that all the schemes converge to another steady state solution which is the supercritical solution everywhere. In this case, it is impossible to catch the steady state solution with two shocks even if the initial conditions are chosen to be the exact steady state solution. This allows us to conclude that the solution with two shocks is not numerically stable. The stability of this solution is affected by the presence of the shock at the left of the bump because the solution with only one shock at the right of the bump is stable, see Figure 5.6.

In this case, the errors shown in Table 5.9 are the L^2 errors (5.3) computed between the numerical solutions and the supercritical steady state solution. Table 5.9 shows that three schemes nearly recover the supercritical steady state solution.

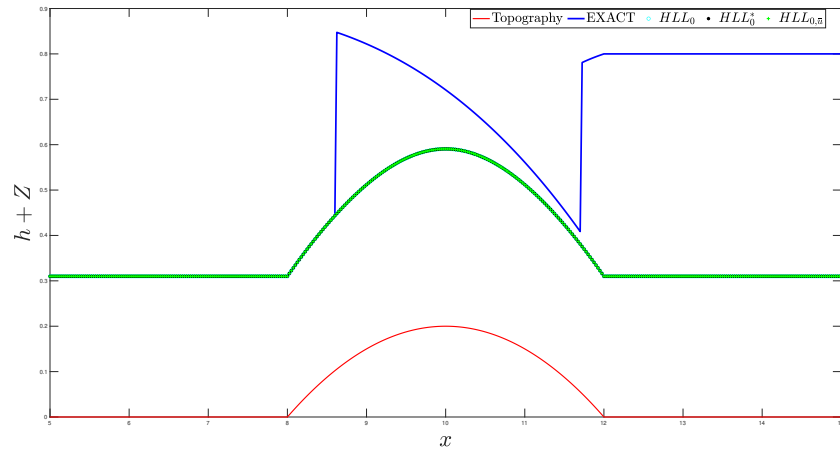


Figure 5.7: Two shocks solution

	$h + Z$	M	S
HLL_0	$5.74e-11$	$1.16e-14$	$1.93e-10$
HLL_0^*	$5.74e-11$	$1.23e-14$	$1.93e-10$
$HLL_{0,\bar{u}}$	$5.74e-11$	$1.13e-14$	$1.93e-10$

Table 5.9: Discharge and shear L^2 errors computed between the numerical solution with two shocks and the exact supercritical steady state solution everywhere.

Conditions on the left	Conditions on the right	Condition on the top	Type of the solution	$h(x) =$
$\psi(h_{K_R}^{sub}(x_L)) < h_L$		$h_{K_L}^{sup}(x_0) < \psi(h_{K_R}^{sub}(x_0))$	One shock at right	$\begin{cases} h_{K_L}^{sup}(x) & \text{if } x < x_{shock}, \\ h_{K_R}^{sub}(x) & \text{if } x > x_{shock}. \end{cases}$
	$\psi(h_{K_L}^{sup}(x_R)) < h_R$	$h_{K_L}^{sup}(x_0) < \psi(h_{K_R}^{sub}(x_0))$	One shock at left	$\begin{cases} h_{K_L}^{sup}(x) & \text{if } x < x_{shock}, \\ h_{K_R}^{sub}(x) & \text{if } x > x_{shock}. \end{cases}$

Table 5.10: The two possible solutions for the supercritical inlet and subcritical outlet boundary condition with $h_R > h_{K_c}^{sub}(x_R)$.

The case $h_R > h_{K_c}^{sub}(x_R)$

For the case, $h_R > h_{K_c}^{sub}(x_R)$, the steady state solution was constructed in Proposition 13. The solution in this case depends on some threshold parameters of K_R and K_L on both sides of the domain and on the top of the topography as seen in Table 5.10. In addition, for the topography defined in (5.1) where $Z(x_L) = Z(x_R)$ the two solutions coexist, see Corollary 1.

For both type of steady state solutions, before the shock, the water height is the C^1 supercritical solution $h_{K_L}^{sup}$ of (5.6) and after the shock it is the subcritical solution $h_{K_R}^{sub}$ of (5.7). At the shock, the solution must verify

$$F^{h\bar{u}}(h_{K_L}^{sup}(x_{shock})) = F^{h\bar{u}}(h_{K_R}^{sub}(x_{shock})).$$

- For the steady state solution with one shock at right, we first fix $h_R = 0.95m$ and we compute all the threshold parameters depending on $K_R = \Phi(h_R, Z_R)$ in Table 5.11. Then, we fix $h_L = 0.3m$ verifying both conditions $\psi(h_{K_R}^{sub}(x_L)) < h_L$ and $h_{K_L}^{sup}(x_0) = 0.366 < \psi(h_{K_R}^{sub}(x_0))$. The numerical results obtained with the three schemes are displayed in Figure 5.8. The three schemes exactly capture the exact solution except in the vicinity of the shock as shown in Table 5.12. The discharge errors are also affected by the shock but this is not the case for the shear errors.
- For the solution with one shock at left, an additional condition on the right of the domain is required. For this reason, we first fix the water height on the left of the domain $h_L = 0.25m$ and we compute all the threshold parameters depending on $K_L = \Phi(h_L, Z_L)$ in Table 5.13. Then, we fix the water height on the right of the domain $h_R = 1m$ to verify $\psi(h_{K_L}^{sup}(x_R)) <$

h_R	0.95
$h_{K_R}^{sub}(x_L) = h_{K_R}^{sub}(x_R)$	0.95
$h_{K_R}^{sup}(x_L) = h_{K_R}^{sup}(x_R)$	0.313
$\psi\left(h_{K_R}^{sub}(x_L)\right) = \psi\left(h_{K_R}^{sub}(x_R)\right)$	0.2459
$\psi\left(h_{K_R}^{sup}(x_L)\right) = \psi\left(h_{K_R}^{sup}(x_R)\right)$	0.8035
$\psi\left(h_{K_R}^{sub}(x_0)\right)$	0.3774
$\psi\left(h_{K_R}^{sup}(x_0)\right)$	0.6641

Table 5.11: Water heights depending on the critical hydraulic head $K_R = 1.0658$

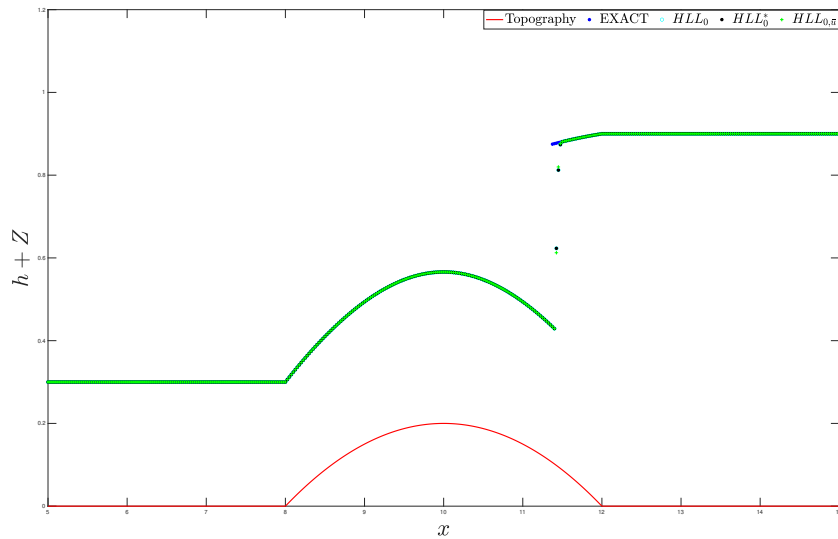


Figure 5.8: One shock at right for $h_R > h_{K_c}^{sub}(x_R)$

	$h + Z$	M	S
HLL_0	$1.5e-02$	$2.1e-03$	$4.4e-15$
HLL_0^*	$1.5e-02$	$2.1e-03$	$4.44e-15$
$HLL_{0,\bar{u}}$	$1.8e-02$	$1.8e-03$	$3.9e-15$

Table 5.12: Free surface, discharge and S errors for the solution with one shock at right for $h_R > h_{K_c}^{sub}(x_R)$

h_L	0.25
$h_{K_L}^{sub}(x_L) = h_{K_L}^{sub}(x_R)$	1.318
$h_{K_L}^{sup}(x_L) = h_{K_L}^{sup}(x_R)$	0.25
$\psi\left(h_{K_L}^{sub}(x_L)\right) = \psi\left(h_{K_L}^{sub}(x_R)\right)$	0.1428
$\psi\left(h_{K_L}^{sup}(x_L)\right) = \psi\left(h_{K_L}^{sup}(x_R)\right)$	0.9396
$\psi\left(h_{K_L}^{sup}(x_0)\right)$	0.8729
$\psi\left(h_{K_L}^{sup}(x_0)\right)$	0.1891

Table 5.13: The water heights depending on the critical hydraulic head $K_L = 1.4267$

	$h + Z$	M	S
HLL_0	$4.5e - 03$	$5.1e - 03$	$2.06e - 10$
HLL_0^*	$4.5e - 03$	$5.1e - 03$	$2.06e - 10$
$HLL_{0,\bar{u}}$	$4.7e - 03$	$4.4e - 03$	$2.06e - 10$

Table 5.14: Free surface, discharge and shear errors when the numerical solution is the solution with one shock at left and the exact solution is the solution with one shock at right.

$$h_R \text{ and } h_{K_L}^{sup}(x_0) < \psi\left(h_{K_R}^{sub}(x_0)\right) = 0.3352m.$$

Figure 5.9 shows that the three numerical schemes converge to the steady state solution with one shock at right which is not the steady state solution we took for the initial conditions. Hence, the steady state with one shock at left solution is not stable. Therefore, we show in Table 5.14 the L^2 norm errors between the numerical solutions and the exact solution with one shock at right. These errors are in accordance with the behavior of the schemes when the solution contains a shock at the right of the bump, see Table 5.14.

5.2.2 Supercritical outlet boundary conditions

In this case, the boundary conditions are supercritical on both sides of the domain. We assume that the right boundary condition is also supercritical, i.e. $h(x_R) < h_c$. The two different steady state solutions are presented in Table 5.15.

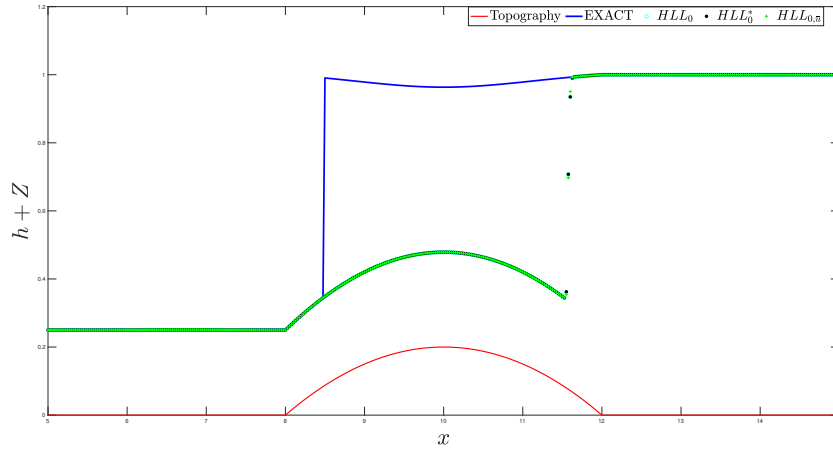


Figure 5.9: One shock at left solution for supercritical inlet and subcritical outlet boundary conditions

Conditions on the left	Type of the solution	$h(x) =$
$h_L < h_{K_c}^{sup}(x_L)$	Supercritical everywhere	$h_{K_L}^{sup}(x)$
$\psi(h_{K_c}^{sub}(x_L)) < h_L < h_{K_c}^{sup}(x_L)$	One shock at left	$\begin{cases} h_{K_L}^{sup}(x) & \text{if } x_L \leq x < x_{shock}, \\ h_{K_c}^{sub}(x) & \text{if } x_{shock} < x < x_0, \\ h_{K_c}^{sup}(x) & \text{if } x > x_0. \end{cases}$

Table 5.15: The two possible solution for the supercritical inlet and outlet boundary condition.

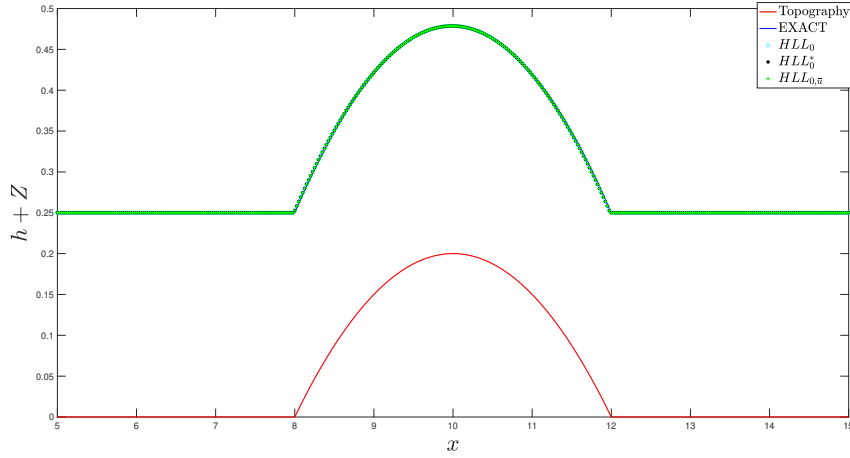


Figure 5.10: Supercritical solution

	$h + Z$	M	S
HLL_0	$5.41e - 14$	$1.87e - 14$	$2.68e - 10$
HLL_0^*	$5.41e - 14$	$1.848e - 14$	$2.68e - 10$
$HLL_{0,\bar{u}}$	$5.41e - 14$	$1.55e - 14$	$2.68e - 10$

Table 5.16: Free surface, discharge and shear errors for the supercritical solution

Supercritical everywhere

For the steady state supercritical solution everywhere, we fix $h_L = 0.25m$. The supercritical water height $h_{K_L}^{sup}$ is the solution of

$$\Phi(h, Z(x)) = K_L \quad \forall x \in I,$$

Since the initial condition is chosen to be equal to the stationary solutions, the three well-balanced schemes have to preserve it by construction. This is observed in Figure 5.10 and in Table 5.16.

	$h + Z$	M	S
HLL_0	6.3e-02	$4.79e - 14$	$5.69e - 10$
HLL_0^*	6.3e-02	$4.68e - 14$	$5.69e - 10$
$HLL_{0,\bar{u}}$	6.3e-02	$1.08e - 14$	$5.69e - 10$

Table 5.17: Free surface, discharge and shear errors for the solution with one shock at left when both boundaries are supercritical.

One shock at left

When the steady state solution contains a shock at the left of the domain, we fix $\psi\left(h_{K_c}^{sub}(x_L)\right) < h_L = 0.32 < h_{K_c}^{sup}(x_L)$. At the left when the flow is supercritical the steady state solution is the C^1 supercritical solution of (5.6) then, a shock occurs and the steady state solution is the C^1 subcritical solution $h_{K_L}^{sup}$ of

$$\Phi(h, Z(x)) = K_c \quad \forall x \in]x_{shock}, x_0],$$

and then, through a continuous transition, the steady state solution becomes the supercritical solution $h_{K_c}^{sup}$ of the same equation for $x \in [x_0, x_R]$. At the shock, the solution satisfies

$$F^{h\bar{u}}\left(h_{K_L}^{sup}(x_{shock})\right) = F^{h\bar{u}}\left(h_{K_c}^{sub}(x_{shock})\right).$$

The numerical simulations showed once again that the solution with one shock at the left is not stable, see Figure 5.11. In fact, the numerical solutions converge to the supercritical solution. We also mention that at the left of the bump and mainly before the shock, the numerical solutions capture exactly the steady state which is not the case at the right of the bump. This is due to the fact that, at the right of the top of the bump, the numerical solution converge to the supercritical solution $h_{K_L}^{sup}$ whereas the exact solution is $h_{K_c}^{sup}$. This explains the L^2 norm errors of the free surface in Table 5.17. In addition, Table 5.17 shows that since the numerical solution converges to a C^1 steady state solution, the schemes are in good behavior regarding M and S .

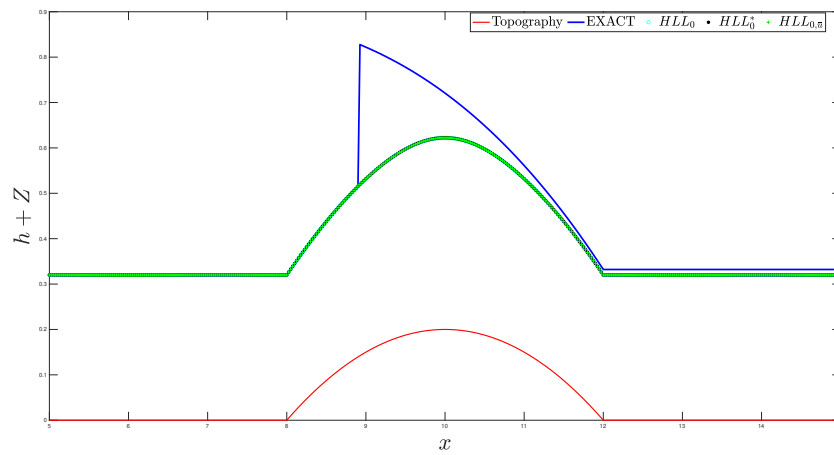


Figure 5.11: One shock at left solution for supercritical inlet and outlet boundary conditions

Conclusion and perspectives

Conclusion

In this thesis, we have studied, the steady state solutions of the Shallow water model with two velocities and a topography source term (SW_2). In addition, we presented several numerical schemes to approach the solutions of the homogeneous model (SW_2^H) and the model with topography.

First, we studied the steady states solutions of (SW_2). We exhibited the C^1 regular solutions following the Bernoulli's principle and the Rankine-Hugoniot jump conditions through a discontinuity where the dissipation of entropy should be verified. Then, for a specific continuous topography, we studied the (non) existence and the (non) uniqueness of the moving steady states. We proved that two steady state solutions with supercritical inlet boundary conditions might coexist and we presented the possible coexistence of the solution depending on the value of the topography on each side of the domain.

Second, using the finite volume method, we constructed three Approximate Riemann Solvers (ARS) to approximate the solution of the homogeneous Shallow water model with two velocities (SW_2^H) to be extended later to approximate the solution of the model with topography (SW_2). The first scheme is the HLL scheme that is not accurate around the contact wave of the model. The second scheme is the HLL^* scheme which can be seen as a 3– waves ARS that takes into consideration the transport of S through the contact wave but considers that the water height and the mean velocity are constant through the transport wave which is not the case for the exact solution of the Riemann problem. The third scheme is a 3– waves ARS named $HLL_{\bar{u}}$ for which the mean velocity is constant through the internal and equal to its celerity. After presenting the-

oretically and numerically the advantages and disadvantages of each ARS, we were able to conclude that the best solver is the $HLL_{\bar{u}}$ solver. This solver

- preserves the positivity of the water height,
- preserves the maximum principle on $S = \frac{\hat{u}}{h}$,
- is accurate for the transport process associated to the shear velocity,
- maintains a stationary isolated contact discontinuity.

However, using a numerical strategy, we proved that the $HLL_{\bar{u}}$ scheme doesn't verify a discrete energy inequality whereas the HLL scheme does.

Third, to approach the solutions of the model with topography (SW_2), we extended the numerical schemes introduced for the homogeneous model. For the model with topography, a stationary wave is added due to the presence of the source term and should be added in the construction of the schemes. Thus, one more property should be considered where the new schemes have to be accurate on the contact discontinuity while verifying the well-balanced property for all regular steady states of the system (SW_2). To do so, we started by approximating the topography source term then, we constructed three well-balanced schemes named HLL_0 , HLL_0^* and $HLL_{0,\bar{u}}$. The first one is an extension of the HLL scheme, the second one is an extension of the HLL^* scheme and the third one can be seen as variation of the HLL_0^* scheme and a combination of HLL_0 and $HLL_{\bar{u}}$ schemes. The three schemes are well-balanced, ensure the positivity of the intermediate water heights, verify the maximum principle on S but don't verify a discrete energy inequality.

Finally, we studied the numerical stability of the moving steady state solutions and the behavior of the numerical schemes on these solutions. Through the numerical results we observed mainly a non-entropic stationary shock on the top of the bump in the $HLL_{0,\bar{u}}$ scheme for the solutions with a transition from the subcritical to the supercritical and that the steady state solutions with one shock at left are not stable.

Perspectives

The different aspects of the thesis have raised questions that still remain open or can be envisioned:

1. For a flat topography, the $HLL_{\bar{u}}$ scheme is better than the other schemes however, this scheme presents a non-entropic stationary shock on the top of the bump for the transcritical solutions contrary to the other schemes. Therefore, we would like to understand the origin the non-entropic stationary shock and then try to correct it.
2. We presented in this scheme three ARS to approach the solution of the model with two velocities and a topography. We proved through a numerical strategy that the three scheme don't verify a discrete energy inequality. In fact, the construction of numerical schemes satisfying the dissipation of entropy remains an open question even for the classical shallow water model. In [44], the authors constructed an entropy dissipative numerical scheme to approach the solution of the classical shallow water model with topography. But, the intermediate states of the scheme are obtained by resolving a non-linear equation which has a large computational cost. To solve this issue, the authors in [45, 16] present a linear formulation to deal with a general form of well-balanced states. However, the scheme presented doesn't verify a discrete energy inequality. Hence, it is very important to develop schemes that satisfy the dissipation of entropy for the shallow water model first and then extend them for the model with two velocities.
3. In [11], the authors proved theoretically that the solutions with a shock on the left of the bump are linearly not-stable. Later on, the authors in [26] proved through a theoretical and experimental approach that if we add a friction source term to the system, the solutions with a left shock can be stable. Hence, we would like to test numerically if this is true for the steady state solutions of the shallow water model with two velocities and a manning friction. Indeed, we have to study first the steady state solutions of the model with a manning friction. Then, for the construction of the numerical schemes, we extend the strategy proposed in [45] for the shallow water model and a manning friction.

List of Figures

1.1	Sketch of the multilayer approach	21
1.2	Representation of the eigenvalues of the $(2DSW_2)$ model. The blue ones correspond to the 1D model (SW_2^H)	26
1.3	Averaged models derived from Euler equations.	28
1.4	Different solutions with subcritical inlet boundaries	33
1.5	Different solutions with supercritical inlet boundaries	34
1.6	The waves representation of the HLL approximate Riemman solver.	40
1.7	The waves representation of the HLL^* approximate Riemman solver.	40
1.8	The waves representation of the $HLL_{\bar{u}}$ approximate Riemman solver.	40
1.9	The one rarefaction one shock: plots of the variables using the HLL scheme for 100, 1000 and 10000 points.	41
1.10	One rarefaction one shock case. Plots of the variables using HLL , HLL^* and $HLL_{\bar{u}}$ solvers for 1000 grid cells	42
1.11	Transcritical solution without shock	45
1.12	The unstable two shocks solution: the numerical solutions converge to a total different regular steady state solution.	46
2.1	Regular moving steady states for $K \geq K_c$	54

2.2	Construction of $h_K^{sub}(x)$ and $h_K^{sup}(x)$, solutions of $\Phi(h, Z(x)) = K$ when $K \geq K_c$	55
2.3	Regular moving steady states for $\bar{K}_L < K < K_c$	57
2.4	Construction of $h_{\bar{K}_L}^{sub}(x)$ and $h_{\bar{K}_L}^{sup}(x)$, solutions of $\Phi(h, Z(x)) = K$ when $\bar{K}_L < K < K_c$	58
2.5	Plot of the function $F^{h\bar{u}}$ and construction of $\psi(h)$	61
2.6	Representation of the eigenvalues for the different type of boundaries	65
2.7	General steady states with subcritical boundary conditions at both sides of the domain	70
2.8	Steady state solution with subcritical boundary conditions at the inlet and supercritical boundary conditions at the outlet	71
2.9	Steady state solution with one shock at right for the supercritical boundary conditions at the inlet and subcritical boundary conditions at the outlet when $K_L > K_c > K_R$	72
2.10	Steady state solution with two shocks for the supercritical boundary conditions at the inlet and subcritical boundary conditions at the outlet when $K_L > K_c > K_R$	73
2.11	Steady state solution with one shock at left for the supercritical boundary conditions at the inlet and subcritical boundary conditions at the outlet when $K_L > K_R > K_c$	77
2.12	Steady state solution with one shock at right for the supercritical boundary conditions at the inlet and subcritical boundary conditions at the outlet when $K_L > K_R > K_c$	77
2.13	Steady state solutions for the supercritical boundary conditions at the inlet and subcritical boundary conditions at the outlet when $K_L > K_c > K_R$ and $Z(x_L) < Z(x_R) = Z(\tilde{x})$	81
2.14	Steady state solutions for the supercritical boundary conditions at the inlet and subcritical boundary conditions at the outlet when $K_L > K_R > K_c$ and $Z(x_L) < Z(x_R)$	81

2.15 Sketch of the different zones of solutions with supercritical boundary condition at the left and subcritical boundary condition at the right for $M = 0.1$, $S = 1$, $g = 9.81$ and $Z(x_L) = Z(x_R)$	83
2.16 Sketch of the different zones of solutions with supercritical boundary condition at the left and subcritical boundary condition at the right for $M = 0.1$, $S = 1$, $g = 9.81$ and $Z(x_L) < Z(x_R)$	84
2.17 Sketch of the different zones of solutions with supercritical boundary condition at the left and subcritical boundary condition at the right for $M = 0.1$, $S = 1$, $g = 9.81$ and $Z(x_L) > Z(x_R)$	84
2.18 General steady states with supercritical boundary conditions at both sides of the domain	86
3.1 Dam Break case: Plots of the variables using the <i>HLL</i> scheme for 100, 1000 and 10000 points.	96
3.2 Dam Break case: Plots of the variables using the <i>HLL</i> and <i>HLL*</i> scheme for 1000 points.	98
3.3 Dam Break case: Plots of the variables using <i>HLL</i> , <i>HLL*</i> and <i>HLL\bar{u}</i> solvers for 1000 grid cells	107
3.4 The two shock problem § 3.6.2. Plots of the variables using <i>HLL</i> , <i>HLL*</i> and <i>HLLC\bar{u}</i> solvers for 1000 grid cells	110
3.5 The two rarefactions case § 3.6.3. Plots of the variables using <i>HLL</i> , <i>HLL*</i> and <i>HLL\bar{u}</i> solvers for 1000 grid cells	111
3.6 Rarefaction/Shock case 2. Plots of the variables using <i>HLL</i> , <i>HLL*</i> and <i>HLL\bar{u}</i> solvers for 1000 grid cells	113
3.7 Dam break problem with change of sign on \hat{u} § 3.6.4. Plots of the $h\hat{u}^2$ using <i>HLL</i> , <i>HLL*</i> and <i>HLL\bar{u}</i> solvers for 1000 grid cells	114
3.8 Stationary contact discontinuity § 3.6.5. Plots of the variables using <i>HLL</i> , <i>HLL*</i> and <i>HLL\bar{u}</i> solvers for 1000 grid cells	118
3.9 Traveling contact discontinuity § 3.6.6. Plots of the variables using <i>HLL</i> , <i>HLL*</i> and <i>HLL\bar{u}</i> solvers for 1000 grid cells	119

4.1	The waves representation of the HLL_0 approximate Riemman solver.	132
4.2	The waves representation of the HLL_0^* approximate Riemman solver with $\lambda^* < 0$ on the left and $\lambda^* > 0$ on the right.	142
4.3	The waves representation of the $HLL_{0,\bar{u}}$ approximate Riemman solver with $\lambda^* < 0$ on the left and $\lambda^* > 0$ on the right.	151
4.4	Riemann problem with negative intermediate water heights	165
5.1	Subcritical Solution	171
5.2	Free surface and topography for the transcritical solution with shock solution	173
5.3	Discharge and shear for the transcritical solution with shock solution	173
5.4	Transcritical solution without shock using the $HLL_{0,\bar{u}}$ scheme for different cell sizes.	174
5.5	Transcritical solution without shock	175
5.6	One shock at right for $h_R < h_{K_c}^{sub}(x_R)$	177
5.7	Two shocks solution	180
5.8	One shock at right for $h_R > h_{K_c}^{sub}(x_R)$	182
5.9	One shock at left solution for supercritical inlet and subcritical outlet boundary conditions	184
5.10	Supercritical solution	185
5.11	One shock at left solution for supercritical inlet and outlet boundary conditions	187

List of Tables

1.1	Number of required boundary conditions	32
3.1	Height error and order of accuracy of the three schemes for the Dam break case	108
3.2	Mean velocity error and order of accuracy of the three schemes for the Dam break case	108
3.3	Standard deviation error and order of accuracy of the three schemes for the Dam break case	109
3.4	Height error and order of accuracy of the three schemes for the two shocks problem § 3.6.2	109
3.5	Mean velocity error and order of accuracy of the three schemes for the two shocks problem § 3.6.2	110
3.6	Standard deviation error and order of accuracy of the three schemes for the two shocks problem § 3.6.2	110
3.7	Height error and order of accuracy of the three schemes for the two rarefactions problem § 3.6.3	112
3.8	Mean velocity error and order of accuracy of the three schemes for the two rarefactions problem § 3.6.3	112
3.9	Standard deviation error and order of accuracy of the three schemes for the two rarefactions problem § 3.6.3	112

3.10	Height error and order of accuracy of the three schemes for the Dam break problem with change of sign on \hat{u} § 3.6.4	116
3.11	Mean velocity error and order of accuracy of the three schemes for the Dam break problem with change of sign on \hat{u} § 3.6.4	116
3.12	Standard deviation error and order of accuracy of the three schemes for the Dam break problem with change of sign on \hat{u} § 3.6.4	116
3.13	Height error and order of accuracy of the three schemes for the stationary contact discontinuity § 3.6.5	117
3.14	Mean velocity error and order of accuracy of the three schemes for the stationary contact discontinuity § 3.6.5	117
3.15	Standard deviation error and order of accuracy of the three schemes for stationary contact discontinuity § 3.6.5	117
3.16	Height error and order of accuracy of the three schemes for the traveling contact discontinuity § 3.6.6	120
3.17	Mean velocity error and order of accuracy of the three schemes for the traveling contact discontinuity § 3.6.6	120
3.18	Standard deviation error and order of accuracy of the three schemes for the traveling contact discontinuity § 3.6.6	120
3.19	Interesting values corresponding to the cases where the schemes are non-dissipative.	122
5.1	Water heights depending on the critical hydraulic head $K_c = 1.0018$	168
5.2	The two possible solutions with subcritical boundary conditions on both sides of the domain.	171
5.3	Free surface, discharge and shear errors for the subcritical solution	172
5.4	Free surface, discharge and shear errors for the transcritical with shock solution	172

5.5	Free surface, discharge and shear errors for the transcritical without shock solution	175
5.6	Free surface errors of the $HLL_{0,\bar{u}}$ scheme for the transcritical without shock solution	176
5.7	The two possible solutions for the supercritical inlet and subcritical outlet boundary condition with $h_R < h_{K_c}^{sub}(x_R)$	177
5.8	Free surface, discharge and shear errors for the solution with one shock at right for $h_R < h_{K_c}^{sub}(x_R)$	177
5.9	Discharge and shear L^2 errors computed between the numerical solution with two shocks and the exact supercritical steady state solution everywhere.	180
5.10	The two possible solutions for the supercritical inlet and subcritical outlet boundary condition with $h_R > h_{K_c}^{sub}(x_R)$	181
5.11	Water heights depending on the critical hydraulic head $K_R = 1.0658$	182
5.12	Free surface, discharge and S errors for the solution with one shock at right for $h_R > h_{K_c}^{sub}(x_R)$	182
5.13	The water heights depending on the critical hydraulic head $K_L = 1.4267$	183
5.14	Free surface, discharge and shear errors when the numerical solution is the solution with one shock at left and the exact solution is the solution with one shock at right.	183
5.15	The two possible solution for the supercritical inlet and outlet boundary condition.	184
5.16	Free surface, discharge and shear errors for the supercritical solution	185
5.17	Free surface, discharge and shear errors for the solution with one shock at left when both boundaries are supercritical.	186

Bibliography

- [1] Nina Aguilon, Emmanuel Audusse, Edwige Godlewski, and Martin Parisot. Analysis of the riemann problem for a shallow water model with two velocities. *SIAM Journal on Mathematical Analysis*, 50(5):4861–4888, 2018.
- [2] Nora Aissiouene, Marie-Odile Bristeau, Edwige Godlewski, and Jacques Sainte-Marie. A combined finite volume - finite element scheme for a dispersive shallow water system. *Networks and Heterogeneous Media*, 11(1):1–27, January 2016.
- [3] Francisco Alcrudo and Fayssal Benkhaldoun. Exact solutions to the riemann problem of the shallow water equations with a bottom step. *Computers & Fluids*, 30(6):643–671, 2001.
- [4] Annalisa AMBROSO, Benjamin BOUTIN, Christophe CHALONS, Frédéric COQUEL, Thomas GALIÉ, Edwige GODLEWSKI, Frédéric LAGOUTIÈRE, Pierre-arnaud RAVIART, and Nicolas SEGUIN. Construction de schémas de type godunov pour les systèmes hyperboliques avec terme source. *Publication du groupe de Travail Couplage de modeles en thermohydraulique, Laboratoire Jacques Louis Lions, Sorbonne Université*. 2008.
- [5] Nikolai Andrianov. Performance of numerical methods on the non-unique solution to the riemann problem for the shallow water equations. *International Journal for numerical methods in fluids*, 47(8-9):825–831, 2005.
- [6] Emmanuel Audusse. A multilayer saint-venant model: derivation and numerical validation. *Discrete & Continuous Dynamical Systems-B*, 5(2):189–214, 2005.
- [7] Emmanuel Audusse, François Bouchut, Marie-Odile Bristeau, Rupert Klein, and Benoit Perthame. A fast and stable well-balanced scheme with

- hydrostatic reconstruction for shallow water flows. *SIAM Journal on Scientific Computing*, 25(6):2050–2065, 2004.
- [8] Emmanuel Audusse, Marie-Odile Bristeau, Marica Pelanti, and Jacques Sainte-Marie. Approximation of the hydrostatic navier–stokes system for density stratified flows by a multilayer model: kinetic interpretation and numerical solution. *Journal of Computational Physics*, 230(9):3453–3478, 2011.
- [9] Emmanuel Audusse, Marie-Odile Bristeau, Benoît Perthame, and Jacques Sainte-Marie. A multilayer saint-venant system with mass exchanges for shallow water flows. derivation and numerical validation. *ESAIM: Mathematical Modelling and Numerical Analysis*, 45(1):169–200, 2011.
- [10] Emmanuel Audusse, Christophe Chalons, and Philippe Ung. A simple well-balanced and positive numerical scheme for the shallow-water system. *Communications in Mathematical Sciences*, 13(5):1317–1332, 2015.
- [11] Peter G Baines and JA Whitehead. On multiple states in single-layer flows. *Physics of fluids*, 15(2):298–307, 2003.
- [12] Adh emar Barr e De Saint-Venant. Th eorie du mouvement non-permanent des eaux avec applications aux crues des rivi eres et   l’introduction des mar ees dans leur lit. *Academie de Sciences. Comptes Rendus*, 73(99):148–154, 1871.
- [13] Alfredo Bermudez and Maria Elena Vazquez. Upwind methods for hyperbolic conservation laws with source terms. *Computers & Fluids*, 23(8):1049–1071, 1994.
- [14] Christophe Berthon and Christophe Chalons. A fully well-balanced, positive and entropy-satisfying godunov-type method for the shallow-water equations. *Mathematics of Computation*, 85(299):1281–1307, 2016.
- [15] Christophe Berthon, Christophe Chalons, S Cornet, and Gianmarco Sperone. Fully well-balanced, positive and simple approximate riemann solver for shallow water equations. *Bulletin of the Brazilian Mathematical Society, New Series*, 47(1):117–130, 2016.
- [16] Christophe Berthon, Meissa M’Baye, Minh H. Le, and Diaraf Seck. A well-defined moving steady states capturing Godunov-type scheme for Shallow-water model. *International Journal on Finite Volumes*, 15, 2021.

- [17] François Bouchut. *Nonlinear stability of finite Volume Methods for hyperbolic conservation laws: And Well-Balanced schemes for sources*. Springer Science & Business Media, 2004.
- [18] François Bouchut and T Morales de Luna. Semi-discrete entropy satisfying approximate riemann solvers. the case of the suliciu relaxation approximation. *Journal of Scientific Computing*, 41(3):483–509, 2009.
- [19] Francois Bouchut, Michael Westdickenberg, et al. Gravity driven shallow water models for arbitrary topography. *Communications in Mathematical Sciences*, 2(3):359–389, 2004.
- [20] Yann Brenier. Homogeneous hydrostatic flows with convex velocity profiles. *Nonlinearity*, 12(3):495, 1999.
- [21] Marie-Odile Bristeau and Benoit Coussin. Boundary Conditions for the Shallow Water Equations solved by Kinetic Schemes. Research Report RR-4282, INRIA, 2001. Projet M3N.
- [22] Manuel J Castro, Alberto Pardo Milanés, and Carlos Parés. Well-balanced numerical schemes based on a generalized hydrostatic reconstruction technique. *Mathematical Models and Methods in Applied Sciences*, 17(12):2055–2113, 2007.
- [23] Praveen Chandrashekar, Boniface Nkonga, Asha Kumari Meena, and Ashish Bhole. A path conservative finite volume method for a shear shallow water model. *Journal of Computational Physics*, 413:109457, 2020.
- [24] Ashwin Chinnayya, Alain-Yves LeRoux, and Nicolas Seguin. A well-balanced numerical scheme for the approximation of the shallow-water equations with topography: the resonance phenomenon. *Int. J. Finite*, 1(1):33, 2004.
- [25] Astrid Decoene and Jean-Frédéric Gerbeau. Sigma transformation and ale formulation for three-dimensional free surface flows. *International Journal for Numerical Methods in Fluids*, 59(4):357–386, 2009.
- [26] Andrea Defina, Francesca Maria Susin, and Daniele Pietro Viero. Bed friction effects on the stability of a stationary hydraulic jump in a rectangular upward sloping channel. *Physics of fluids*, 20(3):036601, 2008.
- [27] Olivier Delestre, Stéphane Cordier, Frédéric Darboux, and Francois James. A limitation of the hydrostatic reconstruction technique for shallow water equations. *Comptes Rendus Mathématique*, 350(13-14):677–681, 2012.

- [28] Olivier Delestre, Carine Lucas, Pierre-Antoine Ksinant, Frédéric Darboux, Christian Laguerre, Thi Ngoc Tuoi Vo, Francois James, and Stephane Cordier. SWASHES: a compilation of Shallow Water Analytic Solutions for Hydraulic and Environmental Studies. *International Journal for Numerical Methods in Fluids*, 72(3):269–300, May 2013.
- [29] Vivien Desveaux. *Contribution à l'approximation numérique des systèmes hyperboliques*. PhD thesis, Université de Nantes, 2013.
- [30] Vivien Desveaux and Alice Masset. A fully well-balanced scheme for shallow water equations with coriolis force. *arXiv preprint arXiv:2105.08357*, 2021.
- [31] Enrique D Fernandez-Nieto, Martin Parisot, Yohan Penel, and Jacques Sainte-Marie. A hierarchy of dispersive layer-averaged approximations of euler equations for free surface flows. *Communications in Mathematical Sciences*, 16(5):1169–1202, 2018.
- [32] Sergey Gavriluk, Kseniya Ivanova, and Nicolas Favrie. Multi-dimensional shear shallow water flows: Problems and solutions. *Journal of Computational Physics*, 366:252–280, 2018.
- [33] Jean-Frédéric Gerbeau and Benoît Perthame. Derivation of Viscous Saint-Venant System for Laminar Shallow Water ; Numerical Validation. *Discrete and Continuous Dynamical Systems - Series B*, 1(1):89–102, 2001.
- [34] Edwige Godlewski and Pierre-Arnaud Raviart. *Numerical approximation of hyperbolic systems of conservation laws*, volume 118 of *Applied Mathematical Sciences*. Springer-Verlag, New York, 1996.
- [35] Sergei Godunov and I Bohachevsky. Finite difference method for numerical computation of discontinuous solutions of the equations of fluid dynamics. *Matematičeskij sbornik*, 47(3):271–306, 1959.
- [36] L Gosse. A well-balanced flux-vector splitting scheme designed for hyperbolic systems of conservation laws with source terms. *Computers & Mathematics with Applications*, 39(9-10):135–159, 2000.
- [37] N Goutal and F Maurel. *Proceedings of the 2nd workshop on dam-break wave simulation*. Electricité de France. Direction des études et recherches, 1997.
- [38] Joshua M Greenberg and Alain-Yves LeRoux. A well-balanced scheme for the numerical processing of source terms in hyperbolic equations. *SIAM Journal on Numerical Analysis*, 33(1):1–16, 1996.

- [39] Emmanuel Grenier. On the derivation of homogeneous hydrostatic equations. *ESAIM: Mathematical Modelling and Numerical Analysis*, 33(5):965–970, 1999.
- [40] Amiram Harten, Peter D Lax, and Bram van Leer. On upstream differencing and godunov-type schemes for hyperbolic conservation laws. *SIAM review*, 25(1):35–61, 1983.
- [41] David D Houghton and Akira Kasahara. Nonlinear shallow fluid flow over an isolated ridge. *Communications on Pure and Applied Mathematics*, 21(1):1–23, 1968.
- [42] Randall J LeVeque. Balancing source terms and flux gradients in high-resolution godunov methods: the quasi-steady wave-propagation algorithm. *Journal of computational physics*, 146(1):346–365, 1998.
- [43] Randall J LeVeque. *Finite volume methods for hyperbolic problems*, volume 31. Cambridge university press, 2002.
- [44] Victor Michel-Dansac, Christophe Berthon, Stéphane Clain, and Françoise Foucher. A well-balanced scheme for the shallow-water equations with topography. *Computers & Mathematics with Applications*, 72(3):568–593, 2016.
- [45] Victor Michel-Dansac, Christophe Berthon, Stéphane Clain, and Françoise Foucher. A well-balanced scheme for the shallow-water equations with topography or manning friction. *Journal of Computational Physics*, 335:115–154, 2017.
- [46] Amélie Rambaud. *Modélisation, analyse mathématique et simulations numériques de quelques problèmes aux dérivées partielles multi-échelles*. Theses, Université Claude Bernard - Lyon I, December 2011.
- [47] Gaël L Richard and Sergey L Gavrilyuk. A new model of roll waves: comparison with brock’s experiments. *Journal of Fluid Mechanics*, 698:374–405, 2012.
- [48] P Ripa. Conservation laws for primitive equations models with inhomogeneous layers. *Geophysical & Astrophysical Fluid Dynamics*, 70(1-4):85–111, 1993.
- [49] P Ripa. On improving a one-layer ocean model with thermodynamics. *Journal of Fluid Mechanics*, 303:169–201, 1995.

- [50] Philip L Roe. Approximate riemann solvers, parameter vectors, and difference schemes. *Journal of computational physics*, 43(2):357–372, 1981.
- [51] Denis Serre. Systèmes hyperboliques de lois de conservation, partie i. *Diderot, Paris*, 1996.
- [52] Denis Serre. *Systems of Conservation Laws 1: Hyperbolicity, entropies, shock waves*. Cambridge University Press, 1999.
- [53] Vladimir Teshukov. Gas-dynamic analogy for vortex free-boundary flows. *Journal of Applied Mechanics and Technical Physics*, 48(3):303–309, 2007.
- [54] Eleuterio F Toro. *Riemann solvers and numerical methods for fluid dynamics: a practical introduction*. Springer Science & Business Media, 2013.
- [55] Eleuterio F Toro, Michael Spruce, and William Speares. Restoration of the contact surface in the hll-riemann solver. *Shock waves*, 4(1):25–34, 1994.